Schweizerische Eidgenossenschaft
Confédération suisse
Confederazione Svizzera
Confederaziun svizra

Federal Department of the Environment, Transport, Energy and Communications DETEC

Swiss Federal Office of Energy SFOE
Energy Research and Cleantech Division

Final report dated 24 August 2023

HydroPilot

Pilot plant for the catalytic hydrothermal gasification of wet biomass



Source: © M. Fischer, PSI, 2020

Date: 24 August 2023

Location: Bern

Publisher:
Swiss Federal Office of Energy SFOE
Energy Research and Cleantech
CH-3003 Bern
www.bfe.admin.ch

Subsidy recipients:
Paul Scherrer Institut
Forschungsstr. 111
CH-5032 Villigen PSI
www.psi.ch

KASAG Swiss AG
Hohgantweg 4
3550 Langnau i. E.
www.kasag.com

TreaTech sàrl
Avenue Alexandre Vinet 22
1004 Lausanne
www.trea-tech.com

ExerGo SA
Avenue des sports 42
1400 Yverdon-les-Bains
www.exergo.com

Afry Schweiz AG
Herostrasse 12
8048 Zürich
www.afry.com

Authors:
Frédéric Vogel, Paul Scherrer Institut, frederic.vogel@psi.ch
Thomas Brunner, FHNW, thomas.brunner1@fhnw.ch
David Baudouin, PSI, david.baudouin@psi.ch
Raquel Zambrano, Treatech, raquel.zambrano@trea-tech.com
Gaël Peng, Treatech, gael.peng@trea-tech.com
Alberto Mian, ExerGo, alberto.mian@exergo.ch
Martin Brandenberger, Afry, martin.brandenberger@afry.com

SFOE project coordinators:
Men Wirz, men.wirz@bfe.admin.ch

Sandra Hermle, sandra.hermle@bfe.admin.ch

SFOE contract number: SI/501793-01

The authors bear the entire responsibility for the content of this report and for the conclusions drawn therefrom.

Zusammenfassung

Zusammen mit den Industriepartnern TreaTech, KASAG, ExerGo und Afry wurde am PSI eine Pilotanlage (TRL 6) für die katalytische hydrothermale Vergasung (cHTG) von nassen Abfallströmen zu Methan konzipiert, gebaut und erfolgreich betrieben. Mit dieser Technologie kann eine breite Palette von nassen Abfallströmen mit hoher Effizienz unter Rückgewinnung aller Nährstoffe verarbeitet werden. Der Schwerpunkt lag dabei auf der P-Rückgewinnung durch das von TreaTech entwickelte Verfahren. Die Pilotanlage mit der Bezeichnung HydroPilot wurde mit Lösungen aus Glycerin, kommunalem Klärschlamm, Industrieabwasser und Lebensmittelabfällen getestet. Alle vier Abfallströme konnten verarbeitet werden und erzeugten einen methanreichen Gasstrom. Das Rohgas enthielt bis zu 70 Vol.-% Methan, der Rest bestand aus CO_2 und H_2. Der Stickstoff im Einsatzmaterial wurde vollständig als Ammonium im Prozesswasser zurückgewonnen, während bis zu 87 % der anderen Mineralien und Nährstoffe im Salzstrom extrahiert wurden. Eine gewisse Anreicherung von Mineralien im Salzabscheider war unvermeidlich und muss weiter optimiert werden, um einen längerfristigen Betrieb zu ermöglichen. Die Herstellung des Vergasungskatalysators wurde erfolgreich hochskaliert und 100 kg davon hergestellt. Seine Aktivität entsprach der unter Laborbedingungen ermittelten Aktivität oder übertraf sie sogar. Während des gesamten Projekts wurden keine Anzeichen einer Desaktivierung festgestellt. Zum Schutz des Katalysators vor den im Einsatzmaterial enthaltenen Schwefelverbindungen wurde ein handelsübliches Absorbermaterial auf der Basis von Zinkoxid dem katalytischen Reaktor vorgeschaltet. Ein statisches und ein dynamisches Wärmeübertragungsmodell wurden entwickelt, um das weitere Scale-up zu unterstützen. Wirtschaftliche Berechnungen und eine Ökobilanz des Verfahrens zur Behandlung von Klärschlamm mit P-Rückgewinnung zeigten Bereiche für weitere Verbesserungen auf, insbesondere die Verringerung der Menge und die Verbesserung des Recyclings des Schwefelabsorbermaterials. Es wurde ein Verfahren zur Rückgewinnung von Phosphor aus dem aus cHTG gewonnenen Salzstrom entwickelt. Der Phosphor wurde erfolgreich durch Säureauslaugung zurückgewonnen und als kristalliner Struvit mit einer Gesamtrückgewinnungsrate von 70-80% ausgefällt, wobei die MinRec-Vorschriften eingehalten wurden. Schließlich wurden die Kapital- und Betriebskosten für das P-Rückgewinnungsverfahren für zwei Phosphorverwertungsszenarien in Form von Phosphorsäure und Struvit geschätzt. Die Verwertung und der Verkauf des Phosphors als Phosphorsäure bei der Integration des cHTG- und P-Rückgewinnungsverfahrens in einem Zementwerk führt zu einem rentablen Szenario, bei dem alle Betriebskosten gedeckt wären.

Résumé

Une installation pilote (TRL 6) pour la gazéification hydrothermale catalytique (cHTG) de flux de déchets humides en méthane a été conçue, construite et exploitée avec succès au PSI, en collaboration avec les partenaires industriels TreaTech, KASAG, ExerGo et Afry. Cette technologie permet de traiter un large éventail de flux de déchets humides avec une grande efficacité, en récupérant tous les nutriments. L'accent a été mis sur la récupération du phosphore par le procédé exclusif de TreaTech. L'installation pilote, appelée HydroPilot, a été testée avec des solutions de glycérol, de boues d'épuration municipales, d'eaux usées industrielles et de déchets alimentaires. Les quatre flux de déchets ont pu être traités et ont produit un flux de gaz riche en méthane. Le gaz brut contenait jusqu'à 70 % de méthane, le reste étant constitué de CO_2 et de H_2. L'azote contenu dans l'alimentation a été entièrement récupéré sous forme d'ammonium dans l'eau de traitement, tandis que jusqu'à 87 % des autres minéraux et nutriments ont été extraits dans le flux de saumure. Une certaine accumulation de minéraux dans le séparateur de sel était inévitable et doit être optimisée pour permettre un fonctionnement à long terme. La production du catalyseur de gazéification a été mise à l'échelle avec succès et 100 kg ont été produits industriellement. Son activité était similaire, voire supérieure, à celle déterminée dans des conditions de laboratoire. Aucun signe de désactivation

n'a été constaté pendant toute la durée du projet. Pour protéger le catalyseur des composés sulfurés présents dans l'alimentation, un matériau absorbant commercial à base d'oxyde de zinc a été placé en amont du réacteur catalytique. Un modèle statique et un modèle dynamique de transfert de chaleur ont été développés pour faciliter la mise à l'échelle ultérieure. Des calculs économiques et une ACV du procédé de traitement des boues d'épuration avec récupération du P ont mis en évidence des domaines susceptibles d'être améliorés, en particulier la réduction de la quantité et l'amélioration du recyclage du matériau absorbeur de soufre. Un procédé a été mis au point pour récupérer le phosphore du flux de saumure extrait du cHTG. Le phosphore a été récupéré avec succès par lixiviation acide et précipité sous forme de struvite cristalline, avec un taux de récupération global de 70 à 80 %, tout en respectant les réglementations MinRec. Enfin, les dépenses d'investissement et d'exploitation pour le processus de récupération du phosphore ont été estimées pour deux scénarios de valorisation du phosphore sous forme d'acide phosphorique et de struvite. La valorisation et la vente du phosphore sous forme d'acide phosphorique lors de l'intégration des processus de cHTG et de récupération du P au sein d'une cimenterie aboutissent à un scénario rentable dans lequel toutes les dépenses d'exploitation seraient couvertes.

Summary

A pilot plant (TRL 6) for the catalytic hydrothermal gasification (cHTG) of wet waste streams to methane was designed, built and successfully operated at PSI, together with the industrial partners TreaTech, KASAG, ExerGo, and Afry. WIth this technology, a wide range of wet waste streams can be processed with a high efficiency, recovering all the nutrients. A focus was set on P-recovery by TreaTech's proprietary process. The pilot plant, called HydroPilot, was tested using solutions of glycerol, municipal sewage sludge, an industrial waste water, and food waste. All four waste streams could be processed and produced a methane-rich gas stream. The raw gas contained up to 70 vol% of methane, the remainder being CO_2 and H_2. Nitrogen in the feed was fully recovered as ammonium in the process water, while up to 87% of the other minerals and nutrients were extracted in the brine stream. Some accumulation of minerals in the salt separator was inevitable and must be further optimized to enable longer term operation. The production of the gasification catalyst was successfully scaled up and 100 kg produced industrially. Its activity was similar to or even exceed the one determined under lab-scale conditions. No signs of deactivation were found during the whole project. To protect the catalyst from sulfur compounds present in the feed, a commercial absorber material based on zinc oxide was placed upstream of the catalytic reactor. A static and a dynamic heat transfer model were developed to aid further scale-up. Economic calculations and an LCA of the process for the treatment of sewage sludge with P-recovery highlighted areas for further improvement, in particular reducing the amount and improving the recycling of the sulfur absorber material. A process was developed to recover phosphorus from the brine stream extracted from cHTG. Phosphorus was successfully recovered through acid leaching and precipitated as crystalline Struvite with an overall recovery rate of 70-80% while complying with MinRec regulations. Finally, the capital and operating expenses for the P-recovery process have been estimated for two phosphorus valorisation scenarios in the form of phosphoric acid and struvite. Valorising and selling the phosphorus as phosphoric acid when integrating the cHTG and P-recovery processes within a cement manufacturing plant, results in a profitable scenario where all the operating expenses would be covered.

Main findings

- Catalytic hydrothermal gasification of wet waste streams to methane was demonstrated at the pilot scale (TRL 6). Waste streams with a low minerals content (< 10 wt%) were processed smoothly with a high efficiency, while sewage sludge with a high minerals content (ca. 45 wt%) posed some challenges in the salt separator. No signs of catalyst deactivation were observed.
- After some adjustments during commissioning, the operation of the high-pressure plant was mostly trouble-free and no hazards occurred. Pumping of sewage sludge did not pose any problems, while the food waste required a more extensive mechanical pretreatment before reliable pumping was possible.
- In the optimal case, up to 87% of the minerals contained in the feed were recovered continuously in the brine stream (ash balance 117%). All feed nitrogen was recovered as ammonium in the process water. This proves that HTG can produce both biomethane and two nutrient-rich streams.
- Building on the results of this project, the design of a demonstration plant at industrial scale should be possible. The few remaining technical risks have been identified. In particular, the choice of materials of construction for the salt separator should be revisited.

Contents

Zusammenfassung **4**

Résumé **4**

Summary **5**

Main findings **6**

Contents **7**

Abbreviations **9**

1 Introduction **11**

1.1 Background and current situation 11
1.2 Purpose of the project 13
1.3 Objectives 14

2 Description of the facility **15**

2.1 General process description 15
2.2 Preheater 16
2.3 Salt separator 17
2.4 Sulfur absorber and catalytic reactors 18

3 Procedures and methodology **20**

3.1 Project organization 20
3.2 Heat transfer measurements 21
3.3 Gasification experiments 22
3.4 Phosphorus recovery 24

4 Results and discussion **25**

4.1 Erection of the pilot plant (WP 1 and 2) 25
4.2 Heat transfer and test campaigns (WP 3) 27
4.2.1 Heat transfer experiments 27
4.2.2 Glycerol test 1 38
4.2.3 Glycerol test 2 40
4.2.4 Conclusions 44
4.3 Processing of sewage sludge (WP 4) 44
4.3.1 Sewage sludge test 1 44
4.3.2 Sewage sludge test 2 46
4.3.3 Sewage sludge test 3 50
4.3.4 Industrial waste water 53
4.3.5 Food waste 57
4.3.6 Corrosion study 62
4.3.7 Conclusions 65

4.4 Phosphorus recovery (WP 5) 65
4.4.1 Phosphorus recovery using solids from the lab-scale prototype (1 kg/h) 65
4.4.2 Phosphorus recovery using solids from HydroPilot (100 kg/h) 79
4.4.3 TOC removal strategy 80
4.4.4 Estimation of the P-recovery costs (CAPEX and OPEX) for an HTG plant treating 6 t/h of sewage sludge 81
4.4.5 Conclusions 90
4.5 Design of an industrial unit (WP 6) 90
4.6 Life Cycle Assessment of HTG of sewage sludge including P-recovery 95
5 Conclusions 98
6 Outlook and next steps 100
7 National and international cooperation 101
8 Publications 102
9 References 102
10 Appendix 104

Abbreviations

ADWO	Swiss ordinance on the avoidance and the disposal of waste
CAGR	Compound annual growth rate
CAPEX	Capital Expenditures
cHTG	catalytic Hydrothermal Gasification
DM	Dry matter
DI	Deionized water
DOE	Design of experiments
DSS	Dry sewage sludge
EDXS	Energy-dispersive X-ray Spectroscopy
EPFL	École Polytechnique Fédérale de Lausanne
EU	European Union
FHNW	Fachhochschule Nordwestschweiz
FIB	Focused ion beam
FM	Functional Module
FOEN	Federal Office of the Environment
FW	Food waste
GC	Gas chromatography
GC-MS	Gas chromatography coupled to mass spectrometry
GHG	Greenhouse gases
G-L	Gas-Liquid
HAZOP	Hazard and operability (study)
HCB	Hexachlorobenzene
HP	High pressure
HTC	Heat transfer coefficient
HTG	Hydrothermal gasification
HX	Heat exchanger
ICP	Inductively coupled plasma
ID	Inner diameter
IPA	Isopropanol
IPCC	Intergovernmental panel on climate change
KIT	Karlsruhe Institute of Technology
KPI	Key performance indicator
LMTD	Logarithmic mean temperature difference
LOD	Limit of detection

LP	Low pressure
MinRec	mineralische Recylingdünger
MWIP	Municipal waste incineration plant
NG	Natural gas
OD	Outer diameter
OES	Optical emission spectroscopy
OFEN	Office fédéral de l'énergie (in German: BFE)
OM	Organic matter
OPEX	Operational expenditures
P	Phosphorus
P&D	Pilot- und Demonstration
PAH	Polycyclic aromatic hydrocarbons
PCB	Polychlorinated biphenyls
PSI	Paul Scherrer Institut
SCCER	Swiss Competence Center for Energy Research
SCW	Supercritical water
SEM	Scanning electron microscopy
SFOE	Swiss federal office of energy
SIG	Services industriels de Genève
SNF	Schweizerischer Nationalfonds (Swiss national science foundation)
SNG	Synthetic natural gas
SS	Sewage sludge
SSC	Swiss safety center
TGA	Thermogravimetric analysis
TIC	Total inorganic carbon
TOC	Total organic carbon
ToS	Time on stream
TS	Total solids
TTR	Temperature transmitter (and recording)
UBP	Umweltbelastungspunkte
VVEA	Verordnung über die Vermeidung und Entsorgung von Abfällen
WP	Work package
WS	Wet solids
WWTP	Waste water treatment plant
XRD	X-ray diffraction
ZHAW	Zürcher Hochschule für angewandte Wissenschaften

1 Introduction

1.1 Background and current situation

General context and challenges

Wet waste biomass such as sewage sludge, manure and food processing waste represent a large energy potential in Switzerland [1]. Digested sewage sludge is already largely used thermally, but the net energy yield of the entire utilization chain is low. This is due in particular to the thermal drying required for incineration of the sewage sludge, e.g. in a cement plant. The use of wet waste biomass is in line with the federal government's strategy to increase the use of biomass for energy [2] and the Energy Strategy 2050 and is therefore significantly supported by the SCCER BIOSWEET.

In general, drying of wet biomass represents a large exergy loss. Anaerobic digestion does not require drying, since the conversion takes place in aqueous phase. However, only the fermentable fractions can be used energetically with this technology. Lignocellulosic components and other components that are difficult to ferment end up in the fermentation residue, which is not used further for energy but is discharged as fertilizer.

Wet municipal waste and wastewater must be disposed of in such a way that no harmful substances are released into the environment. While incineration of municipal waste comes close to this goal, a whole range of harmful substances are not broken down in wastewater treatment plants [3]. These either enter the receiving water via the treated wastewater or end up in the sewage sludge. In Switzerland, sewage sludge must be disposed of thermally, which is a sink for most organic pollutants. In other countries, the application of sewage sludge as fertilizer is still common practice. Prior digestion does not degrade many chemical and biochemical pollutants such as endocrine disruptors (PCBs, HCBs, plasticizers, bisphenol A, nonylphenol, estrogens), optical brighteners, PAHs, polycyclic musks, etc. [3]. If sewage sludge contaminated with such substances is used as fertilizer in agriculture, these substances can be absorbed by humans and animals via the food chain. In Switzerland, the application of sewage sludge has been prohibited since 2006.

However, sewage sludge also contains valuable minerals that would justify its use as a biogenic fertilizer. In particular, the non-renewable element phosphorus must be recovered from sewage sludge from 2026 at the latest, according to the new Ordinance on the Prevention and Disposal of Waste (VVEA). The dry matter of digested sludge in Switzerland contains about 3% P, besides 4% N, 0.2% K, 6% Ca and 0.5% Mg [4]. The FOEN has estimated that about 6,000 t of phosphorus are removed from sewage sludge annually from the fertilizer cycle by incineration in the MWIP or a cement plant [5].

Market situation

In this project, we decided to focus on municipal feedstock (sewage sludge) and industrial feedstock (waste solvent, food waste). TreaTech's business model is based on both municipal and industrial feedstocks with the first industrial HTG unit designed for industrial feedstocks (expected to be commissioned in 2025) and the industrial HTG unit for municipal feedstocks planned for 2027. Waste streams represent value if they can be recycled or converted into energy without over-processing. Biomass waste has little value if biogas can be produced, although its elimination is usually very cheap. One exception is sewage sludge, whose disposal costs can represent up to 40% of wastewater treatment plants operating costs (>400 CHF/t_{DM}). Traditionally, sewage sludge has been used in agriculture due to its high content of inorganic nutrients such as nitrogen and phosphorus, suggesting their use as soil conditioner and fertilizer. However, the presence in sewage sludge of organic micro-pollutants (drugs, hormones, heavy metals, etc.) brought up increasing issues of soil contamination and its consequences for the environment and human health. In response to these issues, new regulations[1] were adopted to control its use and prevent harmful effects on soil, vegetation, animals

[1] Urban Waste Water Treatment Directive 86/278/ EEC; Ordonnance sur la limitation et l'élimination des déchets (VVEA)

and humans. In Switzerland sewage sludge utilization as a fertilizer was prohibited and must be disposed of by incineration. However, incineration generates emissions into the air (particles, acid gases, greenhouse gases, volatile organic compounds, etc.), and residual ashes that are usually disposed of in landfills, since they contain high concentrations of polluting and heavy metals, losing the recovery of phosphates as nutrients for the soil. Despite the loss of recyclable by-products, these standard processes entail high costs to the sludge treatment plants including dehydrating the matter, fossil fuel for thermal drying, a storage zone and transport by truck to incinerators.

Nowadays, more than 60% of sludge disposal is still either incinerated or landfilled causing 2.8% of global GHG emissions, costing up more than € 11.2 B per year in EU and € 142 B globally for wastewater treatment plants [6]. Concerning phosphorus, given an estimated production of 10 million tons of dry sewage sludge per year in Europe, around 600'000 tons of phosphorus could be potentially recovered.

Market – Opportunity

There is a big potential to use hydrothermal gasification solutions for sewage sludge disposal. The feedstock quantities are massive, although it is the economy and the legislation (for example a landfill ban) that will determine the right timing for market penetration.

According to a recent published report [7], The Global Sewage Treatment Plants Market is forecast to grow at a positive CAGR of 9% during 2016 - 2021 to reach € 154 B by 2021, due to an increasing population and emerging stringent regulations. Although for the implementation of our technology, the targeted market is mono-incineration. In Switzerland, considering that P-recovery will be compulsory by 2026, mono-incineration will be required. The planned initial investment is CHF 500-800 M, for around 10-20 mono-incinerators that will be necessary to burn the 200‘000 tons (DM) of sewage sludge produced each year in Switzerland and allow for P-recovery from ashes.

Due to changing trends and new government legislations regarding resource valorization, the European sewage sludge market will obviously orient the main strategy towards mono-incineration solutions. Optimization of actual incinerators won’t be sufficient, new investments for these particular incinerators will be required. If traditional sewage sludge disposal solutions in EU are replaced by incineration, the cost would be of the order of € 650 million per year.

Trends & drivers

The rising urbanization, growth consumption, rapid industrialization and a high rate of capital investments in the waste water treatments are key factors for the rise in the market size of WWTP.

Legislation is undoubtedly the most important driver of growth for sales of wastewater control technologies. EU has one of the most stringent rules in urban wastewater treatment (Directive 91/271/EEC) that aim to protect waterways from the adverse effects of discharges of urban wastewater and from certain industrial discharges. In particular, the Article 14 the Directive states that "Sludge arising from waste water treatment shall be re-used whenever appropriate. Disposal routes shall minimize the adverse effects on the environment." The progressive implementation of the said Directive in all Member States in-creased the quantities of sewage sludge requiring disposal and the effective implementation of Sewage Sludge Directive 86/278/EEC was a necessity. This Directive seeks to regulate the use of sewage sludge in agriculture to prevent harmful effects on soil, vegetation, animals and man.

The Global Biogas Market is expected to grow at a steady 6.5% CAGR from nearly CHF 22 B in 2015 to around CHF 45 B in 2026 due to mounting concerns over depleting fossil reserves and the environmental impact of conventional fuels. The TreaTech solution can produce up to 30% more biogas than current treatment solutions.

The Global Phosphoric Acid Market is worth over CHF 33 B today and is anticipated to reach more than CHF 37 B by 2023. Recovering Phosphate from sewage sludge is a growing trend because this non-renewable resource is being depleted globally. Only few technologies can produce phosphoric

acid from sewage sludge. Treating 200'000 tons (dry matter basis) of sludge per year with our solution we could produce 10‘000 tons of phosphorus. .

1.2 Purpose of the project

Hydrothermal gasification represents a novel thermo-chemical technology that can handle virtually all types of pumpable biomass. Since the process takes place under high pressure, the water remains liquid (or even becomes supercritical) even at high temperature. Thus, the process does not require dried biomass. Typical dry matter contents are between 15 and 30% for the hydrothermal process to operate efficiently. Thus, net biomass-to-methane efficiencies of 60-70% are achievable. Due to the harsh reaction conditions (several minutes in water at 450°C and 28 MPa), it can be assumed that all chemical and biological contaminants (including worm eggs, viruses, etc.) are destroyed. In fact, supercritical wet oxidation, a related process, is used in the United States for the disposal of chemical warfare agents.

Such a gasification process, which yields methane as the main product, has been developed and patented at the Paul Scherrer Institute since 2002 [12]. The worldwide development status was presented in a book article [8]. PSI is at the forefront of research in this area and is one of the few players in the world to have brought hydrothermal gasification to application maturity over such a long period of time. The SFOE has supported this research and development work from the beginning as part of the Bioenergy Research Program. In 2014, a 100-hour campaign was conducted at ZHAW using an algae slurry [9,11], and in 2015, the main apparatus of the process, a salt separator, was successfully tested as a prototype at KIT in Karlsruhe using digestate from a biogas plant [10]. This prototype was funded by the SFOE P&D program. More than ten dissertations have been carried out at PSI on the subject of hydrothermal gasification since 2002, and the findings have been published in 50 scientific articles.

The last logical and necessary step before commercial implementation has been taken in this project: the construction of a pilot plant at PSI for the entire process chain on a semi-industrial scale (TRL 6). With this pilot plant, it also became possible to implement TreaTech’s own mineral extraction process and to produce larger quantities of brine for scaling up the recovery of phosphorus, which TreaTech had developed in parallel to the HTG activities carried out by PSI. Thus, this project aimed at demonstrating the combined hydrothermal gasification and P-recovery from different kinds of waste streams.

Development status of PSI’s hydrothermal gasification process at the beginning of the project

Two components form the core of the PSI technology: the salt separator and the catalytic reactor. Both components were successfully tested in 2015 at KIT's VERENA pilot plant using digestate from a biogas plant [10]. A prototype salt separator was used, which had been developed and built as part of a SFOE P&D project [14]. On a laboratory scale, the process was already demonstrated in 2014 with algae biomass over 100 hours in a field trial at ZHAW [9,11,13]. The following aspects relevant for a commercial implementation are still being worked on at the moment:

- The absorption capacity of the sulfur trap, which protects the catalyst from toxic sulfur compounds, is still insufficient for commercial use. For this purpose, new materials have been developed and tested.
- Due to the susceptibility of the laboratory plant to clogging (small orifices up to 1 mm), it has not yet been possible to carry out a trial with biomass containing solids with a dry matter content > 10%. For economic operation, TS contents of 20% are required with many biomasses.

- The long-term supplier of the ruthenium catalyst, BASF, has discontinued production. New sources of supply have been identified and tested. The production of catalyst quantities in the 100 kg range for the pilot plant are a challenge.
- Further optimization of the catalyst, the sulfur trap and the overall process is being carried out with the laboratory plant in ongoing Innosuisse, SNF, and EU-funded projects.
- The salt separator prototype already achieved 81% P recovery in the first trial at KIT with digestate. The performance limits of the salt separator prototype could not be explored in the KIT trial due to time constraints. Knowledge of these limits is of great importance for further scaling and optimization because the salt separator is the most expensive component in the process.
- The step from laboratory to pilot plant requires a change from high-pressure components specially made for laboratory plants to industrial series components. The behavior of these components under the extreme conditions of hydrothermal gasification is not known.

Development status of TreaTech technology for mineral extraction and P-recovery

- A new mineral extraction unit was developed by TreaTech over the past five years. The latter is an extension of PSI's salt separator and was designed to extract solid minerals during hydrothermal processing of biomass. It was demonstrated that all the minerals can be effectively extracted without altering processing of biomass (digested and undigested sewage sludge).

- Phosphorus was effectively recovered as phosphoric acid from the minerals that were produced during hydrothermal processing of digested and undigested sewage sludge. The P-recovery experiments were performed at the laboratory scale by applying acid leaching (with sulfuric acid) to the minerals. Chemical analysis of the leachate revealed the presence of some contaminants (Fe, Al, Ca, organic compounds) which will require the development and implementation of cost-effective purification methods prior to its commercialization.

1.3 Objectives

- Construction of the world's largest pilot plant for the production of synthetic natural gas (SNG) from wet biomass using catalytic hydrothermal gasification.
- Conduct experimental campaigns with different biomasses to verify the results from the laboratory plant (scale-up).
- Generate first validated cost estimate for commercial plants by the industrial partners KASAG Swiss AG, TreaTech Sàrl, ExerGo Sàrl and Afry.
- Accompanying scientific research within the SCCER BIOSWEET: measurement of material and energy balances, composition of process water and brine, recovery of phosphorus and other minerals from the brine.
- Preparation of a detailed life cycle assessment, including the relevant mass and energy flows, and comparison with alternative solutions in the field of sewage sludge utilization with phosphorus recovery.

2 Description of the facility

2.1 General process description

After feed preparation and size reduction to a pumpable state, the material enters a tube-in-tube heat exchanger via a high-pressure pump at 25 to 30 MPa (Fig. 2.1). In the subsequent salt separator, the temperature is raised to about 420-450 °C, causing dissolved inorganic material to precipitate, together with undissolved minerals, forming a brine. This brine is removed from the hot biomass stream and treated by a patented process developed by TreaTech. The brine is cooled and depressurized. A first absorber, filled with zinc oxide, follows in the main stream, which serves as a "police filter", protecting the subsequent catalytic reactors from sulfur. In the following catalytic reactors, biomass gasification and methanation takes place in supercritical water at 400 to 450 °C. The reactors are filled with a catalyst containing 5% ruthenium on granular activated carbon. Since the heat of reaction is only slightly exothermic, the reactors do not need to be heated or cooled. After passing through the heat exchanger, the product mixture is cooled and split into synthetic natural gas (SNG) and process water via a phase separator operated under high pressure. The process water stream is further depressurized in a vessel, yielding a small stream of weak gas. The process is heated by hot air circulating in a loop around the salt separator. An electric heater provides the process energy to the hot air loop. This electric heater may be replaced by a gas burner fired with a small portion of the SNG in an industrial unit. The resulting SNG has a low level of carbon dioxide because some of it is already removed in the high-pressure phase separator due to the much higher solubility of CO_2 in water than CH_4 and H_2.

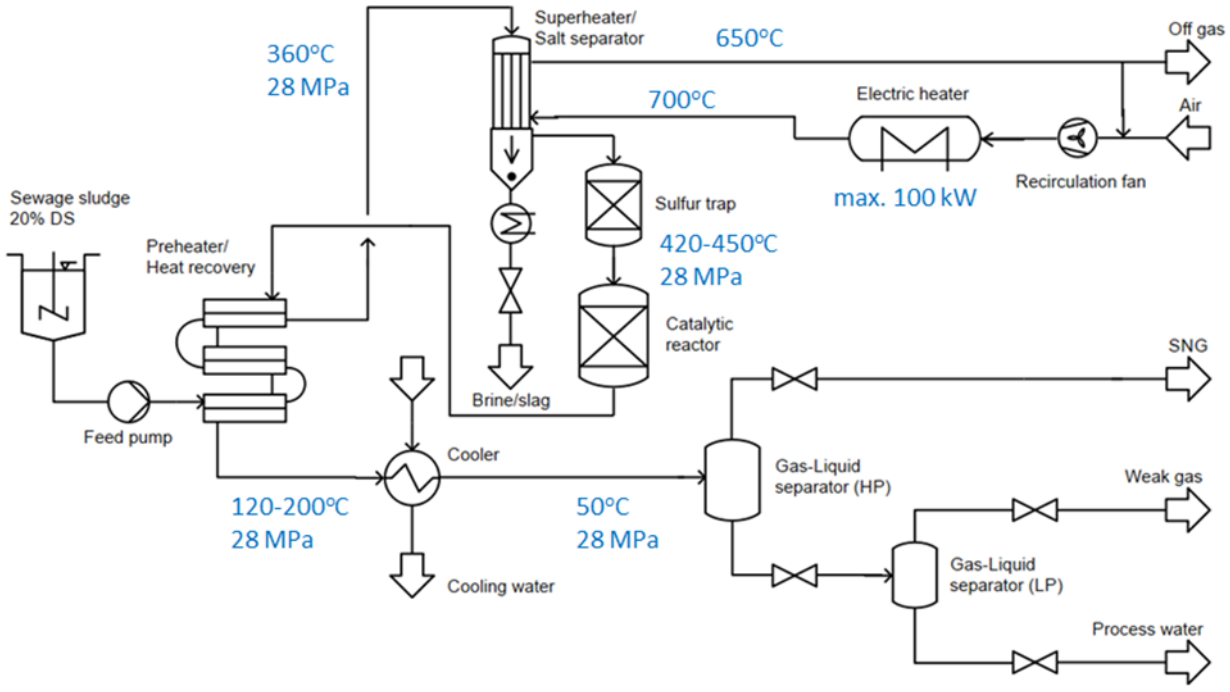


Fig. 2.1: Sketch of the HydroPilot plant. Temperatures and pressures are typical expected values or ranges.

The process gas is burned together with the lean gas in an existing flare, since there is no possibility to use SNG at PSI. The process water is monitored and discharged into the PSI sewer system if the limit values are met. If the limits are exceeded (e.g., if the organic content is too high), the process water is collected and sent for proper disposal. The brine is collected and used for further investigations (especially phosphorus recovery).

These are the design specifications for the HydroPilot plant:

Max. throughput	110 kg/h wet biomass (at max. 20% TS)
Min. throughput	25 kg/h
Max. feed concentration	20% TS
Max. electric heating power	100 kW (at 700°C)
Typical brine mass flow rate	10-20% of the feed mass flow rate
Max. operating pressure	350 bar
Max. fluid temperature	450°C
Max. material temperature	700°C (salt separator)
Materials of construction	Stainless steel 316, except for the salt separator (Inconel 625)

The pilot plant was conceptually subdivided into eight functional modules (FM), FM 10 to FM 80.

2.2 Preheater

The preheater is designed as a heat exchanger and consists of two concentric tubes with the cold fluid in the core (feed stream) and the hot fluid (effluent from the reactor) in the annulus (Figure 2.2). It is built from five equal u-shaped segments placed on top of each other (Figure 2.3 and Table 2.1). Temperature sensors are placed at the inlet and outlet, as well as at the connection between segment three and four.

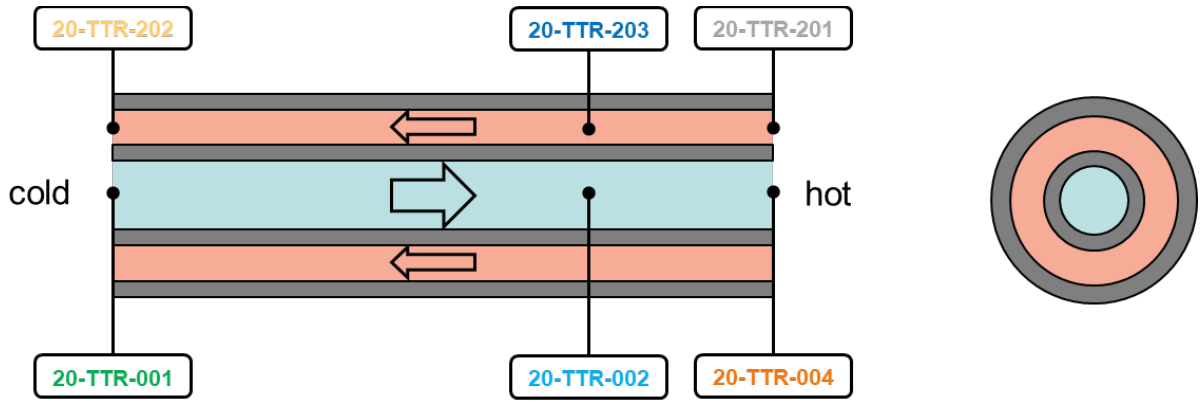


Figure 2.2: Schematic of the preheater with an indication of the approximate positions of the temperature sensors. Blue: Feed stream. Red: effluent from reactor. TTR: temperature transmitters (cp. Fig. 4.12).



Figure 2.3: Picture of the five U-shaped preheater elements of HydroPilot.

Table 2.1: Dimensions of the preheater.

Description	Shortcut	Dimension	Units
Length straight tube	L_{TS}	2.92	m
Length 180° tube bend	L_{TB}	1.13	m
Number of U-Segments	N_{US}	5	-
OD mantle tube	$D_{M,O}$	60.3	mm
ID mantle tube	$D_{M,I}$	38.2	mm
OD core tube	$D_{C,O}$	26.7	mm
ID core tube	$D_{C,I}$	11.0	mm
Heat exchanger area (based on $D_{C,O}$)	$A_{HE,I}$	2.92	m^2

2.3 Salt separator

The salt separator is the only unit where external heat is supplied to the system. It is designed as a tube-bundle heat exchanger. Figure 2.4 shows a schematic of the salt separator. The feed enters through the top and is then distributed into 20 falling tubes. At the bottom, the flow is reversed and exits through the central rising tube. The volume around the tubes shown in red is hot air supplied by an electrical heater and a high temperature fan. Some important dimensions are given in Table 2.2.

Table 2.2: Dimensions of the salt separator. The given lengths correspond to the portion of the tubes that are heated by hot air.

Description	Short	Dimension	Unit
Length falling tube	L_{TF}	1.5	m
Length rising tube	L_{TR}	1.5	m
Number of falling tubes	N_{TF}	20	-
Number of rising tubes	N_{TR}	1	-
OD falling tube	$D_{F,O}$	17.2	mm
ID falling tube	$D_{F,I}$	10.8	mm
OD rising tube	$D_{R,O}$	60.3	mm
ID rising tube	$D_{R,I}$	42.9	mm
Area falling tube (based on $D_{F,O}$)	$A_{HE,F}$	1.62	m^2

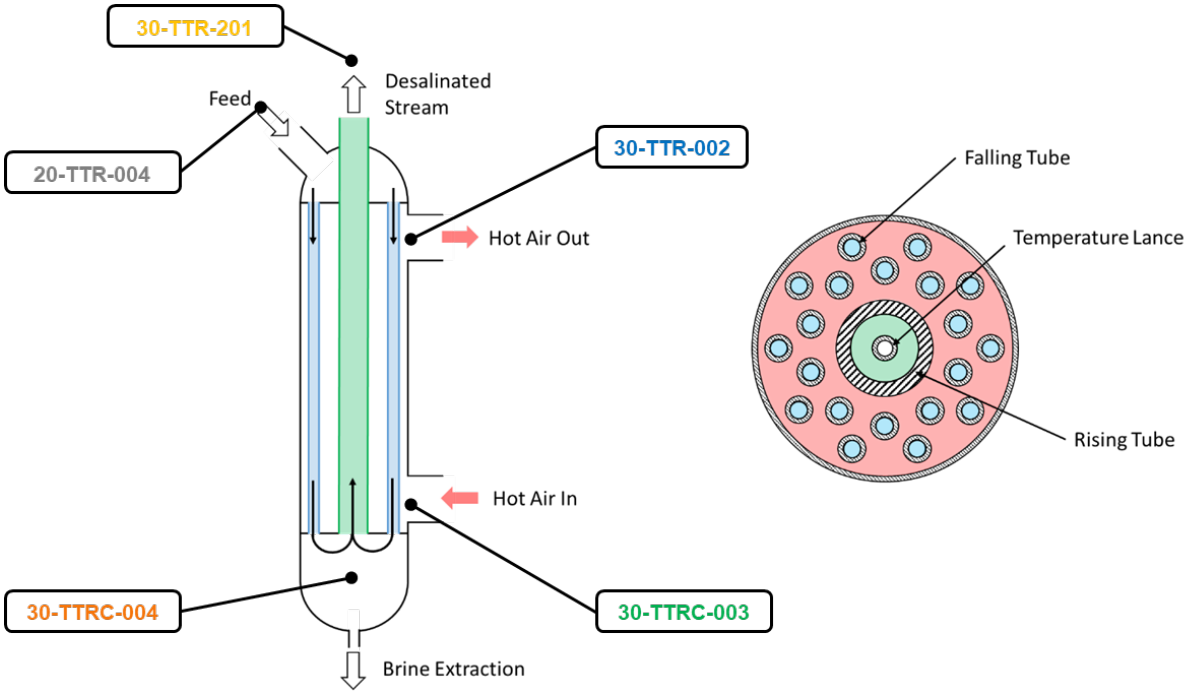


Figure 2.4: Schematic of the salt separator. Left: Lengthwise cut with process streams. Right: cross section showing the tube arrangement. The falling section where the fluid flows downwards is shown in blue. The rising section where the fluid flows upwards is shown in green. The flow reverses in the pot at the bottom of the salt separator. TTR: temperature transmitter; TTRC: temperature controller.

The salt separator takes advantage of the very low solubility of salts and other minerals in supercritical water. They precipitate in the falling tubes and are carried downstream, where they separate from the fluid phase and accumulate in the bottom part. From this salt pot they are continuously removed as a concentrated brine. The salt-free fluid phase leaves the salt separator at the top and enters the sulfur absorber and the catalytic reactors (cp. Fig. 3.2).

2.4 Sulfur absorber and catalytic reactors

HydroPilot contains four reactors (Figure 2.5). The first reactor has a capacity of 100 L and the reactors 2-4 have a capacity of 50 L. The most important dimensions of the reactors are given in Table 2.3. The first reactor (R1) is filled with sulfur absorber materials to protect the catalyst from sulfur poisoning. The second reactor (R2) is filled with the catalyst as well as a protective layer of activated carbon. The third (R3) and fourth reactor (R4) are empty and disconnected. The details of the reactor fillings are listed in Table 2.4. The materials are mentioned in the order following the direction of the flow.



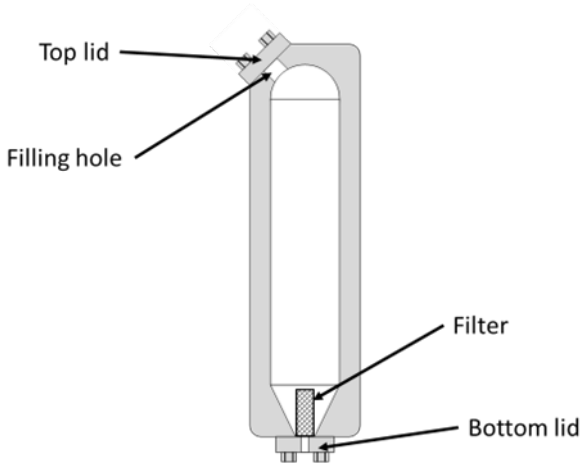


Figure 2.5: Left: Picture of HydroPilot reactors before installing the thermal insulation. Right: Simplified schematic of the reactors. The filter at the bottom prevents the charged solids from being flushed out of the reactors.

Table 2.3: Dimensions of the reactors in HydroPilot. Reactors 2-4 are identical. Reactor 1 is roughly twice as long.

Description	R1	R2 – R4	Units
Length	3.36	1.78	m
Capacity	100	50	L
Inner diameter	0.220	0.220	m
Outer diameter	0.330	0.330	m

Table 2.4: Filling materials of the reactors listed in direction of flow.

Reactor	Material	Amount [kg]
R1	ZnO granules	126
	α-Al_2O_3 granules	54.1
R2	Activated carbon (AC)	5.9
	Ru on AC catalyst	20.7
R3	Empty/not used	-
R4	Empty/not used	-

3 Procedures and methodology

3.1 Project organization

The project was organized and performed along six work packages (WP):

WP 1: Detail engineering[2] and execution planning

WP 2: Construction of the pilot plant

WP 3: Commissioning/initial operation

WP 4: Processing of sewage sludge

WP 5: Phosphorus recovery

WP 6: Design of an industrial unit

Regarding the timeline, the project can be subdivided into the engineering & erection phase (WP 1 & 2), and the commissioning & experimental phase (WP 3 &4). WP 5 and 6 were carried out in parallel to the erection of the pilot plant.

The overall project lead was carried out by PSI. WP 5 and 6 were led by TreaTech and ExerGo, respectively. Fig. 3.1 shows the organizational chart. During the commissioning phase, several key members left the project team: E. De Boni (engineering and plant operation), P. Unverricht (controls), and Y. Bäuerle (controls and process analytics). These team members were replaced by Urs Häseli (PPIH) and Tony Thomas (Treatech).

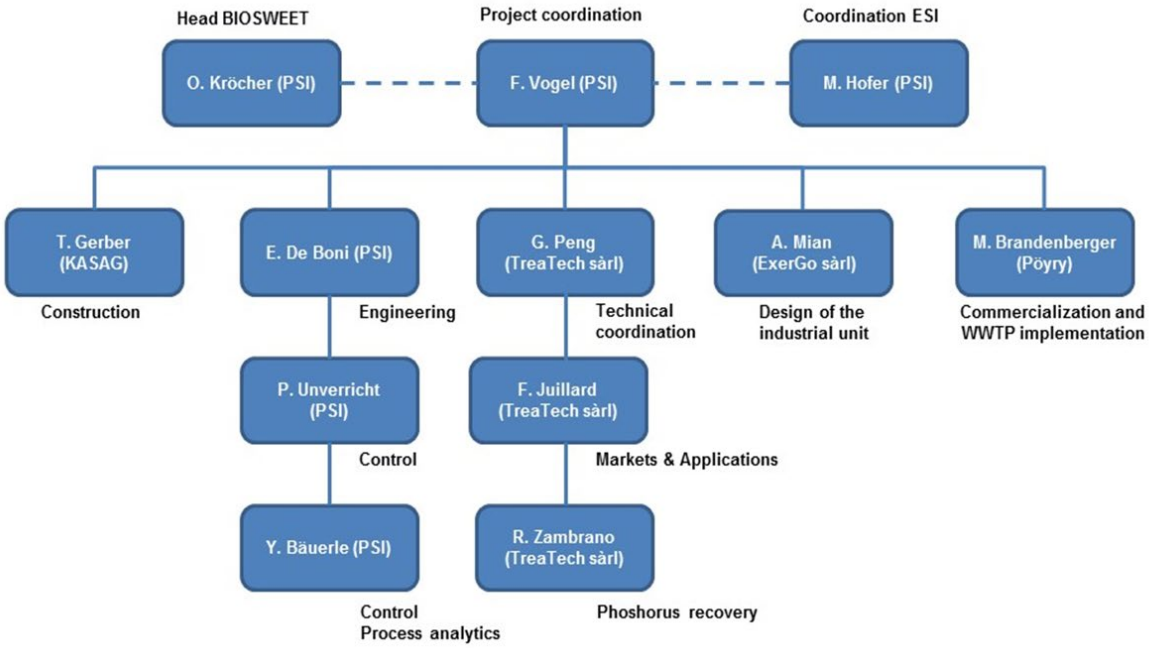


Figure 3.1: Organizational chart of the HydroPilot project as per December 2020.

[2] The basic engineering had already been performed before the HydroPilot project.

The HydroPilot project was embedded in the SCCER BIOSWEET, led by O. Kröcher, and in the Energy System Integration platform at PSI, led by M. Hofer. The overall project coordination was carried out by F. Vogel (PSI and FHNW).

Additional personnel joined the team for the commissioning and testing phase: V. Schnetzler (PSI), G. Koilaridis (Treatech), T. Fovanna (Treatech), P.-C. Vigna (Treatech), M. Nunez (Treatech), V. Jacobsen (Treatech), A. Czechowicz (Treatech), T. Brunner (FHNW), D. Baudouin (PSI), N. Schmid (PSI), D. Erne (PSI).

3.2 Heat transfer measurements

An important question addressed in this P&D project was the scaling up of key components from lab to pilot scale. Underdesigned pieces of equipment would reduce the overall performance of the plant, while overdesigned components would create excessive costs. Thus, it is important for building a commercial plant to be able to accurately design all key components and to keep the safety margin within reasonable limits. The preheater/heat exchanger is such a key component. Thus determining the heat transfer coefficient (HTC) for sub- to supercritical flow was a key question for this P&D project. The HTC was used to validate heat transfer models that now enable the accurate design of a larger, commercial-scale unit. To be able to detect fouling of the heat transfer area, the HTC was first determined using pure water. The value of the HTC under these clean conditions served as a baseline value to be compared to other values determined later with the plant having seen pure organic or biomass feeds.

For the determination of the HTC, several temperatures at the inlet and outlet of the heat exchanger, as well as the mass flow rates and physical properties of all streams must be measured or looked up from the literature. The location of the different temperature measurements is shown in Fig. 3.2. An overview of the operating conditions can be found in Table 4.1.

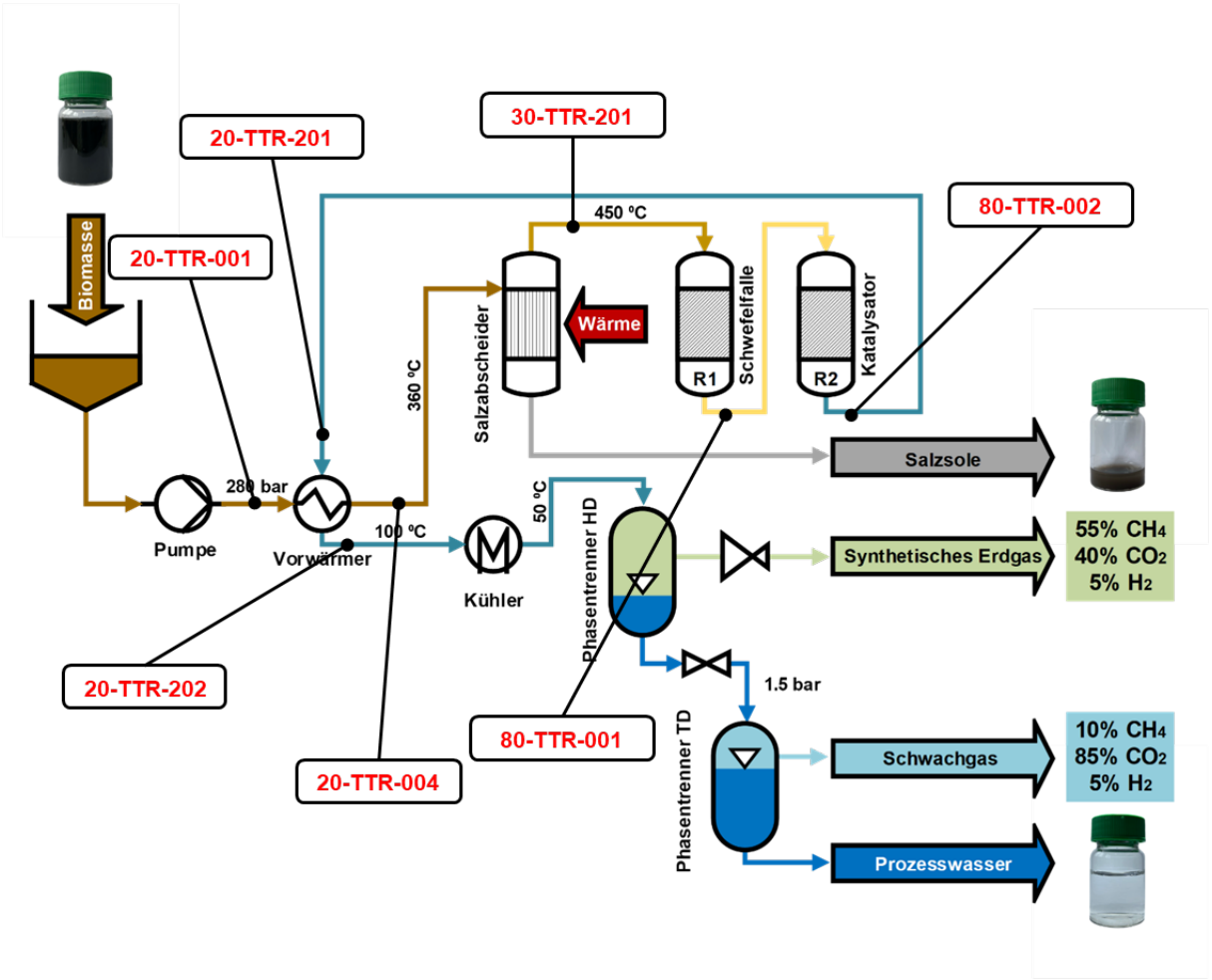


Figure 3.2: Simplified P&ID of HydroPilot with indication of the main temperature sensor positions and typical values for the temperatures and the pressure. TTR: temperature transmitter. The gas compositions for the SNG and the weak gas are indicative only.

3.3 Gasification experiments

After the heat transfer measurements with clean water, first gasification tests with a glycerol solution were performed. Glycerol is a widely used model substance for biomass, and reference data was available from earlier experiments in the lab-scale plant. The operating conditions are summarized in Table 3.1. The plant was heated up by adjusting the temperature setpoint of the hot air stepwise up to its allowed maximum value, as indicated in Table 3.1.

Since the glycerol solution did not contain any salts, the brine outlet of the salt separator was not activated. After some adjustments on the plant, several campaigns with sewage sludge followed. The sludge used was digested sludge from the waste water treatment plant in Wildegg (AG). Compositional data is given in Table 3.2. It was sourced once and stored for several months at 5°C in a ship container.

After the sludge campaigns, a campaign with a waste cleaning solution from industry was processed. Its main component was isopropanol.

The last campaigns were performed with food waste from gastronomy that contained also some plastics and was therefore not suited for anaerobic digestion.

Table 3.1. Experimental campaigns performed. IPA: Isopropanol, DM: dry matter, OM: organic matter. * during steady-state period. **high dilution with flushing water

Date/duration	Campaign	Feed	Feed concentration (wt% DM or OM)	Feed flow rate (kg/h)*	Brine flow rate (kg/h)*	Pressure (bar)*	Max. hot air T (°C)
13.-31.8.2021	Heat transfer	Water	0	50-100	0	240-280	600
21.-22.9.2021	Glycerol test 1	Glycerol/ water	5	ca. 66 (not steady)	0	280-320 (not steady)	600
11.-14.10.2021	Glycerol test 2	Glycerol/ water	4.8	88	0	275	600
14.-15.10.2021	Sewage sludge test 1	Sewage sludge, digested	3	85-91	14.6-21	255	600
20.-24.6.2022	Sewage sludge test 2	Sewage sludge, digested	5	97	12-19	270	700
8.-12.8.2022	Sewage sludge test 3	Sewage sludge, digested	5	98	20-(60**)	270	700
26.-30.9.2022	Industrial waste water	IPA/water	10	80	0	270	700
28.11.-1.12.2022, 12.-16.12.2022	Food waste	Food waste from gastronomy, plastics from packaging	6	60	12-13	275	700

The chosen feedstocks represent a wide range of compositions (Table 3.2). Glycerol and the IPA-waste being representative for liquid industrial wastes free of solids and minerals, and low in sulfur and chloride. At the other end of the range, digested sewage sludge contains almost half of the dry matter in mineral form, and its organic matter contains significant amounts of sulfur and nitrogen. Food waste can be considered an intermediate feedstock with less minerals, nitrogen and sulfur than sewage sludge but with a high chloride content.

Table 3.2. Characteristics of the different feedstocks used. wb: wet basis; db: dry basis. DM: dry matter; OM: organic matter.

Feedstock	DM or OM (wt% wb)	Ash (wt% db)	C (wt% db)	H (wt% db)	N (wt% db)	S (wt% db)	Chloride (mg/L wb)
Glycerol	4.8, 5	0	39	8.7	0	0	0
Sewage sludge	5.2	45	33	1*	9	2	309
IPA	10	< 0.5	60	13.3	0	< 0.01	< 10
Food waste	6.1	10.3	55.9±0.6	3.0±0.4	3.3±0.1	0.74±0.01	1'037

* Measurement probably erroneous

3.4 Phosphorus recovery

The goal of WP5 is to develop a process to recover and valorize the phosphorus contained in the solids extracted from cHTG (Figure 3.3) as well as perform an estimation of the costs of such a process. Due to delays on the HydroPilot campaign, most of the P-recovery and valorization experiments were performed using solids extracted from treating digested sewage sludge with TreaTech's lab-scale prototype (1 kg/h). Specifically, the scope of the work performed within this work package included:

- Phosphorus recovery and valorization using solids from the lab-scale prototype
    - Leaching experiments using a Design of Experiments (DoE) approach
    - Leaching optimization
    - Purification of the leachate
    - Experiments and analysis of the precipitation of phosphorus in the form of calcium phosphates and struvite
    - Compliance with MinRec
    - Preliminary analysis of the presence of organic molecules in the solid residues and leachate
    - Leaching, purification and precipitation experiments using calcined solid residues (ashes)
- Phosphorus recovery using solids from HydroPilot
    - Analysis and phosphorus recovery (leaching) using solids from HydroPilot
- Total organic carbon removal experiments
- Estimation of the P-recovery process costs (CAPEX and OPEX)

Details of the methodology followed for all P-recovery experiments (including experimental protocol and detailed results) as well as the methodology used to calculate CAPEX and OPEX can be found in Annex A.

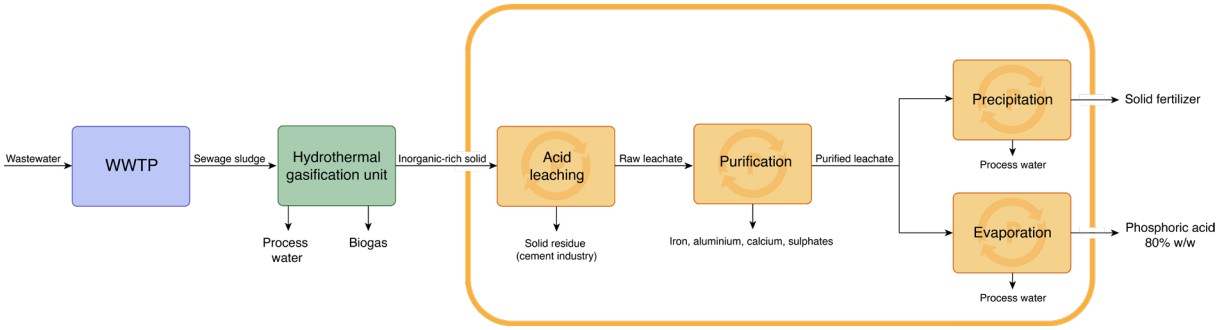


Figure 3.3: Block diagram of the P-recovery process.

4 Results and discussion

4.1 Erection of the pilot plant (WP 1 and 2)

The **main apparatus, piping, vessels, racks**, etc. were delivered to PSI and installed by KASAG. The modules with the main equipment had already been pressure tested by KASAG and accepted by the SSC. An **X-ray inspection** of individual weld seams of the cased modules was successfully performed at PSI. Only isolated problems occurred during production at KASAG, all of which could be solved. The biggest annoyance was the delivery of some defective high-pressure pipes to KASAG for further processing, which had production defects despite a valid material certificate and had to be re-ordered, producing an unexpected delay.

The **salt separator** existing from a previous P&D project [14] and tested at KIT (D) in 2015 was opened and inspected by means of an endoscope by KASAG. The general condition of the apparatus was good, but the heater tubes were internally covered with deposits (but not clogged) stemming from the former campaign. These deposits were first dissolved with descaler and residues removed with brushes. Occasional minor corrosion damage was noted, but not considered critical (thick-walled tubes). The sampling line for the salt brine was adapted to allow the level probe to be inserted axially from below into the salt separator.

The **electrical and pneumatic lines** were installed by the technical department at PSI. All media connections (compressed air, cooling water, nitrogen, electricity, waste water, exhaust air, data) were made in PSI's test hall and connected to the plant.

The exhaust hood and the remaining components of the **ventilation system** including gas sensors were installed and connected to the exhaust stack.

Part of the system was already insulated at KASAG. Insulation of the remaining piping, salt separator and high pressure vessels was completed in March 2021 by an external company.

The concept for the **online process analytics** was implemented. All measuring instruments (gas analysis by means of online sensors and microGC, online TOC, pH, conductivity, various sampling points) were installed.

Figure 4.1 shows the plant from the front on 15.9.2020. The front folding door and some insulation were installed later. Additional photos of the plant can be found in Annex B.



Figure 4.1: Fully installed and piped HydroPilot plant in PSI's test hall under a dedicated fume hood. On the right, one can see the frame with the uninsulated salt separator.

The front of the plant is made inaccessible during operation by a transparent folding door. The back of the plant was also made inaccessible during operation by transparent Plexiglas elements.

The final inspection by the Swiss Safety Center took place on September 8, 2021, and the certificate of conformity was officially issued on Nov. 30, 2021.

Challenges during erection of the plant

The erection of the plant was mostly done by KASAG for the main pieces of equipment, by external suppliers, e.g. for the heating system, and by PSI's technical services. No major technical challenges arose during erection. However, erection was affected by several delays. These were mostly unexpected delays in the delivery of equipment and services, and slowing down of construction work due to COVID-19 restrictions at PSI. Another delay was suffered for the delivery of the catalyst due to difficulties in scaling-up the production method for the catalyst by the manufacturer. Another factor that affected the time schedule negatively was the premature leaving of key team members. This was partly due to reaching the end of employment contracts because of the delays. Another task that used much more time than planned was the public submission for the purchasing of the reactors.

During commissioning, several minor technical issues were identified and solved.

4.2 Heat transfer and test campaigns (WP 3)

4.2.1 Heat transfer experiments

The heat transfer in HydroPilot mainly takes place in two units. The first step occurs in the preheater where the fluid temperature rises from ambient to roughly 370°C. The second step occurs in the salt separator where the fluid is heated to around 430°C. For both the preheater and the salt separator numerical steady-state 1D-models have been created in Python to simulate the heat transfer behavior [16]. For the dynamic behavior of the system, a transient 0D-model has been created in Simulink [17].

Heat transfer in the preheater

To calculate the heat transfer in the preheater, multiple steady states have been evaluated (Table 4.1). It has to be pointed out that a steady state has never been reached for all measured values during water operation. The reason was that the plant took a long time to equilibrate. Nevertheless, data could be extracted during reasonably stable conditions as seen in Figures 4.2a-c. Those figures show the temperatures measured in the preheater (see Section 2.2 for the positions of the temperature sensors and the color code) as well as the flow rate measured by the Coriolis flow meter. The steady states used for evaluation are indicated by vertical black bars.

Table 4.1: List of steady-states considered for the evaluation of the preheater results. The HTC has been calculated based on the tube inner diameter. * This value was not determined by the Coriolis mass flow meter but by the weight difference from the scale beneath the process water tank. The Experiment ID corresponds to the individual tests listed in Table 3.1.

No.	Experiment ID	Time [h]	Mass flow rate [kg/h]
1	2022_06_13_Heat_Transfer_2_Reactors	12	107.3
2	2022_06_13_Heat_Transfer_2_Reactors	28	* 103.2
3	2022_08_08_Sludge_Test_03	29	100.1
4	2022_09_26_Industrial_Feedstok_01	27	77.3
5	2022_09_26_Industrial_Feedstok_01	60	78.7
6	2022_11_18_Industrial_Feedstock_02	35	78.9
7	2022_11_18_Industrial_Feedstock_02	46	78.5
8	2022_12_12_Industrial_Feedstock_03	50	83.5

The transported heat Q_{IN} was calculated based on the heat up of the cold fluid in the core.

$$Q_{IN} = \dot{m} * (h_{20-TTR-004} - h_{20-TTR-001}) \quad (1)$$

The outer area of the core tube $A_{HE,I}$ was used as a base to calculate the heat flux q_{IN}.

$$q_{IN} = \frac{Q_{IN}}{A_{HE,I}} \quad (2)$$

$$A_{HE,I} = N_{US} * (2 * L_{TS} + L_{TB}) * D_{C,O} * \pi \quad (3)$$

The log mean temperature difference (LMTD) was used as the driving temperature difference to calculate the heat transfer coefficient (HTC). This assumption is a rough approximation, as the LMTD is not really applicable in this scenario due to the change in heat capacity along the heat exchanger.

This fact leads to limited comparability of the results to other heat exchangers. However, the HTC can still be used to compare the behavior of the preheater at different times.

$$LMTD = \frac{\Delta T_1 - \Delta T_2}{\ln(\Delta T_1 / \Delta T_2)} \quad (4)$$

$$\Delta T_1 = T_{20-TTR-201} - T_{20-TTR-004}$$

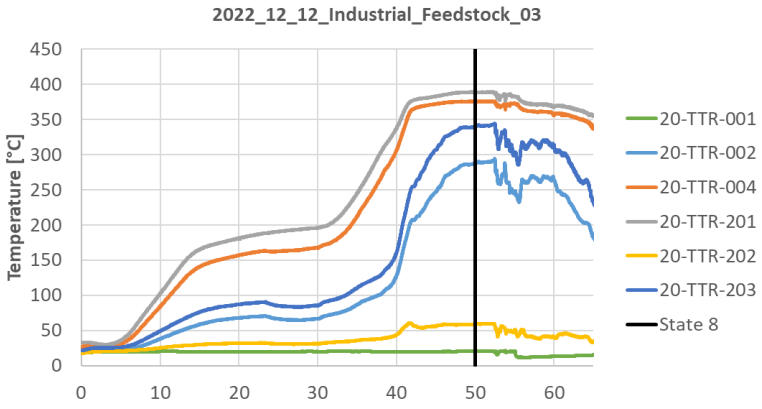
$$\Delta T_2 = T_{20-TTR-202} - T_{20-TTR-001}$$

$$HTC = \frac{q_{IN}}{LMTD} \quad (5)$$

The relevant data to calculate the heat flux and HTC for the preheater are listed in Table 4.2. While steady state 1 was determined with subcritical, i.e., liquid water, states 2-8 were in supercritical state. The HTC in the supercritical cases is roughly 500 W/(m^2 K). One exception is state 3 which shows an HTC of above 700 W/(m^2 K). This is the state with the highest brine extraction rate of roughly 10%. Compared to state 2 this leads to a higher residence time in the annulus. Therefore, the hot fluid cools down more and leads to a lower LMTD. Therefore, even though the heat flux of state 3 is smaller than in state 2, the HTC is higher.

Table 4.2: Inlet temperatures and corresponding enthalpies at the inlet and outlet of the feed side of the preheater. Enthalpy data have been extracted for pure water from the NIST database [15] at a pressure of 250 bar. TTR: temperature transmitter (see Fig. 3.2).

Nr	20-TTR-001 [°C]	20-TTR-004 [°C]	20-TTR-201 [°C]	20-TTR-202 [°C]	$h_{20\text{-}TTR\text{-}001}$ [kJ/kg]	$h_{20\text{-}TTR\text{-}004}$ [kJ/kg]	Q_{IN} [kW]	q_{IN} [kW/m^2]	HTC [W/(m^2 K)]
1	24.2	183.6	212.9	38.1	124.5	791.3	19.9	6.8	329
2	24.8	375.0	392.9	82.6	126.9	1849.4	49.4	16.9	496
3	27.4	367.6	385.8	51.5	137.6	1765.5	45.2	15.5	737
4	23.8	375.0	387.2	67.8	122.8	1849.4	37.1	12.7	512
5	24.9	373.5	388.4	78.0	127.3	1829.9	37.2	12.7	423
6	21.1	374.4	386.4	61.7	111.7	1841.3	37.9	13.0	551
7	21.1	373.1	386.4	56.0	111.7	1824.9	37.4	12.8	571
8	20.3	375.7	388.9	58.9	108.4	1859.1	40.6	13.9	588



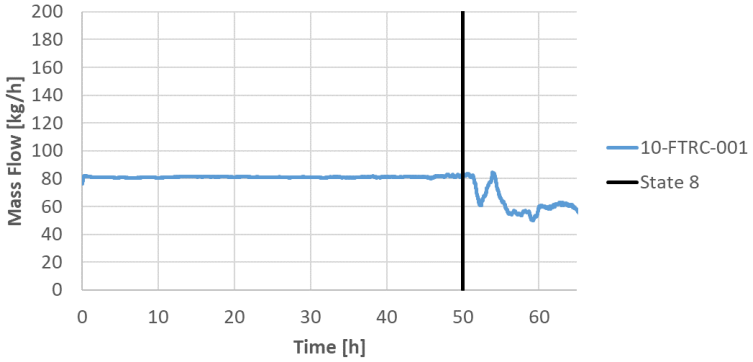


Figure 1: Values from temperature sensors in the preheater (top) and the Coriolis mass flow meter (bottom) extracted from the campaign with food waste. The chosen steady state is indicated by a vertical black line.

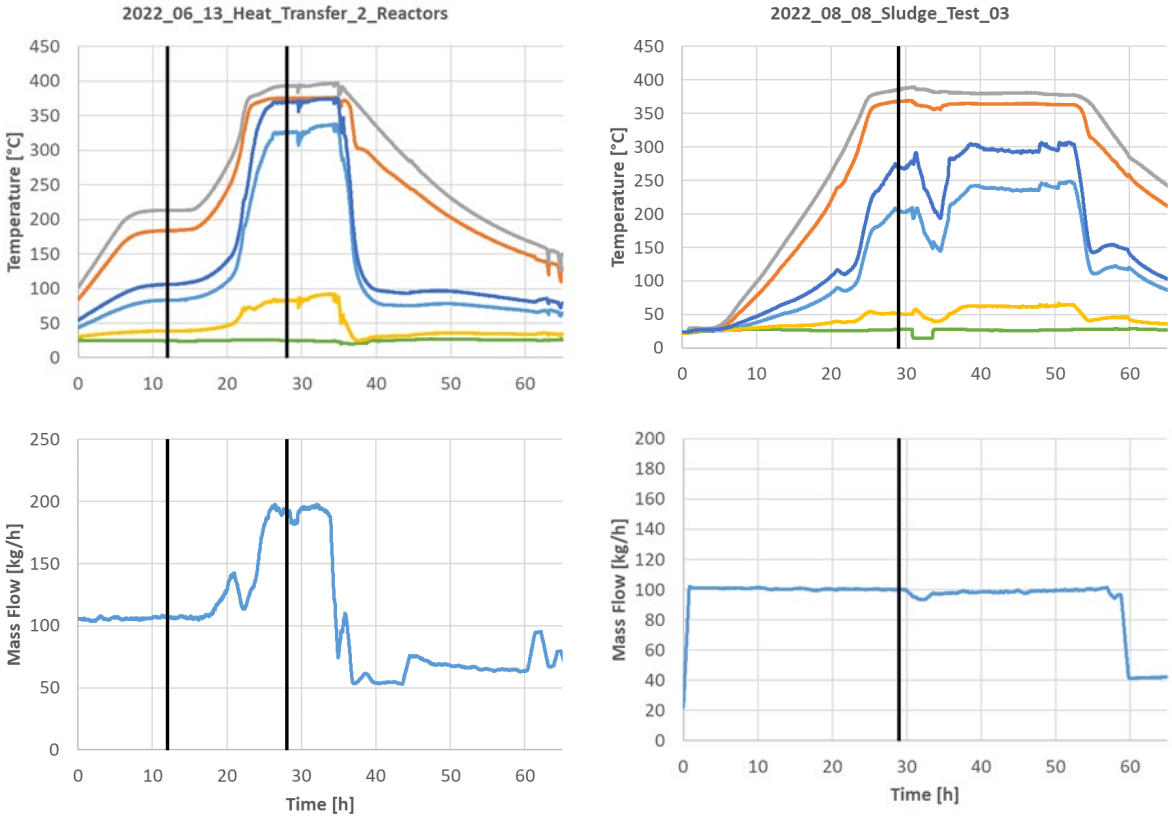


Figure 4.2b: Values from temperature sensors in the preheater (top) and the Coriolis mass flow meter (bottom) extracted from a selection of campaigns. The chosen steady states are indicated by vertical black lines.

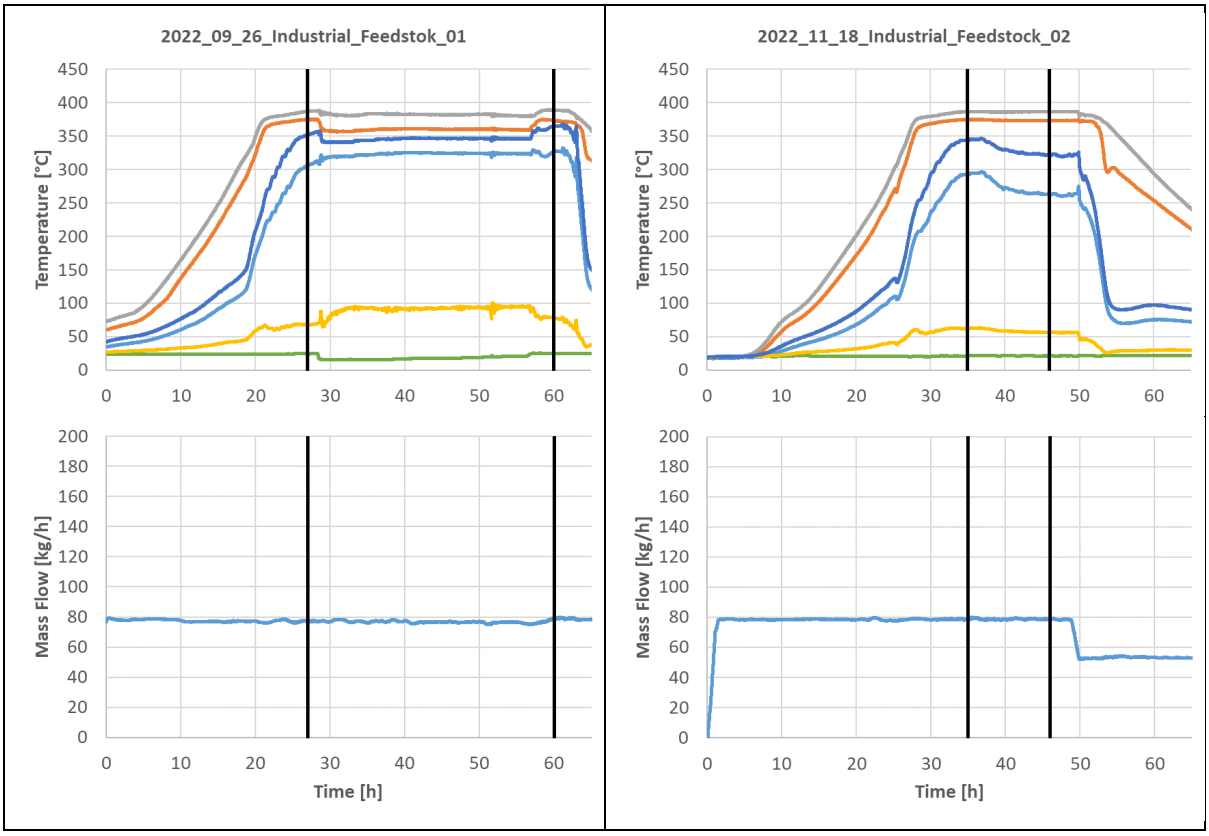


Figure 4.2c: Values from temperature sensors in the preheater (top) and the Coriolis mass flow meter (bottom) extracted from a selection of campaigns. The chosen steady states are indicated by vertical black lines.

Numerical model of the preheater/heat exchanger

A steady state 1D-model has been developed to simulate the heat transfer behavior in the preheater [16]. To calculate the heat transfer, the preheater is divided into segments lengthwise and the energy balance on each segment is solved. Because the model deals with a counter-flow heat exchanger, it assumes initial temperatures and then solves the system iteratively.

To calculate the Nusselt numbers, several correlations from literature have been compared to data collected during the experiments. For the simulations, the inputs from the steady states in Table 4.1 have been used and the domain has been divided into 100 segments. The relative error between the measurement and the simulation has been calculated for each state and found to be below 15% for most cases (Figure 4.3). A positive error means that the model overestimates the heat transfer. Correlation 6 shows the best fit to the experimental data for all states evaluated. However, the conditions of all states were very similar. Therefore, it could be that correlation 6 describes this narrow band of conditions very well, but it may fail if the range of conditions is increased. Correlation 6 describes the correlation developed by Griem [28]. This correlation is shown in equation 6 with ϕ denoting a correction factor for small bulk enthalpies.

$$Nu = 0.0169 * Re^{0.8356} Pr^{0.432} * \phi \tag{6}$$

$$\varepsilon = \frac{\left(Q_{IN,Model} - Q_{IN,Measured}\right)}{Q_{IN,Measured}} \tag{7}$$

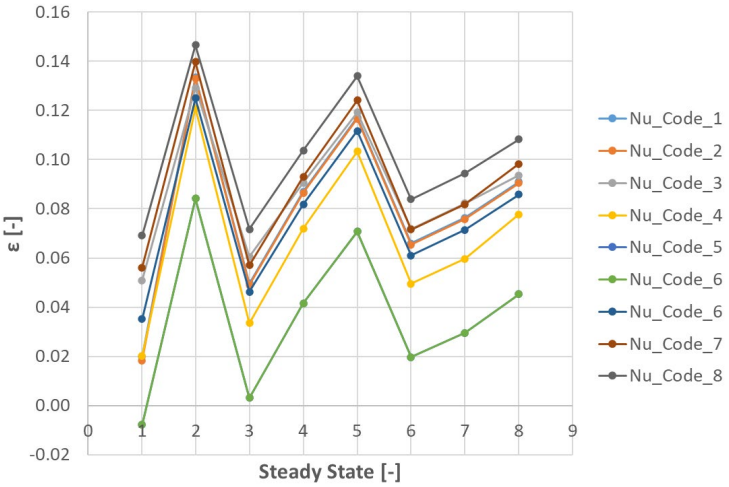


Figure 4.3: Relative error ε between the estimated and the measured exchanged heat for different Nusselt correlations.

Heat transfer in the salt separator

To estimate the heat transfer in the salt separator four steady states have been evaluated (Table 4.3). Although the conditions were not perfectly stable (Figure 4.5a and 4.5b), they were deemed good enough for the evaluation of the heat transfer.

The flow in the salt separator is divided into two sections. The falling section, where the fluid flows downwards through 20 tubes, and the rising section in which the fluid flows upwards through a single tube. Since those two cases are very different, it does not make sense to assign a single heat transfer coefficient to the whole salt separator. Therefore, the falling and rising sections are evaluated individually. A sketch is shown in Fig. 2.4.

Rising Section

A comparison of the temperature in the salt pot (30-TTRC-004) and the temperature at the exit of the salt separator (30-TTR-201) shows that in most cases 30-TTR-201 is colder even though the rising tube passes through the hot air channel again. There are two contributing factors to this behavior.

At the top of the salt separator, the riser tube and the incoming colder fluid are in direct contact. Therefore, some of the heat in the riser tube is transferred to the colder fluid, leading to a lower temperature at 30-TTR-201.

The rather complicated geometry of the salt separator inlet and outlet does not allow for an easy and efficient thermal insulation. As 30-TTR-201 is not measured directly in the salt separator, but in the connection to reactor 1, there might be undetected heat losses in-between. Therefore, the real exit temperature of the salt separator might be higher than the temperature detected by 30-TTR-201.

Falling Section

The transported heat Q_{IN} was calculated based on the enthalpy of the fluid in the salt separator pot ($h_{30\text{-}TTRC\text{-}004}$) and at the exit of the preheater ($h_{20\text{-}TTR\text{-}004}$).

$$Q_{IN} = \dot{m} * (h_{30-TTRC-004} - h_{20-TTR-004}) \quad (8)$$

The outer area of the falling tubes $A_{HE,F}$ was used as a basis to calculate the heat flux q_{IN}.

$$q_{IN,ss} = \frac{Q_{IN}}{A_{HE,F}} \quad (9)$$

$$A_{HE,F} = N_{TF} * L_{TF} * D_{F,O} * \pi \quad (10)$$

The log mean temperature difference (LMTD) was used as the driving temperature difference to calculate the heat transfer coefficient (HTC). This assumption is a rough approximation as the LMTD is not really applicable in this scenario due to the pseudo phase change. This fact leads to limited comparability of the results to other heat exchangers. However, the HTC can still be used to compare the behavior of the salt separator at different times.

$$LMTD = \frac{\Delta T_1 - \Delta T_2}{\ln(\Delta T_1 / \Delta T_2)} \quad (11)$$

$$\Delta T_1 = T_{30-TTRC-003} - T_{30-TTRC-004}$$

$$\Delta T_2 = T_{30-TTR-002} - T_{20-TTR-004}$$

$$HTC, ss = \frac{q_{IN,ss}}{LMTD} \quad (12)$$

Table 4.4 shows the data from two experiments with two states being evaluated each time. The first state is just after heating up with water. The second state has been collected while flushing with water, after the biomass or model solution have been fed to the system. By comparing state 1 and 2 it can be seen that the transported heat (Q_{IN}) and the HTC are almost equal. Therefore, it is assumed that no considerable amount of fouling has occurred during this experiment. The raw material in this experiment was Isopropanol (IPA) that contained almost no inorganic matter. By comparing the states 3 and 4 in Table 4.4 it can be seen that both the transported heat and the HTC have dropped significantly. In fact, they have dropped to a level that prevented continuation of the experiment, as supercritical conditions could not be maintained. In this experiment food waste was used as a raw material which contained inorganic matter. It is assumed that those inorganic materials caused deposits in the salt separator, which led to a large thermal resistance. In addition, an endoscope analysis after the experiment with food waste showed large deposits on the tube walls (Fig. 4.4). As the data did not suggest fouling after the IPA campaign (section 4.4.4), the salt separator tubes were not inspected. Therefore, it is not certain that no deposits were formed.



Figure 4.4: Left: Endoscope picture from one falling tube after the experiment with food waste. Right: Endoscope picture after the last cleaning of the same tube.

Table 4.3: List of steady states considered for the evaluation of the salt separator results.

No.	Experiment ID	Time [h]	Mass flow rate [kg/h]
1	2022_09_26_Industrial_Feedstok_01	27	77.3
2	2022_09_26_Industrial_Feedstok_01	60	78.7
3	2022_12_12_Industrial_Feedstock_03	50	83.5
4	2022_12_12_Industrial_Feedstock_03	72	44.6

Table 4.4: Temperatures and corresponding enthalpies at the inlet and the salt pot of the salt separator. Enthalpy data have been extracted for pure water from the NIST database [15] at a pressure of 250 bar. The transported heat is based on the fluid temperature between the inlet and the salt pot.

No.	30-TTRC-003 [°C]	30-TTR-002 [°C]	20-TTR-004 [°C]	30-TTRC-004 [°C]	$h_{30\text{-}TTRC\text{-}004}$ [kJ/kg]	$h_{20\text{-}TTR\text{-}004}$ [kJ/kg]	Q_{IN} [kW]	$q_{IN,ss}$ [kW/m^2]	HTC,ss [W/(m^2 K)]
1	611.3	541.3	375.0	430.0	2837.8	1849.4	21.2	13.1	75.3
2	621.8	551.3	373.5	433.0	2856.9	1829.9	22.4	13.8	75.5
3	614.0	544.0	375.7	427.7	2823.1	1859.1	22.4	13.8	77.9
4	682.8	630.5	326.8	380.4	1944.1	1477.7	5.8	3.6	11.8

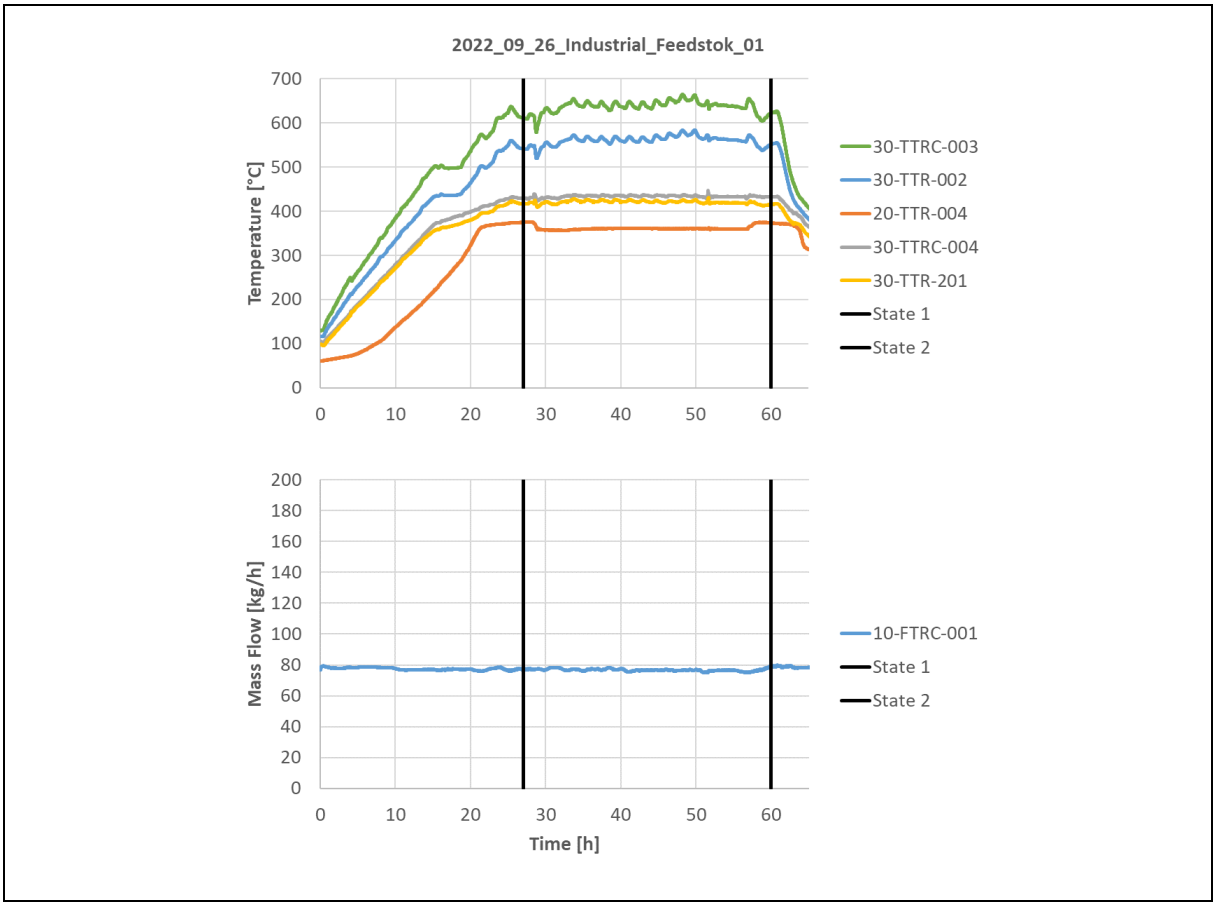


Figure 2.5a: Values from temperature sensors in the salt separator (top) and the Coriolis mass flow meter (bottom) extracted from the IPA campaign. Each steady state is indicated by one vertical black bar. The labels refer to the names of the different temperature sensors in function modules 20 (heat exchanger), 30 (salt separator).

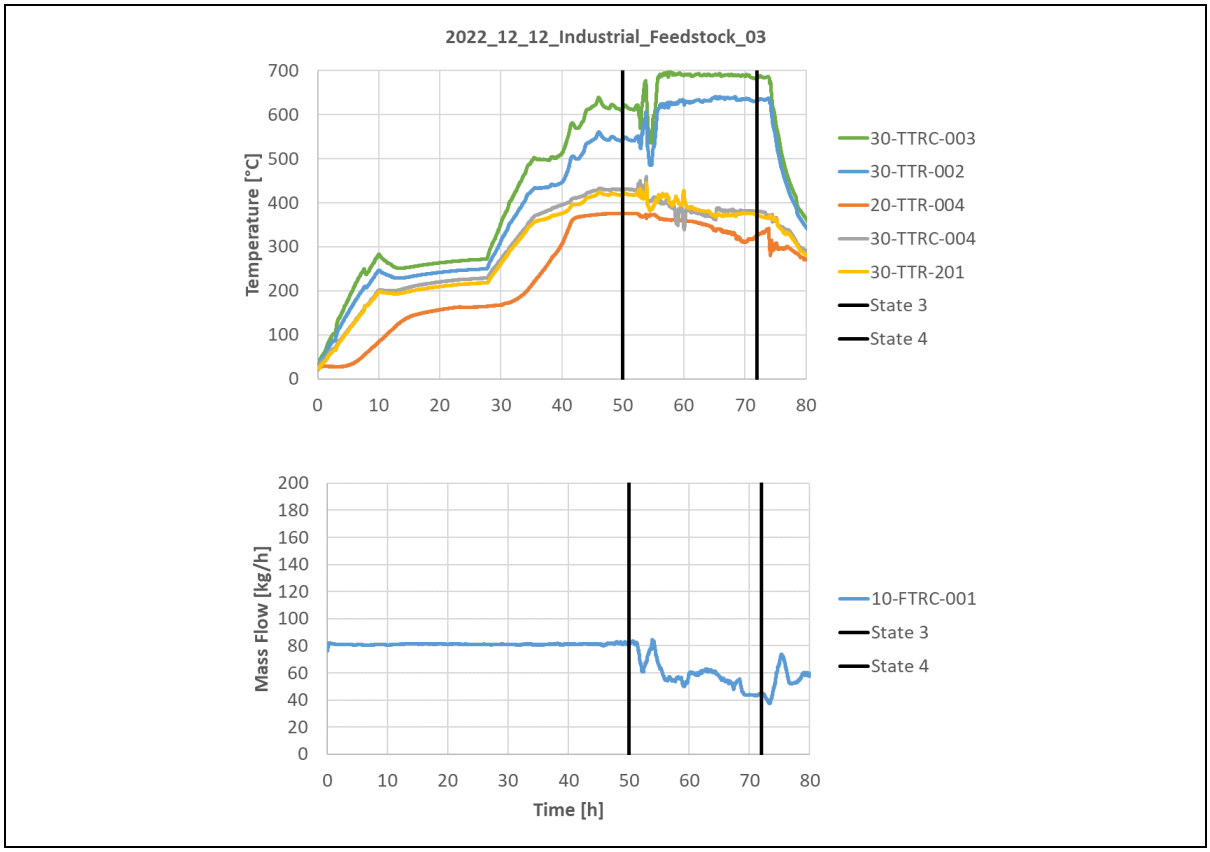


Figure 4.5b: Values from temperature sensors in the salt separator (top) and the Coriolis mass flow meter (bottom) extracted from the FW campaign. Each steady state is indicated by one vertical black bar. The labels refer to the names of the different temperature sensors in function modules 20 (heat exchanger), 30 (salt separator).

Dynamic model of complete plant

Apart from the two steady state models for the main heat transfer units, a zero-dimensional dynamic model has been created in Simulink to estimate the transient behavior of the entire plant [17]. The model simulates the thermal behavior of the plant using the thermodynamic data of pure water, also taking losses to the environment into account. Figure 4.6 shows the results from one heat up test conducted on HydroPilot. Figure 4.7 shows the simulation results obtained by the dynamic model. It can be seen that the model delivers a rather accurate estimate of the time that the system needs to equilibrate, as well as the steady state temperatures. It is therefore a useful tool for the planning of experiments.

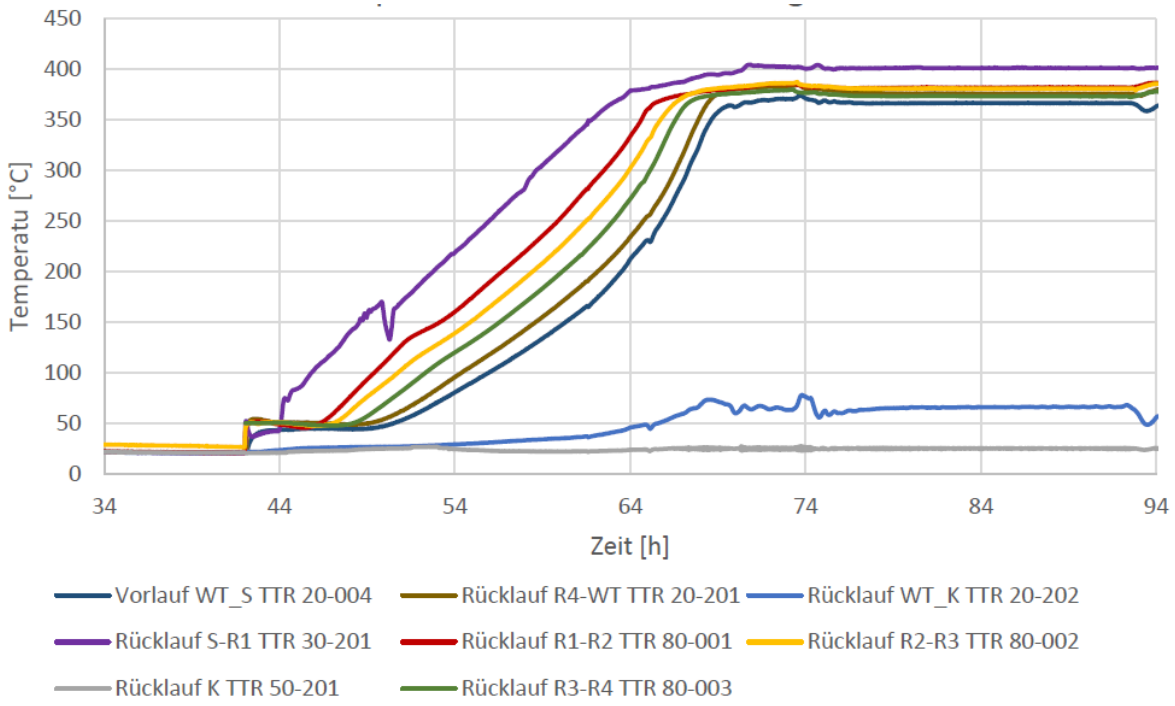


Figure 4.6: Measured temperature profiles during a HydroPilot campaign [17]. X-axis: time on stream.

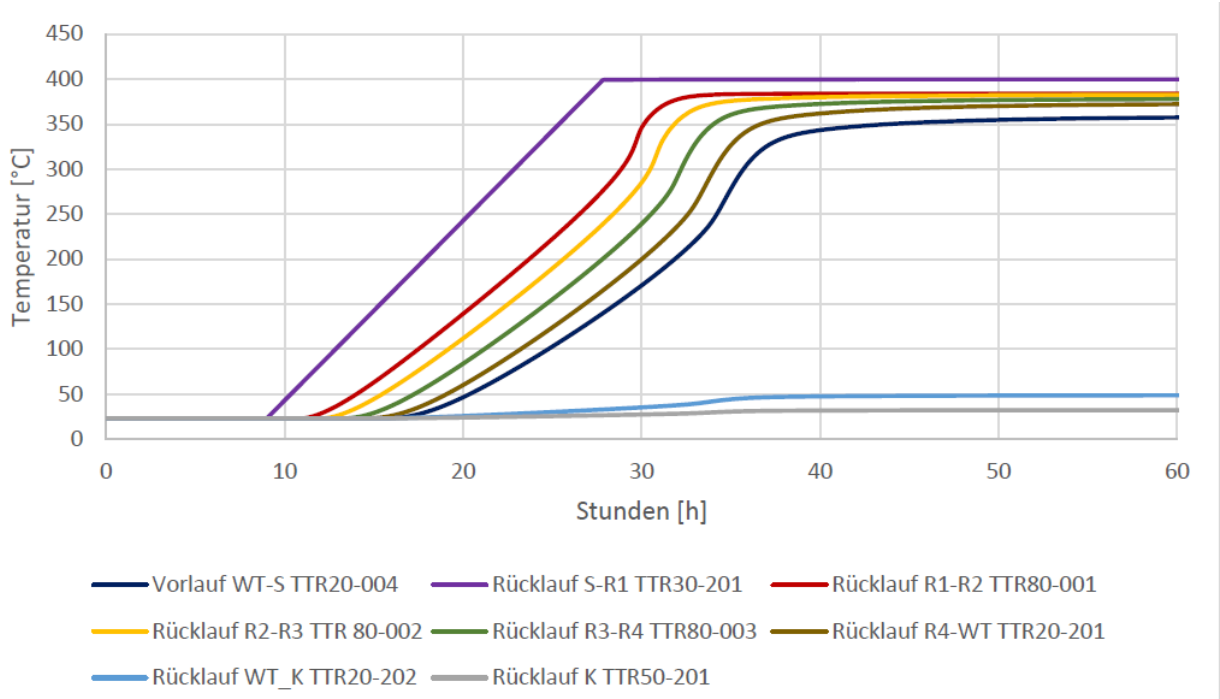


Figure 4.7: Simulated temperature profiles, predicted by the dynamic model [17]. X-axis: time.

Estimation of heat losses

The heat losses in HydroPilot were not directly measured but they were estimated by comparison of the fluid temperatures inside the system. Two approaches were used for this estimation. In the first

approach, the values of two consecutive temperature sensors are compared to estimate the heat loss in individual segments. In the second approach, the major energy streams entering (Q_{IN}) and leaving (Q_{OUT}) the system are compared. Both approaches were calculated based on the campaign with industrial feedstock 01 (section 4.4.4) at the time on stream 60 h (Table 4.5 and Figure 4.8). An overview of the sensor locations is given in Figure 3.2.

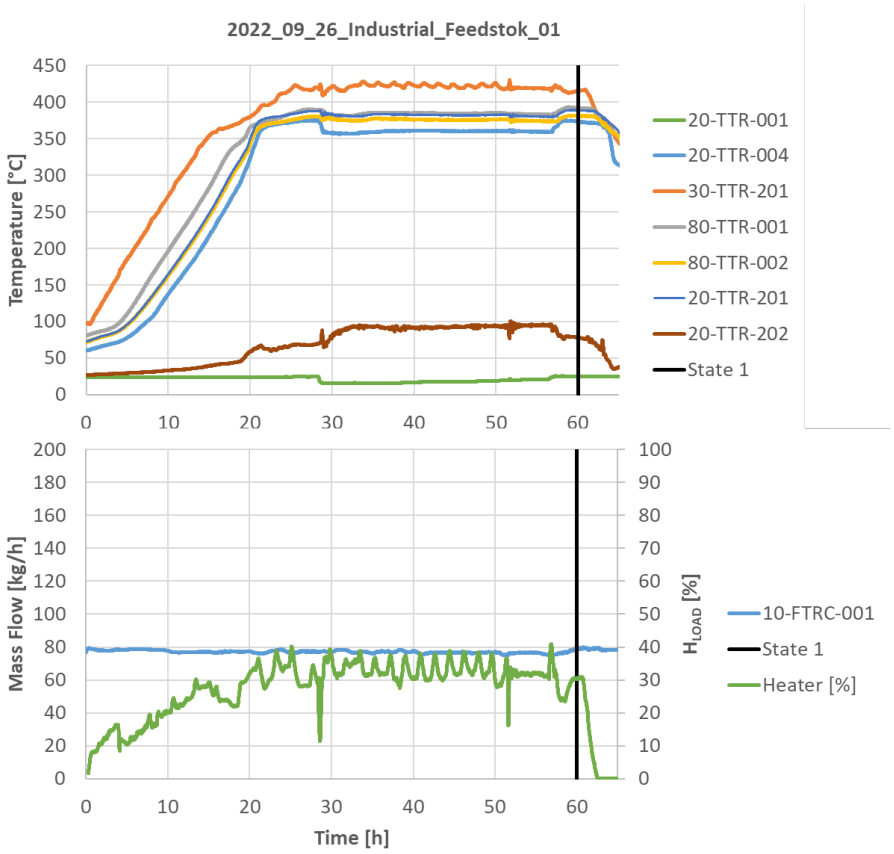


Figure 4.8: Values from temperature sensors, the Coriolis mass flow meter and the heater from the experiment “2022_09_26_Industrial_Feedstock_01” (section 4.4.4). The labels refer to the names of the different temperature sensors in function modules 20 (heat exchanger), 30 (salt separator), and 80 (sulfur trap and catalytic reactors).

Table 4.5: Temperatures and enthalpies for specific locations in the system (cp. Fig. 3.2). Enthalpy data have been extracted for pure water from the NIST database [15] at a pressure of 250 bar.

Property	20-TTR-001	20-TTR-004	30-TTR-201	80-TTR-001	80-TTR-002	20-TTR-201	20-TTR-202
Temperature [°C]	24.9	373.5	416.1	391.4	381.2	388.4	78.0
Enthalpy [kJ/kg]	127.3	1829.9	2739.4	2431.8	1967.2	2344.9	346.6

Heat loss based on individual segments

The following segments have been used to estimate the heat loss in the system (Table 4.6). The heat losses (Q_{Loss}) have been calculated based the enthalpy difference at the inlet and the outlet.

$$Q_{Loss} = \dot{m} * (h_{Start} - h_{End}) \quad (13)$$

For segment 3 the heat loss cannot be calculated this way as 20-TTR-201 (hot side entrance to the heat exchanger) shows a higher temperature than 80-TTR-002 (at the exit of the catalytic reactor) which would result in a negative heat loss (compare Table 4.6). Skipping 80-TTR-002 and directly comparing 80-TTR-001 and 20-TTR-201 leads to a loss of 1.9 kW in this combined section. At the moment it is not clear if 80-TTR-002 is indeed lower than 20-TTR-201 or if it is a measurement error. This will be further investigated.

For the preheater the heat losses can also be estimated. In steady state conditions, the heat from the hot fluid can only go to the cold fluid or is lost to the environment. If the salt extraction is running, there will be a different mass flow on the product and on the feed side. For this evaluation, only states where both flows are equal (salt extraction flow rate = 0) were considered.

$$Q_{Loss} = \dot{m} * [(h_{20-TTR-202} - h_{20-TTR-201}) - (h_{20-TTR-004} - h_{20-TTR-001})] \quad (14)$$

Table 4.6: Heat losses of the individual segments.

Segment	Start	End	Q_{loss} [kW]
1	30-TTR-201	80-TTR-001	6.7
2	80-TTR-001	80-TTR-002	10.2
3	80-TTR-002	20-TTR-201	-8.3
Preheater			6.5
Total			**15.1**

Table 4.6 shows that the total heat loss is approximately 15 kW. It also shows that 20-TTR-201 measures a higher temperature than 80-TTR-002 even though it is further downstream. Therefore, by comparing these two temperatures, the calculation results in a negative heat loss for segment 3. This could be an error in the temperature measurement and will be further investigated.

Heat loss based on the complete system

During water operation without brine extraction, the only energy streams leaving the system are the water on the product side and the heat losses. The main energy streams entering the system are the fluid on the feed side and the power consumed by the electrical heater (Q_{Heater}). For this calculation, the percentage (H_{LOAD}) of the maximum heater capacity (Q_{Heater_Max}) has been used to estimate the power used by the heater.

$$Q_{Heater} = H_{LOAD} * Q_{Heater\_Max} \quad (15)$$

$$Q_{OUT} = \dot{m} * h_{20-TTR-202} \quad (16)$$

$$Q_{IN} = \dot{m} * h_{20-TTR-001} + Q_{Heater} \quad (17)$$

$$Q_{Loss} = Q_{IN} - Q_{OUT} \quad (18)$$

The heat loss calculated for the total system was 25.6 kW and therefore significantly higher than the loss calculated based on the individual segments. The reason for this difference is that the salt separator and the hot air loop also contribute to the total losses but have not been covered in the calculation for the individual segments.

4.2.2 Glycerol test 1

As the very first reactive test, an aqueous solution of **5% glycerol** was processed at a nominal flow rate of 100 kg/h. The temperature of the hot air was increased stepwise up to the maximum temperature of 600°C by adjusting the power of the electric heater. After the plant reached near steady-state around ToS = 27.3 h, the feed was switched from water to the glycerol solution. At ToS = 36.2 h a fault of the gas oven stopped the feed flow and switched to the emergency water pump. This caused a short interruption of the flow in the system, which can be seen in the temperatures rising quickly in Fig. 4.9. The temperatures fluctuated and did not reach a steady-state during the period when the glycerol solution was fed. T reached 455°C in the salt separator when stopping the feed flow at ToS ca. 36 h (30-TTRC-004; brown line in Fig. 4.9).

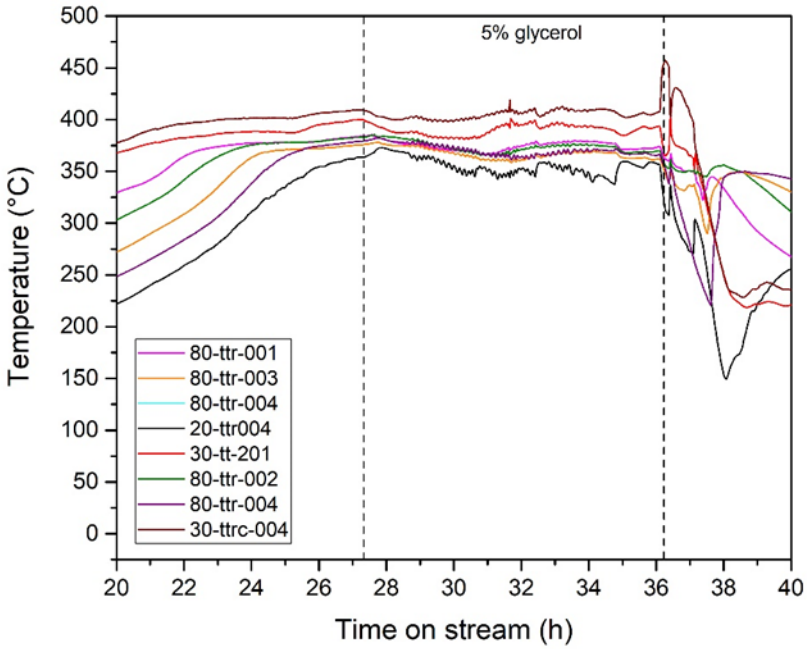


Figure 4.9: System temperatures after heating up (glycerol test 1). The dashed lines denote the beginning and the end of feeding a 5% glycerol solution. The labels refer to the names of the different temperature sensors in function modules 20 (heat exchanger), 30 (salt separator), and 80 (sulfur trap and catalytic reactors).

The trend in the temperatures was likely due to fluctuations of system pressure. While the pressures at the different locations in the plant reached a steady-state of 260-280 bar during heating up with water, switching to the glycerol solution led to pressure fluctuations between 280 and 320 bar (Fig. 4.10). This was likely caused by pressure regulation issues in the HP phase separator. According to the logbook, control valve 50-RV-401 froze at some point, which can explain this pressure increase. Pressure fluctuations lead to density and heat capacity fluctuations of the supercritical fluid mixture, which would lead to the observed temperature and flow rate fluctuations.

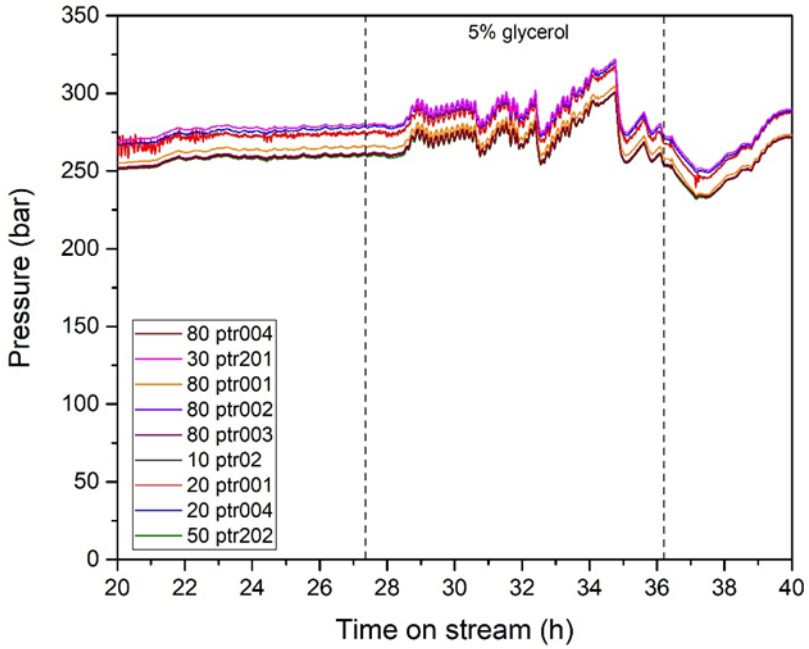


Figure 4.10: System pressures after heating up (glycerol test 1). The dashed lines denote the beginning and the end of feeding a 5% glycerol solution. The labels refer to the names of the different pressure sensors in function modules 10 (feeding), 20 (heat exchanger), 30 (salt separator), 50 (cooling and phase separation) and 80 (sulfur trap and catalytic reactors).

The SNG composition is shown in Fig. 4.11. The composition did not reach steady state within the time window. While H_2 remained nearly constant, methane still increased. This may be linked to the pressure increase in the system, and consequently also in the HP phase separator, which would dissolve more CO_2 and thus enrich the gas with methane. The methane concentration reached 43 vol.% on an N_2-free basis, which is higher than the expected equilibrium value for 285 bar and 380°C, i.e. 55 vol% [18]. The HP phase separator proved to be effective for washing out CO_2. The weak gas composition could not be measured because of a technical problem.

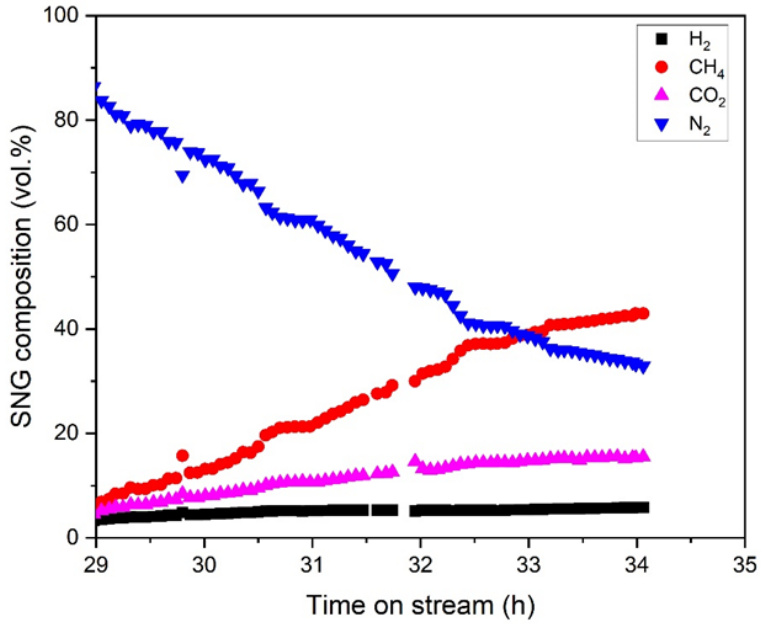


Figure 4.11: SNG composition from glycerol test 1, starting at time on stream of 29 h. The weak gas composition was not recorded due to a problem with the pressure in the gas sampling line. Note that the HP phase separator is pressurized with N_2 before heating up. This N_2 is then displaced over time by the SNG produced.

4.2.3 Glycerol test 2

The following improvements were made to the HydroPilot plant after Glycerol test 1:

The second experiment with a 5% glycerol solution went much smoother than glycerol test 1. There were no pressure and temperature fluctuations during the operation with glycerol. Both p and T reached a steady-state for almost 20 h (Figs. 4.12 and 4.13). The only noticeable change was an increase of all pressure readings by ca. 15 bar after switching to the glycerol feed (Fig. 4.13).

SNG composition is shown in Fig. 4.14. Note that the G-L phase separator is pressurized with N_2 during heating up. This N_2 is then displaced over time by the SNG produced. CH_4 concentration stabilizes after 18 hours to ca. 70 vol% with still a few percent of N_2 remaining. The high CH_4 concentration (70 vol%) and low CO_2 concentration (20 vol%) obtained underline the good performance of the HP phase separator (integrated water scrubbing of the CO_2).

Fig. 4.15 shows the weak gas composition. It contains ca. 70 vol% CO_2, 20 vol% CH_4, and 5 vol H_2. This composition correlates with the partial pressures of these gases in the HP phase separator and their respective solubilities in water.

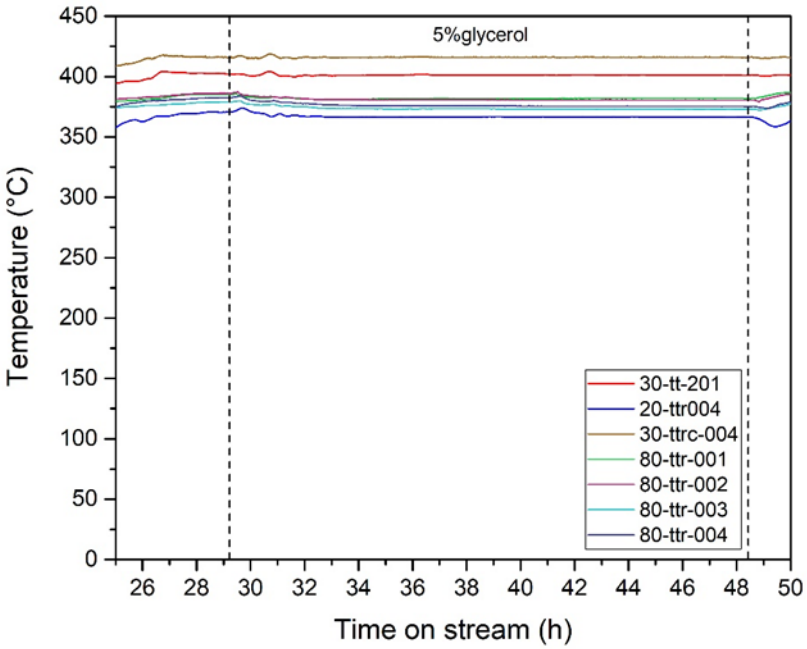


Figure 4.12: System temperatures after heating up (glycerol test 2). The dashed lines denote the beginning and the end of feeding a 5% glycerol solution. The labels refer to the names of the different temperature sensors in function modules 20 (heat exchanger), 30 (salt separator), and 80 (sulfur trap and catalytic reactors).

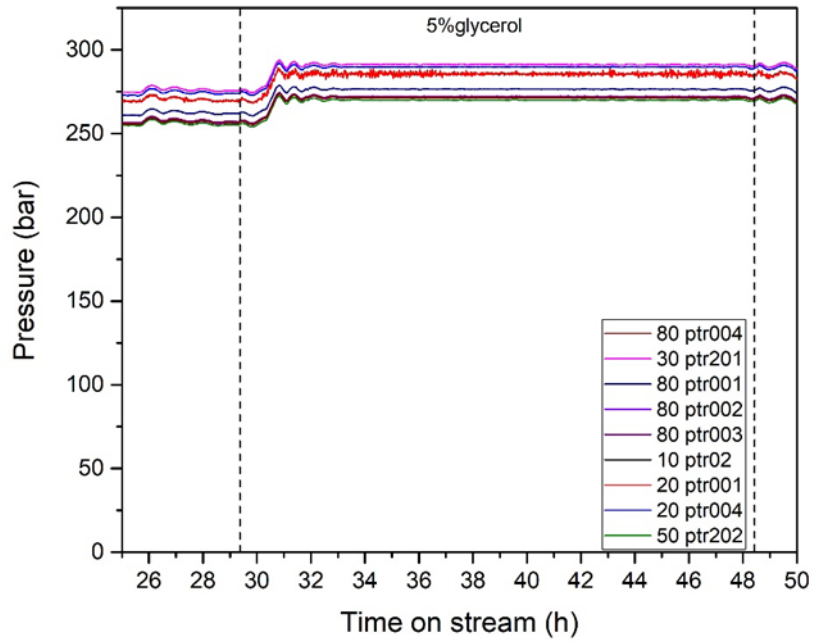


Figure 4.13: System pressures after heating up (glycerol test 2). The dashed lines denote the beginning and the end of feeding a 5% glycerol solution. The labels refer to the names of the different pressure sensors in function modules 10 (feeding), 20 (heat exchanger), 30 (salt separator), 50 (cooling and phase separation) and 80 (sulfur trap and catalytic reactors).

During the steady-state operation with glycerol (ToS 29-48 h), the efficiency of the heat exchanger was evaluated. The specific enthalpies *h* were taken as those of pure water at the respective temperature and 275 bar. “hot” and “cold” denote the hot stream and the cold stream, respectively.

$$\eta = \frac{h_{hot,in} - h_{hot,out}}{h_{hot,in} - h_{cold,in}} \cdot 100\% = 91\%$$

This value is the baseline value for the heat exchange efficiency in the clean heat exchanger when no brine flow is extracted.

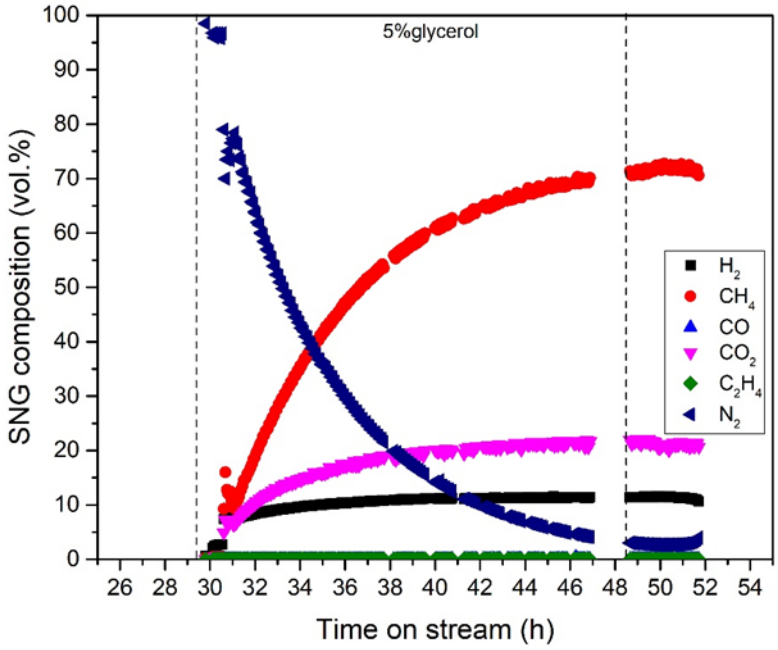


Figure 4.14: SNG composition from glycerol test 2, starting at time on stream of 29 h. Note that the HP phase separator is pressurized with N_2 before heating up. This N_2 is then displaced over time by the SNG produced. The dashed lines denote the beginning and the end of feeding a 5% glycerol solution.

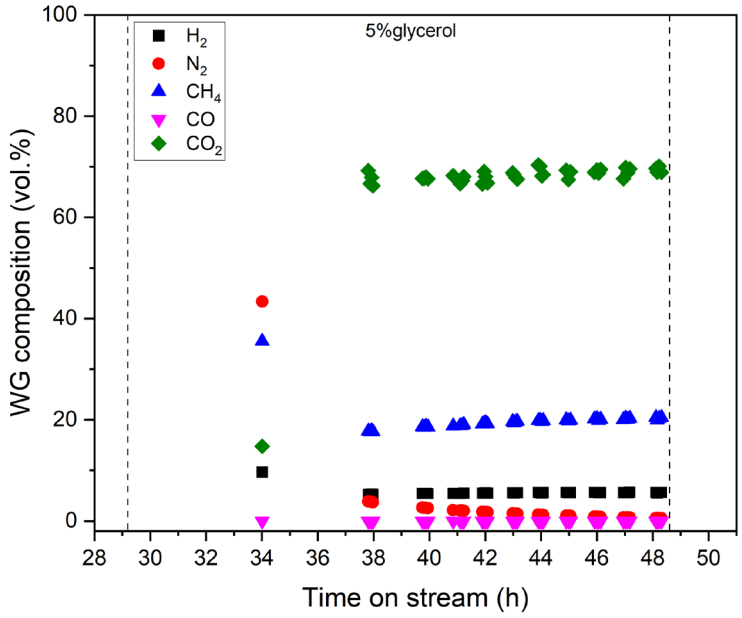


Figure 4.15: Weak gas composition from glycerol test 2, starting at time on stream of 29 h. The N_2 comes from the HP phase separator, which is pressurized with N_2 before heating up. This N_2 is then displaced over time by the SNG produced. The dashed lines denote the beginning and the end of feeding a 5% glycerol solution.

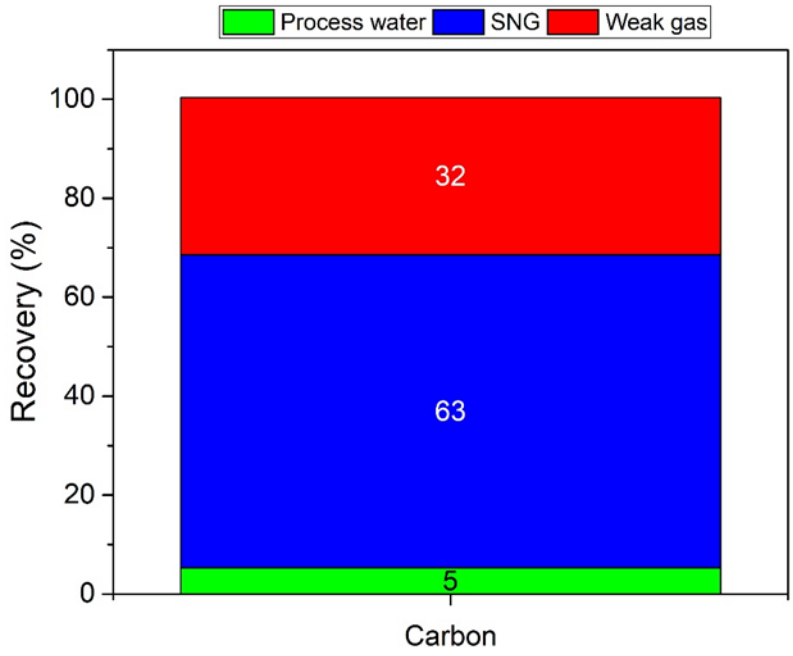


Figure 4.16: Total carbon balance of glycerol test 2. Feed carbon = 100%. The brine extraction was not activated, thus there was no brine flow to be accounted for.

The total carbon balance is depicted in Fig. 4.16. 100% of the feed carbon could be accounted for in the SNG, in the weak gas, and in the process water. 63% of the feed carbon were recovered as CH_4

and CO_2 in the SNG, while 32% were recovered in the weak gas. Only 5% of the feed carbon ended up as dissolved carbon in the process water.

4.2.4 Conclusions

The heat transfer tests under clean conditions (no fouling of heat transfer surfaces) confirmed the correct design of the heat exchanger, achieving measured heat transfer efficiencies of up to 91%. Its overall heat transfer coefficient (fluid to fluid) is significantly higher than the one for the salt separator (hot air to supercritical fluid). Heat loss estimations revealed the major heat losses and represent a good basis for further increasing the process efficiency. A dynamic model of the plant's thermal behavior matched the measured temperatures during start-up well. The results from the gasification of glycerol validated the values from lab-scale experiments. In particular, the catalyst used for the first time at this scale performed as expected and led to full conversion of the glycerol with a gas composition corresponding to the chemical equilibrium. However, the methane content of the depressurized SNG was significantly higher than in the lab-scale experiments due to the high-pressure phase separation in the HydroPilot plant that washed out some of the CO_2 from the SNG. Overall, we conclude from this work package that the HydroPilot plant was well designed and reaches the target specifications with a clean feed, free of solids and minerals.

4.3 Processing of sewage sludge (WP 4)

Processing sewage sludge posed much higher challenges than gasifying a glycerol solution. The digested sludge was provided by the WWTP Langmatt in Wildegg (AG). First, the sewage sludge had to be macerated and ground to a fine particle size with a corundum disk mill, which was required by the pump manufacturer. Additionally, the ground sludge was filtered through a 400 µm mesh to ensure a smooth feeding with the high pressure pump. The energy required for this pretreatment could not be measured and thus it was not included in the overall energy balance. The different pretreatment steps were not automated and took a lot of manpower because of a batch-wise operation. For a commercial plant, continuous pretreatment units should be installed.

4.3.1 Sewage sludge test 1

This first test was conducted within the campaign of glycerol test 2. At ToS = 72 h, the feed was switched from water to **3% digested sewage sludge.**

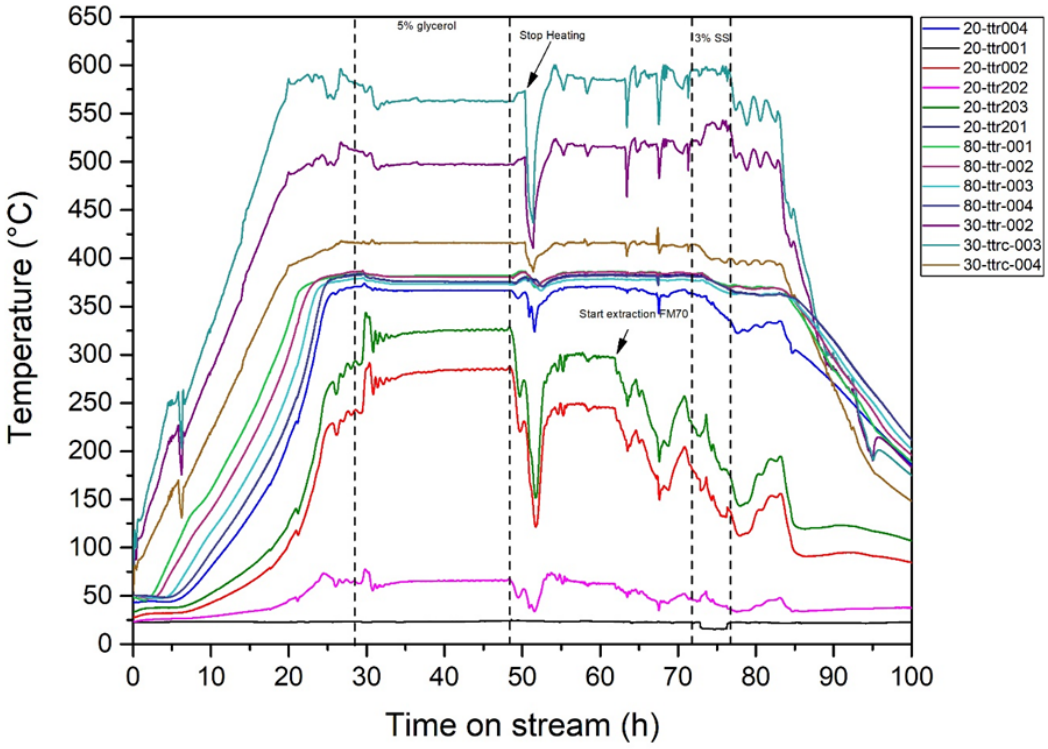


Figure 4.17: System temperatures overview for glycerol test 2 and sewage sludge test 1, conducted within the same campaign. In between the glycerol and the sewage sludge feed, the plant was flushed with water to test the brine extraction system FM 70. Sewage sludge was fed during ToS 72-76 h. The labels refer to the names of the different temperature sensors in function modules 20 (heat exchanger), 30 (salt separator), and 80 (sulfur trap and catalytic reactors).

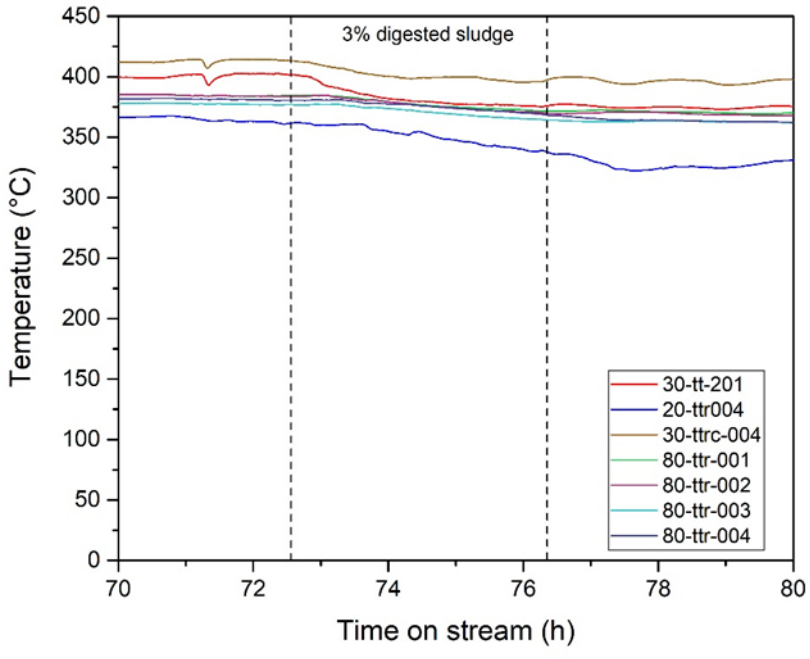


Figure 4.18: System temperatures overview for sewage sludge test 1. The labels refer to the names of the different temperature sensors in function modules 20 (heat exchanger), 30 (salt separator), and 80 (sulfur trap and catalytic reactors).

Upon feeding sewage sludge, the fluid temperatures decreased slowly. On the other hand, the hot air temperature exiting the salt separator increased (compare Fig. 4.17, signal 30-ttr-002). This indicates a reduced heat transfer from the hot air to the supercritical fluid inside the salt separator, most likely due to fouling of the salt separator tubes. The situation in the heat exchanger is more difficult to interpret because the extraction of brine in FM70 also caused a temperature decrease in the heat exchanger (due to the smaller mass flow rate of the hot stream entering the heat exchanger; Fig. 4.18; 20-ttr-004).

Because the temperature of the desalinated stream exiting the salt separator dropped below the critical temperature, the feeding of sewage sludge was stopped. Under these subcritical conditions, the salts would not be separated efficiently anymore and all the minerals would be carried into the sulfur trap and catalytic reactors, which must be avoided.

Gas production

The gas production was below the minimum flow rate to allow the high pressure control valve to open. As a consequence, all the gasses left the HP phase separator dissolved in the process water and ended up in the weak gas. Therefore, no analysis of the SNG and no carbon balance could be performed.

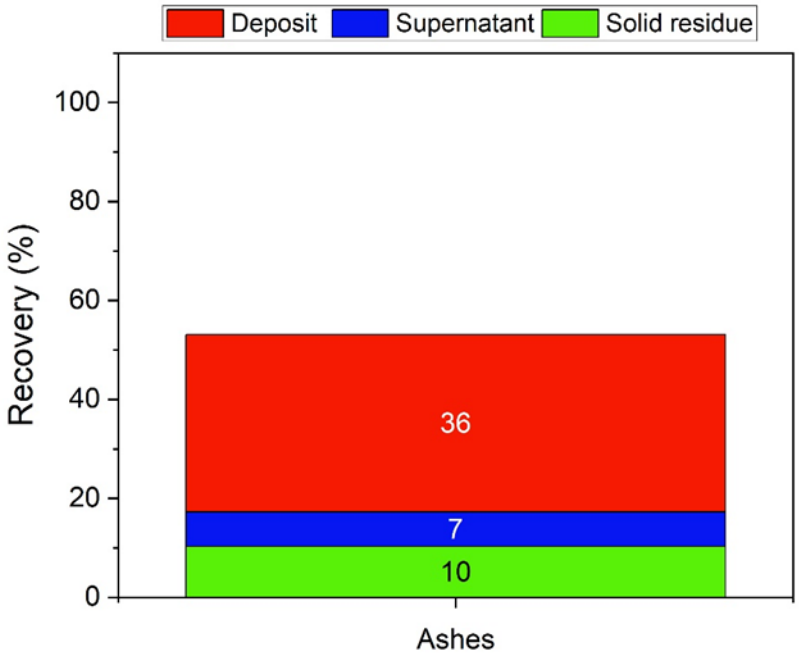


Figure 4.19: Recovery of ash content for sewage sludge test 1. Deposit = inside the salt separator, flushed out after the experiment, including cleaning; supernatant = aqueous phase of the extracted brine after centrifugation; solid residue = solid phase of the extracted brine after centrifugation.

4.3.2 Sewage sludge test 2

Several improvements were made on the HydroPilot between the two sludge campaigns:

- Increasing the maximum hot air temperature in the salt separator to 700°C, including an updated risk assessment
- Removal of the side exit for the brine, extraction now performed from the bottom of the salt separator
- Bypassing of the brine vessel cooling. This cooling turned out to be unnecessary and it drew a lot of heat from the salt separator, which made it difficult to reach supercritical conditions at the exit.
- Installing a bypass of reactor vessels 3 and 4, allowing for faster heat up and less heat losses.
- Installing a scale beneath the feed container to measure the flow rate. This was added because the Coriolis mass flow meter did not perform well in some cases.
- Replacing the needle valves for the brine extraction by ball valves.
- Several smaller improvements to increase the operability

A more concentrated **digested sludge with 5% Total Solids** was processed during only 1.6 h due to some issues with FM70. The new extraction sequence (without backflushing a valve with water) caused the accumulation of minerals in the collector, which were then transported downstream, contaminating the extraction unit. The compositional data of the sludge is given in Table 3.2.

The heat exchanger efficiency dropped only slightly to 89%, compared to 91% for the baseline case with 5% glycerol. This indicates only minor fouling in the heat exchanger.

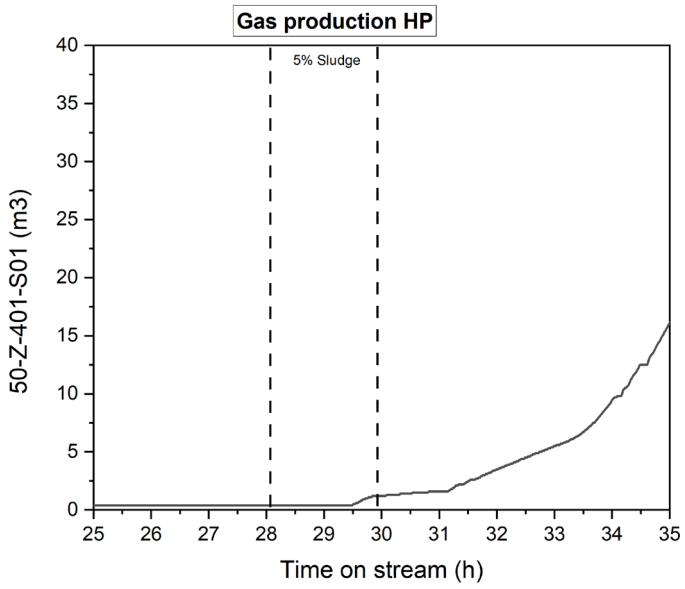


Figure 4.20: Cumulative SNG production (from the high pressure phase separator) for sewage sludge test 2. The dashed vertical lines denote the period when sludge was fed.

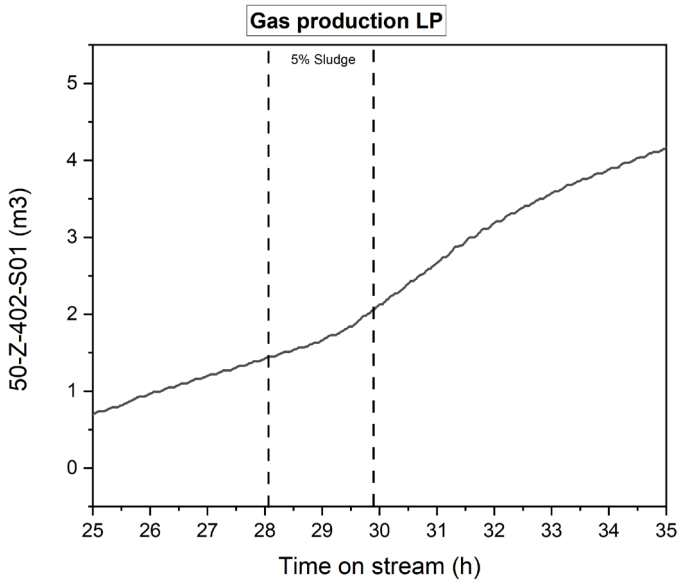


Figure 4.21: Cumulative weak gas production (from the low pressure phase separator) for sewage sludge test 2. The dashed vertical lines denote the period when sludge was fed.

The cumulative volumes of gas produced are depicted in Figs. 4.20 and 4.21. Gas production starts at ToS = 30 h (2 hours after having started feeding sludge). Total gas production: 25 m^3 of SNG and 4 m^3 of weak gas = 29 m^3 total (including N_2). The maximum gas flow rate was 10 m^3/h for SNG (obtained at ToS = 35-36 h, including N_2). The gas flow rate without N_2 was 3.1 m^3/h for SNG and 0.3 m^3/h for weak gas = 3.4 m^3/h total. Since the steady state could not be reached, the further calculations were done at the maximum gas flow rate (ToS = 35-36 h) and highest CH_4 content (ToS = 31.5-32.5 h).

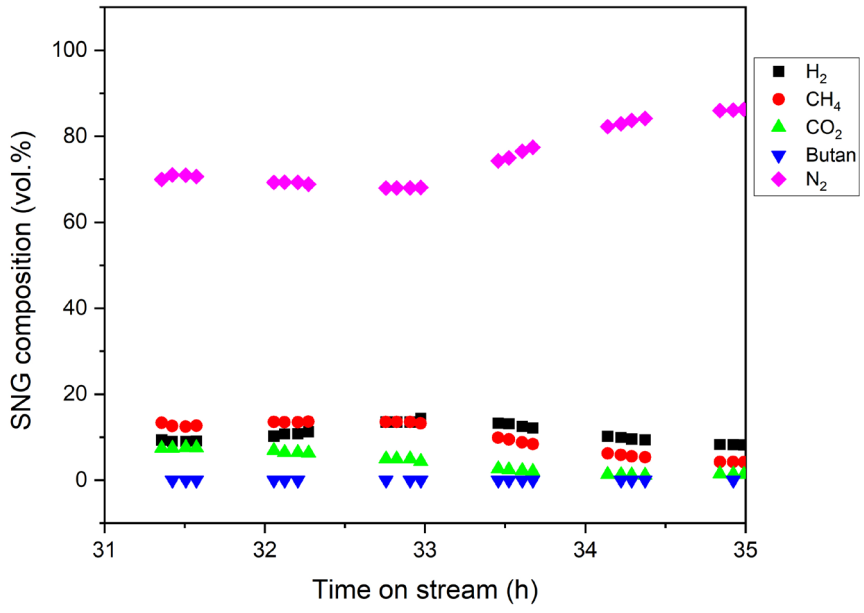


Figure 4.22: SNG composition from sewage sludge test 2, starting at time on stream of 31 h. Note that the HP phase separator is pressurized with N_2 before heating up. This N_2 is then displaced over time by the SNG produced.

SNG composition is shown in Fig. 4.22. At ToS = 31.5-32.5 h, the composition is: CH_4 = 14 vol.%; H_2 = 11 vol.%; CO_2 = 7 vol.%; N_2 = 69 vol.%

The weak gas composition is shown in Fig. 4.23. It reflects again the much higher solubility of CO_2 vs. CH_4 and H_2.

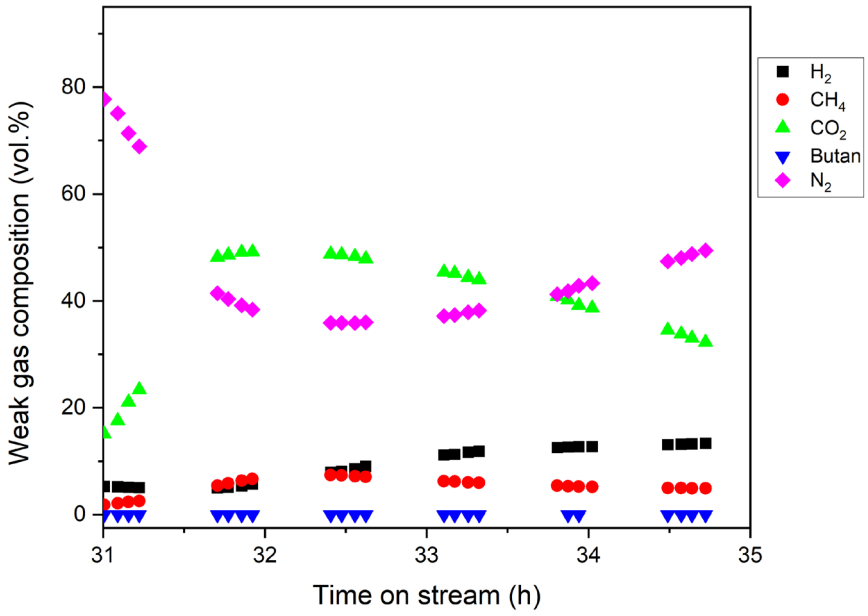


Figure 4.23: Weak gas composition from sewage sludge test 2, starting at time on stream of 31 h. Note that the HP phase separator is pressurized with N_2 before heating up. This N_2 is then displaced over time by the SNG produced.

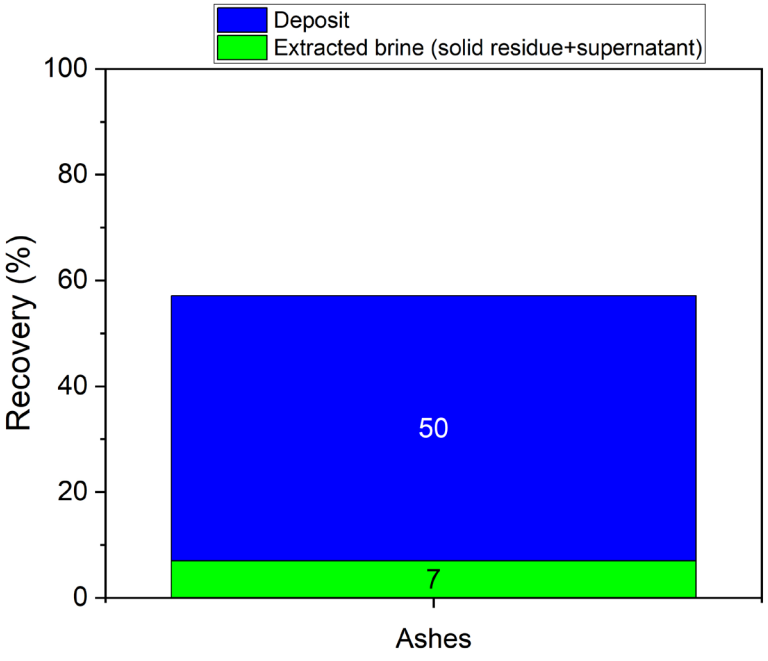


Figure 4.24: Recovery of ash content for sewage sludge test 2. Deposit = inside the salt separator, flushed out after the experiment, including cleaning; Extracted brine = solid and liquid phases of the extracted brine after centrifugation.

Fig. 4.24 shows the ash recovery. In total, 57% of the ashes could be recovered but only 7% in a continuous way with the brine during the experiment. The 50% were flushed out of the salt separator during cooling down and when cleaning. 43% could not be recovered at all.

4.3.3 Sewage sludge test 3

Digested sludge (DM = 5 wt.%) was processed during 2.8 h but had then to be stopped due to some issues coming from the accumulation of mineral salts in the salt separator. In fact, due to this accumulation, the salt separator could not be heated properly (increased heat transfer resistance). An overview of some of the temperatures is given in Fig. 4.25 and 4.26.

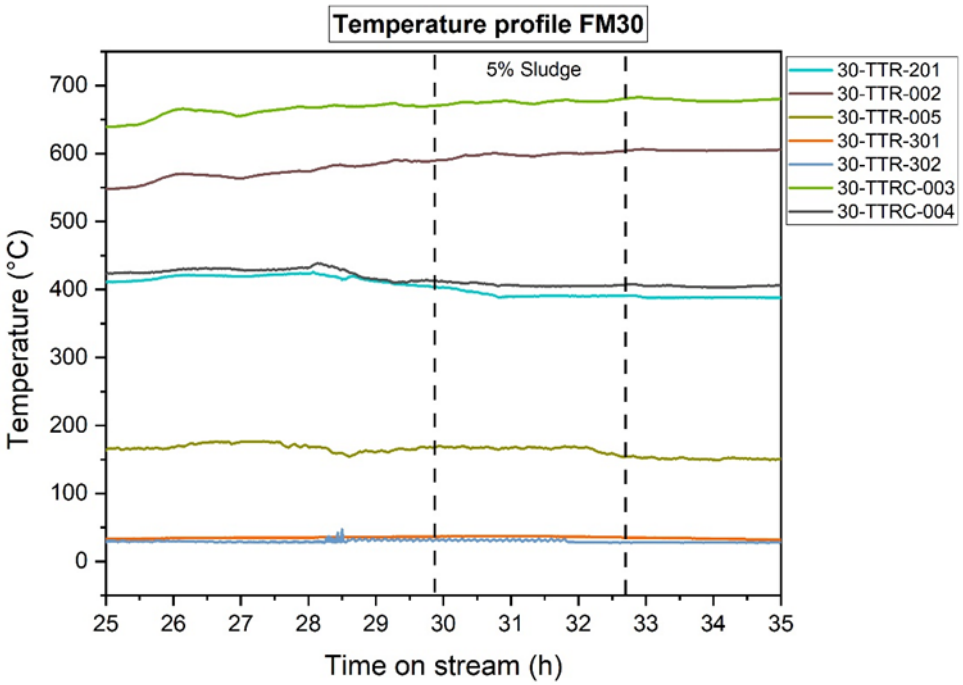


Figure 4.25: Temperatures in the FM 30 (salt separator) during sewage sludge test 3. The dashed vertical lines denote the period when sludge was fed.

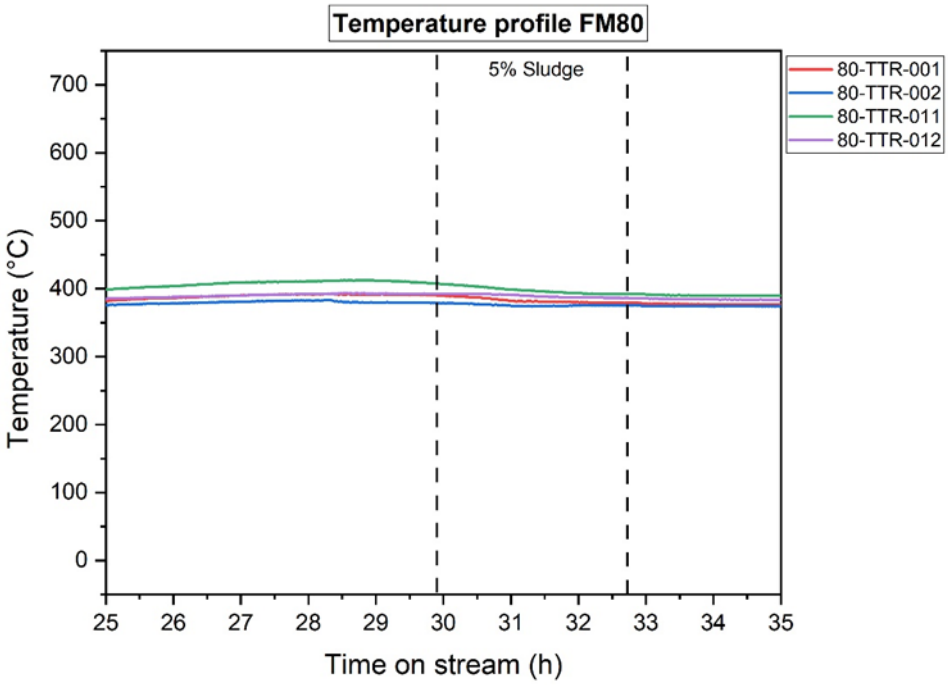


Figure 4.26: Temperatures in the FM 80 (sulfur trap and catalytic reactor) during sewage sludge test 3. The dashed vertical lines denote the period when sludge was fed.

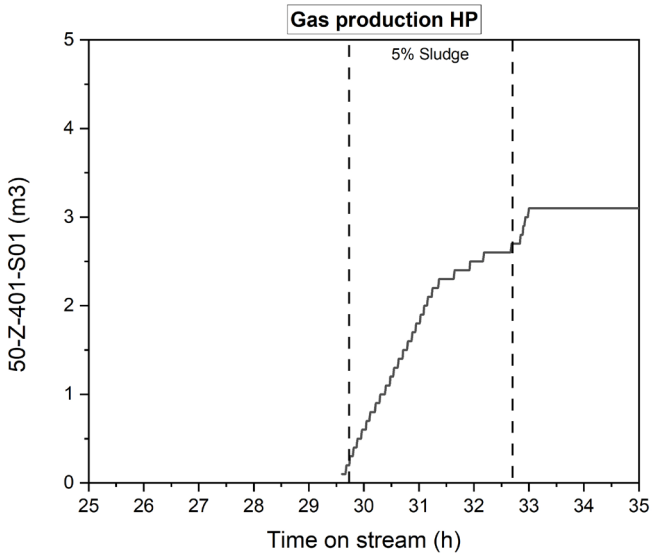


Figure 4.27: Cumulative SNG production (high pressure) for sewage sludge test 3. The dashed vertical lines denote the period when sludge was fed.

Gas production started at ToS = 30 h and remained very low (ca. 1 m^3/h). The composition of the SNG is shown in Fig. 4.28. Due to problems with the pressure control in the gas sampling line, the composition fluctuated. The problem could be fixed for subsequent campaigns.

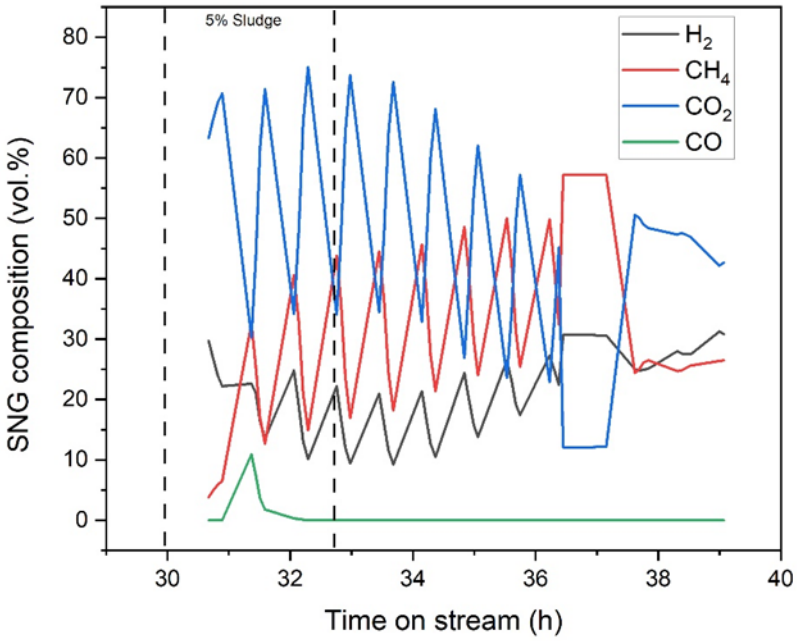


Figure 4.28: SNG composition from sewage sludge test 3, starting at time on stream of 30 h.

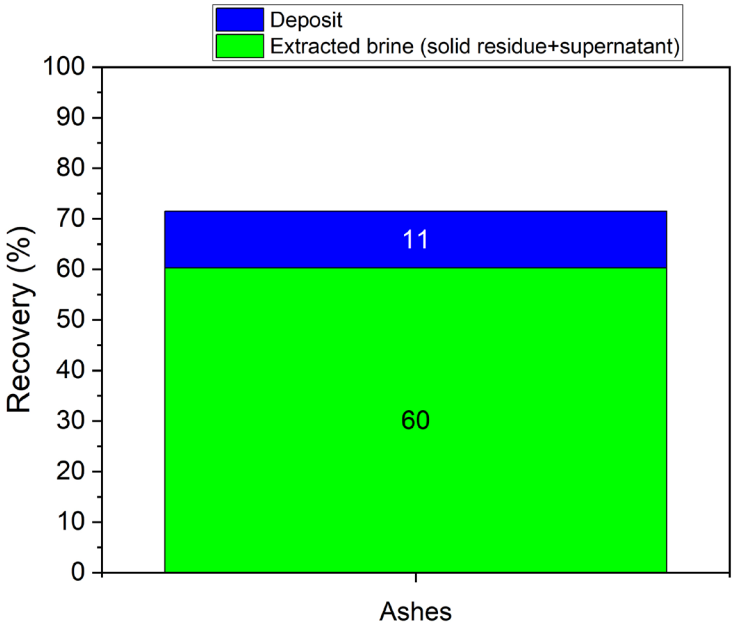


Figure 4.29: Recovery of ash content for sewage sludge test 3. Deposit = inside the salt separator, flushed out after the experiment; Extracted brine = solid and liquid phases of the extracted brine after centrifugation. .

60% of the ashes were extracted in the brine effluent and 11% in the deposits after the test. Total ashes recovery is 71% (Fig. 4.29). The ash extraction worked much better in this test compared to sewage sludge tests 1 and 2.

4.3.4 Industrial waste water

A hydrothermal gasification (HTG) campaign with isopropanol (IPA) waste (conc: 10 wt.%) provided by Cridec was conducted. Located in Eclépens (VD), Cridec is one of Switzerland's leading special waste treatment companies, processing around 50,000 tons of waste per year. The feed consisted of IPA that was mainly used as cleaning solvent in the industry. Cridec's motivation for assessing HTG with this feedstock is to compare economic benefits of HTG versus incineration (current disposal route for IPA waste).

The whole test campaign was carried out for 5 days (including the heating phase, gasification, and cooling phase) on HydroPilot unit. As shown in Figure 4.30, hydrothermal gasification of the IPA waste was carried out during 27 hours at an average mass flow rate of 80 $kg \cdot h^{-1}$. The fact that the pressure remained stable during the whole experiment demonstrates the good stability of the process during operation with the IPA waste. The observed pressure build-up at time on stream 67 h was caused by the formation of ice on the gas regulation valve due to a failure of the heating mantle surrounding the regulation valve. This minor incident could be fixed easily by restarting the heater on the heating mantle. As it can be seen in Figure 4.31, the temperature profile inside the sulfur trap and catalytic reactor remained stable during the experiment.

As shown in Figure 4.32 and 4.33, the gas composition in the HP and LP gas was stable during the whole gasification test demonstrating the high activity and stability the catalyst for effectively converting IPA waste into a methane-rich gas. The low concentrations of CO and ethane reflects the high selectivity of the catalyst for the methanation of IPA waste. As a result, a process water containing solely traces of TOC was obtained (< 10 $mg \cdot L^{-1}$) (see Table 4.7). The presence of inorganic carbon (TIC) in process water is due to the dissolution of a part of the CO_2 coming from the gas, which is of course dependent on the pH of the effluent. The fact that the LP gas contains a high CO_2 content (ca. 74 vol.%) reveals that the high-pressure gas/liquid separation is effective at separating a high fraction of the CO_2 from the methane-rich gas.

At time on stream from 60 h to 65 h, the total gas flow rate corresponds to about 9.4 m^3 per hour. Based on the amount of IPA injected into the process and the characteristics of the produced gas, a specific gas production of 1'230 m^3 per ton of IPA and a high heating value (HHV) of 27 $MJ \cdot m^{-3}$ and 8 $MJ \cdot m^{-3}$ were estimated for the HP and LP gas, respectively. The energy recovered in the gas, based on the HHV of both the feed and gas, is 91% which demonstrates the high performance of the technology in converting the chemical energy of IPA waste to the gas. As a result, a specific energy production of 8'637 kWh per ton of IPA waste was calculated. The carbon mass balance also confirms that most of the carbon in the feed was recovered in the gas (96%; see Figure 4.34).

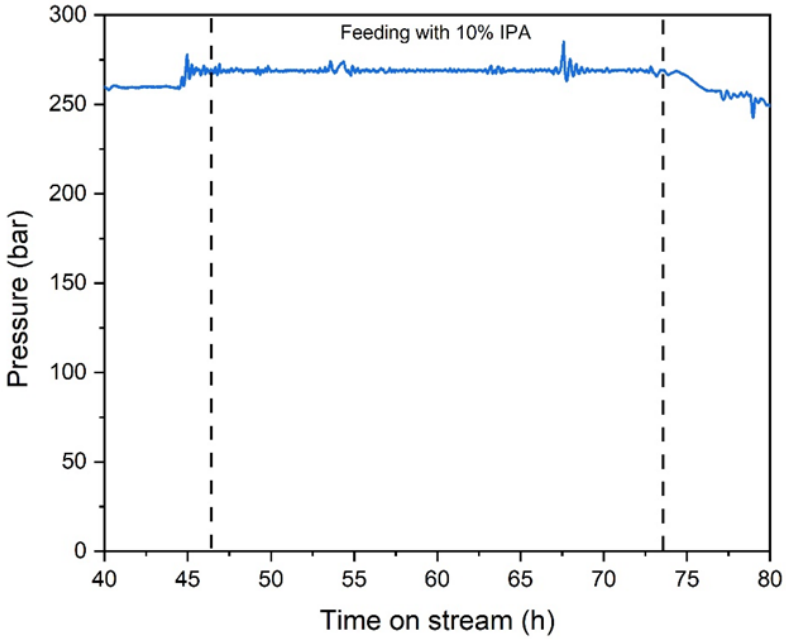


Figure 4.30: Pressure evolution during hydrothermal gasification of the IPA waste.

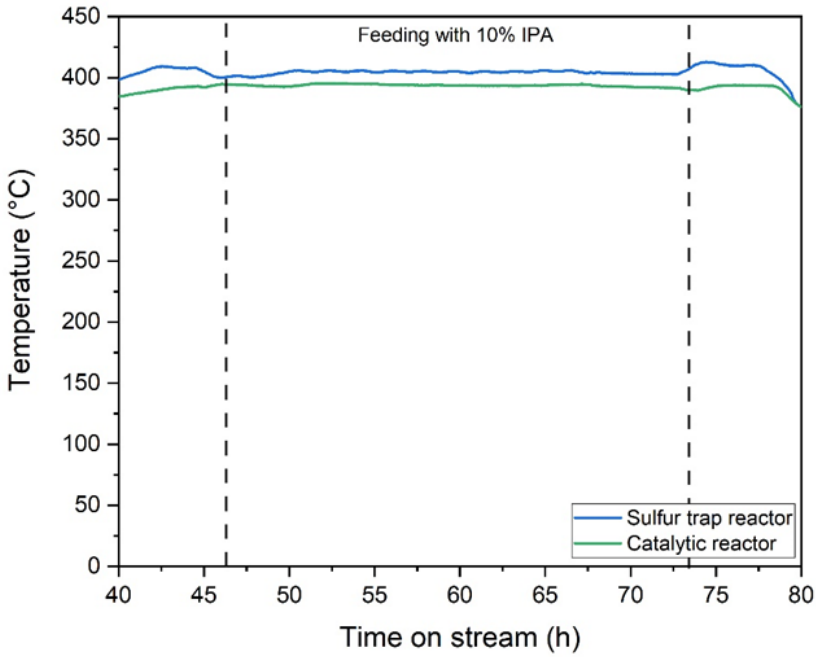


Figure 4.31: Evolution of the temperature during hydrothermal gasification of the IPA waste in the sulfur trap and catalytic reactor.

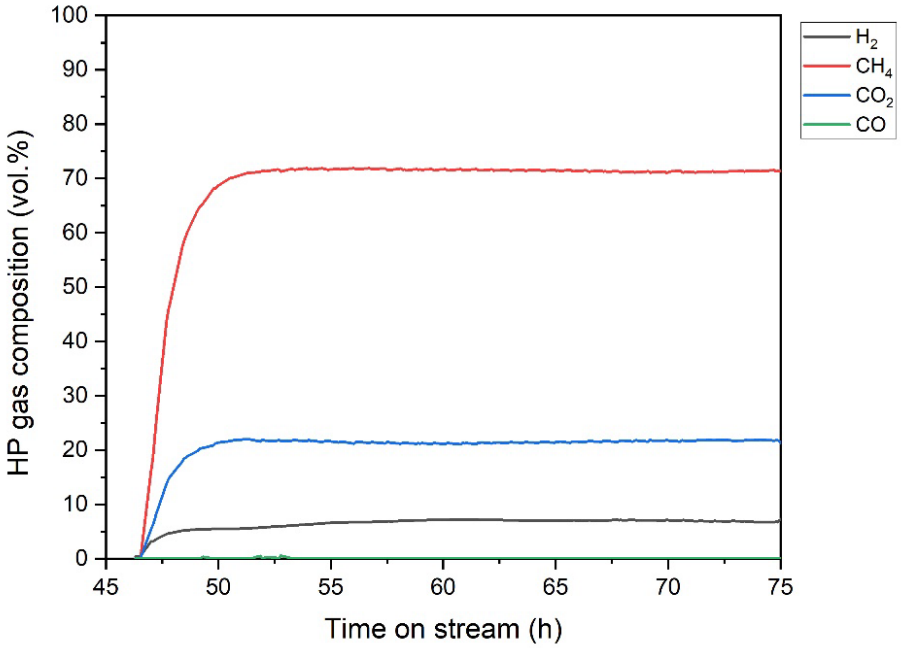


Figure 4.32: Evolution of the HP gas composition during hydrothermal gasification of the IPA waste.

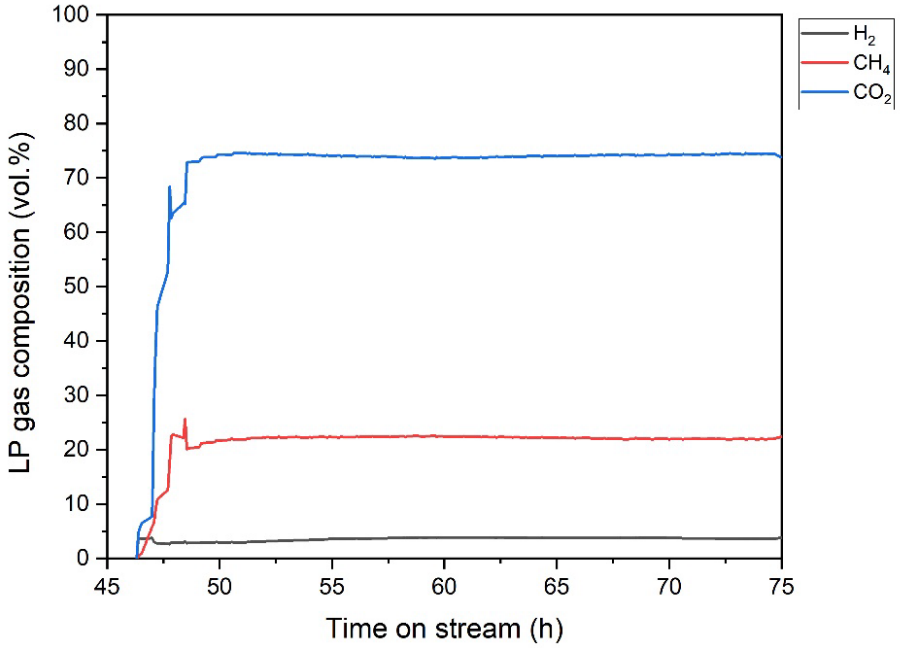


Figure 4.33: Evolution of the LP gas composition during hydrothermal gasification of the IPA waste.

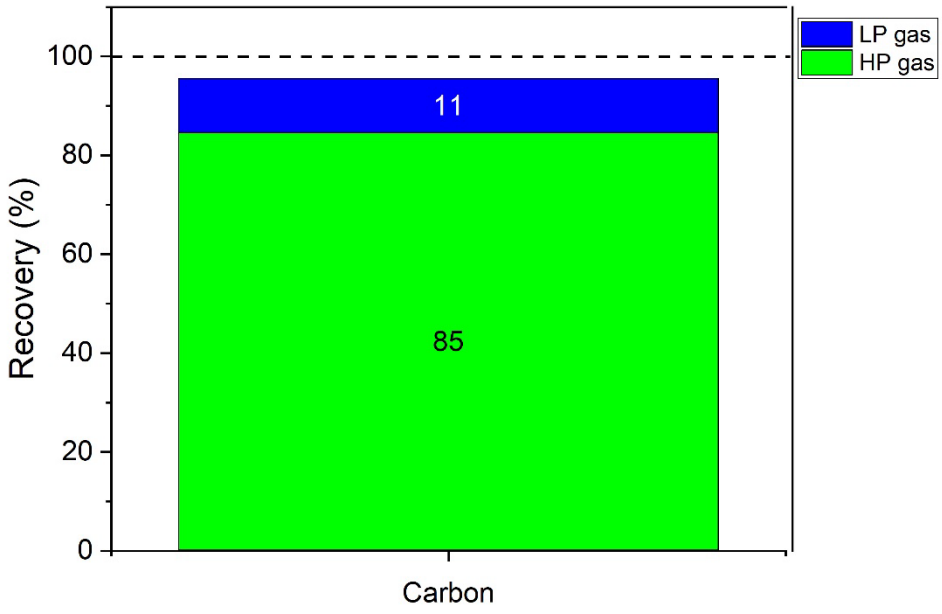


Figure 4.34: Carbon mass balance calculated during hydrothermal gasification of the IPA waste.

Table 4.7: Overview of the key parameters obtained during the test with IPA. N.D. = not detected

Feeding rate ($kg \cdot h^{-1}$)	80
Gas production ($m^3 \cdot h^{-1}$)[a]	9.4
Specific gas production ($m^3 \cdot ton_{IPA}^{-1}$)[a]	1'230
Specific energy production ($kWh \cdot ton_{IPA}^{-1}$)[a]	8'637
Concentration (wt.%)	10
Gas HP composition[a]:	
CH_4 (vol.%)	72
CO_2 (vol.%)	21
H_2 (vol.%)	7
CO (vol.%)	N.D.
Ethane (vol.%)	<0.005
Gas LP composition[a]:	
CH_4 (vol.%)	22
CO_2 (vol.%)	74
H_2 (vol.%)	4
CO (vol.%)	N.D.

C recovery in gas (% of feed)[a]	96
Energy recovery $(HHV_{gas} \times m_{gas})/(HHV_{feed} \times m_{feed}) \times 100$[a]	91
HHV_{gasHP} ($MJ \cdot m^{-3}$)[a]	27
HHV_{gasLP} ($MJ \cdot m^{-3}$)[a]	8
Composition of the process water[a]: TOC ($mg \cdot L^{-1}$) TIC ($mg \cdot L^{-1}$)	 <10 30-50

[a] Calculated at the steady state (time on stream from 60 h to 65 h)

4.3.5 Food waste

A hydrothermal gasification (HTG) campaign with food waste (FW) (concentration: 6 wt.%) provided by Ecorecyclage SA was conducted on HydroPilot. The feed consisted of food waste coming from restaurants, plastic residues (mostly food packaging material), and terpenes, whose chemical composition is depicted in Table 4.8. Ecorecyclage's motivation for assessing HTG with this feedstock is the difficulty for removing the plastic residue from the FW prior to anaerobic digestion. Consequently, the plastic residues end up in the digestate causing some environmental issues such as soil contamination.

The sample was successfully converted into gas (*HP gas composition*[3]: CH_4: 69 vol%., CO_2: 25 vol.%, H_2: 6 vol.%; *LP gas composition*[4]: CH_4: 19 vol%., CO_2: 78 vol.%, H_2: 3 vol.%) for a period of 13 hours. At the steady state, about 72% of the chemical energy contained in the feed was recovered in the gas leading to a specific energy production of 4'526 $kWh \cdot ton_{FW}^{-1}$. Only small amounts of total organic carbon (TOC) (< 50 $mg \cdot L^{-1}$) were measured in the process water which demonstrates the high performance of the catalyst to convert the organic carbon into gas.

Table 4.8: Chemical composition of FW.

pH	**DM (wt.%)**	**Ash content (wt.%)[a]**	**NH_4^+ ($mg \cdot L^{-1}$)**	**Cl^- ($mg \cdot L^{-1}$)**	**TOC (wt.%)**
3.7	6.1	10.3	N.A.	1'037	N.A.

Elemental analysis (wt.%)[a]				**HHV ($MJ \cdot kg^{-1}$)[a]**	**LHV ($MJ \cdot kg^{-1}$)[a]**
C	**N**	**H**	**S**		
55.9±0.6	3.3±0.1	3.0±0.4	0.74±0.01	20.1±0.5	19.4±0.5

[a] Calculated on a DM basis

The whole test campaign was carried out for 4 days (including the heating phase, gasification, and cooling phase) on HydroPilot unit. As shown in Figure 4.35, hydrothermal gasification of the FW was

[3] HP gas refers to the gas obtained after gas/liquid separation at high pressure (ca. 280 bar).
[4] LP gas refers to the gas obtained after gas/liquid separation at atmospheric pressure.

carried out during 13 hours at an average mass flow rate of 60 $kg \cdot h^{-1}$. The fact that the pressure remained stable during the whole experiment demonstrates the good stability of the process during operation with the FW. As it can be seen in Figure 4.36, the temperature profile inside the sulfur trap and catalytic reactor steadily decreased from 395 to 375 °C and 385 to 355 °C in the sulfur trap and catalytic reactor, respectively. The reason for such a decrease was a progressive accumulation of ashes inside the inner falling tubes of the salt separator (I.D. 17 mm) which deteriorated the heat transfer from the hot air loop to the salt separator. Consequently, the conditions of supercritical water could not be achieved anymore and feeding with FW was stopped. Such an issue was already observed when gasifying digested sludge and reveals that the salt separator developed by PSI is not adapted for mineral-rich feedstock.

As shown in Figure 4.37 and 4.38, a CH_4-rich gas (ca. 69 vol%.) and CO_2-rich gas (78 vol%.) was obtained in the HP gas and LP gas, respectively. This result demonstrates the good performance of the catalyst for effectively converting FW into a CH_4-rich gas as well as the good performance of the high-pressure gas/liquid phase separator for separating a high fraction of CO_2 from the CH_4-rich gas. The low concentrations of CO and ethane reflects the high selectivity of the catalyst for the methanation of FW. As a result, a process water containing solely traces of TOC was obtained (< 50 $mg \cdot L^{-1}$; see Table 4.9). The presence of inorganic carbon (TIC) in process water is due to the dissolution of a part of the CO_2 coming from the gas, which is of course dependent on the pH of the effluent.

At time on stream from 66 h to 68 h, the total gas flow rate corresponds to about 2.6 m^3 per hour. Based on the amount of FW injected into the process and the characteristics of the produced gas, a specific gas production of 801 m^3 per ton of FW and a high heating value (HHV) of 26 $MJ \cdot m^{-3}$ and 7 $MJ \cdot m^{-3}$ were estimated for the HP and LP gas, respectively. The energy recovered in the gas, based on the HHV of both the feed and gas, is 72%, which demonstrates the high performance of the technology in converting the chemical energy contained in the FW to the gas. As a result, a specific energy production of 4’526 kWh per ton of FW was calculated.

The carbon mass balance also confirms that most of the carbon in the feed was recovered in the gas (69%) and 10% in the process water as dissolved CO_2 (see Figure 4.39). The fact that most of the nitrogen (119±17%) was recovered in the process water demonstrates the capacity of the technology to convert nitrogen into ammonium.

During the whole gasification test (56-69 h), about 87% of the mineral salts were recovered in the mineral effluent while 30% were harvested from the deposit after the test. Such a high recovery shows that the mineral salts can be effectively extracted from the process, thus avoiding any risk of clogging due to the accumulation of mineral salts in the salt separator. The fact that the recovery was above 100% can be explained by the presence of corrosion products in the deposits that were collected after the test. In fact, some corrosion products were detected in the deposits (see section 4.4.6).

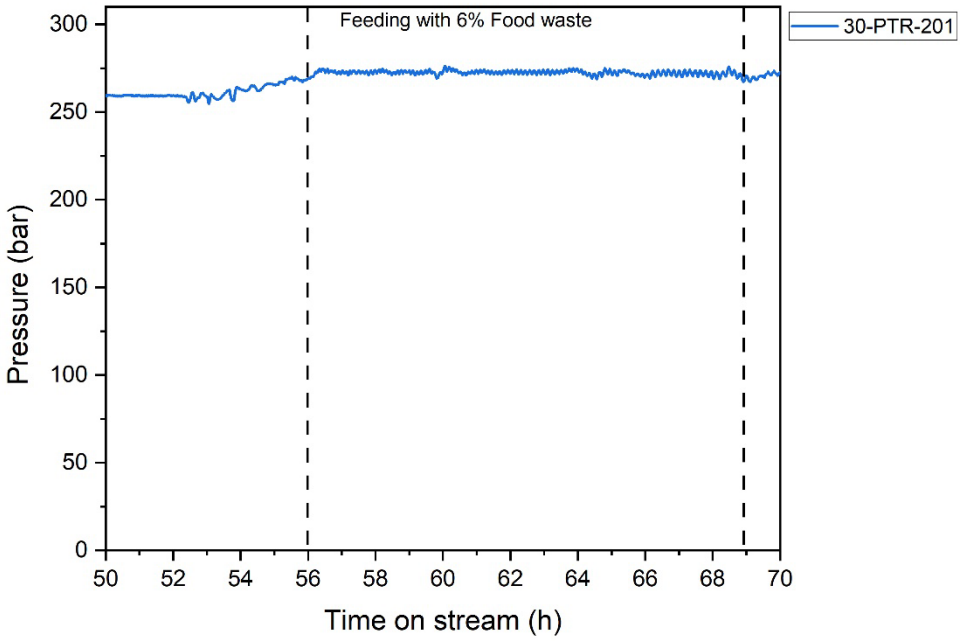


Figure 4.35: Pressure evolution during hydrothermal gasification of FW. The pressure sensor 30-PTR-201 was located at the exit of the salt separator.

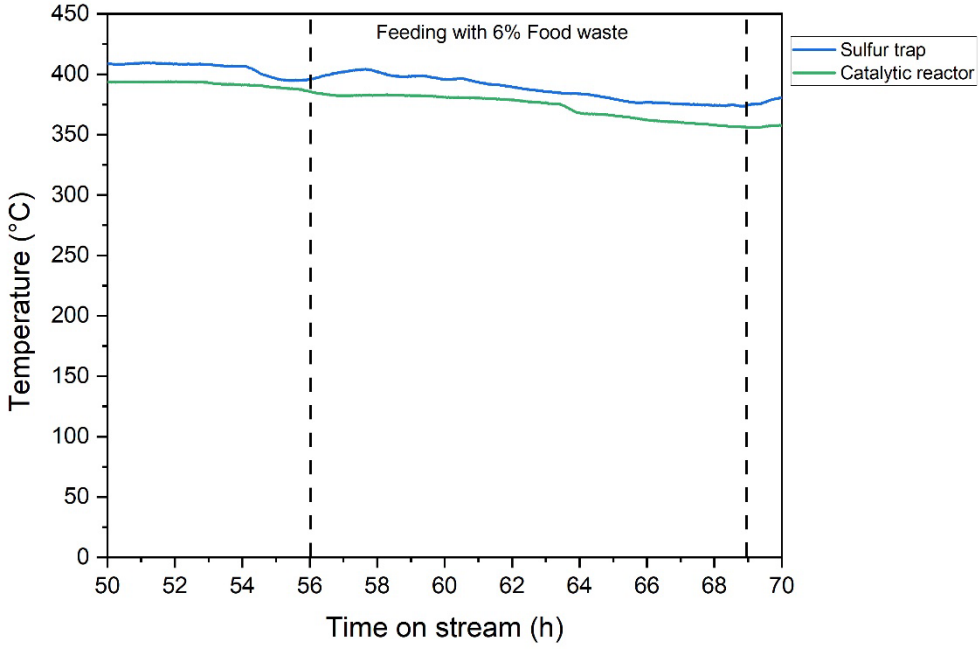


Figure 4.36: Evolution of the temperature during hydrothermal gasification of FW in the sulfur trap and catalytic reactor.

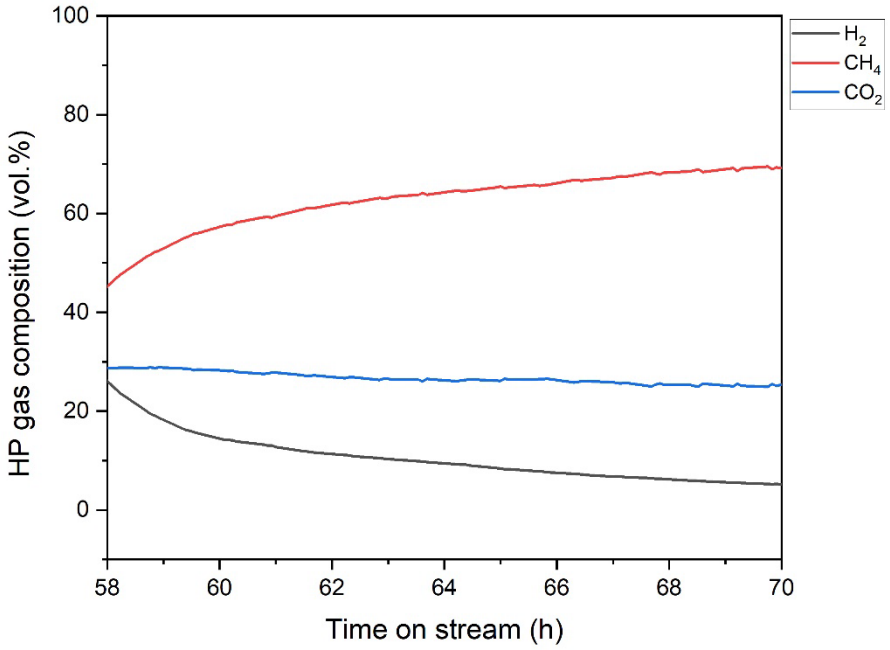


Figure 4.37: Evolution of the HP gas composition during hydrothermal gasification of FW.

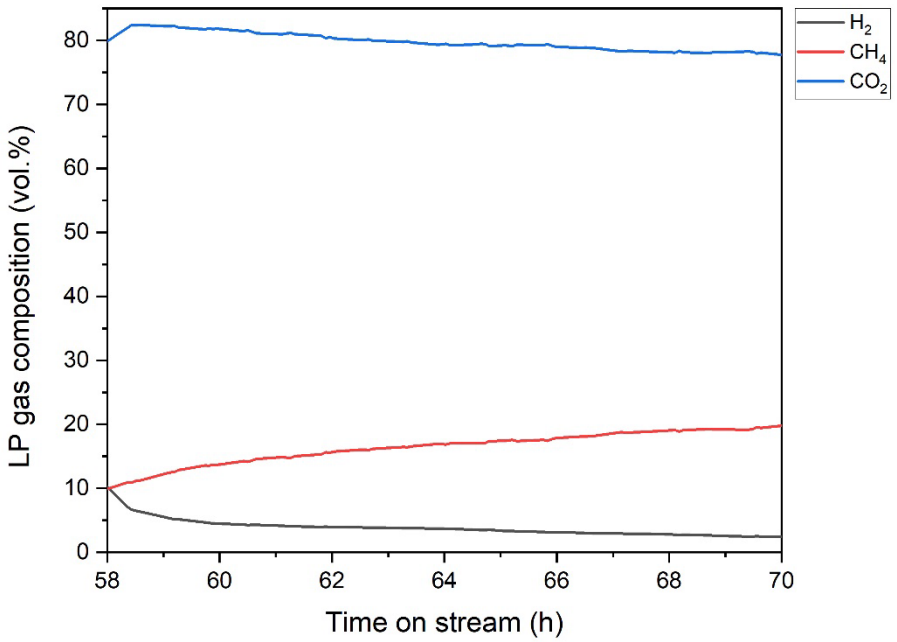


Figure 4.38: Evolution of the LP gas composition during hydrothermal gasification of FW.

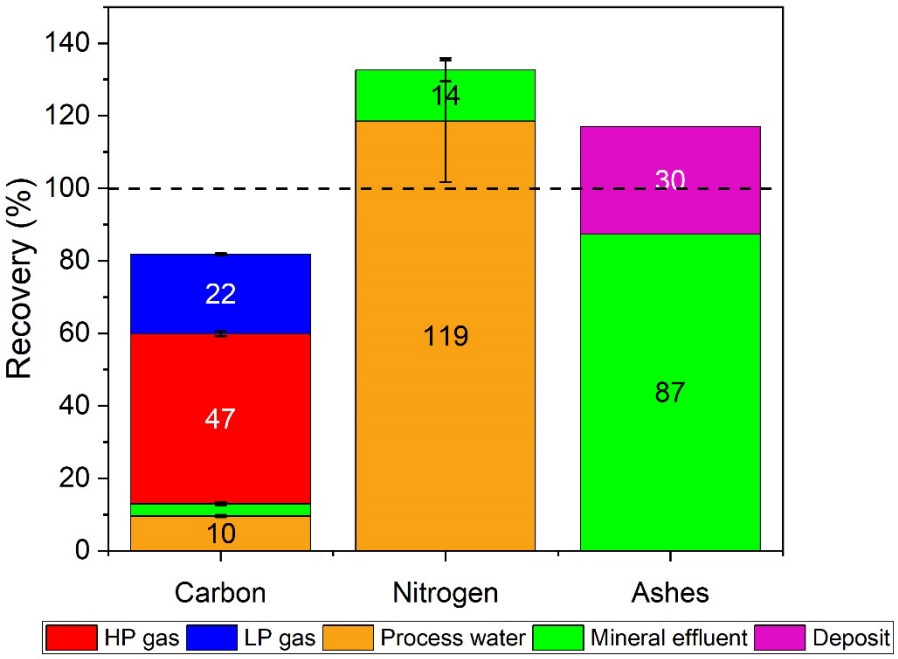


Figure 4.39: Mass balance calculated during hydrothermal gasification of the FW. The mass balances of carbon and nitrogen were both calculated at the steady state (time on stream from 66 h to 68 h) whereas the one for the ashes was calculated for the whole gasification test (time on stream from 56 h to 69 h).

Table 4.9: Overview of the key parameters obtained during the test with FW. N.D. = not detected

Feeding rate ($kg \cdot h^{-1}$)[b]	60
Specific gas production ($m^3 \cdot ton_{FW}^{-1}$)[a]	801
Specific energy production ($kWh \cdot ton_{FW}^{-1}$)[a]	4'526
Dry matter content (wt.%)	6
HP gas composition[a]:	
CH_4 (vol.%)	69
CO_2 (vol.%)	25
H_2 (vol.%)	6
CO (vol.%)	N.D.
Ethane (vol.%)	<0.2
Propane (vol.%)	<0.1
Butane (vol.%)	<0.03
LP gas composition[a]:	
CH_4 (vol.%)	19

CO_2 (vol.%)	78
H_2 (vol.%)	3
CO (vol.%)	N.D.
Ethane (vol.%)	<0.04
Butane (vol.%)	<0.002
C recovery in gas (% of feed)[a]	69±1
N recovery in process water (% of feed)[b]	114±16
Ashes recovery in the mineral effluent (% of feed)[b]	87
Energy recovery ($HHV_{gas} \times m_{gas}$)/($HHV_{feed} \times m_{feed}$)x100[a]	72±2
HHV_{gasHP} ($MJ \cdot m^{-3}$)[a]	26
HHV_{gasLP} ($MJ \cdot m^{-3}$)[a]	7
Composition of the process water[b]:	
TOC ($mg \cdot L^{-1}$)	<50
TIC ($mg \cdot L^{-1}$)	~3'300
TN ($mg \cdot L^{-1}$)	~2'400

[a]Calculated at the steady state (time on stream from 66 h to 68 h)

[b]Calculated for the whole gasification test (time on stream from 56 h to 69 h)

4.3.6 Corrosion study

After all the gasification campaigns performed on HydroPilot, the plant was thoroughly flushed and parts of the plant, such as the salt separator, were opened and inspected for signs of corrosion and mineral deposits. As it can be seen in Figure 4.40 A, the inlet tubes of the salt separator suffered from important corrosion as depicted by the shallow holes observed (image taken after the last campaign). These shallow holes clearly correspond to the metallic flakes collected at the bottom of the salt separator after cleaning with high pressure water jet (Figure 4.40 B&C). After the last campaign, about 1 kg of these dense and metallic flakes could be collected.

The corrosion product samples were analyzed by Inductively Coupled Plasma (ICP) and Thermogravimetric Analysis (TGA) and the results are presented in Table 4.10 along with the composition of Inconel 625. It can be seen that the composition of the corrosion products pictured in Figure 4.40 B&C (2nd line in Table 4.10) has similarities with that of Inconel 625, indicating it probably originates from the vessel walls. However, these corrosion residues are much richer in nickel than in Cr or Fe, compared to Inconel. Interestingly, some sulfur was detected in these solids as well. Residues collected from the first three inlet tubes and from the central outlet tube of the salt separator showed a composition very similar to the solids collected at the bottom of the separator, with the exception of a much higher sulfur content reaching 11 wt% for the salt separator outlet. The loss on ignition in the corrosion residues from the inlet tubes and outlet tube was lower than 1.8 wt% and 10.4 wt%, respectively, and can be explained by the oxidation of the sulfur (to gaseous SO_x) present in the samples, as outlined by elemental composition measured by ICP. Note that the balance from the elemental composition determined by ICP reaches 43 to 58 wt% for the three corrosion samples.

Oxygen can cover 20 to 30 % of the balance (if all the metals are in oxide form), indicating that other non-volatile elements make-up a significant part of the sample, possibly Mo and Nb (from Inconel) or other metals deposited from the feedstock.

Table 4.10: Inductively Coupled Plasma (ICP) and Thermogravimetric Analysis (TGA) of corrosion samples collected from the first three inlet tubes, the outlet tube and the bottom of the salt separator, as well as the salt separator alloy composition it is built from.

Sample	Loss on combustion (wt.%)	Elemental analysis (wt.%)										
		Ni	Cr	Fe	Mo	Nb	Co	Mn	Al	Ti	Si	S
Inconel 625	≈ 0	>58,0	20,0-23,0	<5,0	8,0-10,0	3,15-4,15	<1,0	<0,50	<0,40	<0,40	<0,50	0
Residues collected at the bottom of the salt separator	n.d.	37.4	3	1	n.d.	n.d.	n.d.	< LOD		n.d.	n.d.	0.5
Residues from tubes 1, 2, 3 (salt separator inlet)	1.8	37.9	2	0.8	n.d.	n.d.	n.d.	< LOD	< LOD	n.d.	n.d.	3.8
Residues from the central tube (salt separator outlet)	10.4	40.2	4.1	1.2	n.d.	n.d.	n.d.	< LOD	< LOD	n.d.	n.d.	11

n.d. stands for not determined
LOD stands for limit of detection

A metallic flake (corrosion products) collected during a cleaning following a series of campaigns, where the second to last and last tests were with sewage sludge and with glycerol (section 4.3.3), was analyzed by Scanning Electron Microscopy (SEM), see Figure 4.40 D. A Gallium Focused Ion Beam (FIB) was used to dig in the sample for a depth analysis, revealing a layered structure going down to 10 µm at the measured area, followed by an area exhibiting random unlayered dealloying (Figure 4.40 E.). Energy Dispersive X-Ray Spectroscopy (EDXS) was used to determine the elemental composition of the layers observed. It revealed that the successive layers are strongly enriched in Ni (lighter grey area), and in Cr (darker grey area).

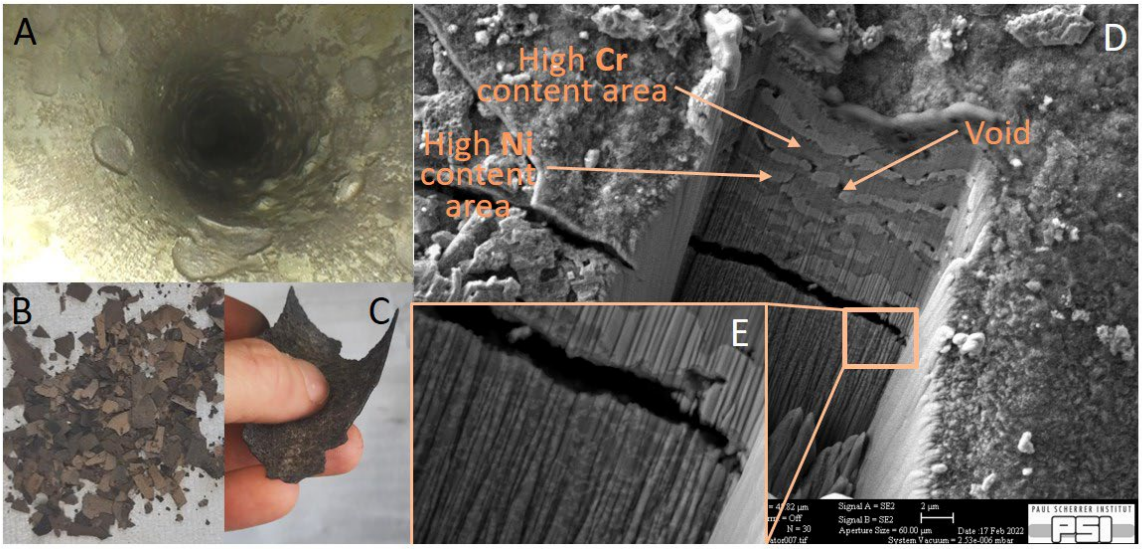


Figure 4.40: A: Endoscope image from the first inlet tube of the salt separator after thorough cleaning, after the last campaign on HydroPilot; B&C: Metallic corrosion products (flakes) collected from the high pressure water cleaning of the salt separator after the last campaign; D&E: Scanning Electron Microscopy (SEM) images of the convex side of a flake collected during a cleaning following the campaign glycerol test 2. A Gallium Focused ion beam (FIB) was used to dig in the sample. The darker grey areas are high Cr content, while the light grey areas are high Ni content as indicated by Energy Dispersive X-Ray Spectroscopy (EDXS).

Note that a part of the corrosion sample collected at the bottom of the salt separator showed a clear ferromagnetism, while Inconel 625 is paramagnetic. This is in line with the phase segregation observed by FIB-SEM-EDXS which indicated the formation of very high nickel content zones, pure nickel(0) being a known ferromagnetic material. The average composition was however the same, independent of the magnetic properties.

Carbonate and hydroxides are known to inhibit and/or passivate nickel-based alloys in oxidative/neutral hydrothermal and supercritical water [19]. However, carbonate mixed with organics (reducing conditions) lead to fast corrosion by carbonate [20], but also to a lower extent by hydroxide [21]. With carbonate, a depletion of (reduced) Ni and Mo from the surface was observed, while Cr and Nb were oxidized. This dealloying leads to changes in the material properties (ductility, tensile strength) which in turn leads to embrittlement [22]. Both dealloying and embrittlement are in line with our own observations. Hydrosulfide has been observed to lead to critical corrosion in reductive SCW on nickel-base alloys but with a corrosion mechanism very different to the one observed with carbonate [23].

From the literature, it appears that corrosion induced by carbonates in the presence of organics is the main type of corrosion observed in our salt separator. However, the presence of reduced sulfur species (hydrogen sulphide leading) is likely to play a role in the corrosion observed, but it is most likely not the main cause of the dealloying observed by SEM-FIB. The role of carbonate and sulphides on corrosion under these conditions has not been studied, particularly questions of synergy between the anions. The presence of other compounds are likely to have a small impact on corrosion on this material and under these conditions. Note that even in the absence of carbonate or sulfur in the feed in some of the campaigns, metallic flakes (corrosion products) could still be collected during the cleaning. This was the case in the last campaign (1 kg of metallic residues collected), whose feedstock contained a negligible carbonate content. This indicates that decarboxylation of organics and/or gasification of organics at the surface of the walls might play an important role. Studying the corrosion mechanism at stake under

these conditions and testing various classes of materials should help improving the process and decreasing the risks for future operation.

4.3.7 Conclusions

Solids-containing feedstocks could be processed after proper conditioning by macerating, milling, and filtering. The heat transfer efficiency in the preheater decreased only slightly, compared to the case with a glycerol solution. The biggest challenges with these feedstocks occurred in the salt separator. Heat transfer was seriously deteriorated with sewage sludge, and to a lesser extent also with food waste, which was found to be due to an incrustation of the inner surfaces of the falling tubes with mineral matter. Feed passage was not blocked but the heat transfer decreased, which made it impossible to keep supercritical temperatures from the exit of the salt separator to the catalytic reactor for those feedstocks. To conclude, the current design of the salt separator is not able to separate and concentrate most of the minerals in sewage sludge as an extractable brine at the bottom. Thus, for feedstocks rich in solids and minerals, a redesign of the salt separator is needed.

Even though supercritical conditions could not be maintained in the catalytic reactor during all campaigns, conversion of the organic fraction was almost complete in all campaigns and the gas composition reached the expected values close to the chemical equilibrium. This underlines the exceptional performance of the Ru/C catalyst also for solids and minerals-containing feedstocks, along with the good protection of the catalyst by the upstream sulfur trapping bed.

After some optimization of the extraction module (FM 70), the continuous extraction and recovery of minerals was high for the food waste but lower for the sewage sludge. This is clearly an area that needs further improvement for long-term operation.

Corrosion was observed exclusively in the high-pressure tubes within the salt separator. This was surprising since these tubes were made from a higher-quality alloy than other parts of the plant. The mechanism for the corrosive attack was not investigated in detail but fortunately, only general corrosion occurred, the consequences of which could be kept within limits and did not prevent further operation of the plant. However, this issue must be considered in future designs of the salt separator.

An additional campaign with an industrial waste water, free of solids and minerals, performed completely trouble-free and validated the excellent performance and readiness of HTG for this type of feedstock.

4.4 Phosphorus recovery (WP 5)

4.4.1 Phosphorus recovery using solids from the lab-scale prototype (1 kg/h)

4.4.1.1 Leaching experiments using Design of Experiments approach

During the first months of the project, WP5 was dedicated to the optimization of the acid leaching experiments. Since the pilot plant was not available yet, the minerals used for these experiments were produced from digested sewage sludge coming from Villeneuve by using TreaTech's lab-scale prototype. In order to evaluate the effect of several parameters during acid leaching (e.g. temperature, residence time, solid/ liquid ratio), a Design of Experiment (DOE) strategy was adopted. The latter allows us to determine the conditions for maximum P-recovery through the least experiments possible. The factors and levels of the design have been selected by literature research and experiments. The selected factors were: temperature (room temperature or 50 °C), pH (1 or 2), residence time (30 or 90 minutes) and liquid/solid ratio (6 or 10). This design would require 16 experiments per replica. However, by sampling after 30 minutes for the experiments that were performed during 90 minutes, the residence time factor was hence discarded, which decreases the number of experiments from 16 to 8.

Before starting the P&D project HydroPilot, only leaching experiments with very high liquid to solid ratio (160) had been carried out which means a high dilution factor. This is why prior to beginning the DOE, preliminary experiments were carried out in order to determine the lowest liquid/solid ratio. It was found that a homogeneous and stable mixing could be achieved with a minimum liquid/solid ratio of 4.5. However, leaching experiments performed at such a low liquid/solid ratio did not allow to achieve a high P recovery (ca. 50% at pH 1). Consequently, liquid/solid ratios above 4.5 were selected for the DOE (6 or 10).

Two replicas of the 8 experiments mentioned above were carried out. Additionally, two digestions of the feed (dried sewage sludge) using aqua regia (a HCl/HNO_3 mixture) were performed in order to determine its chemical composition. All the collected liquid samples (34 samples) were sent to an external laboratory (FHNW, Muttenz) for ICP-OES and elemental analyses (e.g. total organic carbon). Whereas the solid fractions (32 samples) recovered after the leaching experiments as well as the dried feedstock were sent to another laboratory (EPFL) for elemental analysis (CHN)

The results show that pH is the main factor affecting the performance of the process (Figure 4.41). In addition, as shown in Figure 4.43, at pH 1, the percentage of phosphorus recovery is more than 3 times higher than at pH 2, reaching an average maximum of 77% for experiments at pH 1, L/S=10, 30 minutes and 50°C. This same trend is followed by iron, aluminum and, although with less differentiation, magnesium (Figure 4.44). However, it is at these harsh conditions where we find the highest error, since at low pH and high T the process is highly sensitive to changes in the parameters. As a result, recovery can go from 50% to a 100% using these conditions. We find that experiments at pH 1, L/S=10, 30 minutes and room temperature are more stable with a lower average recovery but a much lower variance as well. Besides, working at room temperature would significantly reduce the cost of the process at industrial scale. From now on, we will consider pH 1, L/S=10, 30 minutes and room temperature the base conditions to keep improving the recovery percentage either by fine tuning the parameters (increasing L/S ratio, lowering pH) or by recycling the solid phase to perform a second leaching.

Finally, as shown in Figure 4.42 most of the carbon (>87%) remains in the solid phase for all the conditions and there is no clear trend that would link the variation on the parameters to the amount of carbon leached. In fact, for every experiment, the difference between samples after 30 or 90 minutes are very subtle which could mean that all the soluble carbon is leached quickly before the first 30 minutes.

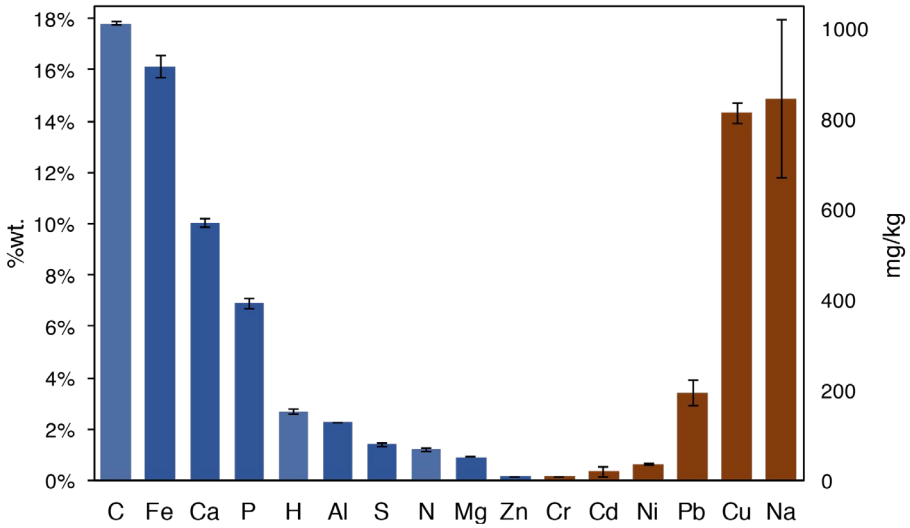


Figure 4.41: Solid residue composition before leaching.

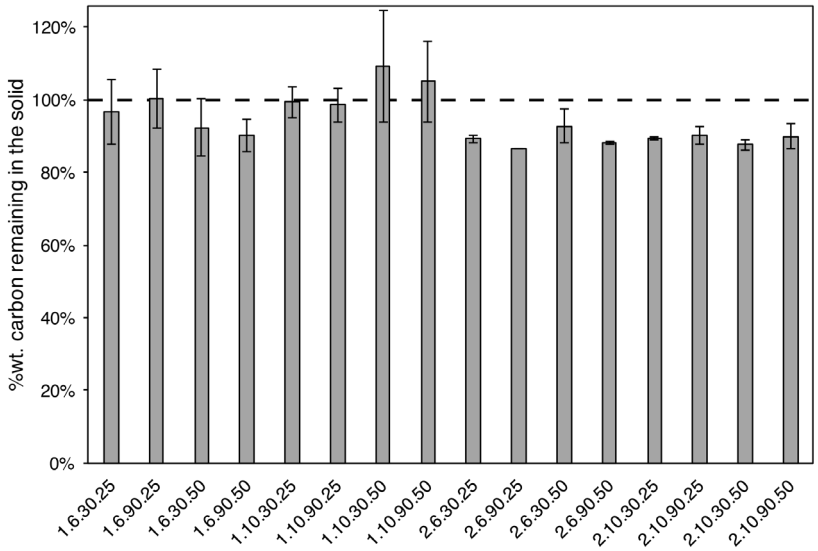


Figure 4.42: Weight percentage of the total carbon from the dried sewage sludge (feed) that remains in the solid after leaching. Each experiment is tagged as W.X.Y.Z where W is the pH (1 or 2), X is the solid to liquid ratio (6 or 10), Y is the residence time (30 or 90 minutes) and Z is the temperature (25 or 50 °C)

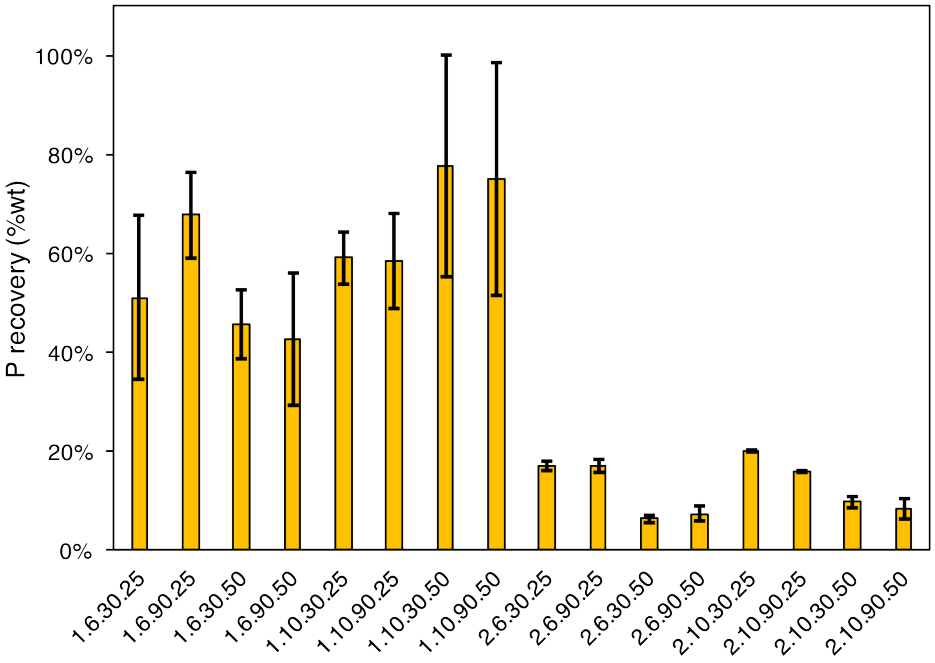


Figure 4.43: Weight percentage of phosphorus recovered from the solid residue into the leachate. Each experiment is tagged as W.X.Y.Z where W is the pH (1 or 2), X is the solid to liquid ratio (6 or 10), Y is the residence time (30 or 90 minutes) and Z is the temperature (25 or 50 °C)

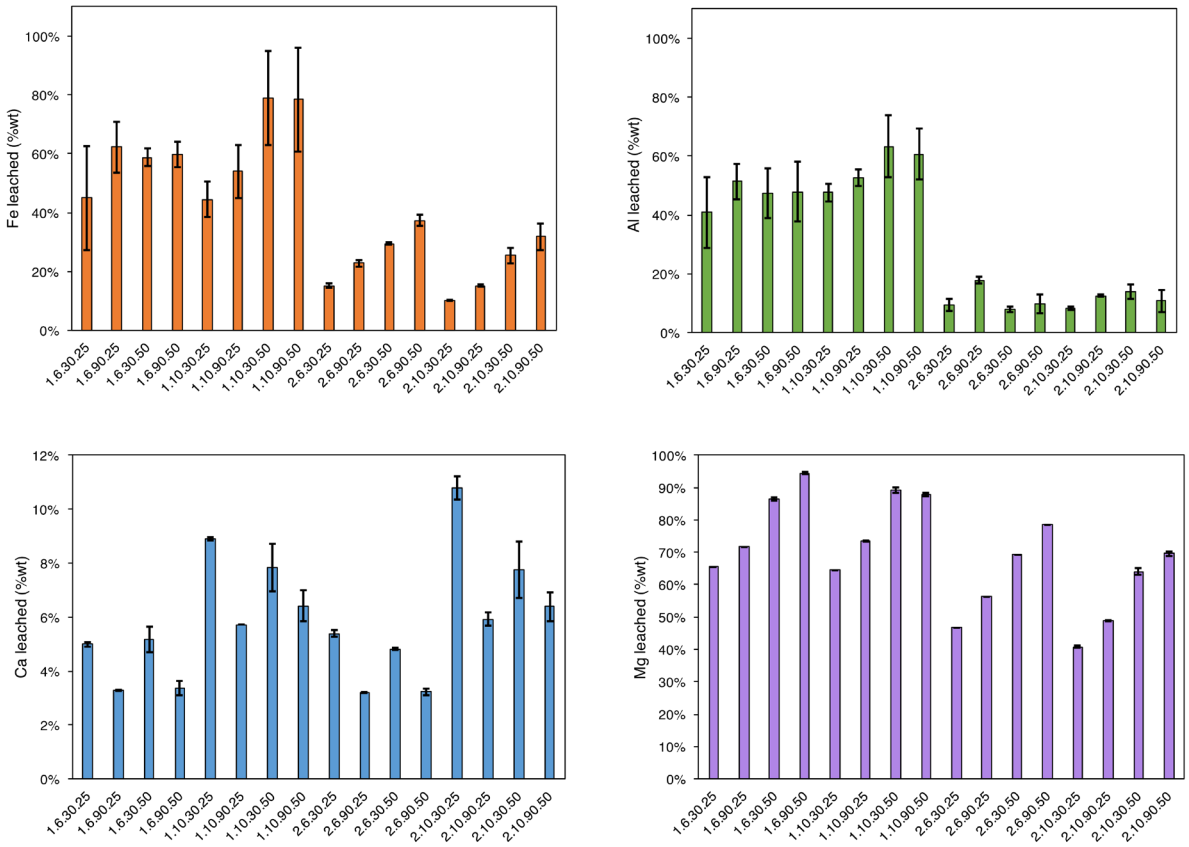


Figure 4.44: Weight percentage of iron, aluminum, calcium and magnesium leached from the solid residue into the leachate. Each experiment is tagged as W.X.Y.Z where W is the pH (1 or 2), X is the solid to liquid ratio (6 or 10), Y is the residence time (30 or 90 minutes) and Z is the temperature (25 or 50 °C).

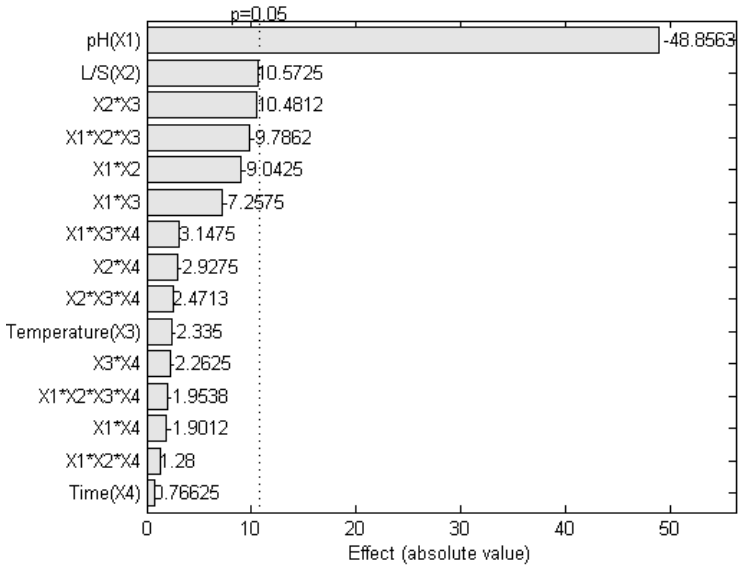


Figure 4.45: Pareto's chart for the effect of pH, temperature, liquid to solid ratio and time on P recovery.

4.4.1.2 Leaching optimization, purification and preliminary experiments for phosphorus valorization

During the period between April and September 2019, WP5 was dedicated to pushing further the recovery of phosphorus from the solid fraction, performing the first purification tests of the leachate and conducting preliminary experiments for the final valorization of phosphorus. Since the pilot plant was not yet available, the minerals used for these experiments were produced from digested sewage sludge from SIG by using TreaTech's lab-scale prototype (1 kg/h).

i. Leaching optimization

Even though we found that pH was the main factor affecting phosphorus leaching, the liquid to solid ratio has an important role as well since it directly affects the mass transfer rate of phosphorus to the liquid phase. This is why it has been decided to perform new leaching experiments tuning liquid to solid ratio and pH. Specifically, we run triplicate experiments at pH 1 and liquid to solid ratio of 20 as well as experiments at pH 0.5 and liquid to solid ratio of 10. Following the same method followed for experiments of section 4.4.1.1, the solids were analyzed before (Figure 4.46) and after leaching. We were able to push the P-recovery up to 87% by using a liquid to solid ratio of 20 at pH 1 and up to 84% by using a liquid to solid ratio of 10 at pH 0.5 (Figure 4.48 left). Regarding the rest of the elements analyzed, concentrations of Mg, Al, Fe, Ni, Cu, Zn, Cd and K are higher for lower pH while only Ca, Cr and Pb have slightly higher concentrations for a higher pH. This means that working at a higher pH will contaminate less our leachate. We should take special precautions when analyzing the behavior of Cd, Pb, Ni and Cr since they have very low concentrations in the solid residue. This results in bigger inaccuracies and errors (Figure 4.48 right). Finally, in average, 87% and 97% of the carbon remains in the solid for the experiments at pH 1 and 0.5 respectively (Figure 4.47). As

the experiment at pH 0.5 is performed at half the liquid to solid ratio (10), we think that less carbon can solubilize in the liquid and hence, more carbon remains in the solid.

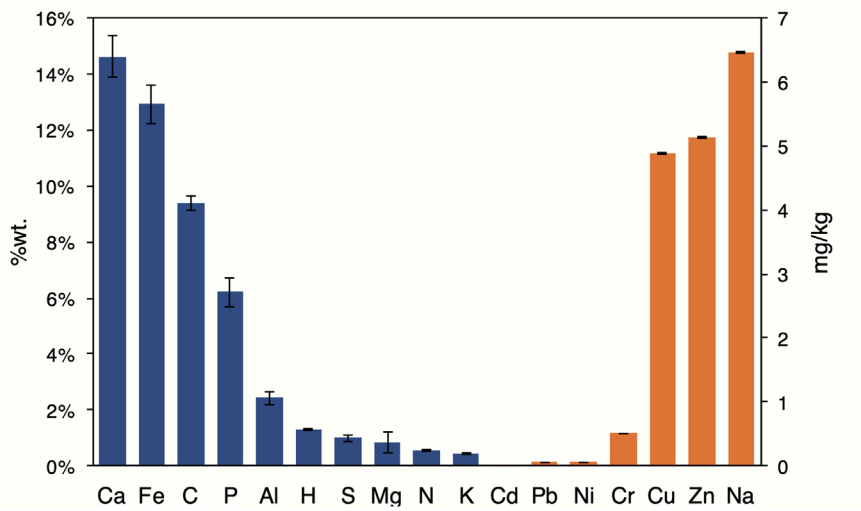


Figure 4.46: Composition (%wt in blue, mg/kg in orange) of the solid residue mix before leaching.

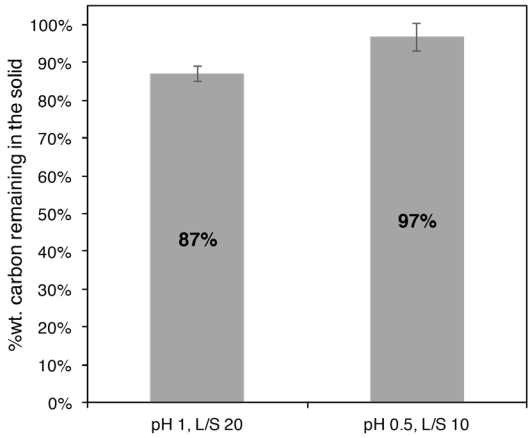


Figure 4.47: Percentage of the carbon in the solid residue that remains in the solids after leaching.

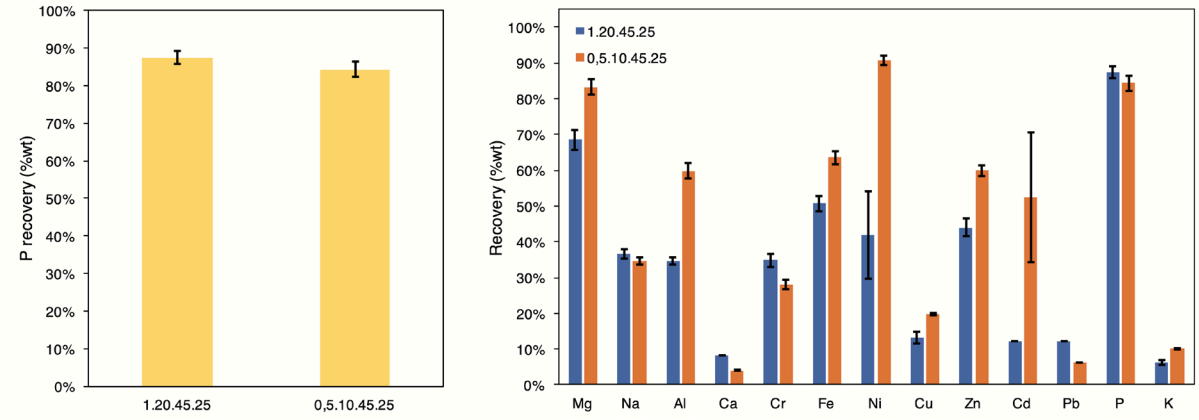


Figure 4.48: [Left] Percentage of P recovered in the leachate from the solid residue. [Right] Percentage recovered of all the elements analyzed.

ii. Purification experiments

Following the leaching experiments, we used ion exchange resins (Purolite MTC1600H) to purify the leachate by removing most of the cations present in the samples. In fact, the resins have proven to work as expected at lab scale (Figure 4.49). We were able to recover, in the purified stream, 91% and 87% of the P that was present in the dirty leachate for conditions 1.20.45.25 and 0,5.10.45.25, respectively. Starting from the P in the solid residue, the overall recovery rate is 80% wt and 73% wt for conditions 1.20.45.25 and 0,5.10.45.25, respectively. However, we found that, especially for Na and P, 14 to 20% of the amount present in the dirty leachate ended up in the cleaning water. In view of these results, we changed the protocol of the purification experiments for the next trials.

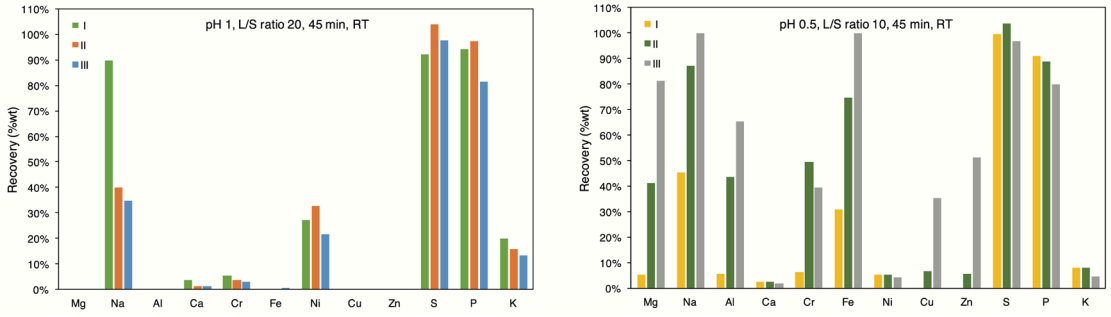


Figure 4.49: Percentage of each element that remains in the purified leachate with respect to the mg of each element present in the dirty leachate.

iii. Preliminary precipitation experiments

Finally, we have performed 3 preliminary precipitation experiments with dirty leachate. The results showed that amorphous, and not crystalline, calcium phosphates were precipitated. Figure 4.50 shows that 95%, 100% and 70% of the phosphorus in the dirty leachate was precipitated. In the next months, we performed precipitation experiments with the purified leachate in order to explore if the reason for this poor performance was the fact that the leachate is not purified or if it lies within the carbon-containing nature of the solid fraction.

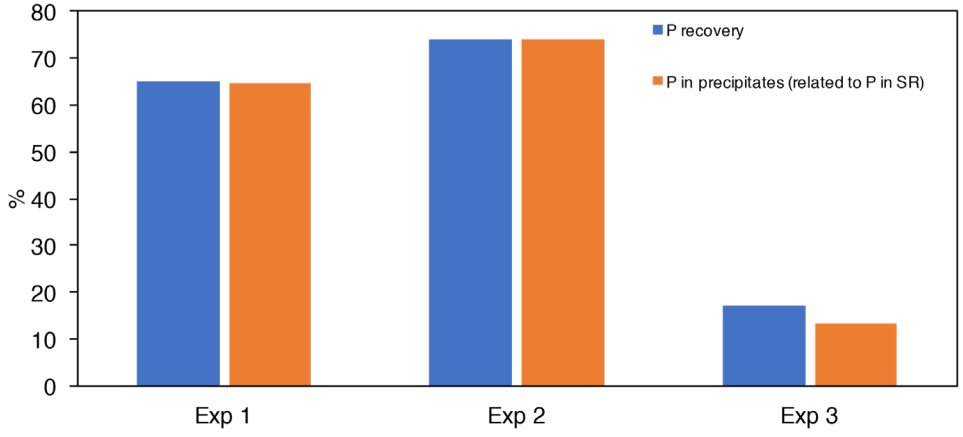


Figure 4.50: P recovery from the solid residue to the leachate and recovery of this P in the precipitates for the preliminary experiments. [Exp1] Feedstock: solid residue. Leaching conditions: pH 1, 90

minutes, L/S 6, room temp. Precipitation conditions: 1.2% Ca(OH)2, 120 minutes, room temp. [Exp 2] Feedstock: sewage sludge ashes. Leaching conditions: pH 1, 90 minutes, L/S 6, room temp. Precipitation conditions: 2% Ca(OH)2, 120 minutes, room temp. [Exp 3] Feedstock: solid residue + Ca(OH)2 (15% w/w). Leaching conditions: pH 4, 90 minutes, L/S 6, room temp. Precipitation conditions: 1.1% Ca(OH)2, 120 minutes, room temp.

4.4.1.3 Phosphorus valorization

Between October 2019 and March 2020, WP5 was dedicated to valorizing the extracted phosphorus from the solid residue into a solid P-based fertilizer by precipitating calcium phosphates and magnesium ammonium phosphate (struvite). In addition, the solid residue and leachate were tested to verify its compliance with MinRec (regulation for recycled fertilizers from waste). Since the pilot plant was not yet available, the minerals used for these experiments were produced from digested sewage sludge from SIG (Services Industriels de Genève) by using TreaTech's lab-scale prototype (1 kg/h) (Figure 4.51).

i. Leaching and purification

Leaching experiments were performed at pH 1 (sulfuric acid), liquid to solid ratio of 20 and a residence time of 45 min (optimized parameters from section 4.4.1.2). The carbon content of the hydrothermally treated sewage sludge was low (~6 %wt.). On average, 78 %wt. of the phosphorus was recovered in the liquid phase (Figure 4.52).

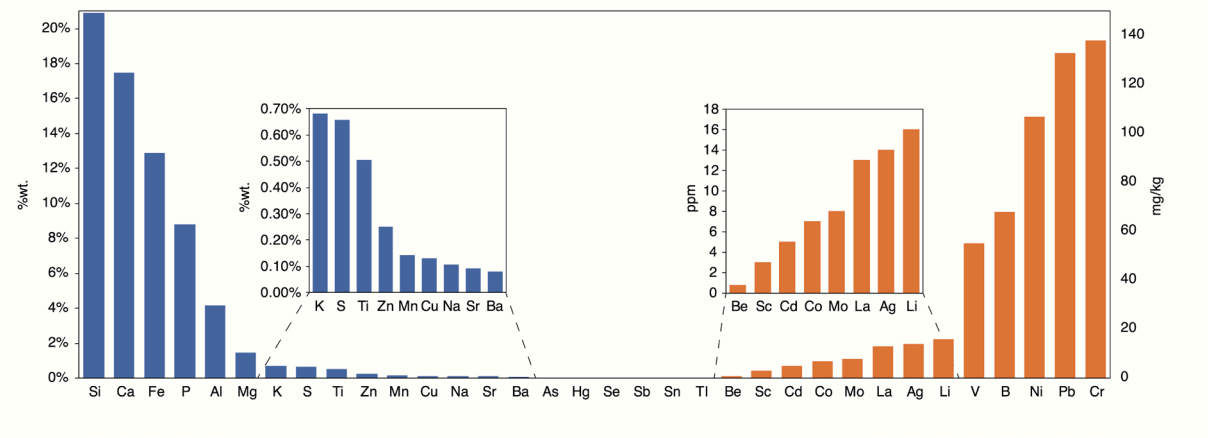


Figure 4.51: Composition (%wt in blue, mg/kg in orange) of the deposits before leaching.

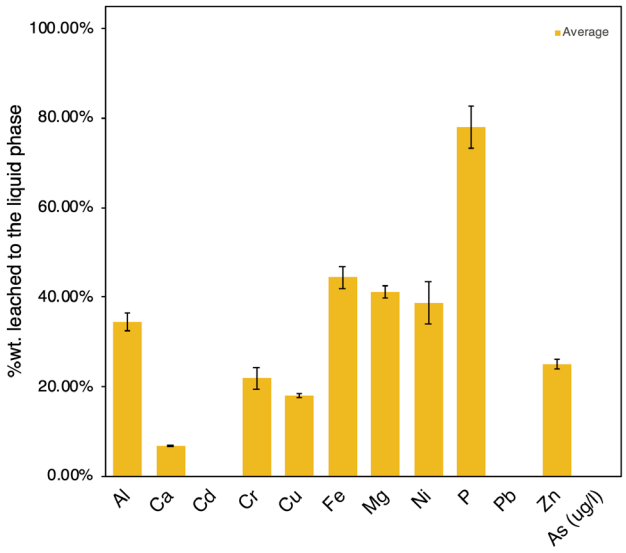


Figure 4.52: Average %wt. leached to the liquid phase from the solid before purification.

Following, the liquid phase (leachate) containing phosphorus and impurities, was purified using ion exchange resins (Purolite MTC1600H). It was shown that more than 99 %wt. of the cations present in the samples can be removed thanks to the ion exchange resins. After this purification step, about 80%wt. of the phosphorus still remained in the purified leachate (Figure 4.53).

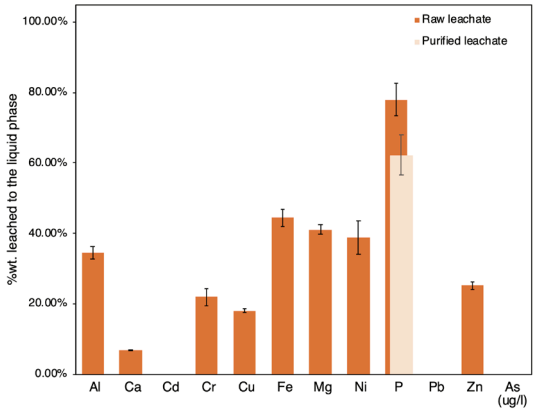


Figure 4.53: Average %wt. leached to the liquid phase from the solid before and after purification for both replicates.

ii. Precipitation

The next step concerns the precipitation experiments to produce either calcium phosphates or struvite (magnesium ammonium phosphate) by using the purified leachate.

- Calcium phosphates

Phosphorus was precipitated by adding excess calcium hydroxide to the purified leachate under stirring during 2 hours at room temperature. The solid samples were analyzed using XRD.

No crystalline calcium phosphate was found in either of the samples. The samples were mainly composed of a mixture of bassanite and gypsum.

In addition, CHN analysis of the solids and TC/TOC of the liquid phases were performed to study the distribution of carbon during precipitation. According to the results, in average, after leaching, 9.4% of the carbon is transferred to the leachate, then about 3.7% is trapped in the ion exchange column and finally all carbon remaining in the clean leachate precipitates during the precipitation experiment. This means that, in average, if we start with 100 grams of solid residue, 5.7 grams of it will be carbon (5.7% carbon in the residues) and 0.52 grams of this carbon will end up in the precipitates.

- Struvite

Struvite was precipitated by adding magnesium chloride hexahydrate as the magnesium source, then the pH was adjusted to 9 thanks to sodium hydroxide and finally ammonium chloride was added as the nitrogen source. The mixture was stirred for 2 hours at room temperature as well. In both cases, the solids were filtered out under vacuum and dried overnight at 50 °C.

All the solid samples were analyzed using XRD. Figure 4.54 shows the results and the reference pattern.

High purity crystalline struvite was found in all cases confirming that a solid P-based fertilizer can be produced from hydrothermally treated sewage sludge.

Regarding carbon balance, after precipitation of Struvite, all carbon remaining in the clean leachate precipitates during the precipitation experiment. The concentration of carbon in the Struvite precipitates is lower than in the calcium phosphate precipitates (1.45% vs 3.79% for experiment I) because the total mass in the case of Struvite is bigger. The reason for this is that Struvite molecules are heavier than

gypsum or bassanite, which are the main molecules, found in the calcium phosphate precipitates.

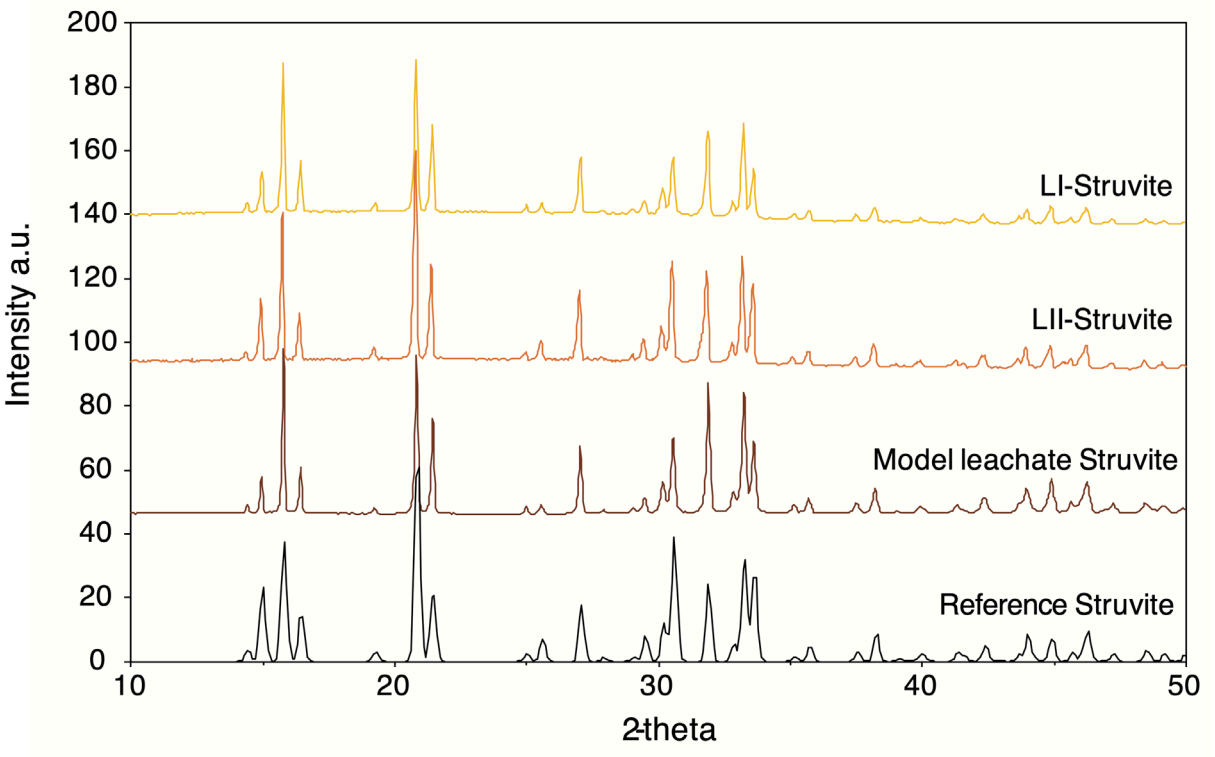


Figure 4.54: XRD patterns for struvite precipitates from hydrothermally treated sewage sludge (LI-Struvite and LII-Struvite), for struvite precipitates from a model leachate (diluted phosphoric acid with equivalent concentration to the leachate obtained in section 4.4.1.3.i) and XRD reference substance pattern.

4.4.1.4 Compliance with MinRec

Solid residue samples, extracted during hydrothermal gasification experiments, were tested to find the concentration of organic and inorganic pollutants that require an upper limit according to the MinRec regulation.

Concerning organic pollutants, we have performed analysis to determine the concentration of PCBs and PAHs. According to the results (Tables 4.11 and 4.12), the concentrations of PCBs (average 0.07 g/t of P) and PAHs (average 5.76 g/t of P) comply with MinRec requirements (0.5 g/t of P for PBCs and 25 g/t of P for PAHs). Due to a lack of resources at the moment of the performance of these analysis, the concentration of PCDD/F could not be measured. Compliance concerning this contaminant will be assessed as part of the moRECo project in collaboration with FHNW Muttenz (https://www.aramis.admin.ch/Grunddaten/?ProjectID=49236).

Table 4.11: Concentration of PCBs in a sample of solid residue from hydrothermally treated sewage sludge (digested).

PCBs	LOD	Concentration in sample	Concentration by P content
	ng/g	ng/g	g/t of P
CB 28	0.05	0.55	0.009
CB 52	0.05	0.55	0.009
CB 101	0.05	0.91	0.015
CB 138	0.05	0.89	0.014
CB 153	0.05	1.07	0.017
CB 180	0.05	0.39	0.006
∑ PCBs		4.34	**0.070**
MinRec limit			0.5

Table 4.12: Concentration of PAHs in a sample of solid residue from hydrothermally treated sewage sludge (digested).

PAHs	LOD	Concentration in sample	Concentration by P content
	ng/g	ng/g	g/t of P
Naphthalene	10.0	15.7	0.252
Acenaphthylene	1.0	2.0	0.031
Acenaphthene	2.1	2.9	0.046
Fluorene	0.7	5.3	0.085
Phenanthrene	2.1	44.3	0.712
Anthracene	0.8	7.6	0.123
Fluoranthene	1.3	56.8	0.912
Pyrene	1.1	36.6	0.588
Benzo (a) anthracene	0.3	20.6	0.331
Chrysene	0.4	43.0	0.692
Benzo (b) fluoranthene	2.5	41.2	0.662
Benzo (k) fluoranthene	0.7	16.5	0.266
Benzo (a) pyrene	0.8	23.6	0.380
Indeno (1,2,3-cd) pyrene	2.0	4.4	0.071
Dibenzo (a,h) anthracene	0.2	8.3	0.134
Benzo (g,h,i) perylene	1.3	29.4	0.472
∑ PAHs		358.1	**5.758**
MinRec limit			25

Regarding inorganic pollutants, the concentrations of cadmium, arsenic, mercury, nickel, zinc, chrome, lead and copper are below the MinRec requirements as well (Table 4.13). The same tests were done for the liquid phase after phosphorus extraction, and purification with ion exchange resins, resulting in total compliance with MinRec as well (Table 4.13). Therefore, we can confirm that the precipitates (P-based fertilizer) from this liquid phase will comply as well with the regulation.

Table 4.13: Concentration of inorganic pollutants in a solid residue sample and a purified leachate sample that must comply with MinRec.

	Limit value MinRec (mg/kg P)	Solid Residue %wt.	Solid Residue mg/kg P	Purified leachate mg/l	Purified leachate mg/kg P
Cadmium	25	<LOD	<LOD	<LOD	<LOD
Arsenic	100	0.0007	208	<LOD	<LOD
Mercury	2	0.0002	62	<LOD	<LOD
Nickel	500	0.0042	1310	0.017	15
Zinc	10000	0.0813	25347	<LOD	<LOD
Chrome	1000	0.0048	1487	0.017	15
Lead	500	<LOD	<LOD	0.117	104
Copper	3000	0.0489	15252	<LOD	<LOD
P		3.21		1121	

LOD for solid samples (ppm): Cd 1.015, As 12.6, Hg 4.325, Ni 1.59, Zn 2.185, Cr 0.068, Pb 8.8, Cu 1.6.
LOD for liquid samples is 0.5 mg/l for all elements except As which has a LOD of 0.5 μg/l.

4.4.1.5 Organic molecules in the final product

After leaching of the solids with diluted sulfuric acid, in average 9 wt.% of the carbon originally present in the solids is transferred to the leachate, then about 1 wt.% is trapped in the ion exchange column during purification and finally all carbon remaining in the clean leachate precipitates during the Struvite precipitation experiments. The concentration of carbon in the Struvite precipitates is 1.6 wt.% on average. Nonetheless, as stated in the previous report, XRD analysis confirmed that the presence of this carbon does not affect the crystallinity of the Struvite.

Regarding the nature of the organic molecules in the leachate, we previously demonstrated that the concentration of PCBs and PAHs in the purified leachate are below the limits of detection. Nonetheless, we observed that the total organic carbon (TOC) in the purified leachate is about 100 mg/l. Therefore, even though we have discarded that these organic molecules correspond to PCBs and PAHs, it is still interesting to identify them. We performed some preliminary liquid-liquid extractions using an organic solvent (hexane) and purified leachate. After extraction, the organic phase was analyzed using GC-MS but the results were not conclusive and only ethyl acetate (reliability of 90.5%) was found. On the other hand, we performed solid-liquid extractions using solid residues (before leaching) as the solid phase and organic solvents (hexane and toluene) as the liquid phase to identify organic molecules in the solid residues. The spectra obtained through GC-MS for all the extractions were very similar to each other. The main detected molecules were stigmastane, coprostane, cholestane and bisphenol (Figure 4.55)

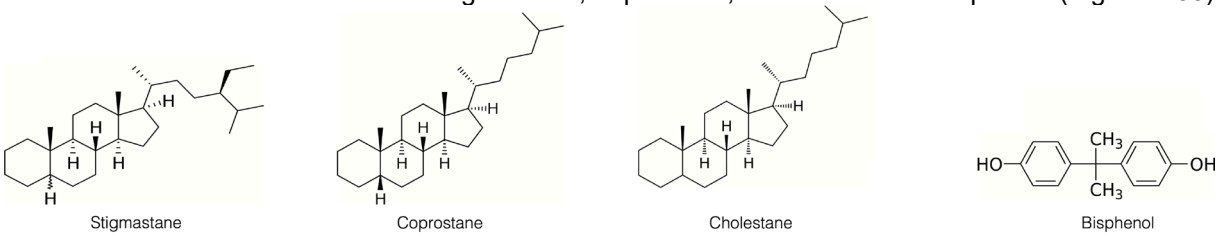


Figure 4.55: Structural formula of the main molecules found in the solid residues through solid-liquid extraction and GC-MS.

4.4.1.6 P-recovery experiments using calcined solid residue (ashes)

The solid residue was calcined at 900°C for 3 hours in order to transform it into ashes. The main difference in composition between the solid residue (before calcination) and the ashes is the volatile matter content (refer to Figures 4.51 and 4.56 for detailed composition before and after calcination). In fact, during calcination, volatile matter is burned resulting in the decrease of carbon content. For

instance, the calcined solids (ashes) contain 1.4 %wt. of carbon (vs 6 wt.% in the solids) which can be mostly attributed to carbonates which only decompose at temperatures above 900°C.

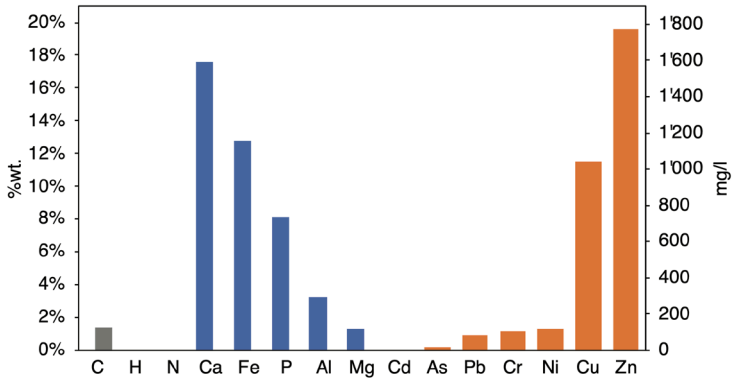


Figure 4.56: Composition (%wt in blue and gray, mg/kg in orange) of the calcined solid residue (ashes) before leaching.

The ashes were leached following the same protocol as for the solid residues (section 4.4.1.3i). Results show that the percentage of P recovered is very similar (around 80 wt.%. for the solids vs 83 wt.% for the ashes). Then, purification experiments were performed using ion exchange resins. In average, 82 wt.% of the P that was originally present in the raw leachate, was recovered in the purified leachate. For the rest of the elements, between 99 and 99.99 wt.%. were removed by the column (Figure 4.57).

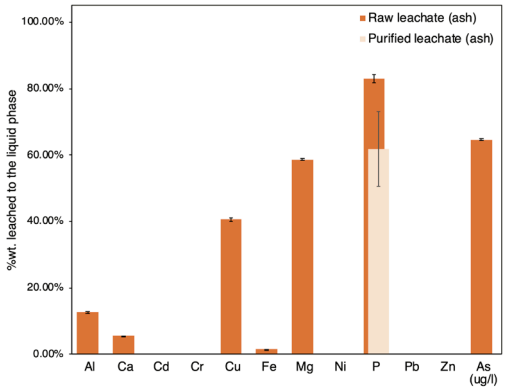


Figure 4.57: Average %wt. leached to the liquid phase from the solid before and after purification for both replicates.

Afterwards, we precipitated phosphorus as calcium phosphates (CaP) compounds and as Struvite using the purified leachates. The solid precipitates were analyzed by XRD in order to identify the crystalline phases formed. In the case of the CaP precipitation, we found that the crystalline phases were composed by 60% Brushite ($CaHPO_4$)$2H_2O$) and 40% calcium carbonate ($CaCO_3$) confirming that, when using ashes as feedstock, phosphorus precipitates as crystalline dicalcium phosphate dihydrate (Brushite). In the case of Struvite precipitation, the results confirmed that we were able as well to precipitate phosphorus as crystalline Struvite when using ashes. Moreover, ICP analysis of the purified leachate and waste liquid after both CaP and Struvite precipitations, confirmed that all the phosphorus in the purified leachate had precipitated.

The results confirm that the carbon present in the leachate, after leaching of hydrothermally treated sewage sludge solids, has an effect in the crystallinity of the CaP species precipitated but not in the crystallinity of Struvite.

4.4.2 Phosphorus recovery using solids from HydroPilot (100 kg/h)

The goal for the second part of WP5 was to apply the P-recovery method developed in section 4.4.1 to the solids produced by the HydroPilot unit when running campaigns using sewage sludge as a feedstock. Due to the numerous challenges faced to process sewage sludge with HydroPilot, only a small amount of usable solids were produced in August 2022. The work performed on these solids resulted in the following findings in relation with the goals set for the second part of WP5.

4.4.2.1 Comparison of the chemical composition of the solids from HydroPilot with that obtained with the lab-scale prototype

Solid residues from the experiments performed in the lab-scale prototype and HydroPilot were analyzed (TOC and elemental analysis through ICP) for comparison. The main difference between the solids was found in the TOC content. Solids from HydroPilot contained, on average, 56% less TOC than those extracted from the lab-scale unit. This difference reaches 68% if compared to the solids left inside the salt separator of HydroPilot and that were extracted after the campaign was completed and hence had a longer residence time. This difference between lab-scale and HydroPilot solids can be explained by the fact that the lab-scale unit does not have a heat exchanger where the feedstock is preheated. Hence, the residence time of sewage sludge under supercritical water conditions is lower than in HydroPilot. In addition, the salt separator entry point was placed too close to the extraction point and consequently, some unconverted sewage sludge was being extracted together with the converted solid residues. In fact, after modification of the lab-scale salt separator reactor, the difference on TOC dropped to 10-15%. A lower TOC concentration in the solids means that less organic carbon will be transferred to the leachate and hence the purification process to remove it will be easier.

Concerning the elemental analysis, the same major elements were found in both solid samples (P, Fe, Al, S, Ca, Mg, K, Na) without significant quantitative differences for most of them if we take into account the heterogeneous nature of sewage sludge. Notably, the P content was around 7% wt. for both samples. Only sulfur was remarkably lower (76% lower) for solids from HydroPilot which could be attributed to the hypothesis that sulfur can react with the material of the walls of the salt separator (Inconel, high Ni content) at supercritical conditions, assuming that most sulfur is in a reduced form in the feed. Drawing any sulfur mass balance to investigate this hypothesis is however not possible. Another explanation may lie in the difference in brine extraction and salt separation efficiencies between the setups leading to extraction efficiency being particle size dependent and then sulfur sensitive if the S concentration in the particles varying with their size.

4.4.2.2 Extracting phosphorus from the solids produced with HydroPilot

Similarly, as it was done for the solids from the lab-scale prototype (section 4.4.1.3.i), phosphorus was extracted from the solids from HydroPilot using acid leaching with similar results. Recovery can reach 100% at low pH (0-1). Hydrochloric and Sulfuric acid were tested with similar results. Nonetheless, sulfuric acid remains the acid of choice due to the corrosion risk hydrochloric acid poses. As observed with solids from the lab scale prototype, when performing the extraction experiments with the solids from HydroPilot not only phosphorus is leached but also heavy metals, minerals and organic compounds. Hence, as anticipated in previous experiments, the leachate needs to be purified.

Scale-up and further optimization of the leaching process is performed within the moRECo project in collaboration with FHNW Muttenz and with the support of FOEN.

4.4.2.3 Leachate purification

Purification of the leachate is a crucial step to obtain a commercially viable phosphoric acid. Several purification methods are available for the removal of cations and heavy metals such as ion exchange (successfully tested with solids from the lab-scale prototype) and membrane filtration. Due to the delays within the HydroPilot project, purification tests using solids from HydroPilot have not been performed within this project. Nonetheless, preliminary nanofiltration tests within the moRECo project have shown promising results. Further investigation of the purification of the leachate, scale-up and characterization of the product to fulfill the legal standards for its commercialization are performed within the moRECo project.

4.4.3 TOC removal strategy

As opposed to the ashes after incineration, the solids after HTG contain organic carbon. Even though the solids from HydroPilot contain less organic carbon than those from the lab-scale prototype, part of this organic carbon (1-5%) is still leached during acid leaching. Removal of this organic carbon using membrane filtration will also be explored within the moRECo project.

Nonetheless, after separation of the leachate from the remaining leached solids (cake) different routes have been explored for the valorization of this stream. The most promising one being its reuse within cement manufacturing processes. Another option for safe disposal, instead of valorization, would be landfilling as type D and E solids if compliant with maximum TOC content according to ADWO regulation. In both cases (valorization in cement manufacturing or safe disposal) organic carbon on this stream should also be limited.

To this end, we carried out a viability study with FHNW Muttenz at the beginning of 2021 (with solids from the lab-scale prototype) to test removal of organic carbon before phosphorus extraction with the goal of limiting both the organic carbon in the leachate to facilitate downstream purification and in the cake for its further utilization and compliance with cement manufacturing requirements. The main conclusions from the study were the following:

- Only the most recalcitrant fraction of organics is expected to remain in the solids since the solid residue after HTG has undergone harsh conditions (i.e. anaerobic digestion, and extraction at supercritical conditions). Although this fraction is expected to be stable, the oxidative processes investigated in this exploratory work were capable of eliminating residual TOC in the solids after hydrothermal gasification.
- Among the investigated processes, oxidation by the means of hydrogen peroxide is the most promising process for different reasons: (1) it achieves the highest TOC elimination (i.e. 44 %), (2) limited additional CAPEX costs are expected (i.e. it can be performed in the same reactor as the leaching for nutrient recovery) on the contrary to ozone; and lower OPEX compared to ozone, Fenton oxidation, and Fe(II)-activated persulfate which needs peroxide and Fe(II).
- Furthermore, it was confirmed in this study that peroxide oxidation is also capable of degrading TOC from deposits from HTG (extracted after stopping the lab-scale unit and opening the salt separator) which contains lower amounts of TOC (5-18%). However, when peroxide oxidation is applied for the treatment of these solids, the efficiency of the process decreases by 52% on average compared to the same conditions applied for the solid residues containing higher amounts of TOC (~23%). It is hypothesized that the less TOC remaining in the solid after extraction at

supercritical conditions, the more resistant to oxidant those organics are. Hence, it is expected that the efficiency of TOC oxidation by H_2O_2 oxidation depends on the reactivity of the carbon species in the solids.

- However, these results indicate that, at the highest H_2O_2 dosage tested in this project, H_2O_2 oxidation alone will not be sufficient to comply with ADWO for safe disposal in type D and E landfill. Nonetheless, we also report that the plateau of TOC elimination in the solids by H_2O_2 may not have been reached yet. Therefore, higher concentrations of H_2O_2 should be tested in the future to demonstrate whether higher elimination is technically possible.

4.4.4 Estimation of the P-recovery costs (CAPEX and OPEX) for an HTG plant treating 6 t/h of sewage sludge

i. Introduction

In Q1 2021, we performed an assessment with the collaboration of a leading cement manufacturer in Switzerland, for the complete integration of the cHTG technology within their manufacturing process.

Cement industry is responsible for about 7% of the total CO_2 emissions in Switzerland whose 34% come from the fuels used to heat the burners and 66% from the CO_2 release from the limestone. Reducing these emissions is therefore a major ecological challenge for this industry. As Switzerland is among the countries with the highest CO_2 tax in the world (101.5 USD/ton of CO_2), there is also a strong economic motivation.

In order to achieve this objective of CO_2 emissions reduction, the following steps were identified by cement industry:

- increasing energy efficiency in the use of thermal and electrical energy
- reducing the proportion of clinker, the intermediate product burned in cement, by using other materials
- substituting primary fossil fuels by renewable fuels

In addition, by 2026 Switzerland will be the first country to establish a strict regulation regarding phosphorus recovery from sewage sludge and slaughterhouse waste, as described in the Swiss ordinance on the avoidance and the disposal of waste (ADWO). This implies that cement manufacturers need to find a solution to recover phosphorus before or after using it as fuel.

As shown in Figure 4.58, for this case study, the cement plant requires a significant amount of energy for heating the rotary kiln (33 MW) and the calciner (43 MW). For heating both burners, a mix of several materials are used (e.g. coal, tires, plastic, sewage sludge, bone meal, wood chips).

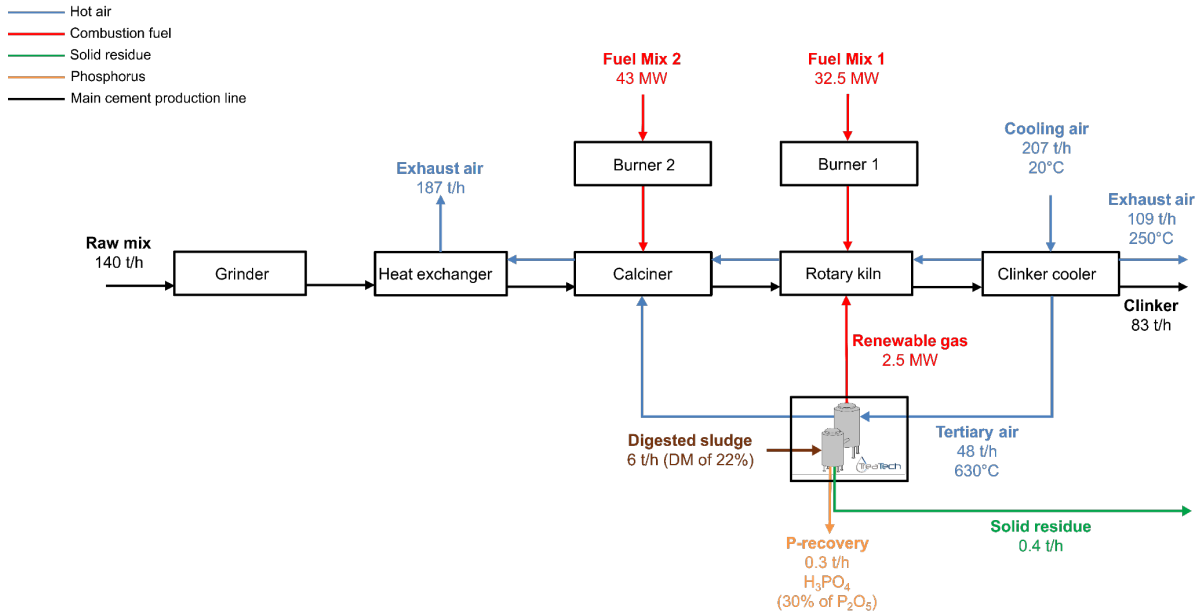


Figure 4.58: Simplified overview of the cement production process with cHTG integration. Fuel mix calculated based on numbers from 2019 provided by the cement manufacturer.

In this study, several synergies were identified between the two processes:

- The available mass flow and temperature level of the tertiary air (T = 630°C), taken from the clinker cooler, is well suited for heating the cHTG process
- The renewable gas produced by the cHTG process can be used on site to substitute some of the natural gas (NG) for the rotary kiln without a need for prior gas upgrading
- Thanks to the cHTG process, more than 80% of phosphorus can be recovered and valorized into phosphoric acid or fertilizers. In absence of P-recovery at the cement plant, sewage as well as slaughterhouse waste could not be used anymore by 2026.

As a result of integrating hydrothermal gasification in their process, a cHTG plant treating 6 tons/h of sewage sludge (dry matter of 22%) would lead to a renewable gas production of 2.5 MW thermal power, which corresponds to about 7% of the total power of rotary kiln burner. Since this burner is not relying on a high purity of natural gas, the renewable gas can be burned without prior upgrading. Replacing the natural gas with renewable gas would reduce the purchase of fossil gas by saving about USD 500'000 per year.
Integrating a P-recovery process directly at the cement plant is beneficial for both the cHTG and cement plants. Besides allowing the cement plant to fulfill the new regulation, the use of the tertiary air for concentrating the phosphoric acid (one of the possible phosphorus products) and the valorization of the solid residue after phosphorus extraction in the cement production would reduce the total operating costs of the cHTG process by 60%.

In fact, TreaTech's P-recovery process allows phosphorus to be recovered from hydrothermally treated sewage sludge in high yield (above 80%). Due to current regulation, phosphorus-based products obtained from recycled waste are to be used in fertilizers production. For this purpose, two valorization scenarios have been selected and investigated, scenario A being in the form of struvite and scenario B being in the form of phosphoric acid (PA) (refer to Figure 4.59 for details).

For both scenarios, the feedstock represents a flow of 6000 kg/h of digested SS and produces 1217 kg/h of hydrothermally treated wet solid (WS). WS are rich in P (36 kg/h) and are further treated in TreaTech's P- recovery process to obtain phosphorus-derivative products via the two possible selected valorization routes. After P-recovery, 29 kg/h of phosphorus are recovered in the form of Struvite or phosphoric acid. Additionally, 1126 kg/h of final solid residue (cake after leaching, 40% DM), to be re-used in the cement production or landfilled, are produced. Finally, Scenario A and B generate 5350 kg/h of permeate water and 4800 kg/h of evaporated water respectively. For both scenarios, permeate water and evaporated water is recovered and re-used in the leaching step.

ii. Economic analysis for the implementation of a P-recovery unit treating the solid residue from a cHTG unit processing 6 t/h of digested sewage sludge

The CAPEX and OPEX estimations were performed in collaboration with Afry Schweiz AG. The costs are estimated for a plant treating 6 t/h of sewage sludge corresponding to a P-Recovery plant treating 1.2 t/h of WS from cHTG. In the following sections, CAPEX and OPEX are presented and discussed for scenario A (struvite production) and scenario B (PA production). Note that prices per ton basis are expressed per ton of wet sludge (22% DM).

The economic study was performed based on the following assumptions:

- TreaTech's P-recovery process will be integrated in a cement plant in Switzerland
- The residual solids are valorized in the cement production instead of being landfilled
- 70% of the deionized (DI) water needed for leaching and purification processes is recycled from the permeate (Struvite) / evaporate (PA)
- Product revenues are defined as product sales according to the product market price found for Struvite (> 95%) and phosphoric acid (54% P_2O_5) at the time the study was performed (Q1 2021).

SCENARIO A

The total capital investment is given in Table 4.14. It includes the direct costs, indirect costs and the working capital investment and give a total of 4.4 MCHF or 91 CHF/t_{SS}.

In the case of struvite production, the major part of the costs is due to direct costs more specifically to the purchase of equipment (1.1 MCHF) and installation costs (0.4 MCHF). The approximate costs of equipment as tanks, dosing units, press filters and centrifuge are mainly based on providers' quotes. The land's price is set to zero due to the assumption of integrating the process in an existing site.

The main expenses included in the indirect cost are equally allocated to the construction (0.4 MCHF), contingency budget (0.4 MCHF), engineering and supervision (0.4 MCHF).

Table 4.14: Fixed Capital Investment for TreaTech's P-Recovery process for scenario A (struvite) ±30% for a plant treating 6t/h of SS, corresponding to 1.2 t/h of WS from cHTG.

	Ratio Factors (%) used in the Economy Analysis	CHF
Direct Costs		
Major Purchased Equipment	100%	1'114'950
Installation Cost	39%	435'000
Instrumentation and Control	26%	290'000

Piping	31%	346’000
Electrical	10%	112’000
Buildings	18%	201’000
Service Facilities	25%	279'000
Total Direct Costs		2’777’950
Indirect Costs		
Engineering and Supervision	35%	391’000
Construction Expenses	40%	446’000
Contractor's Fee	5%	181’000
Contingency	10%	362’000
Total Indirect Costs		1’380’000
Total Fixed Capital Investment		**4’157’950**
Working Capital Investment	5%	208’000
Total Capital Investment		**4’365’950**
Price per ton of wet sludge @ 22% DM		**91**

The total operating expenditure (OPEX) includes the chemical consumption, waste disposal, amortization, insurance, staff, maintenance and power consumption.

Regarding the chemical consumption, the assumed recycled DI water is provided by the filtrate water after precipitation and centrifugation of struvite. The process requires for the treatment (incl. leaching, purification and precipitation) of 9600 t/y of WS and producing 1900 t/y of struvite, an annual fresh input of 3 kt/year of concentrated acid (H_2SO_4 and HCl), 21 kt/year of DI water and 5 400 t/year of precipitation agents.

Power is essentially needed in the centrifugation step of the process. The annual power consumption to produce 1 900 t/y of struvite is estimated between 200 and 430 MWh. Taking into account an average of 315 MWh, the power consumption per ton of wet solid is 33 kWh/t_{WS}.

The total operating expenditure (OPEX) is given in detail in Table 4.15 that depicts the difference in costs between reusing the residual solids in the cement industry or disposing them at a landfill site. The use of the residual solids, after P-recovery results in 0.56 MCHF savings per year and gives a total operating costs of 2.76 MCHF/y or 57 CHF/tSS/y.

The biggest cost corresponds notably to the purchase of chemicals (67%) followed by the waste disposal expenses (16%) and the staff costs (8%).

Taking into account a market sale price of 0.25 CHF/kg (Chembid Q1 2021), selling the Struvite would generate 462'284 CHF/year of revenues that would cover 17% of the costs of operation.

Table 4.15: Detailed operation expenditure for scenario A (struvite) for a plant treating 6t/h of SS, corresponding to 1.2 t/h of WS from cHTG ±30%. All costs are in CHF.

	CHF/y	
	Reuse of solids by the cement producer	**Landfill of solids**
Chemicals	1'881'621	1'881'621
Waste disposal	439'100	1'027'227
Amortization	62'676	62'676
Maintenance	104'000	104'000
Insurance	26'000	26'000
Staff	240'000	240'000
Power	34'350	34'350
Total costs	**2'757'286**	**3'345'413**
Cost per ton of wet sludge @ 22% DM	**57**	**70**

SCENARIO B

The total capital investment is given in detail in Table 4.16. It includes the direct costs, indirect costs and the working capital investment and adds up to 4.9 MCHF or 103 MCHF/t_{SS}.
Similar to investment costs for scenario A (struvite), in scenario B (PA), the major part of the costs is dedicated to the purchase of equipment (1.3 MCHF) and installation costs (0.5 MCHF) for the direct costs and the construction (0.5 MCHF), contingency budget (0.4 MCHF) and engineering and supervision (0.4 MCHF) for the indirect costs. The approximate costs of equipment as tanks, the dosing unit, press filters and the vacuum evaporator are mainly based on providers quotes. Again, the land's price is set to zero.

Table 4.16: Fixed Capital Investment for TreaTech's P-Recovery process for scenario B (PA) for a plant treating 6 t/h of SS corresponding to 1.2 t/h of WS from cHTG ± 30%.

	Ratio Factors (%) used in the Economy Analysis	CHF
Direct Costs		
Major Purchased Equipment	100%	1'260'900
Installation Cost	39%	492'000
Instrumentation and Control	26%	328'000
Piping	31%	391'000
Electrical	10%	127'000

Buildings	18%	227’000
Service Facilities	25%	316’000
Total Direct Costs		3’141’900
Indirect Costs		
Engineering and Supervision	35%	442’000
Construction Expenses	40%	505’000
Contractor's Fee	5%	205’000
Contingency	10%	409’000
Total Indirect Costs		1’561’000
Total Fixed Capital Investment		**4’702’900**
Working Capital Investment	5%	236’000
Total Capital Investment		**4’938’900**
Price per ton of wet sludge @ 22% DM		**103**

From the total 4.9 MCHF, purchasing the equipment represents the higher cost (25%) followed by the installation cost (10%), the construction expenses (10%) and the engineering and supervision costs (9%).

The content of the OPEX costs includes the chemical consumption, waste disposal, amortization, insurance, staff, maintenance and power consumption. Regarding chemical consumption, the considered recycled DI water comes from the evaporated water during the concentration of PA. For the treatment (incl. leaching and purification) of 9600 t/y of wet solid and producing 1890 t/y of phosphoric acid 54% (P2O5), an annual fresh input of 3 kt/year of concentrated acid and 21 kt/year of DI water is needed.

Power is essentially needed for the energy intensive process of water evaporation. The overall power consumption to produce 1980 t/y of PA 54% (P_2O_5) is estimated between 10 and 20 GWh (thermal and electrical). Taking into account an average of 15 GWh, the power consumption per ton of wet solid is 1875 kWh/tWS.

The thermal energy needed for evaporation could be in the form of hot water (80°C), steam, thermal oil or 30% ethylene glycol. It is important to note that the utilization of thermal energy from the cement production plant would notably decrease the power consumption costs by 80%

The total operating expenditure (OPEX) is given in detail in Table 4.17. The total operating expenditure including the reuse of solids and without heat integration adds up to 1.77 MCHF/y or 37 CHF/tSS/y.

Table 4.17 also highlights the difference in costs between reusing the solids in the cement industry or disposing them at a landfill site. The use of the residual solids, after P-recovery, in cement manufacturing results in 0.59 MCHF savings per year.

Taking into account a market sale price of 1 CHF/kg (Chembid Q1 2021), selling the phosphoric acid would generate 1'980'000 CHF/year of revenues that would cover 100% of the costs of operation (when the solids are reused) and generate additional benefits.

Table 4.17: Detailed operation expenditure for scenario B (PA) for a plant treating 6 t/h of SS, corresponding to 1.2 t/h of WS from cHTG ±30%. All costs are in CHF.

	CHF/y	
	Reuse of solids by the cement producer	**Disposal of solids (type D)**
Chemicals	511'205	511'205
Waste disposal	439'100	1'027'227
Amortization	59'634	59'634
Maintenance	98'800	98'800
Insurance	24'700	24'700
Staff	240'000	240'000
Power (electrical + thermal)	394'525	394'525
Total costs	**1'773'489**	**2'361'616**
Cost per ton of wet sludge @ 22% DM	**37**	**49**

In this sub-scenario, with reuse of solids but without heat integration, the largest cost corresponds to the purchase of chemicals (29%) followed by waste disposal (26%) and power expenses (23%). The latter are mainly due to thermal energy needed for evaporation, which accounts to 0.39 MCHF/year.

On the other hand, in the sub-scenario in which solids are reused and the thermal energy needed for evaporation is integrated from the excess heat in the cement production process, the benefits would increase 14%. In this case, costs associated with power consumption decrease remarkably to 80%. The highest cost is associated with the purchase of chemicals (35%) followed by the waste disposal costs (30%).

iii. Possible optimizations

A fully dedicated project (moRECo) on optimizing and scaling up TreaTech's P-recovery process is taking place in collaboration with FHNW Muttenz and with the support of FOEN. The results of the project will allow us to address questions such as the influence of the carbon concentration in the leachate on the quality of the final product as well as to determine more accurately the costs of the P-recovery process.

One example of a parameter that could directly influence cost when optimized is the liquid to solid ratio during the leaching process, which is directly related to the amount of DI water needed. A reduction of the DI water needed will result in a leachate with higher phosphoric acid concentration and thus, in the case of phosphoric acid production, less water will need to be evaporated to reach the desired concentration. As an example, if the amount of DI water needed is reduced by 30% the OPEX (without

taking into account the revenues) would decrease from 1.77 MCHF/y to 1.59 MCHF/y meaning that we could save 180 kCHF/y.

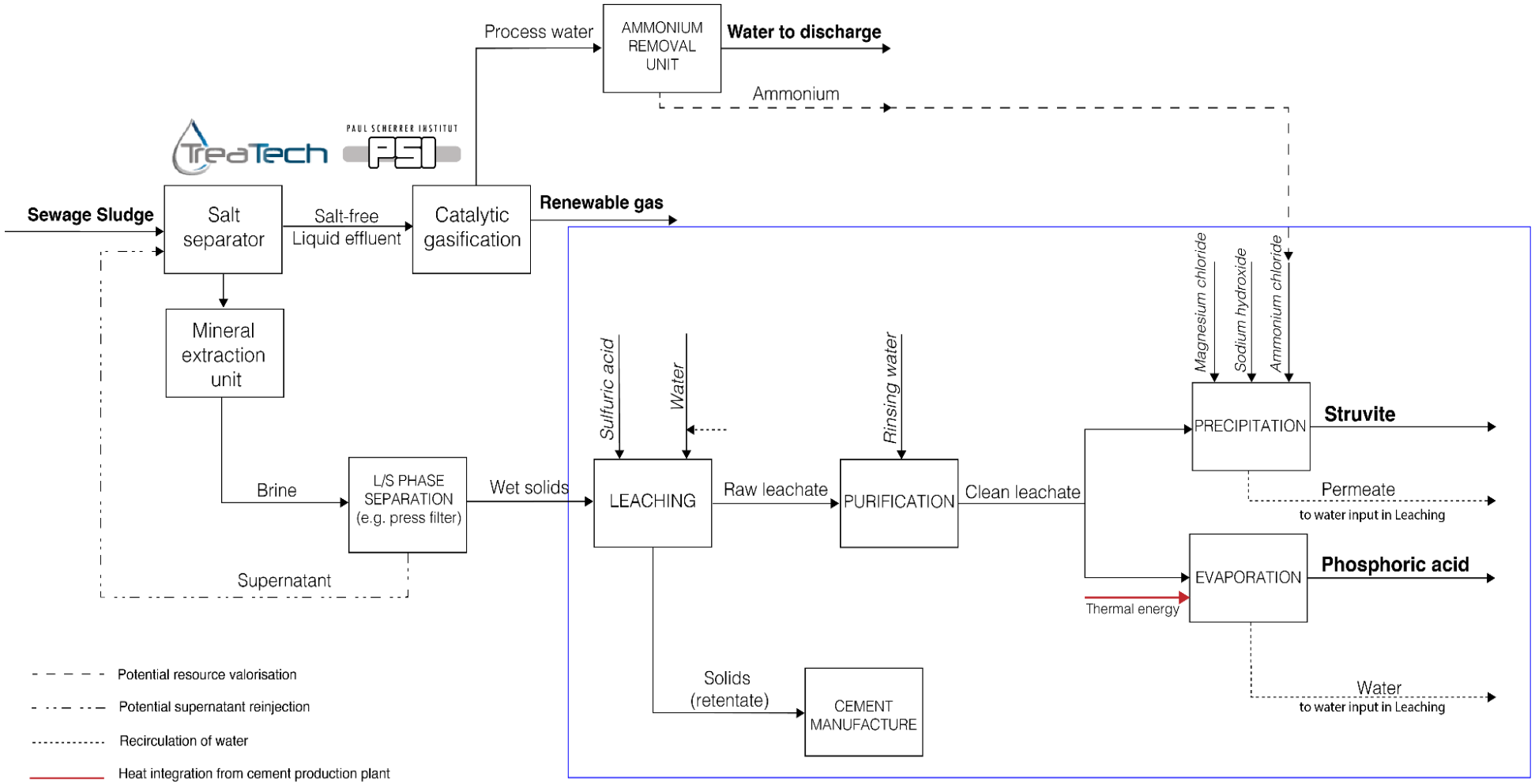


Figure 4.59: Block diagram of the P-recovery process with two different valorization routes: Struvite precipitation and concentration of diluted phosphoric acid.

4.4.5 Conclusions

The tasks performed within WP5 revealed that high purity crystalline Struvite can be produced from phosphorus extracted from the solids of cHTG confirming that a solid P-based fertilizer can be produced from hydrothermally treated sewage sludge. In the case of calcium phosphates, no crystalline forms were found. Nonetheless, when the feedstock is calcined residue (ashes) with no organic carbon, both crystalline struvite and dicalcium phosphate can be identified. We hypothesize that, in the case of hydrothermally treated sewage sludge (not calcined), phosphorus in the liquid phase might be attached to organic functional groups and that, calcium cations (from calcium hydroxide) are unable to precipitate phosphorus and only precipitate sulphates in the form of bassanite and/or gypsum.

Regarding regulation, the analysis performed are very positive since our purified leachate complies with MinRec for organic and inorganic pollutants (pending PCDD/F).

Moreover, the viability study carried to test removal of organic carbon before phosphorus extraction with the goal of limiting both the organic carbon in the leachate and in the cake showed that the oxidative processes investigated were capable of eliminating residual TOC in the solids after hydrothermal gasification. Among the investigated processes, oxidation by the means of hydrogen peroxide is the most promising process since it achieves the highest TOC elimination (i.e. 44 %), and it implies lower additional CAPEX costs.

Finally, the results from the economic study showed that, in an annual basis, a cHTG unit integrated in a cement manufacturing site and treating 48000 tons of digested sewage sludge (22% dry matter) would produce 9736 tons of wet solids from which 232 tons of phosphorus would be recovered. The phosphorus would then be transformed into 1848 tons of Struvite (>95% purity) with an estimated CAPEX of 91 CHF/tSS and OPEX of 57 CHF/tSS; or 1900 tons of phosphoric acid (54% P_2O_5) with an estimated CAPEX of 103 CHF/tSS and OPEX of 37 CHF/tSS. Taking into account the revenues from selling the products, the OPEX for Struvite would decrease to 48 CHF/tSS and the OPEX for phosphoric acid would be 100% covered with additional benefits of 4 CHF/tSS.

4.5 Design of an industrial unit (WP 6)

The design of an industrial unit has been the target of ExerGo's activities. In collaboration with PSI and TreaTech, the partners have focused on three key development activities:

1. Implementation of a numerical model of the HydroPilot setup, including validation using data acquisition from the pilot plant
2. Use of the numerical model developed in (1) in combination with an optimization algorithm to generate optimized configurations (geometry, size) of the heat recovery heat exchangers. These routines allow to highlight the techno-economic trade-offs, propose optimal tubes positioning and configurations, also taking into account external energy hot sources (utility) used to fulfill the high temperature energy needs of the salt separator (different temperature-enthalpy profiles).This approach provides a method to evaluate alternative solutions based on cost-efficiency and performance indicators.
3. Development of a simple computer tool for the fast screening of industrial business cases. The less complex, more graphical approach allows to consider simplifications with respect to numerical models developed in (1) and (2) and ease the iterative value proposition between the technology provider (TreaTech) and their future customers.

ExerGo and project partners have organized the workflow and set up activities involving students from EPFL, with the reference contact being Prof. François Maréchal, and students from PSI and FHNW where Prof. Frédéric Vogel has teaching activities.

Exchanges with industrial partners TreaTech, Kasag and Afry allowed to take into account implementation limitations and economic constraints imposed by industry for future technology scale-up.

The design of an industrial size unit is part of TreaTech's roadmap for the next two years. However, before TreaTech can design such a unit, the technology needs to be validated in real environment. This is why a demonstration unit (100-200 kg/h) that will run continuously at a client site will be installed in Switzerland next year. Hence, scale-up parameters of an industrial cHTG unit could not be provided within the scope of the HydroPilot project.

WP 6.1 : Implementation and validation of a numerical model of the industrial unit.

WP6.1 allowed the development of new numerical models and the adaptation of the existing ones concerning the supercritical gasification process. The thermodynamic process modelling task was organized in collaboration with an EPFL student (Tim Dosso) and a civil service intern at FHNW (Nicola Hagger).

During the modeling activities, particular attention was given to heat transfer mechanisms and waste-to-fuel conversion rates. The objective being to adapt the physico-chemical relationships to the specific geometry of the pilot and to derive from it future design specifications with particular reference to heat transfer phenomena.

For this WP6.1, PSI supervised the civil service project of Nicola Hagger, who developed a thermodynamic model for the calculation of the heat recovery heat exchanger of the HydroPilot unit (Fig. 4.60). Several modelling approaches and solving strategies were defined and are presented in the report of Nicola Hagger [16]. The results generated by these models were compared and showed a dependency of the target temperature used for the comparison.

Based on the data validation on HydroPilot, it appears that with the tested conditions the most appropriate correlation to estimate the outlet temperature of the supercritical flow leaving the heat recovery heat exchanger is correlation 6 shown in equation 6 in section 4.3.1.

ExerGo supervised the EPFL student Tim Dosso, who contributed in a semester project to the development of a numerical model for the energy modelling of the salt-separator unit where hot air is cooled down to provide the process with the amount of energy required to sustain the salt separation process.

The model accounts for the changing physical properties along the flow path. An equation-oriented approach was implemented in Python and validated during periodic exchanges between the partners and ExerGo. Similarly to the approach adopted for the heat recovery heat exchanger, several correlations for the estimation of the heat transfer coefficient of the supercritical fluid where implemented and tested, showing the need to validate the model and identify the most accurate correlation for given operating conditions (pressure, composition of the feedstock, geometry and flow velocities).

This model was extended and improved by Nicola Hagger, who also performed an integration of such simulation package with an existing publicly available multi-objective optimization package (PyMoo).

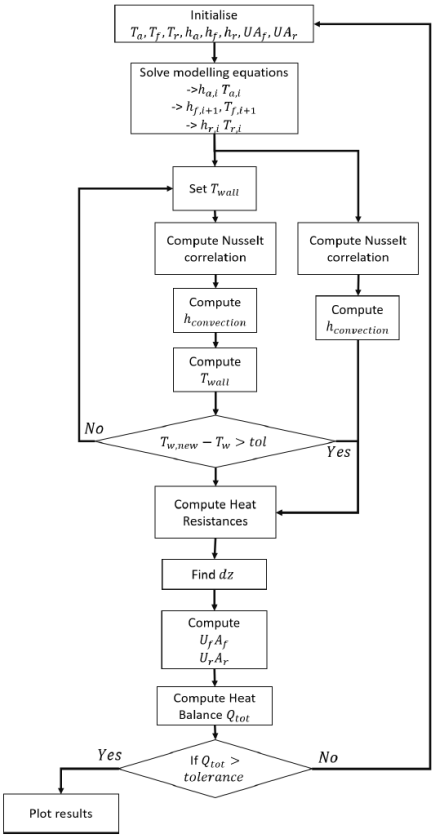


Figure 4.60: Flowchart of the HydroPilot heat recovery heat exchanger numerical model

WP 6.2 : Development of an optimization model for the design of industrialized units.

Activities in WP6.2 have allowed to link numerical models developed for WP6.1 with an optimization framework.

Initially, the infrastructure approach proposed by Grossmann [26] and the corresponding SYNHEAT superstructure was implemented and tested without the need of including the detail numerical models. This approach was selected as it allows to automatically generate optimal heat exchange matches between a given set of hot/cold streams with pre-defined flowrates, target temperatures, heat transfer coefficients as well as approach temperature difference bounds (Fig. 4.61). Such approach allows also taking into account forbidden/restricted matches between hot/cold streams, making it a reference model also for the process design of industrial units. Tests performed showed using the student version of the optimization software AMPL allowed to identify the bottleneck of such approach, showing that the use of the Synheat superstructure in presence of non-linear temperature-enthalpy profiles (supercritical heating/cooling) leads to a numerical complexity of the model that is difficult to handle without the use of parallel calculation and supercomputers. The solution found to avoid computational complexity was to pre-assign the matches

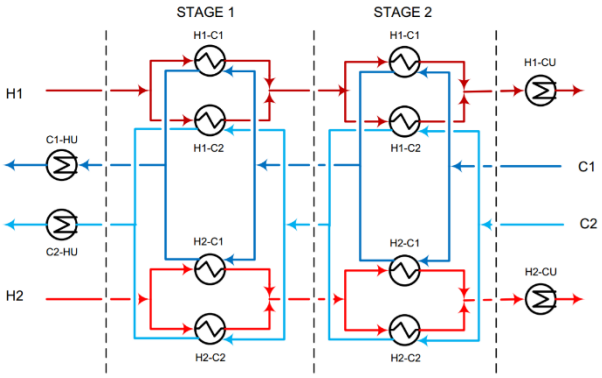
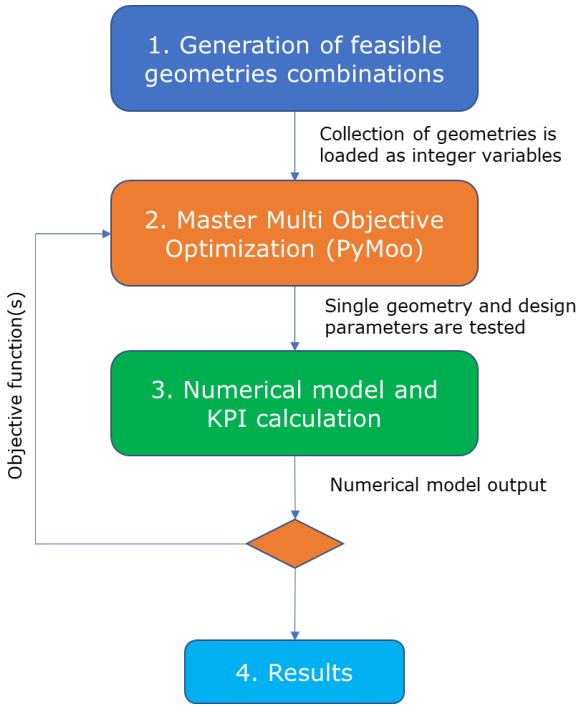


Figure 4.61: Synheat superstructure representation for two hot and two cold streams and heating/cooling utilities [26]

between hot/cold streams with non-linear temperature enthalpy profiles (feedstock heating and water gas cooling). The tested configurations were thus easier to solve using the simplified superstructure approach, and the resulting model will be used in future to assess future configurations of the supercritical gasification system (e.g. industrial integration with other existing processes).



It was agreed between partners to modify the objectives of WP 6.2 and to mainly focus on the optimized design of the heat recovery heat exchanger (two supercritical fluids) and the salt separator. The original approach of using numerical models in combination with optimization algorithm was kept as proposed in the previous project intermediate report.

The models developed for WP6.1 were modified to be integrated with the Python Multi Objective optimization platform (PyMOO; Fig. 4.62). This choice allow to profit from an open source tool that is supported by a large community of optimization problem experts, which reduces the risk to experience programming issues and numerical problems during the resolution of the optimization problem.

Figure 4.62: Simplified flowchart of the multi objective optimization framework

WP 6.3 Determination of techno-economic trade-offs: generation using optimization of best geometries and utility integration with corresponding cost-efficiency performance indicators.

During WP6.3 sensitivity analysis and optimization were used to define the design optimization problem of an industrial unit.

The use of PyMOO in combination with the models developed during the project made it possible to define a semi-automated methodology for calculating the best plant configurations in terms of equipment geometry and footprint. In order to account for realistic geometries and system configurations, the model is fed with industry-validated parameters (e.g only market available and certified stainless steel pipes specifications are considered).

Results of the optimization problems tested and the corresponding results can be found in [16].

It is important to mention that the considered modeling technique will make it possible in the future to update the numerical models used, as well as the input data concerning the standard dimensions of the options linked to certain plant components (pipe diameters and lengths, materials and their thermal properties, etc.) for the analysis of possible options can be improved. The methodology that has been defined up to this point will use the models and methods developed for WP 6.1 and WP 6.2 and use them as a subroutines in the multi-objective optimization framework here proposed. The industrial plant design will be automatically generated including a set of Pareto trade-off solutions with respect to conflicting objectives (e.g. plant efficiency vs investment costs).

WP 6.4: Development of a user-friendly computer tool for the fast screening of industrial business cases

The object of WP6.4 is to provide TreaTech with a fast screening tool to quickly estimate techno-economic trade-offs and system key performance indicators. Such an instrument will be used by the TreaTech technical sales and integration team during first contacts with technology adopters and customers. Given few input data such as composition and flow of the feedstock and utility integration options, the tool would allow to visualize economic and energy indicators of a pre-defined set of plant configurations. For the gas composition estimation, it was not possible to consider any correlations, and the numerical software Belsim Vali was integrated to the Python numerical model. This particular aspect of the solving strategy should be improved in future.

The exchange of information with the industrial partners KASAG AG and Afry allowed to define internal economic parameters and aligned on a shared database for equipment cost. The tool was implemented during the semester project of the EPFL student Alfonso Villegas, who translated the specifications and exchanges between partners into a Python interface which includes a scalable cost model for full-scale plant costs.

The developed approach allows to generate plant configurations and provide graphical outputs in the form of parallel coordinates plotting of KPIs, and Sankey type costing specifications, detailing the cost of each system subsystem.

Parallel coordinates plot allow to quickly analyze multiple configurations with respect to technical, energy and financial performance indicators (see Example in Figure 4.63)

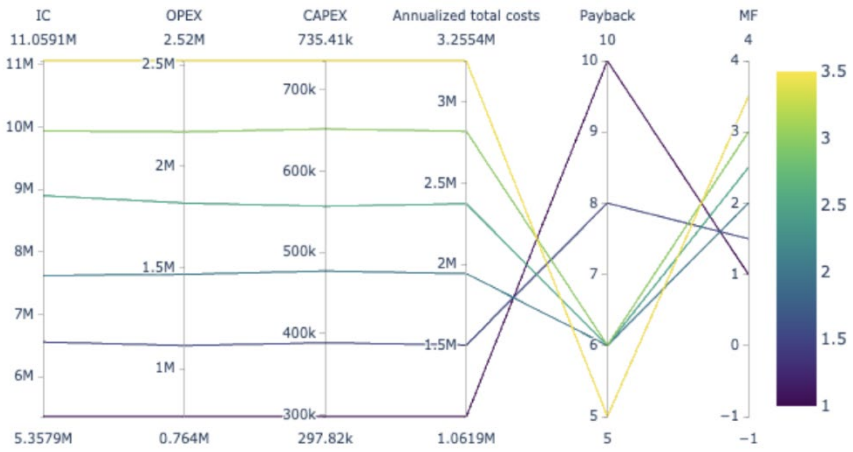


Figure 4.63: Output of the fast screening tool: comparison of KPI for multiple solutions using parallel coordinates visualization, where every line corresponds to a system configuration)

For each system configuration, a Sankey diagram for CAPEX and OPEX is produced to help the user identifying the cost drivers (see Example in Figure 4.64)

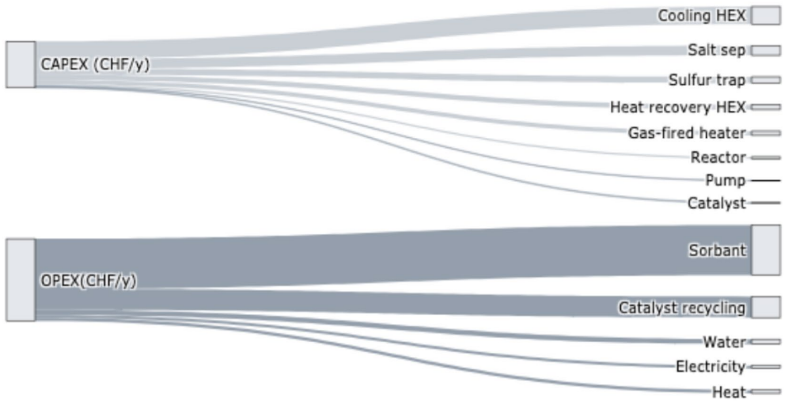


Figure 4.64: Example of CAPEX and OPEX Sankey diagrams generated by the fast screening tool, for a given system configuration

During the industrialization path of the technology, TreaTech and its business partners will be able in future to keep updating the economic and technical parameters that are internally used by the tool to generate such results themselves.

4.6 Life Cycle Assessment of HTG of sewage sludge including P-recovery

This section was adapted from Reference [27], where the full study can be found.

The environmental impact of the PSI TreaTech process was assessed by means of a life cycle assessment analysis. The procedure for preparing a life cycle assessment can be divided into the following steps:

- Determining the target system, setting the framework conditions and choosing a functional unit
  - 100 kg of digested sludge with 20% dry matter (DS) was chosen as the functional unit. The elemental composition of the digested sludge was given.
- Identify relevant material and energy flows, as well as other impacts
- Create a life cycle inventory from the above information
- Determine the effects on the environment with the impact balance sheet
- Interpretation or evaluation of the life cycle inventory
  - The life cycle assessment methods used were the IPCC 100a 2013 and the Ecological Scarcity 2013 method
- Elaboration of optimizations

For the comparison with alternative technologies, different methods were first evaluated and then selected for comparison using defined criteria. Thereby the following processes were selected for comparison: the EuPhoRe, PyroPhos and the Phos4Life process. A life cycle assessment was also prepared for these processes and compared with that of the PSI TreaTech process.

Input parameters

A summary of the input parameters used in the LCA is given in Table 4.18.

Table 4.18. Input parameters and main assumptions used for the reference model of the cHTG process including P-recovery [27]. The footnotes refer to reference [27].

Parameter	Werte
Edukt	Modellschlamm
TS-Gehalt [%]	0.2
Material Anlage	NiCr22Mo9Nb
Gewicht Anlage [kg] **1)**	30000.00
Durchsatz Anlage[kg/h]	4400
Leerlauf Reinigung pro Jahr	100
Betriebsstunden pro Jahr [h/a]	7500
Lebensdauer Anlage	15
Anzahl Reaktoren Schwefelfalle	2
Anzahl Reaktoren Katalysator	1
Katalysatorinventar	Aktivkohle und Ruthenium
Katalysatorinventar [kg]	1500
Ruthenium Anteil Katalysator **2)**	0.05
Inventar Schwefelfalle **5)**	Zinkoxid und Kupferoxid
Verwendeter Strommix	electricity, medium voltage//[CH] market for electricity, medium voltage
Kühlung **6)**	Wasser(Fluss/Quelle)
Transportdistanz Edukt [km]	20
Energie überhitzen	Synthesegas aus Eigenproduktion
Säure auslaugen	Schwefelsäure (95%)
Säure Aufreinigung	Salzsäure (37%)
Wasser TreaTech	Wasser deionisiert
Aufkonzentration Phosphorsäure	Eindampfen
Entsorgung **3)**	Deponierung
Phosphorhaltiges Endprodukt **7)**	Phosphorsäure (54%) für Düngerherstellung, Salzsäure
Energetischer Output	Synthese Gas
Verwendeter Datensatz Phosphorsäure **4)**	phosphoric acid, fertiliser grade, without water, in 70% solution state//[GLO] market for phosphoric acid, fertiliser grade, without water, in 70% solution state
Phosphor Rückgewinnungsgrad	79%
Verwendung Energetischer Output	Blockheiztkraftwerk (BHKW)

Main results

The recycling of 100 kg model sludge with the PSI-TreaTech process resulted in the reference variant in 17.39 kg CO2 eq. or 31’790 UBP. The greatest effect on the CO2-eq. balance is the energy for concentrating the phosphoric acid with 14.69 kg CO2-eq. Furthermore, the consumption of HCl with 4.44 kg CO2-eq. is also a relevant expense. In the struvite variant of the PSI-TreaTech process, the recycling of 100 kg model sludge results in 8.34 kg CO2-eq. or 28'360 UBP. The difference of these variants, especially in the CO2-eq. balance, resulted from the fact that for the struvite variant no energy is required for concentration. In comparison with the alternative processes, with the exception of the CO2 eq. balance of the PyroPhos process, the PSI TreaTech process and its variants have comparatively high emissions. The high emissions of the reference variant of the PSI TreaTech process can be explained by the high energy input required to concentrate the phosphoric acid. In the

case of the struvite variant, it is a combination of high input costs (11.3 kg CO2 eq. or 35’520 UBP) and comparatively small credits (5.40 kg CO2-eq. or 13'060 UBP). In addition, the substitution of phosphoric acid is weighted less than that of phosphate fertilizer. This has a strong influence on the good performance of the EuPhoRe process. Table 4.19 lists the values of all processes for comparison.

Table 4.19: Results from the LCA and comparison to other P-recovery processes

Process	**kg CO2-Eq.**	**UBP**
PSI-TreaTech	17.39	31’790
PSI-TreaTech Struvit	8.34	28’360
PyroPhos	14.31	8’930
Phos4Life	0.24	-3’360
EuPhoRe	0.58	-9’260

Optimization potential

The greatest potential for optimization lies in the concentration of phosphoric acid. It was determined that if the waste heat flow from burning some of the synthesis gas was also used to concentrate the phosphoric acid, 4.67 kg CO2 eq. could be saved. This would be an optimization of 26.9% compared to the reference variant of the PSI-TreaTech process. Furthermore, by comparison with the Phos4Life process, it was determined that iron(III) chloride could be produced and isolated as a by-product in the phosphoric acid production process, thereby saving 4.95 kg CO2 eq. This would be an optimization of 28.5 % compared to the reference process. Together, this would result in an optimization of 55.3% compared to the reference process, so the new total emissions would be 7.77 kg CO2-eq. In the struvite variant, optimization would only be possible by means of iron(III) chloride. This would lead to an optimization of 59.4 % and would reduce the emissions to 3.39 kg CO2-eq. Thus, the PSI-TreaTech process in both variants would still have higher emissions than the EuPhoRe and the Phos4Life process. The reasons for this are that the EuPhoRe process generally has a very small cost and thus comes very close to offsetting the expenses even with a smaller credit. Compared to the Phos4Life process, the difference lies in the attributed energy, or waste heat of the sludge incineration plant.

Conclusion

The PSI-TreaTech process meets the federal requirements. In comparison, it performs worse than alternative processes. There is potential for optimization in the area of waste heat utilization, or the energy for concentrating the phosphoric acid. In the reference variant, and in the struvite variant, the recovery of iron(III) chloride could result in an additional credit. If a waste heat source were available to the PSI TreaTech process and the synthesis gas were fed to the high-pressure gas network, as shown in the best-case scenario, the process would even be the only process to show a negative balance of -2.28 kg CO2 eq. Uncertainties in the comparison are the substitution of oil heating by district heating for all processes, except for the PSI-TreaTech-process. Here, of course, first enough customers would have to be found, who would buy the product district heating, as well as the network must be available. Furthermore, the phosphate-containing end products of the PyroPhos and EuPhoRe processes are not yet MinRec compliant and would currently require a purification step. Based on the results of the work, it is recommended to investigate the optimization of the iron(III) chloride recovery in more detail. In addition, a more detailed investigation of the phosphorus-containing end product of the EuPhoRe and PyroPhos process, which was not within the scope of this

work, is recommended. Likewise, a follow-up work, which would compare the production of phosphoric acid and phosphate fertilizer in the PSI-TreaTech process with the primary production, is recommended. Reasons for this would be that the idea behind the production of own phosphorus should reduce the dependence on suppliers and the environmental pollution caused by the production process can be avoided. Thus, the comparison with primary production would be interesting, and the same would apply to the production of the synthesis gas. From this point of view, the PSI-TreaTech-process has a very high potential. For this reason, it is recommended that a follow-up work to clarify these aspects be performed.

5 Conclusions

Findings & learnings

- Pumping certain sludges reliably to high pressures is a challenge. Defining a maximum particle size alone is not sufficient to ascertain pumpability. Mechanical pretreatment of the sludges is a crucial step. It was easier to produce a pumpable slurry from digested sewage sludge than from a food waste sludge.
- Pretreatment of the feed (milling, filtering, filling/emptying) was performed batch-wise and needed a lot of manpower. These tasks should be automatized in a commercial plant.
- The high pressure tube-in-tube heat exchanger can be designed for supercritical water operation using the well-known design equations. It worked as designed, achieving a thermal efficiency of up to 91% with a glycerol-water mixture. With sewage sludge, the thermal efficiency dropped slightly to 89%, indicating that fouling was not a big problem.
- Heating up of the plant is a critical phase for a leak-free operation. The heat-up rate of the hottest components must be kept below a certain value to prevent leaks from differences in thermal expansion.
- Providing hot air from an electric heater within a recirculation loop leads to a very efficient usage of the heating energy, as the air has to be reheated only to its initial temperature but not starting from ambient temperature. The recirculation system with a siphon to the atmosphere for pressure balancing could be operated trouble-free and with only very small losses of hot air.
- The capacity of the plant was limited by the heat transfer in the salt separator. The heat transfer coefficient between the hot air and the supercritical fluid was estimated to be ca. 75 W/m2/K in the absence of fouling.
- Fouling of the vertical tubes in the salt separator was an issue. Upon feeding sewage sludge, and to a lesser extent also with food waste, the heat transfer from the hot air to the fluid inside the tubes deteriorated continuously. Because the maximum temperature of the hot air was limited, the temperature gradient across the tubes was not sufficient anymore to heat up the fluid to supercritical conditions in all cases.
- A significant fraction of the minerals fed into the plant, i.e. 11-50%, accumulated inside the salt separator. These minerals were washed out during cooling down, or were recovered from the cleaning water after the campaign.
- Some general corrosion was found in the falling tubes of the salt separator made of Inconel 625. They were exposed to the harshest conditions: highest temperatures, largest temperature differences across the tube cross-section, concentrated salts and minerals at the

surface. Corrosion could be tentatively linked to carbonates or (organic) sulfur compounds. Another contributing factor could be the steep temperature gradient across the high pressure tubes (outside T up to 680°C, inside T ca. 380°C). The stainless steel tubes of the preheater/heat exchanger did not suffer apparent corrosion.

- Scaling up catalyst production from the laboratory (gram scale) to the pilot scale (100 kg scale) was successfully achieved. The catalyst had the same performance in the pilot plant as in the lab-scale plant (100 times smaller throughput).
- A cumulated amount of 236 kg of OM were fed per kg of catalyst. The Ru/C catalyst, manufactured by a commercial supplier after scaling up a lab-scale procedure, was very active and stable, and did not show any signs of deactivation during all the campaigns performed in this project.
- The autothermal operation of the catalytic reactors could be validated at the pilot scale. Isothermal conditions were established in the well-insulated, but not actively heated reactors.
- Salt brine extraction performed less than expected for sewage sludge, where up to 60% of the minerals could be extracted continuously in the brine. For the food waste slurry, up to 87% of the minerals could be continuously extracted.
- We could demonstrate phosphorus valorization into phosphoric acid and crystalline Struvite using the solids produced by the lab scale prototype. However, applying the same valorization steps to the solids produced by the HydroPilot unit was not possible since only a small amount of usable solids were produced during the campaigns with sewage sludge.
- Although the estimated Capex and Opex for the P-recovery process look promising when integrated with cHTG within the cement manufacturing process due to energy and disposal costs savings, further research, optimization and scale-up activities need to be performed in order to obtain a more accurate estimate. These questions will be addressed as part of the moRECo project that is carrying out by FHNW Muttenz in collaboration with TreaTech and with the support of FOEN. Moreover, the adequacy of the solids of cHTG to be treated by other P-recovery processes will be studied.

Main conclusions

The results of the HydroPilot campaigns confirmed that the catalytic hydrothermal gasification technology can valorize biogenic waste with good potential for gas production and mineral recovery. Nonetheless, we have also confirmed that sewage sludge is one of the most challenging substrates to be treated and that further technical optimization is needed to be able to valorize this type of waste in a continuous manner at industrial scale (8000 hours per year). On the contrary, treating substrates with low concentration of minerals have demonstrated excellent performance of the technology, which reveals the potential to treat this type of waste streams at industrial scale in the short term.

One of the issues that is harder to solve is fouling by minerals. Deposition on the walls depends on several factors such as type and concentration of minerals, particle size and morphology, flow pattern, surface temperature. Being able to cope with a wide range of minerals would make cHTG widely applicable. Thus, additional effort should be directed towards an improved design for the salt separator for feedstocks with a high minerals content such as sewage sludge.

Pretreatment of the feed is expected to become easier and less demanding as the process is scaled up further. Larger pumps can cope with larger particles, which directly reduces the need for milling and filtering. A future commercial plant should be able to process most wet feedstocks, including sewage sludge, with a minimum of pretreatment, e.g. just a screen for removing coarse particles.

Another challenge is to reconsider the choice of materials for the construction of the salt separator. Although a corrosion study was performed in an earlier project, including testing of specimen under load up to 1’000 h, unexpected corrosion of Inconel 625 occurred in this project. To guide the choice

of materials, another corrosion study should be performed using the learnings from this project. The reason for the specific corrosion must be identified and used to test other alloys, starting with stainless steel 316, as used for other parts of the pilot plant and that suffered no apparent corrosion.

6 Outlook and next steps

- The pilot plant needs several small improvements for further campaigns. A more significant improvement is needed for the handling of inorganics. The current salt separator should be replaced by a new design that is able to cope with high amounts of inorganics.
- The extraction of salts and other minerals should be further improved to avoid an accumulation of minerals in the salt separator.
- After these improvements will have been implemented, further experimental campaigns with sewage sludges and other industrial feedstocks (food processing wastes, liquid wastes) can be carried out to confirm the performance measured in this project.
- Using the results of this project, in particular from WP 6, a fully automated demo plant is being designed by TreaTech (TRL 7, capacity 100-200 kg/h) This demo plant will be able to operate 24/7 at a client's site with a minimum of operator manipulations.
- The reason for the observed general corrosion in the salt separator tubes should be investigated in more detail. Alloys other than Inconel 625 should be evaluated for the salt separator and tested under HTG conditions.
- In the latest campaign, power measurements have been installed in HydroPilot. For future campaigns, the power used by the heater can be measured directly.
- The scale up of the P-recovery process, as well as further investigation of the purification of the leachate and characterization of the product to fulfil the legal standards for its commercialization will be performed within a project carried out by the University of Applied Sciences and Arts Northwestern Switzerland (FHNW) in Muttenz in collaboration with TreaTech and with the support of the FOEN.
- The learnings from the HydroPilot project had an impact on TreaTech's industrialization and commercialization strategy of the technology. TreaTech has just closed their Series A financing round which has a main goal the installation of a demonstration unit at a client site that will run continuously (24/7) to validate the technology in real environment. The learnings from the heat transfer experiments, the challenges faced during the sewage sludge campaigns as well as the performance of the unit during the rest of campaigns have directly helped in the design of the new demonstration unit. In addition, as stated in chapter 5, the challenging nature of sewage sludge confirmed that industrialization will be faster for units treating waste streams with low inorganic content. TreaTech expects to install their first industrial-size unit, treating industrial effluents, in 2025 and their first full scale unit treating municipal sewage sludge in 2026 (Figure 6.1).

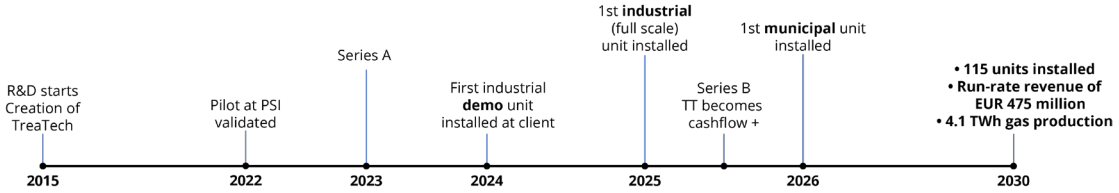


Figure 6.1: TreaTech's roadmap for the cHTG technology including P recovery.

7 National and international cooperation

National cooperation was already expressed in the project team, which brought together two partner companies from French-speaking Switzerland with three partners from German-speaking Switzerland. A cooperation with other partners took place within SCCER BIOSWEET. There we cooperated on topics of analytics and techno-economic evaluation with colleagues at PSI (Ch. Ludwig), at FHNW (T. Griffin, M. Bösch), and EPFL (F. Maréchal).

Collaborations with GRTGaz (F) and Services Industriels de Genève (SIG) were established. Trials on injecting H_2 into hydrothermal gasification of sewage sludge to increase methane content were discussed.

A feasibility study on the hydrothermal gasification of slurry and hydrolyzed biowaste for the French company LIGER, together with TreaTech and Afry, was carried out. The final results are confidential. LIGER is interested in operating a demonstration plant at one of its sites in France.

In December 2019, a visit of the company SUEZ (F) to PSI, together with TreaTech, took place. Possibilities of collaboration were discussed.

Afry has been in discussions with Marafiq for some time to possibly conduct a gasification campaign with their industrial sludge. Marafiq is a company specialized in seawater desalination, provision of cooling water and wastewater treatment in Saudi Arabia. Unfortunately, no agreement could be reached as the costs were apparently too high for Marafiq. Also presented was TreaTech and hydrothermal gasification at a utility provider in Oman. In both countries the disposal of sewage sludge to landfills will be banned in the near future and therefore there is a lot of interest. In addition, a MoU was signed with Andean Dragon in Chile for further cooperation for potential customers in Chile.

Afry has presented TreaTech to an integrated fuel supplier as a possible option to offset CO_2 emissions under REDII (Renewable Energy Directive II). It is evident that without an existing pilot on a semi-industrial scale, discussions are unfortunately often not productive.

Together with a cement manufacturer and TreaTech, a study was performed at PSI in 2020 to examine the integration of an HTV plant including phosphorus recovery in a cement plant (confidential information).

TreaTech, together with FHNW in Muttenz, School of Life Sciences, has started the project "Phosphorus recovery from hydrothermally treated sewage sludge", sponsored by FOEN. This is intended in particular to address the scale-up of TreaTech's P-recycling technology.

Discussions with Nestlé have been continued. They are interested in applying HTG for the energy recovery of coffee waste.

The cooperation with GRTGaz (F) was continued. This company promotes hydrothermal gasification and the use of biogas in all media. An easy-to-understand promotional film was published on Youtube: https://www.youtube.com/watch?v=byDwof5Wzfg

At PSI, the Horizon2020 project "Black Liquor to Fuel" was launched in April 2020. This is about the hydrothermal liquefaction of lignin in black liquor and the recovery of pulping chemicals for the pulping process. PSI is working on salt separation under hydrothermal conditions.

In collaboration with SIAAP (F), PSI has performed hydrothermal gasification experiments with sewage sludge from the greater Paris area. A continuation of the collaboration is planned for performing a techno-economic study for the valorization of sewage sludge in the contect of SIAAP.

Afry Switzerland Ltd. continued to support TreaTech in its pathway to commercialization. We provided support in the elaboration of the Hydrothermal Gasification Whitebook [29], prepared by a French gas consortium which was released recently at the Bio360 exposition. The Whitebook is a first concise compendium for the implementation of the technology in the French market.

Furthermore, Afry Germany's Process Industry Branch prepared a new Technical Due Diligence to support TreaTech's search for investors. This study, which lasted several weeks was done free of charge.

Sewage sludge disposal and organic sludge in general remain a huge challenge. Across Afry's activities, they have pointed out the technology to their clients on several occasions. Afry being involved in several mega projects in the utility sector in Saudi-Arabia, they see a great potential for the technology. However, without further progress on the industrial demonstration plant, it will be difficult to reach a larger audience.

8 Publications

Burg, V.; Bowman, G.; Thees, O.; Baier, U.; Biollaz, S.; Damartzis, T.; Hersener, J.-L.; Luterbacher, J.; Madi, H.; Maréchal, F.; Moioli, E.; Rüsch, F.; Studer, M.; Van herle, J.; Vogel, F.; Kröcher, O., 2021: White Paper: Biogas from animal manure in Switzerland: energy potential, technology development and resource mobilization. SCCER-BIOSWEET; Birmensdorf, Swiss Federal Research Institute WSL. 20 pp., DOI

Berndorff, J. *Aus Biomasse das Maximum an Energie herausholen*, online-Beitrag, 27. Oktober 2021, Paul Scherrer Institut, https://www.psi.ch/de/media/forschung/aus-biomasse-das-maximum-an-energie-herausholen

Website of the HydroPilot plant: https://www.psi.ch/de/cpe/hydropilot

9 References

[1] Thees, O.; Burg, V.; Erni, M.; Bowman, G.; Lemm, R. Biomassepotenziale der Schweiz für die energetische Nutzung, Ergebnisse des schweizerischen Energiekompetenzzentrums SCCER BIOSWEET, Eidg. Forschungsanstalt für Wald, Schnee und Landschaft WSL, Birmensdorf, Heft 57, 2017, ISSN 2296-3448.

[2] Binggeli, D.; Guggisberg, B.; Gutzwiller, L.; Hermle, S.; Schärer, H.-U.; Volken, T. Strategie für die energetische Nutzung von Biomasse in der Schweiz, Bundesamt für Energie, Bern, 28.9.2010.

[3] Kupper, T.; Becker van Slooten, K.; Tarradellas, J.; Organische Schadstoffe im Klärschlamm - Quellen, Verbleib, Risiken für die Umwelt, 58. VSA-Hauptmitgliederversammlung, 19. April 2002, Basel, Schweiz.

[4] Gujer, W. Siedlungswasserwirtschaft, 2. Aufl., 2002, Springer.

[5] Hermann, L. 2009: Rückgewinnung von Phosphor aus der Abwasserreinigung. Eine Bestandesaufnahme. Umwelt-Wissen Nr. 0929. Bundesamt für Umwelt, Bern. 196 S.

[6] Global Atlas of excreta, wastewater sludge, and biosolids management: moving forward the sustainable and welcome uses of a global resource, UN-HABITAT, 2008.

[7] Azoth Analytics research report: “Global Sewage Treatment Plant Market: Trends, Opportunities and Forecasts (2016-2021)”.

[8] Vogel, F. Hydrothermale Verfahren. In: *Energie aus Biomasse*, 3. Aufl., M. Kaltschmitt, H. Hartmann, H. Hofbauer, (Hrsg.), Springer: Berlin, 2016, Kapitel 15, 1267-1337, ISBN 978-3-662-47437-2.

[9] Peng, G.; Vogel, F.; Refardt, D.; Ludwig, C. Catalytic Supercritical Water Gasification: Continuous Methanization of Chlorella vulgaris, *Ind. Eng. Chem. Res.* 2017, 56, 6256−6265.

[10] Boukis, N.; Hauer, E.; Herbig, S.; Sauer, J.; Vogel, F. Catalytic gasification of digestate sludge in supercritical water on the pilot plant scale, *Biomass Conversion and Biorefinery*, published online January 13, 2017, DOI 10.1007/s13399-017-0238-x.

[11] Laukenmann, J. *Wenn Algen Gas geben*, Sonntagszeitung, 5. Oktober 2014.

[12] US Patent 8,475,549 B2 (2013-07-02), “Process for generating methane and/or methane hydrate from biomass”, Patent application WO 2007/038996 A1 (2007-04-12), Paul Scherrer Institut, Inventors: Vogel, F.; Waldner, M.; Truong, T.-B.; De Boni, E.; Stucki, S., 2005.

[13] Peng, G.; Ludwig, C.; Vogel, F. Catalytic Supercritical Water Gasification: Interaction of sulfur with ZnO and the Ruthenium catalyst, *Appl. Catal. B* 2017 202, 262–268.

[14] Vogel, F. Nährsalzabscheidung bei der hydrothermalen Methanierung von Biomasse im Pilotmassstab, Schlussbericht, Bundesamt für Energie, 20. November 2015.

[15] Linstrom, P.J. and Mallard, W.G., Eds., NIST Chemistry WebBook, NIST Standard Reference Database Number 69, National Institute of Standards and Technology, Gaithersburg MD, 20899, https://doi.org/10.18434/T4D303

[16] Hagger, Nicola, Heat Exchanger Model V 2.2, internal report, FHNW, 5 February 2021.

[17] Zeyer, Silvan, Dynamisches Modell Hydropilot, “Digital Twin” einer Forschungsanlage zur hydrothermalen Vergasung von Biomasseschlämmen, Bachelorthesis, Studiengang EUT, FHNW, Juli 2022.

[18] Zöhrer, Hemma, Hydrothermal gasification of fermentation residues for SNG-production, PhD thesis, ETH Zürich, 2013.

[19] Brunner, G. Chapter 12 - Corrosion in Hydrothermal and Supercritical Water, Vol 5, 2014, Elsevier

[20] Boukis N., Habicht W., Franz G. and Dinjus E., Behavior of Ni-base alloy 625 in methanol-supercritical water systems, Materials and Corrosion, 2003, 54, 326-330

[21] R. Fujisawa, M. Sakaihara, Y. Kurata and Y. Watanabe, Corrosion behaviour of nickel base alloys and 316 stainless steel in supercritical water under alkaline conditions, Corrosion Eng., Science Tech., 2013, 40244-248

[22] W. Habicht, N. Boukis, G. Franz and E. Dinjus, Investigation of Nickel-Based Alloys Exposed to Supercritical Water Environments, Microchim. Acta, 2004,145, 57-62

[23] R. Wang, R. Deplazes, F. Vogel and D. Baudouin, Continuous Extraction of Black Liquor Salts under Hydrothermal Conditions, Ind. Eng. Chem. Res. 2021, 60, 4072-4085

[24] Pöyry Switzerland Ltd., Technical report on Supercritical Water Gasification of Sewage Sludge and business case study of sewage sludge treatment options, 2018 (confidential)

[25] Nättorp, A., Remmen, K., Sustainable sewage sludge management fostering phosphorus recovery and energy efficiency, Report on LCC of European P recovery processes (P-REX).

[26] Yee, T. F and I. E. Grossmann, Simultaneous Optimization Models for Heat Integration-II. Heat Exchanger Network Synthesis, Computers chem. Engng. Vol. 14, No. 10, pp.1165-1184, 1990.

[27] Dill, Florian, Ökobilanzierung der Hydrothermalen Vergasung aus Klär- und Faulschlämmen, Bachelor thesis, Studiengang EUT, FHNW, 21 March 2021.

[28] Griem, H. A new procedure for the prediction of forced convection heat transfer at near-and supercritical pressure, Heat and Mass Transfer 31.5 (1996), pp. 301-305.

[29] GAZÉIFICATION HYDROTHERMALE LIVRE BLANC, Robert Muhlke (GRTgaz), Jean-Baptiste Castaing (Cerema), Mathieu Morel (Sia Partners), Violette Donat (Yélé Consulting), January 2023

10 Appendix

Annex A: P-recovery protocol and CAPEX/OPEX calculations

To keep the page numbers, this Annex has been added after p. 111.

Annex B: Additional pictures



Figure B1: High-pressure phase separator (left), low pressure phase separator and process water collection vessel (foreground, right), brine collection vessel (back, right). © M. Fischer, PSI, 2020



Figure B2: Cooler (left, uninsulated), tube-in-tube heat exchanger (right). © M. Fischer, PSI, 2020



Figure B3: Hot air heating system during site acceptance test. Hot air fan (left), electrical heater (horizontal insulated, middle), connecting tubing and salt separator bypass (right, U-shaped, uninsulated). © PSI, 2020



Figure B4: Salt separator, uninsulated; hot air loop (back, insulated). © PSI, 2020



Figure B5: Electrical cabinets, plant control with touch screen (left), hot air system (right).
© M. Fischer, PSI, 2020



Figure B6: Online monitoring. TOC of process water (middle, grey box), microGC for gas composition (blue box, foreground). © PSI, 2020



Figure B7: Combustion oven for the gasses on the roof of the building (pre-existing). © PSI, 2020

Phosphorus recovery from hydrothermally treated sewage sludge: Leaching optimisation

June 2019

ABSTRACT

Technologies for phosphorus recovery from sewage sludge and sewage sludge ashes are experiencing a very rapid development due to the new regulations enforcing the recovery of this element since its production from fossil resources is expected to peak between 2035 and 2075 ([1,2]). Most of the technologies are based on leaching the phosphorus from the solid using a basic or an acid solution. However, the solid residue obtained from hydrothermally treated sewage sludge at supercritical conditions differs from sewage sludge and sewage sludge ashes. This is why a design of experiments of 4 factors and 2 levels have been performed to find the optimal conditions for phosphorus leaching. The results show that pH is the main factor affecting the performance of the process and that at pH 1, the percentage of phosphorus recovery is more than 3 times higher than at pH 2, reaching an average maximum of 77% for experiments at pH 1, L/S=10, 30 minutes and 50 ºC. However, is at this harsh conditions where we find the highest error, since at low pH and higher temperature the process is highly sensitive to changes in the parameters. As a result, recovery can go from 50% to a 100% using these conditions. We find that experiments at pH 1, L/S=10, 30 minutes and room temperature are more stable with a lower average recovery but a much lower variance as well. Besides, working at room temperature would significantly reduce the cost of the process at industrial scale. From now on, we will consider pH 1, L/S=10, 30 minutes and room temperature the base conditions to keep improving the recovery percentage either by fine tuning the parameters or by recycling the solid phase to perform a second leaching.

List of Figures

1 Summary of the process. . . . 2
2 Composition (%wt in blue, mg/kg in orange) of the solid residue before leaching. . . . 4
3 Weight percentage of the total carbon from the dried sewage sludge (feed) that remains in the solid after leaching. 4
4 Weight percentage of phosphorus recovered from the solid residue into the leachate. . . . 5
5 Weight percentage of iron (a), aluminium (b), calcium (c) and magnesium (d) leached from the solid residue into the leachate. . . . 6
6 Pareto's chart for the effect of pH, temperature, liquid to solid ratio and time on P recovery. . . . 6
A.1 Weight percentage recovered from the solid into the leachate of the analysed elements. . . . 10
A.2 Surface graphs for liquid to solid ratio, temperature (C) and time (min) vs pH for all the conditions. . . . 11
A.3 Pressure and temperature profile for experiments LI and LII - 1.6.25 . . . 12
A.4 Pressure and temperature profile for experiments LI and LII - 1.6.50 . . . 12
A.5 Pressure and temperature profile for experiments LI and LII - 1.10.25 . . . 13
A.6 Pressure and temperature profile for experiments LI and LII - 1.10.50 . . . 13
A.7 Pressure and temperature profile for experiments LI and LII - 2.6.25 . . . 14
A.8 Pressure and temperature profile for experiments LI and LII - 2.6.50 . . . 14
A.9 Pressure and temperature profile for experiments LI and LII - 2.10.25 . . . 15
A.10 Pressure and temperature profile for experiments LI and LII - 2.10.50 . . . 15

List of Tables

1 Factors and levels for experiment design. RT= room temperature. . . . 3
A.1 Composition of the solid residue before leaching (ICP). . . . 8
A.2 CHN analysis of the solid residue. . . . 8
A.3 CHN analysis of the solid residues after leaching. . . . 8
A.4 Composition of the leachate and recovery . . . 9

Contents

1 Aim, framework and scope **2**

2 Experimental protocol **3**
2.1 Digestion of solid samples . . . 3
Materials • Method
2.2 Leaching experiments . . . 3
Materials • Method
3 Results and discussion **3**
3.1 Recovery of elements . . . 3
3.2 Effect of parameters over P recovery . . . 5
4 Conclusions **7**
References **7**
A Appendix I **8**
A.1 Solid residue composition . . . 8
A.2 Composition of the leachate and recovery . . . 8
A.3 Surface plots . . . 11
A.4 Temperature and pH profiles . . . 12

1 Aim, framework and scope

Aim

The goal of this report is to show the results of the optimization of the acid leaching of hydrothermally treated sewage sludge (SS) in order to recover the maximum amount of phosphorus.

Framework

Around 9 millions of tons of SS are produced every year in Europe as a side product of the treatment of wastewater, one of the major volumes of waste directly linked to the existence of humans. The current sludge disposal routes (landfilling, biosolids production, and incineration) cause severe environmental impacts (e.g. soil contamination, toxic gas emissions) and do not valorise its energetic and mineral content such as performing phosphorus (P) recovery.

P is a key component in crop growth and animal feeding and it is almost exclusively obtained through mining of phosphate rock. The concern of depleting the current sources of this element has raised exponentially since its production from fossil resources is expected to peak between 2035 and 2075 ([1,2]). Switzerland is the first country to establish a new regulation regarding P-recovery from SS and the latter will enter into force in 2026. Although several companies have developed promising P-recovery technologies, all of them either have low efficiencies or suffer from high capital and operating costs. Treatech has developed a cost-efficient and eco-friendly technology for transforming waste (among which SS) into clean water, renewable gas and fertilizers (phosphoric acid). Treatech's technology uses the unique properties of supercritical water to efficiently recover the valuable minerals and convert the organic compounds to renewable gas (refer to figure 1).

Most of the P-recovery technologies extract P from SS incineration ashes using either acid leaching or thermal treatment.

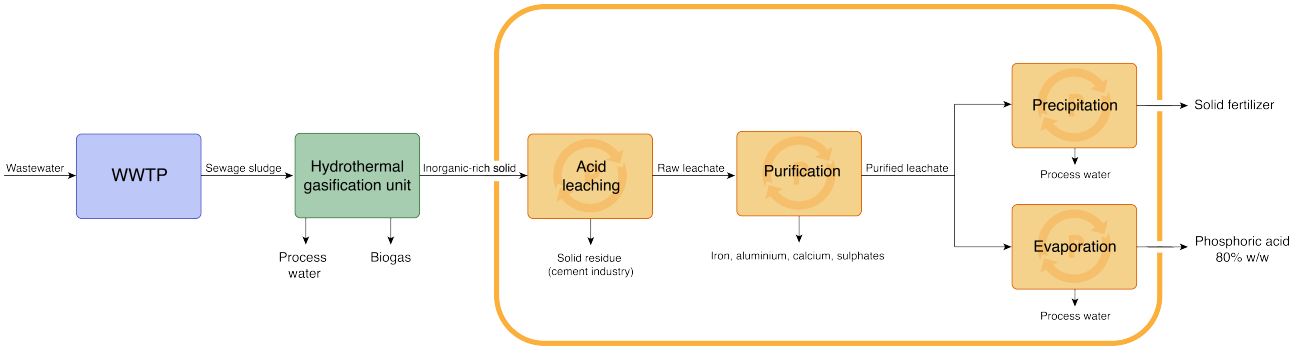


Figure 1. Summary of the process.

Although the P-recovery yield of these processes is high (>90%), SS must be dehydrated, transported to incinerators, and combusted using natural gas. These costs can reach 50% of the operating expenses of a wastewater treatment plant. Moreover, the energetic content of the sludge is not valorised as a renewable energetic vector (e.g. biogas) since the organic compounds are combusted. Besides reaching a high P recovery yield without dehydration steps, TreaTech's technology allows to convert efficiently most of the organic compounds to renewable gas.

Scope

As indicated before, the first step towards the valorization of the phosphorus trapped in the solid residue is to transfer it to the liquid phase. This can be achieved through acid and/or basic leaching in aqueous phase[3–6]. In this case, after a preliminar screening of different leaching agents, sulfuric acid was selected as the proton donor. In order to reach the optimum conditions through the least number of experiments possible, a design of experiments of 4 factors and 2 levels was performed (table 1). The solid residue used was a representative sample from the deposits extracted during the hydrothermal liquefaction campaign performed at EPFL on March 2018.

Before the start of this project, only experiments with very high liquid to solid ratio (160) had been carried out. This is why prior to the performance of the designed experiments, preliminary experiments were performed to find the correct values for the ratio factor. Simple water-dried sewage sludge mixing experiments showed that homogeneous and stable mixing was possible up to 4.5. However leaching experiments at this ratio showed low P recovery (around 50%) at pH 1. This is why, ratios above 4.5 were selected for the design of experiments.

Factor \ Level	Low	High
pH	1	2
Temp. (°C)	RT	50
L:S	6	10
time (min)	30	90

Table 1. Factors and levels for experiment design. RT= room temperature.

2 Experimental protocol

2.1 Digestion of solid samples

2.1.1 Materials

65% Nitric Acid was acquired from Sigma-Aldrich. 95-98% Sulphuric Acid was acquired from Merck. Nylon membrane filters (0.2 μm pore size) were acquired from Whatman.

2.1.2 Method

Pre-digestion Three grams of previously dried solid residue mix are mixed with 28 ml of freshly prepared aqua regia (3:1, 37% HCl:65% HNO_3) in a round bottom flask provided with a magnetic stirrer. The mixture is stirred for sixteen hours at room temperature.

Digestion[7] The mixture is then refluxed for two hours at 130°C using an oil bath and a reflux system, trapping the NOx gases in a basic solution.

Filtration After digestion, the mixture is left to cool down and filtered through 0.2 μm pore size membrane filters, rinsing the flask with ultrapure water. The diluted filtrate is sent to perform ICP analysis.

2.2 Leaching experiments

2.2.1 Materials

95-98% Sulphuric Acid was acquired from Merck. Nylon membrane filters (0.2 μm pore size) were acquired from Whatman. Ultrapure water (Mili-Q) was used to reach the desired liquid to solid ratio. The experiments were performed in a 100 ml glass beaker provided with a magnetic stirrer. Continuous stirring was achieved using a hotplate (Heidolph Hei-Tec) and an oil bath was used for the experiments performed at 50°C.

2.2.2 Method

Around 7 grams of previously dried solid residue were mixed up with 38 ml or 67 ml of ultrapure water. The mixture was stirred at room temperature or 50°C during 90 minutes with temperature and pH control. Sulfuric acid was added gradually throughout the experiment in order to maintain the mixture at the desired pH (1 or 2). A 10 ml sample was extracted from the beaker and vacuum filtered using a 0.2 μm nylon filter after 30 minutes. After another 60 minutes of experiment, the rest of the mixture was vacuum filtered using a 0.2 μm nylon filter. The liquid samples were analysed by ICP for total phosphorus determination. This experiment was performed in duplicate for each set of conditions.

3 Results and discussion

3.1 Recovery of elements

For every experiment, the weight percentage recovered from the solid samples into the leachate is calculated for fourteen elements (P, Al, Ca, Fe, S, K, Mg, Na, Cr, Ni, Cu, Zn, Cd, Pb) using formula 1.

$$\%wt.\,Recovery\,of\,element\,X = \frac{m_{elementX}\ in\ leachate}{m_{elementX}\ before\ leaching} \cdot 100 \tag{1}$$

The amount of each element originally present in the solid samples is determined from the concentration of those elements in the extracted liquid phase after digestion with aqua regia. Refer to figure 2 for the results (table A.1 in the appendix). The mass of each element in the leachate is calculated through its concentration on the liquid phase after leaching.

Figure A.1 in the appendix shows the recovery results for all the leaching experiments performed. A table with the ICP concentrations and the recovered percentages can be consulted in the appendix (table A.4) as well.

Elemental analysis (CHN) was also performed to know the percentage of carbon in the solid residue (table A.2 in the appendix) as well as in the residues after leaching (table A.3 in the appendix) to evaluate the amount of carbon that stays

on the solid phase. The average CHN composition (% weight) of the solid residue before leaching is 17.8%, 2.7% and 1.2% respectively (figure 2). These percentages are compared with the composition of the solids after leaching. For all the experiments, 87-100% of the original amount of hydrogen, and 72-94% of the original amount of nitrogen remained in the solid phase after leaching. Since the content of hydrogen and nitrogen is quite low, we will focus on the carbon. Results for carbon are shown in figure 3. As it can be seen, most of the carbon (>87%) remains in the solid phase for all the conditions and there is no clear trend that would link the variation on the parameters to the amount of carbon leached. In fact, for every experiment, the difference between samples after 30 or 90 minutes are very subtle which could mean that all the soluble carbon is leached quickly before the first 30 minutes.

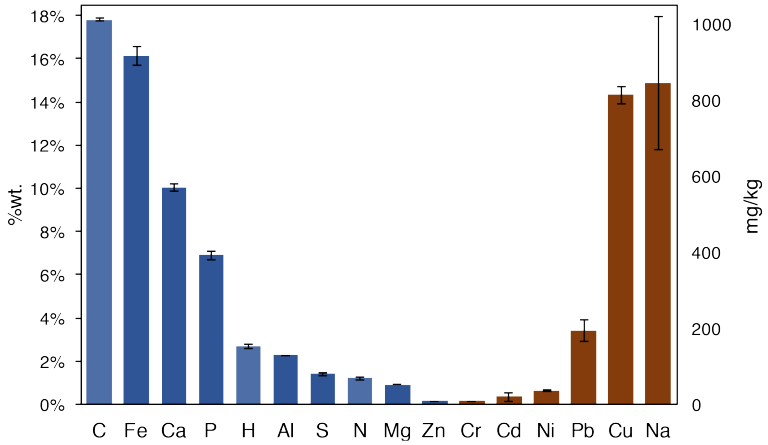


Figure 2. Composition (%wt in blue, mg/kg in orange) of the solid residue before leaching.

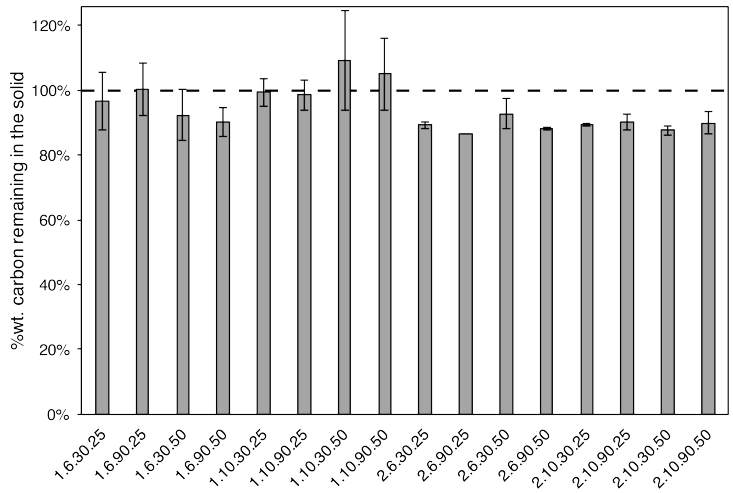


Figure 3. Weight percentage of the total carbon from the dried sewage sludge (feed) that remains in the solid after leaching.

3.2 Effect of parameters over P recovery

As mentioned beforehand, to find the optimal leaching conditions for maximum P recovery with the least experiments a design of experiments of 4 factors and 2 levels was performed. The factors selected were temperature, pH, liquid to solid ratio and residence time. For every condition, two replicates were performed. Figure 4 summarizes the performance of the experiments regarding P recovery.

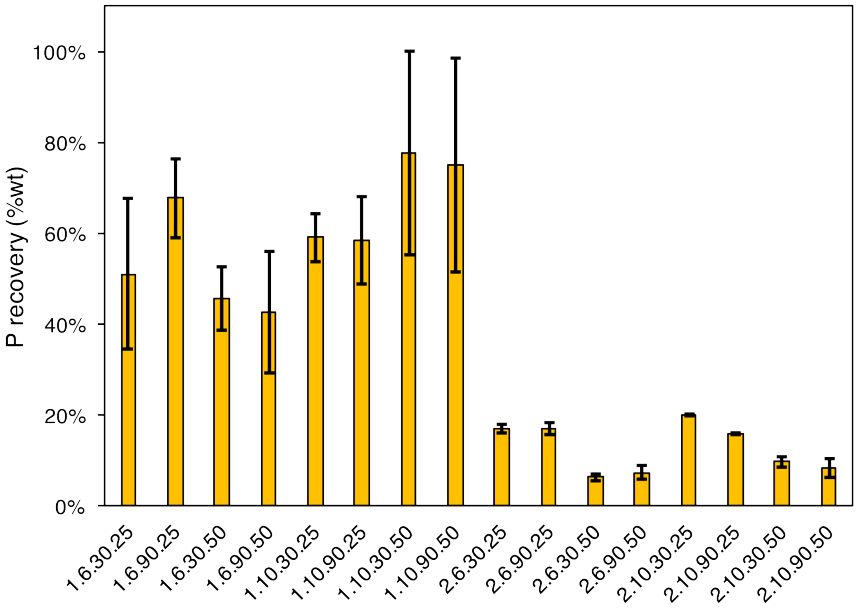


Figure 4. Weight percentage of phosphorus recovered from the solid residue into the leachate.

We can clearly state that, as expected, the recovery rates are remarkably higher for pH 1 experiments since there are more protons in solution to leach the phosphorus. This same trend is followed by iron, aluminium and, although with less differentiation, magnesium (Figure 5).

Regarding residence time, there is practically no increase nor decrease of phoshorus concentration after 30 minutes for all the experiments performed. This indicates that 30 minutes are enough to reach the maximum transfer of phosphorus to the liquid phase. Nonetheless, iron, calcium and magnesium behave differently whereas aluminium does not present a clear trend. The concentration of iron increases with time, for all experiments, between 5 and 17% except for harsh conditions at pH 1 and 50°C, for which it remains constant after 30 minutes. Magnesium concentration increases with time between 5 and 9% except for the experiment with the harshest conditions (L/S=10, pH 1 and 50°C) for which it remains constant after 30 min. Calcium follows the reverse trend due to the leaching-precipitation dynamic involved. The low pH environment leaches calcium to the liquid phase where it reacts with the sulphates from sulfuric acid to precipitate as calcium sulphates. The decrease of concentration with time is a result of this precipitation process. From 30 to 90 minutes the concentration of calcium in the liquid phase decreases between 2 and 5%.

In general, the liquid to solid ratio does not present a strong effect on the phosphorus recovery. Nonetheless, for experiments at 50°C, where the influence of the parameters is amplified, results for a ratio of 10 are slightly better than those for a ratio of 6. This is mainly due to the fact that at a ratio of 10, a better solid-liquid mixing is achieved.

Finally, increasing the temperature does not have a positive effect on P recovery for most of the conditions. Only for experiments at pH 1 and L/S=10, results at 50°C look better than at room temperature. However, we can not draw any conclusion looking at the average values, since precisely for experiments at pH 1, L/S=10 and 50°C, the error is the biggest.

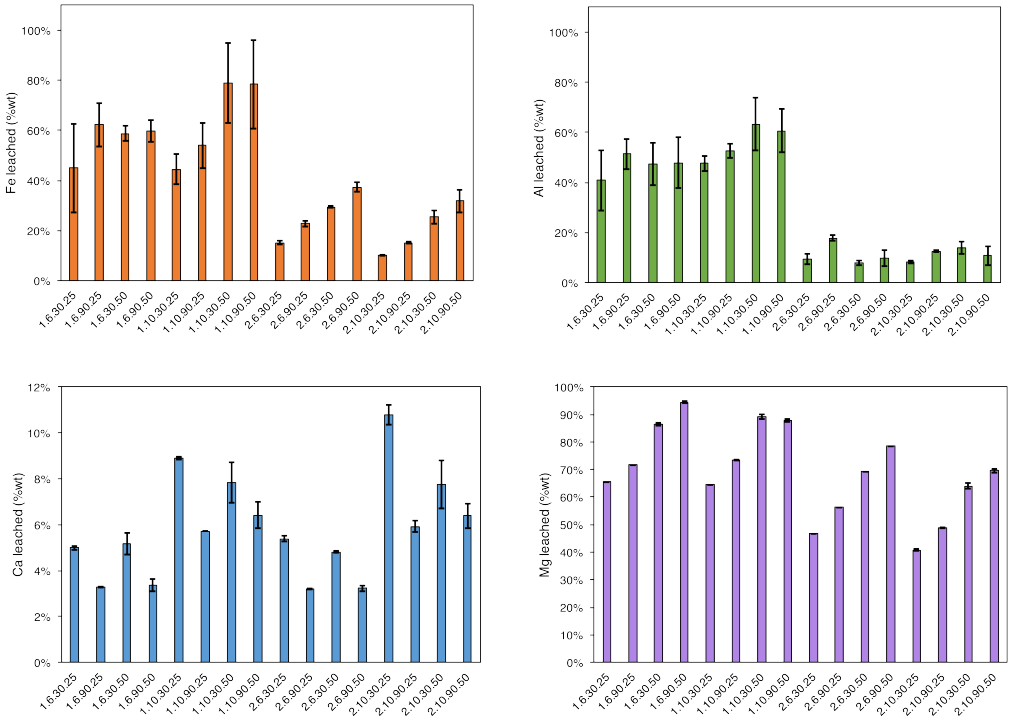


Figure 5. Weight percentage of iron (a), aluminium (b), calcium (c) and magnesium (d) leached from the solid residue into the leachate.

Using the open source software Chemoface, the effect of the factors was evaluated statistically to strengthen and give support to the hypothesis above. As expected, pH is the only significant factor on P recovery (figure 6, linear regression R-squared=0.8755). Looking at the surface representations of the parameters vs pH, we can confirm that liquid to solid ratio, temperature and time have little influence on P recovery into the liquid phase (Figure A.2 in the appendix).

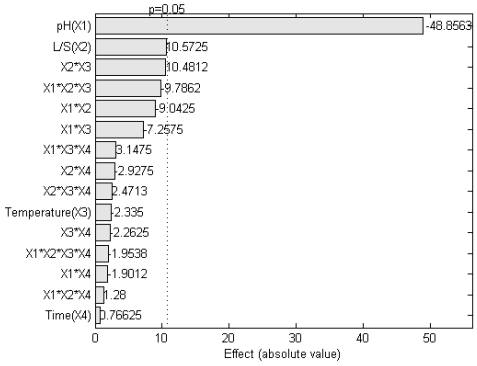


Figure 6. Pareto's chart for the effect of pH, temperature, liquid to solid ratio and time on P recovery.

4 Conclusions

Technologies for phosphorus recovery from sewage sludge and sewage sludge ashes are experiencing a very rapid development due to the new regulations enforcing the recovery of this element since its production from fossil resources is expected to peak between 2035 and 2075 ([1,2]). Most of the technologies are based on leaching the phosphorus from the solid using a basic or an acid solution. Then this liquid phase is purified and phosphorus is valorised as phosphoric acid or precipitated to form solid fertilizers. However, the solid residue obtained from hydrothermally treated sewage sludge at supercritical conditions differs remarkably from sewage sludge and sewage sludge ashes. This is why we need a tailored solution to recover phosphorus from this stream. As a first step, a design of experiments of 4 factors and 2 levels have been performed to find the optimal conditions for phosphorus leaching. The results show that pH is the main factor affecting the performance of the process and that at pH 1, the percentage of phosphorus recovery is more than 3 times higher than at pH 2, reaching an average maximum of 77% for experiments at pH 1, L/S=10, 30 minutes and 50°C. However, is at this harsh conditions where we find the highest error, since at low pH and high T the process is highly sensitive to changes in the parameters. As a result, recovery can go from 50% to a 100% using these conditions. We find that experiments at pH 1, L/S=10, 30 minutes and room temperature are more stable with a lower average recovery but a much lower variance as well. Besides, working at room temperature would significantly reduce the cost of the process at industrial scale. From now on, we will consider pH 1, L/S=10, 30 minutes and room temperature the base conditions to keep improving the recovery percentage either by fine tuning the parameters (increasing L/S ratio, lowering pH) or by recycling the solid phase to perform a second leaching.

References

1. White, S. & Cordell, D. Peak phosphorus: the sequel to peak oil. *Phosphorus Futur.* (2009).
2. Mohr, S. & Evans, G. New projection of peak phosphorus. *Philica* (2013).
3. Acelas, N. Y., López, D. P., Brilman, D. W., Kersten, S. R. & Kootstra, A. M. J. Supercritical water gasification of sewage sludge: Gas production and phosphorus recovery. *Bioresour. Technol.* **174**, 167–175, DOI: 10.1016/j.biortech.2014.10.003 (2014).
4. Petzet, S., Peplinski, B. & Cornel, P. On wet chemical phosphorus recovery from sewage sludge ash by acidic or alkaline leaching and an optimized combination of both. *Water Res.* **46**, 3769–3780, DOI: 10.1016/j.watres.2012.03.068 (2012).
5. Egle, L., Rechberger, H., Krampe, J. & Zessner, M. Phosphorus recovery from municipal wastewater: An integrated comparative technological, environmental and economic assessment of p recovery technologies. *Sci. The Total. Environ.* **571**, 522–542, DOI: 10.1016/j.scitotenv.2016.07.019 (2016).
6. Donatello, S., Tong, D. & Cheeseman, C. Production of technical grade phosphoric acid from incinerator sewage sludge ash (issa). *Waste Manag.* **30**, 1634–1642, DOI: 10.1016/j.wasman.2010.04.009 (2010).
7. Santoro, A., Held, A., Linsinger, T., Perez, A. & Ricci, M. Comparison of total and aqua regia extractability of heavy metals in sewage sludge: The case study of a certified reference material. *Trends Anal. Chem.* **89**, 34–40, DOI: 10.1016/j.trac.2017.01.010 (2017).

A Appendix I

A.1 Solid residue composition

	P	Al	Ca	Fe	S	Mg	Na	Cr	Ni	Cu	Zn	Cd	Pb
ICP(mg/l)	2559.2	834.4	3721.7	5979.5	515.4	337.8	31.4	0.3	1.3	30.1	58.2	0.7	7.2
%wt. feed	6.90	2.25	10.04	16.12	1.39	0.91	0.08	0.001	0.0004	0.08	0.16	0.002	0.02
Error %	2.74	0.90	1.84	2.53	4.04	1.20	20.80	0.15	7.10	2.61	1.90	53.76	13.73

Table A.1. Composition of the solid residue before leaching (ICP).

	C	H	N
%wt.	17.80	2.66	1.19
% Error	0.42	3.5	3.14

Table A.2. CHN analysis of the solid residue.

A.2 Composition of the leachate and recovery

	C		H		N	
Experiment	**%wt. C remains**	**Error %**	**%wt. H remains**	**Error %**	**%wt. N remains**	**Error %**
1.6.30.25	96.83%	8.86%	99.68%	0.27%	91.03%	9.26%
1.6.90.25	100.39%	8.13%	100.99%	1.91%	89.04%	10.71%
1.6.30.50	92.35%	7.80%	97.75%	1.44%	93.89%	1.11%
1.6.90.50	90.16%	4.37%	96.66%	0.60%	87.47%	9.04%
1.10.30.25	99.41%	4.31%	94.61%	1.72%	84.67%	4.42%
1.10.90.25	98.52%	4.73%	97.09%	8.24%	83.64%	4.03%
1.10.30.50	109.27%	15.27%	98.88%	7.30%	91.59%	16.25%
1.10.90.50	105.00%	11.06%	100.16%	4.15%	87.67%	10.92%
2.6.30.25	89.29%	1.04%	84.85%	0.97%	72.45%	2.26%
2.6.90.25	86.61%	0.06%	92.17%	1.61%	73.87%	0.81%
2.6.30.50	92.67%	4.70%	88.93%	0.29%	76.84%	4.09%
2.6.90.50	88.15%	0.40%	92.04%	0.03%	75.96%	0.21%
2.10.30.25	89.40%	0.38%	84.77%	1.36%	74.23%	0.32%
2.10.90.25	90.19%	2.56%	87.38%	10.32%	76.45%	4.17%
2.10.30.50	87.60%	1.38%	87.05%	3.66%	75.57%	2.21%
2.10.90.50	89.99%	3.51%	88.77%	0.06%	76.83%	1.15%

Table A.3. CHN analysis of the solid residues after leaching.

		P	Al	Ca	Fe	S	Mg	Na	Cr	Ni	Cu	Zn	Cd	Pb
1.6.30.25	ICP,ave mg/l	6162.518	1606.053	875.893	12672.033	9443.433	1043.486	81.701	0.456	1.334	3.979	123.922	0.227	5.088
	Error, ICP	0.461	0.411	0.027	0.556	0.461	0.243	0.217	0.013	0.616	1.307	0.201	0.460	0.055
	%wt Recov	51.05%	40.80%	4.99%	44.93%		65.46%	55.31%	31.99%	21.63%	2.80%	45.11%	6.87%	15.05%
	Error, Recov	0.327	0.292	0.020	0.394		0.172	0.154	0.010	0.436	0.924	0.143	0.324	0.039
1.6.90.25	ICP,ave mg/l	8180.930	2020.600	577.489	17562.207	12357.229	1142.083	84.260	0.301	1.631	6.697	125.938	0.226	4.592
	Error, ICP	0.179	0.161	0.006	0.198	0.167	0.111	0.086	0.002	0.325	0.587	0.097	0.787	0.052
	%wt Recov	67.76%	51.32%	3.29%	62.26%		71.64%	57.03%	21.14%	26.44%	4.72%	45.84%	6.83%	13.58%
	Error, Recov	0.127	0.114	0.005	0.141		0.079	0.062	0.000	0.230	0.415	0.070	0.556	0.038
1.6.30.50	ICP,ave mg/l	3426.843	1155.863	894.643	12438.229	9919.448	1244.350	75.768	0.451	2.031	0.301	136.457	0.150	5.113
	Error, ICP	1.214	1.295	0.164	0.575	0.572	0.304	0.392	0.001	0.577	0.001	0.376	0.001	0.126
	%wt Recov	45.54%	47.45%	5.18%	58.81%		86.58%	58.43%	31.01%	24.23%	0.26%	42.81%	2.27%	9.05%
	Error, Recov	0.153	0.179	0.091	0.049		0.090	0.115	0.017	0.903	0.184	0.462	1.000	0.811
1.6.90.50	ICP,ave mg/l	3538.976	1277.581	611.259	15377.107	11776.690	1580.279	87.791	0.301	2.911	0.201	173.867	0.125	4.090
	Error, ICP	1.059	1.126	0.062	0.259	0.315	0.060	0.208	0.003	0.168	0.003	0.143	0.285	0.040
	%wt Recov	42.58%	47.86%	3.36%	59.78%		94.45%	59.64%	20.74%	27.05%	0.17%	54.34%	1.51%	6.76%
	Error, Recov	0.198	0.211	0.076	0.073		0.088	0.137	0.012	0.942	0.188	0.276	1.000	0.830
1.10.30.25	ICP,ave mg/l	4115.774	1081.611	903.605	7251.022	6651.274	594.235	51.042	0.450	0.751	8.219	72.961	0.150	4.429
	Error, ICP	0.120	0.085	0.003	0.186	0.166	0.040	0.034	0.001	0.001	0.162	0.028	0.001	0.143
	%wt Recov	59.03%	47.56%	8.91%	44.52%		64.53%	59.81%	54.73%	21.06%	10.02%	45.97%	7.86%	22.66%
	Error, Recov	0.090	0.065	0.007	0.137		0.033	0.029	0.005	0.005	0.119	0.025	0.005	0.097
1.10.90.25	ICP,ave mg/l	4075.654	1194.513	580.597	8787.576	7207.596	676.703	48.867	0.300	0.774	8.919	76.592	0.100	3.374
	Error, ICP	0.229	0.067	0.002	0.227	0.153	0.009	0.042	0.003	0.316	0.302	0.007	0.003	0.133
	%wt Recov	58.47%	52.52%	5.72%	53.96%		73.48%	57.26%	36.45%	21.76%	10.88%	48.25%	5.24%	17.28%
	Error, Recov	0.166	0.052	0.003	0.166		0.012	0.035	0.002	0.228	0.218	0.010	0.002	0.099
1.10.30.50	ICP,ave mg/l	5632.610	1603.019	1002.595	12495.485	13322.662	869.060	63.113	0.472	1.331	13.317	101.357	0.157	5.887
	Error, ICP	0.466	0.022	0.020	0.347	0.421	0.056	0.003	0.065	0.103	0.924	0.006	0.065	0.247
	%wt Recov	77.63%	63.26%	9.29%	78.87%		89.25%	69.56%	56.66%	26.38%	13.71%	42.70%	5.51%	21.17%
	Error, Recov	0.290	0.166	0.094	0.201		0.090	0.093	0.042	0.600	0.690	0.706	0.709	0.638
1.10.90.50	ICP,ave mg/l	5333.605	1435.007	678.839	12357.747	12688.534	821.137	57.092	0.403	1.563	16.622	103.632	0.101	4.306
	Error, ICP	0.525	0.209	0.096	0.390	0.527	0.039	0.082	0.346	0.038	1.043	0.112	0.008	0.365
	%wt Recov	75.10%	60.68%	6.41%	78.47%	0.00%	87.79%	64.42%	44.88%	30.24%	19.39%	52.77%	3.53%	15.42%
	Error, Recov	0.313	0.142	0.089	0.225	0.000	0.036	0.078	0.258	0.642	0.637	0.350	0.707	0.685
2.6.30.25	ICP,ave mg/l	2092.887	382.064	963.358	4372.249	3797.518	759.089	62.469	0.454	0.833	0.303	102.320	0.151	3.669
	Error, ICP	0.098	0.327	0.022	0.084	0.087	0.036	0.024	0.008	0.136	0.008	0.012	0.008	0.094
	%wt Recov	16.99%	9.50%	5.38%	15.19%		46.69%	41.46%	31.26%	13.25%	0.21%	36.52%	4.49%	10.63%
	Error, Recov	0.062	0.224	0.023	0.052		0.018	0.010	0.013	0.104	0.013	0.001	0.013	0.060
2.6.90.25	ICP,ave mg/l	2110.932	715.227	572.241	6551.438	5466.793	915.701	61.041	0.302	1.159	0.202	111.656	0.101	2.847
	Error, ICP	0.117	0.101	0.005	0.089	0.073	0.062	0.068	0.007	0.006	0.007	0.045	0.007	0.081
	%wt Recov	17.13%	17.80%	3.20%	22.76%		56.31%	40.50%	20.82%	18.42%	0.14%	39.84%	2.99%	8.25%
	Error, Recov	0.076	0.064	0.003	0.056		0.037	0.041	0.012	0.012	0.012	0.024	0.012	0.050
2.6.30.50	ICP,ave mg/l	775.655	317.034	857.919	8410.071	6976.267	1120.675	67.840	0.451	1.616	0.301	120.456	0.150	3.946
	Error, ICP	0.167	0.179	0.006	0.021	0.018	0.014	0.027	0.001	0.100	0.001	0.017	0.001	0.015
	%wt Recov	6.33%	7.94%	4.82%	29.39%		69.31%	45.27%	31.21%	25.83%	0.21%	43.22%	4.49%	11.50%
	Error, Recov	0.116	0.125	0.006	0.013		0.011	0.021	0.003	0.072	0.003	0.013	0.003	0.012
2.6.90.50	ICP,ave mg/l	883.346	385.368	574.605	10687.215	7936.007	1268.545	68.193	0.312	2.256	0.208	134.303	0.104	3.504
	Error, ICP	0.295	0.472	0.053	0.071	0.088	0.038	0.084	0.046	0.100	0.046	0.072	0.046	0.028
	%wt Recov	7.22%	9.65%	3.23%	37.35%		78.46%	45.51%	21.60%	36.06%	0.14%	48.20%	3.10%	10.21%
	Error, Recov	0.210	0.336	0.039	0.052		0.029	0.061	0.031	0.073	0.031	0.053	0.031	0.021
2.10.30.25	ICP,ave mg/l	1412.828	188.671	1107.407	1663.988	2026.440	380.902	45.000	0.451	0.751	0.300	59.421	0.150	3.306
	Error, ICP	0.016	0.090	0.062	0.008	0.016	0.028	0.168	0.001	0.001	0.001	0.017	0.001	0.001
	%wt Recov	19.99%	8.19%	10.77%	10.08%		40.81%	52.05%	54.05%	20.80%	0.36%	36.94%	7.77%	16.70%
	Error, Recov	0.015	0.067	0.040	0.009		0.016	0.122	0.004	0.004	0.004	0.009	0.004	0.004
2.10.90.25	ICP,ave mg/l	1117.096	290.409	609.457	2491.234	2407.423	455.585	38.518	0.301	0.527	0.201	59.580	0.100	2.508
	Error, ICP	0.019	0.030	0.059	0.043	0.050	0.062	0.113	0.003	0.064	0.003	0.046	0.003	0.081
	%wt Recov	15.80%	12.60%	5.93%	15.08%		48.81%	44.55%	36.10%	14.58%	0.24%	37.04%	5.19%	12.67%
	Error, Recov	0.017	0.024	0.039	0.027		0.040	0.083	0.006	0.042	0.006	0.029	0.006	0.054
2.10.30.50	ICP,ave mg/l	683.442	318.013	795.178	4203.269	3978.114	596.399	44.921	0.406	0.707	0.271	67.973	0.135	2.928
	Error, ICP	0.173	0.253	0.195	0.149	0.177	0.159	0.036	0.158	0.092	0.158	0.133	0.158	0.223
	%wt Recov	9.69%	13.82%	7.75%	25.50%		64.02%	52.06%	48.83%	19.63%	0.33%	42.34%	7.02%	14.81%
	Error, Recov	0.118	0.174	0.133	0.101		0.108	0.030	0.108	0.060	0.108	0.089	0.108	0.153
2.10.90.50	ICP,ave mg/l	586.756	249.173	654.087	5239.307	4403.788	648.303	63.521	0.326	0.960	0.217	72.356	0.109	2.898
	Error, ICP	0.365	0.500	0.115	0.206	0.236	0.204	0.453	0.110	0.208	0.110	0.188	0.110	0.070
	%wt Recov	8.31%	10.82%	6.38%	31.77%		69.58%	73.72%	39.16%	26.63%	0.26%	45.06%	5.63%	14.67%
	Error, Recov	0.254	0.350	0.086	0.141		0.140	0.325	0.082	0.143	0.082	0.129	0.082	0.054

Table A.4. Composition of the leachate and recovery

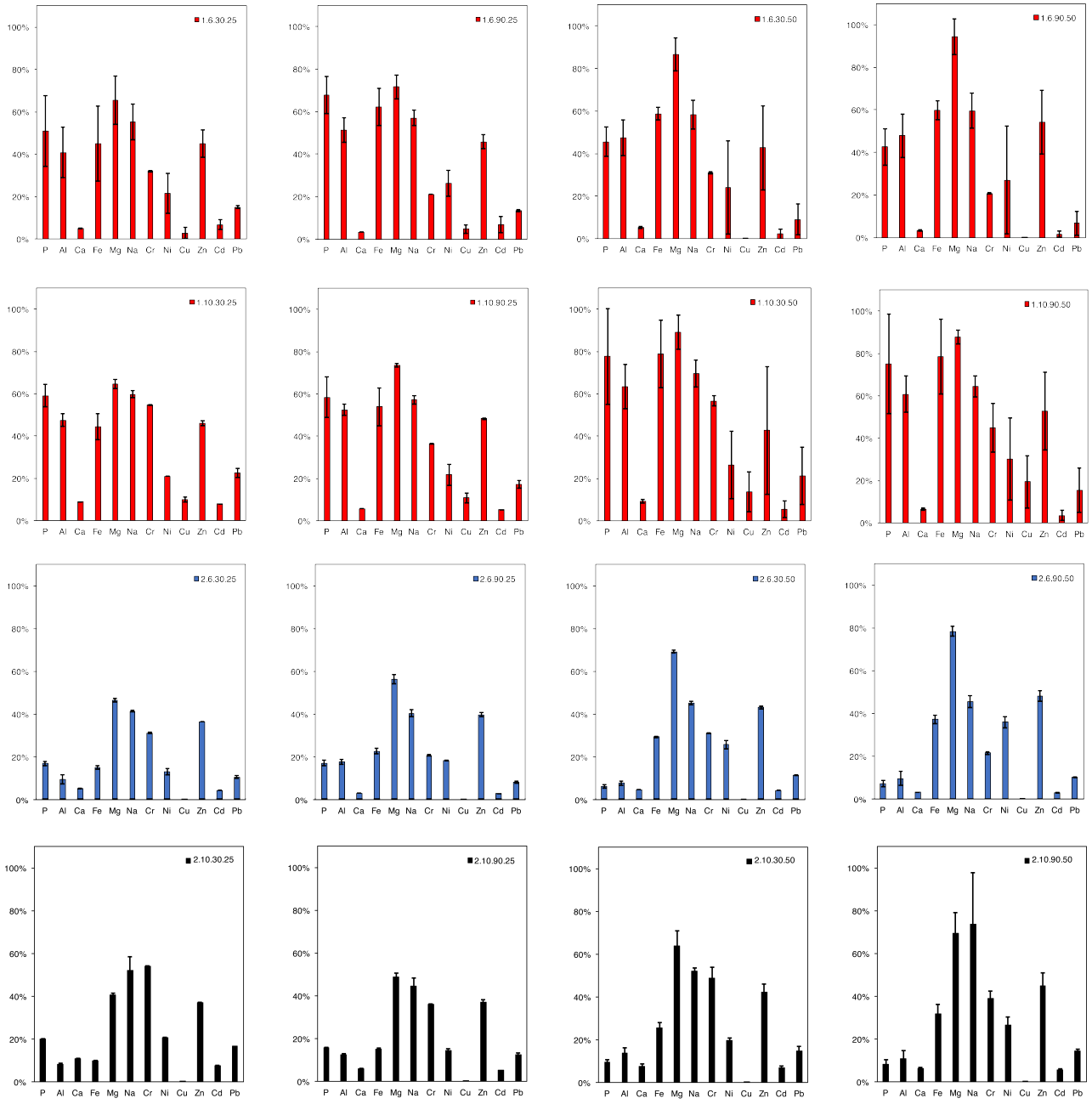


Figure A.1. Weight percentage recovered from the solid into the leachate of the analysed elements.

A.3 Surface plots

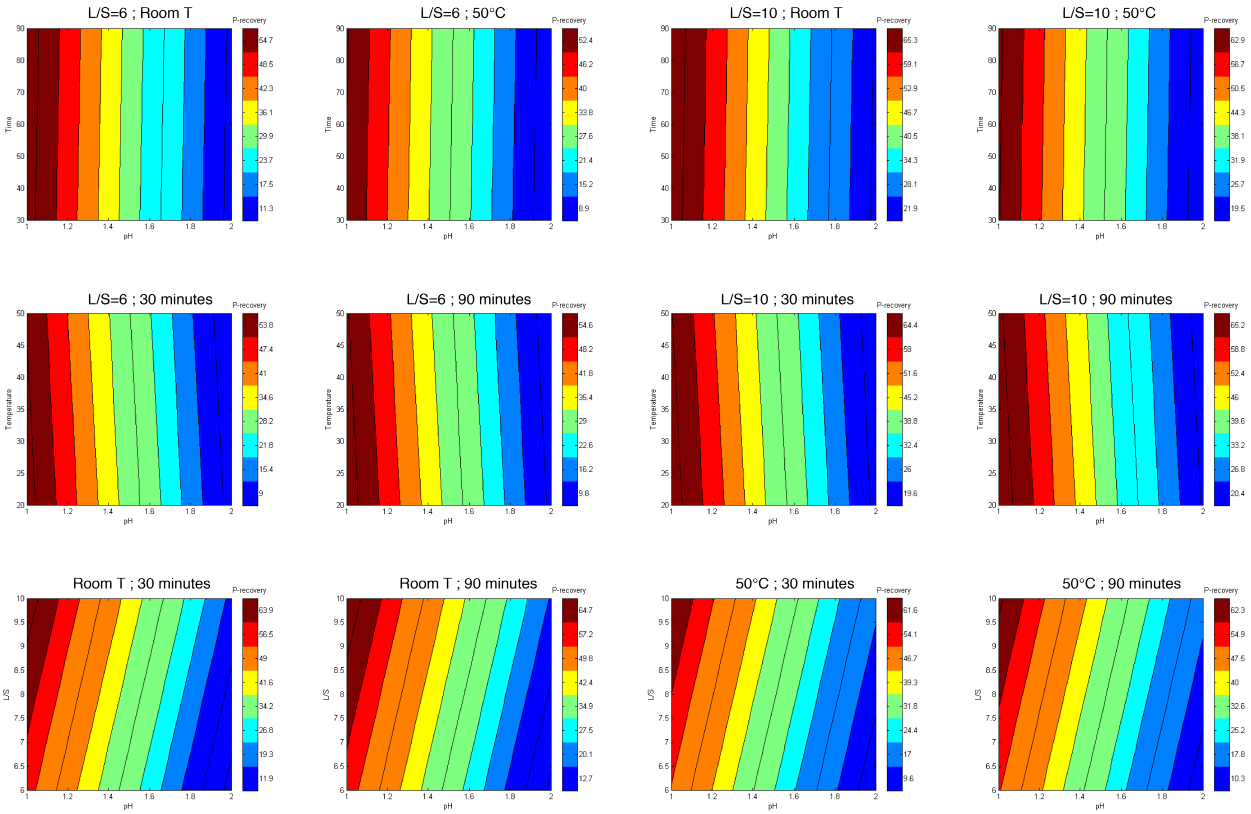


Figure A.2. Surface graphs for liquid to solid ratio, temperature (C) and time (min) vs pH for all the conditions.

A.4 Temperature and pH profiles

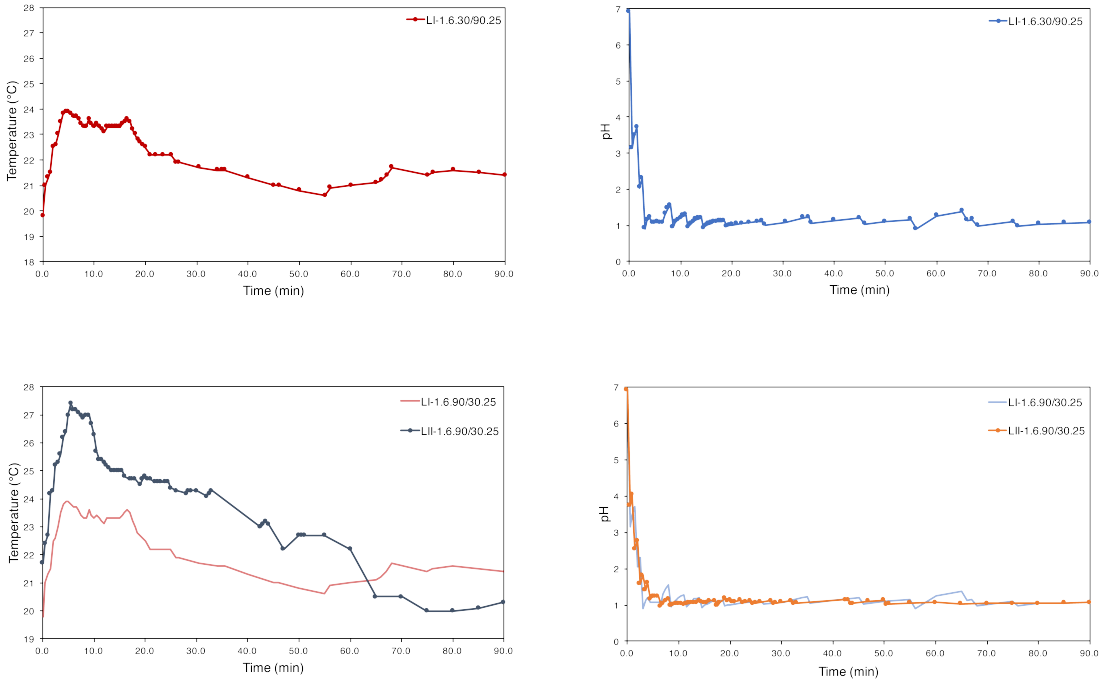


Figure A.3. Pressure and temperature profile for experiments LI and LII - 1.6.25

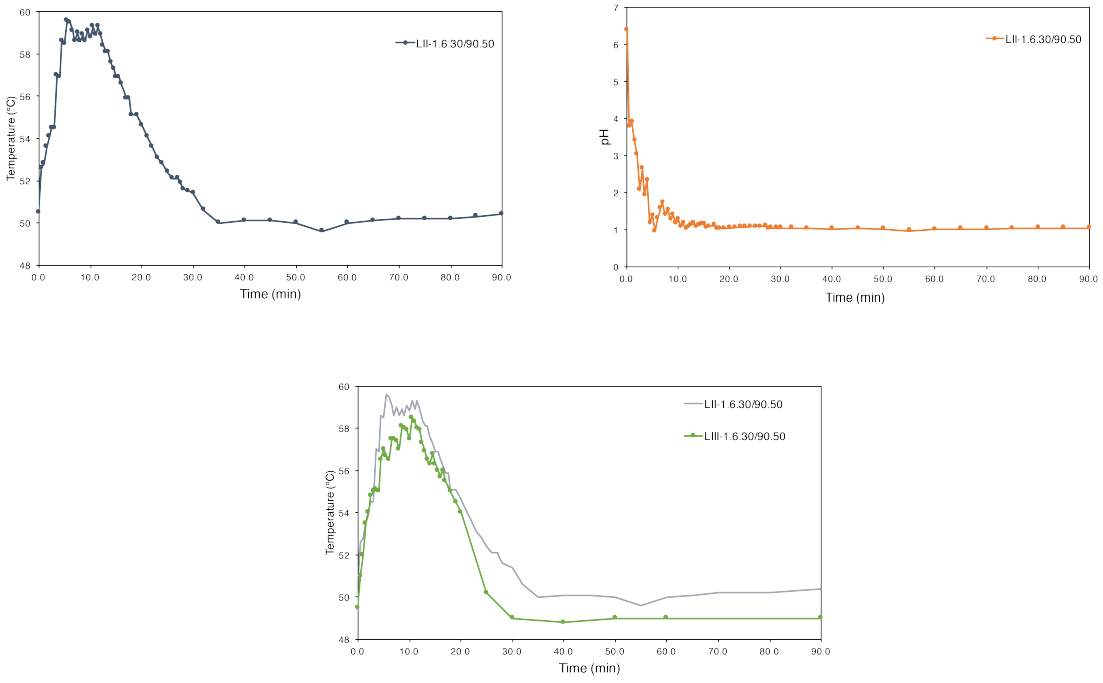


Figure A.4. Pressure and temperature profile for experiments LI and LII - 1.6.50

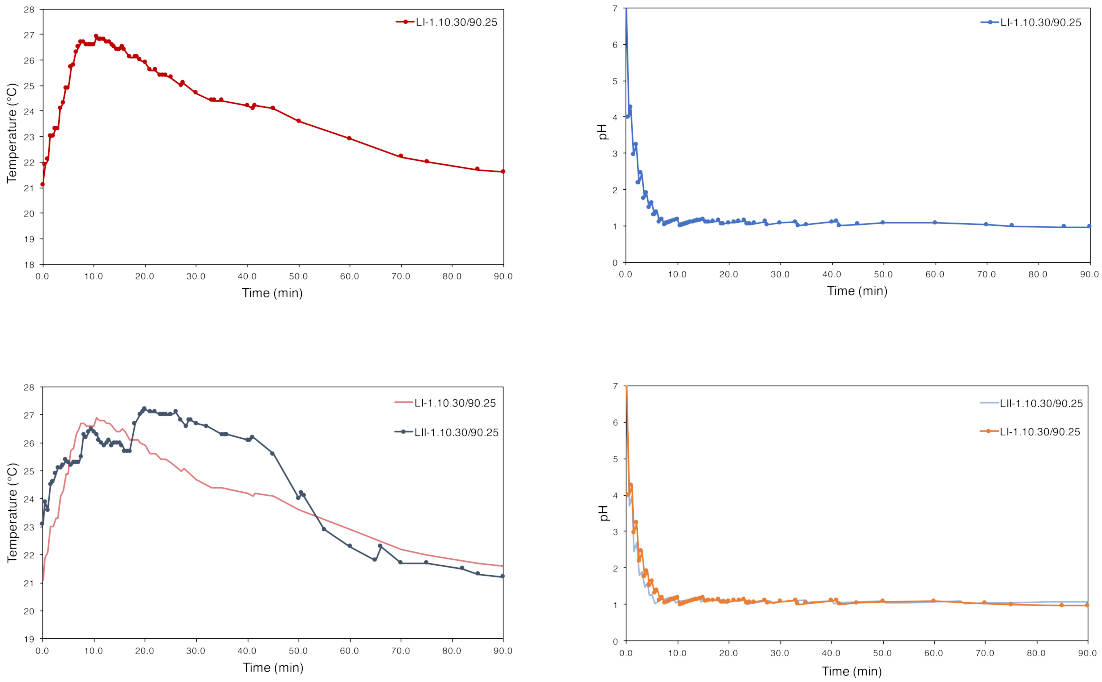


Figure A.5. Pressure and temperature profile for experiments LI and LII - 1.10.25

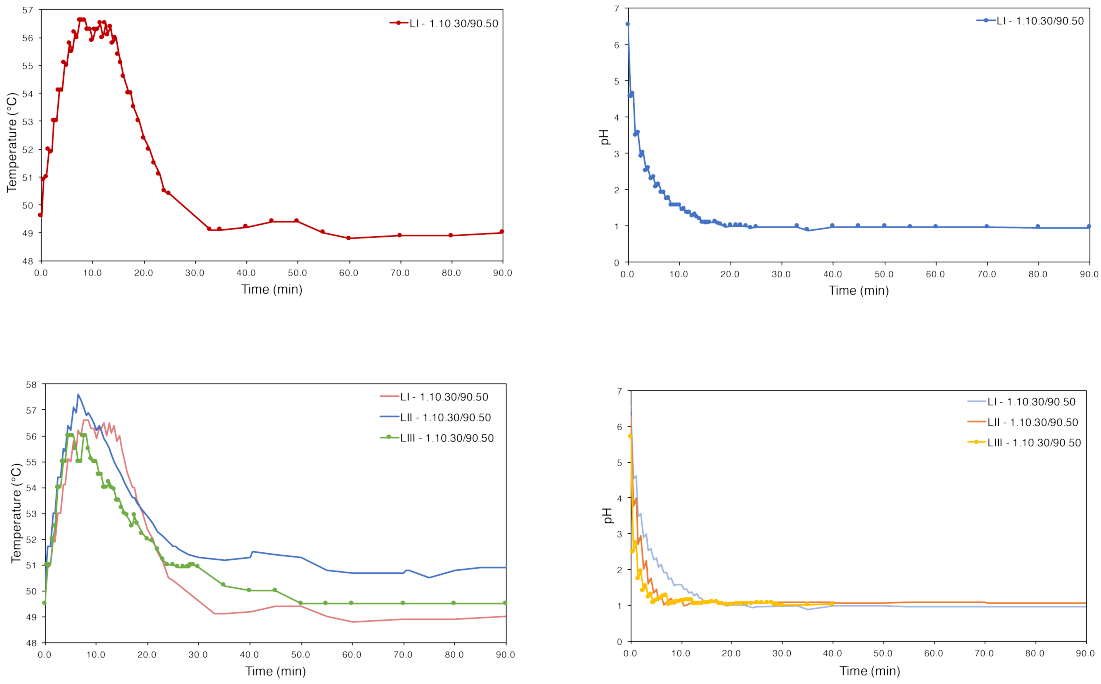


Figure A.6. Pressure and temperature profile for experiments LI and LII - 1.10.50

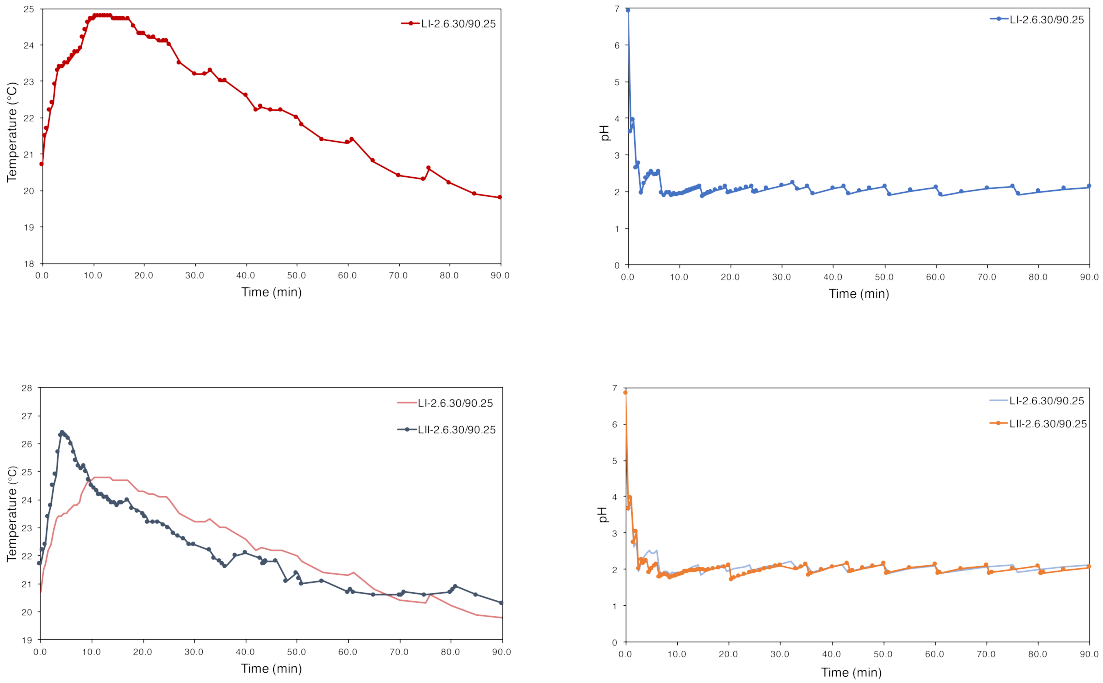


Figure A.7. Pressure and temperature profile for experiments LI and LII - 2.6.25

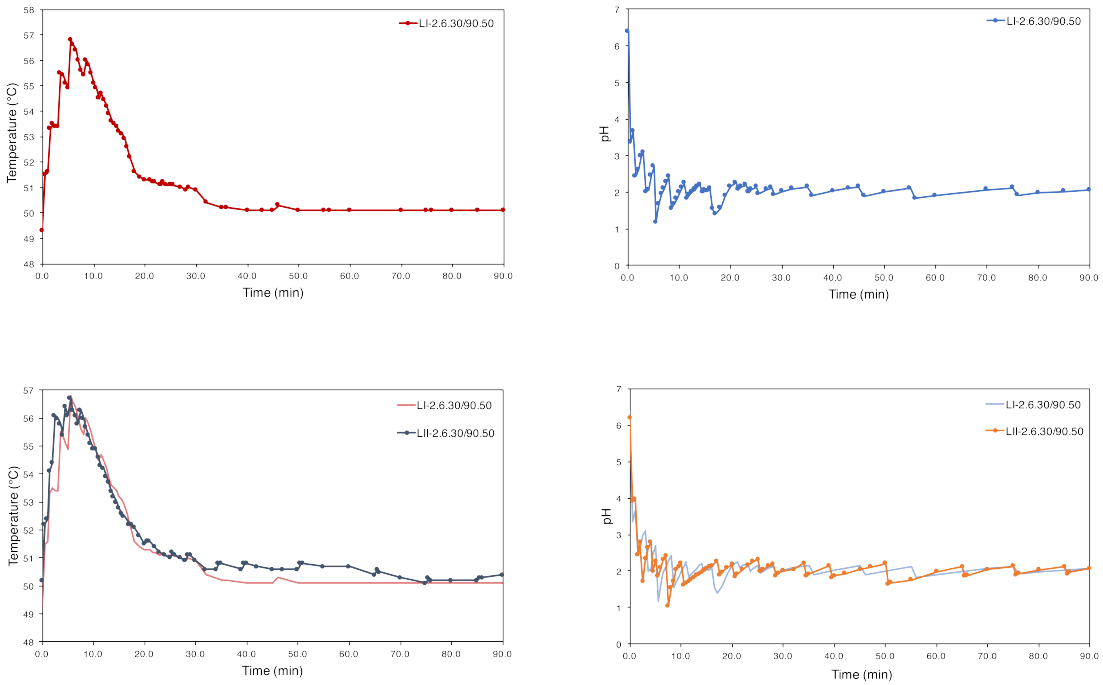


Figure A.8. Pressure and temperature profile for experiments LI and LII - 2.6.50

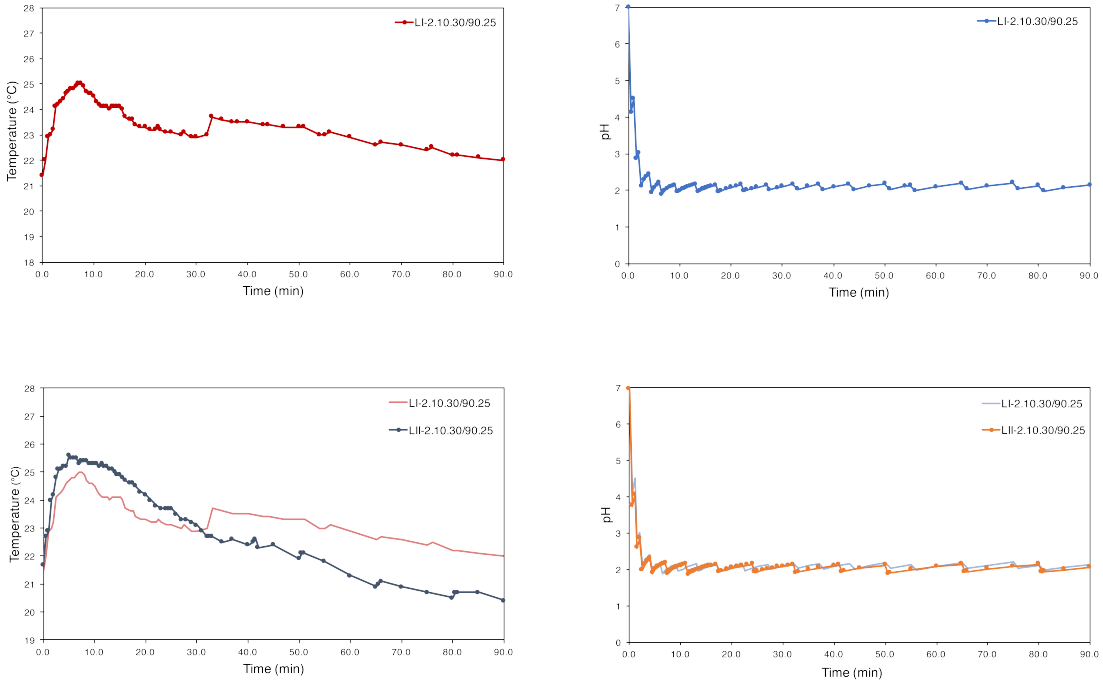


Figure A.9. Pressure and temperature profile for experiments LI and LII - 2.10.25

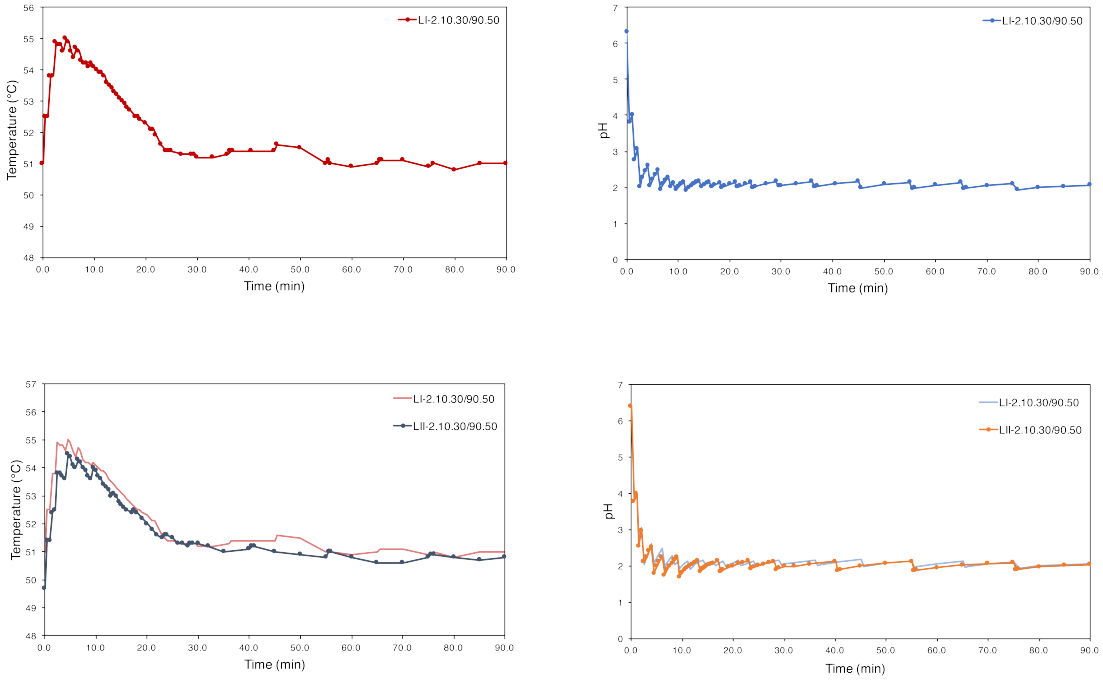


Figure A.10. Pressure and temperature profile for experiments LI and LII - 2.10.50

Phosphorus recovery from hydrothermally treated sewage sludge: Optimization, purification and precipitation

October 2019

ABSTRACT

This second part of the phosphorus recovery project has focused its activity on pushing the recovery of phosphorus from the solid residue by changing the leaching conditions. We were able to push the recovery up to 87% by using a liquid to solid ratio of 20 at pH 1 and up to 84% by using a liquid to solid ratio of 10 at pH 0.5. In addtion, we used ion exchange resins to purify the leachate by removing most of the cations present in the samples. In fact the resins have proven to work as expected for the experiments with a liquid to solid ratio of 20. Up to 91% of the phosphorus remained in the purified leachate. For experiments with a liquid to solid ratio of 10, the column gradually stopped retaining cations because it got saturated and needed regeneration. Finally, we have performed some preliminar precipitation experiments with dirty leachate. The results showed that no crystalline calcium phosphates were precipitated. Next, precipitations experiments with the purified leachate will be performed in order to see if the reason for this poor performance is the fact that the leachate is not purified or if it lies within the nature of the solid residue.

List of Figures

1 Summary of the process. . . . 3
2 Composition (%wt in blue, mg/kg in orange) of the solid residue mix before leaching. . . . 6
3 P recovery from the solid residue to the leachate and in the precipitates for the preliminar experiments 6
4 Composition (%wt in blue, mg/kg in orange) of the solid residue mix before leaching. . . . 7
5 Percentage of the carbon in the solid residue that remains in the solids after leaching. . . . 7
6 [Left] Percentage of P recovered in the leachate from the solid residue. [Right] Percentage recovered of all the elements analysed. . . . 7
7 Percentage of each element that remains in the purified leachate (+ cleaning water) with respect to the mg of each element present in the dirty leachate. . . . 8
A.1 Lab setup for the purification experiments. . . . 11
A.2 Change in pH throughout purification of the leachate and cleaning of the column with ultra pure water. . . . 11
A.3 XRD spectra from top to bottom: solid residue, precipitates Exp1 and precipitates Exp1 II. . . . 13
A.4 XRD spectra from top to bottom: precipitates Exp2, waste solid after leaching Exp3, precipitates Exp3. . . . 14

List of Tables

1 Conditions for the leaching experiments to push P recovery. RT= room temperature, 25°C. . . . 6
2 For conditions 1.20.45.25, percentage of the elements present in the purified leachate, discarded water and cleaning water taking as a reference the mg of each element present in the dirty leachate. . . . 8
3 For conditions 0,5.10.45.25, percentage of the elements present in the purified leachate, discarded water and cleaning water taking as a reference the mg of each element present in the dirty leachate. . . . 8
A.1 ICP results (mg/l) for the leaching experiments performed. . . . 12
A.2 ICP results (mg/l) for the purification experiments performed. . . . 12

Contents

1 Aim, framework and scope 3
2 Experimental protocol 4
2.1 Materials . . . 4
2.2 Method . . . 4
Digestion and leaching experiments • Dicalcium phosphate precipitation • Purification experiments

3 Results and discussion **5**
3.1 Preliminar precipitation experiments . . . 5
3.2 Leaching experiments to push P recovery . . . 5
3.3 Purification of the leachate . . . 7
4 Conclusions **8**
References **10**
A Appendix **11**
A.1 Purification experiments . . . 11
A.2 ICP results . . . 12
A.3 XRD spectrum . . . 13

1 Aim, framework and scope

Aim

The goal of this report is to show the results of purification experiments in order to remove the cations present in the liquid phase after leaching. Besides, on the basis of the leaching conditions chosen as the best after the design of experiments performed in the previous report, we aim to find the conditions under which we can achieve 80 to 90% recovery.

Framework

Around 9 millions of tons of sewage sludge (SS) are produced every year in Europe as a side product of the treatment of wastewater, one of the major volumes of waste directly linked to the existence of humans. The current sludge disposal routes (landfilling, biosolids production, and incineration) cause severe environmental impacts (e.g. soil contamination, toxic gas emissions) and do not valorise its energetic and mineral content such as performing phosphorus (P) recovery. Treatech has developed a cost-efficient and eco-friendly technology for transforming waste streams (among which SS) into clean water, renewable gas and fertilizers precursors using the unique properties of supercritical water (refer to figure 1).

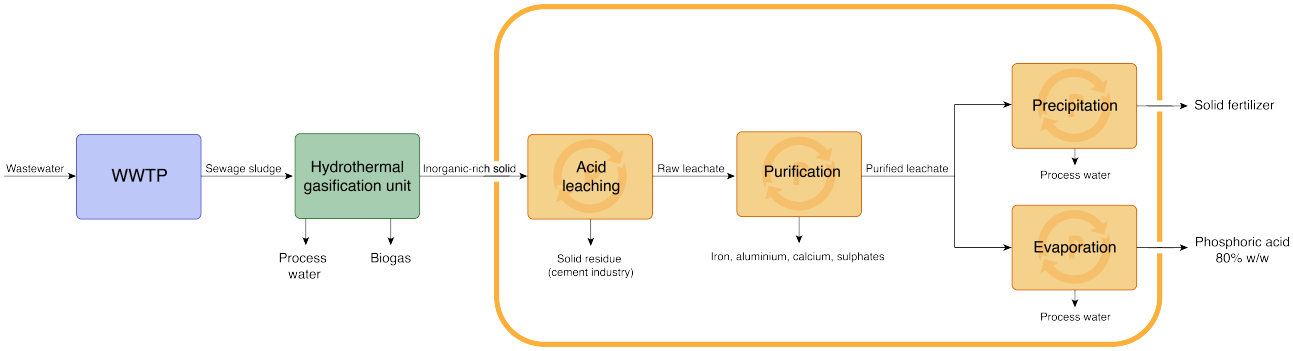


Figure 1. Summary of the process.

Phosphorus is a key component in crop growth and animal anf human food production. Nowadays it is almost exclusively obtained in the form of phosphoric acid through mining of phosphate rock. The concern of depleting the current sources of this element has raised exponentially since its production from fossil resources is expected to peak between 2035 and 2075[1,2]. The phosphoric acid extracted through mining, is mainly consumed by the fertilizer industry which, for instance, demanded in 2015 around 4 million tonnes of phosphorus (in Europe, expressed as P_2O_5). This number is expected to increase 2.2% by 2020. Around 3.5% of this phosphorus (expressed as P_2O_5) will end up in sewage sludge.[3–8]

Switzerland is the first country to establish a new regulation regarding P-recovery from sewage sludge and the latter will enter into force in 2026. Although several companies have developed promising P-recovery technologies, all of them either have low efficiencies or suffer from high capital and operating costs.

Scope

Pushing P recovery. We could reach a maximum average of 65% phosphprus recovery through acid leaching after 30 minutes at pH 1, room temperature and liquid to solid ratio of 10. We could reach 90% by lowering the pH to 0. However at this low pH, intensive leaching of heavy metals also occurs.

We think that even though we found that pH was the main factor affecting phosphorus leaching, the liquid to solid ratio has an important role as well since it directly affects the mass transfer rate of phosphorus to the liquid phase. Besides, according to previous studies[9], recovery reaches 90% from a liquid to solid ratio of 20 which is double the highest value we used for our previous study. This is why we decided to perform new leaching experiments tuning liquid to solid ratio and pH. Specifically, we run experiments at pH 1 and liquid to solid ratio of 20 as well as experiments at pH 0.5 and liquid to solid ratio of 10.

Purification. After leaching, not only phosphorus is transferred to the liquid phase. As we observed in the previous report, iron, aluminium, calcium and magnesium are the most abundant ions found in the leachate (apart from phosphorus) but we can also find nickel, zinc, cadmium, chrome, lead, copper, sodium and potasium in low concentrations. The percentage of

each ion that is transferred to the liquid phase depends on the conditions of the leaching process. Low residence times and higher pH will result in lower concentration of these elements but these conditions also decrease the amount of phosphorus recovered. As phosphorus leaches to the liquid faster than most of the rest of the ions, keeping the residence time as low as possible (30-45 minutes) will guarantee the lowest concentration of undesired ions while achieving high recovery.

The level of purification needed depends on the final product. If the targeted product is phosphoric acid, intensive purification is needed in order to comply with the commercial phosphoric acid requirements[9]. On the other hand, to produce a solid phosphate we would need to remove the main ions prior to precipitation (to avoid impurities in the solid) and then check if the quality of the residual liquid is good enough for discharge.

Valorization of P after leaching. We considered two possibilities for the valorization of phosphorus after leaching and purification: precipitation as phosphates and concentration as phosphoric acid.

The easiest phosphate to precipitate is dicalcium phosphate dyhydrate (DCPD). Corresponding to the formula $CaHPO_4 \cdot 2H_2O$, it can be produced from phosphoric acid by precipitation with $Ca(OH)_2$ in aqueous media at room temperature (5 steps reaction). Then, the anhydrous form (DCP) can be produced the same way as DCPD but at around 100 °C. Tricalcium phosphate (TCP, $Ca_3(PO_4)_2$) can also be precipitated from phosphoric acid and calcium hydroxide at high temperature in aqueous phase or low temperature in organic solvents.[10–13]

We also considered struvite as a product. Magnesium Amounium Phosphate (MAP, $MgNH_4PO_4.6H_2O$) is a crystalline solid with low solubility in water or alkaline solutions. As its name indicates, it consists of magnesium, amonium and phosphate in a 1:1:1 molar ratio and it is normally hydrated by six water molecules. Struvite can be used as a low nutrient release fertilizer since it is a direct source of phosphorus (13%), nitrogen (6%) and magnesium (10%). Many wastewater plants precipitate struvite to prevent scaling of the equipment due to a natural precipitation of struvite along the subsequent steps of the waste water treatment[14]. To ensure an efficient precipitation of phosphprus in the form of MAP, pH should between 8 and 9 for municipal waste[15,16]. Besides, although precipitation starts when the ratio between the three ions is 1:1:1, the process is favoured when the NH_4:PO_4 molar ratio is increased[15,17,18]. Finally, the presence of calcium in the mixture, as it is our case, decreases the availability of phosphorus for the precipitation of struvite since dicalcium phosphate is formed.

On the other hand, we investigated the posibility of chosing phosphoric acid as our final product. In this case, the leachate has to be purified and then water must be evaporated to reach a phosphoric acid concentration of 80%. The low purity of the diluted phosphoric acid after leaching is mainly due to the presence of iron, sulphur, aluminium, calcium and magnesium. Zinc, sodium, copper, lead, nickel, chrome and cadmium are also present in low quantitites.

2 Experimental protocol

2.1 Materials

65% Nitric Acid was acquired from Sigma-Aldrich. 37% Chlorhydric Acid was acquired from Sigma-Aldrich. 95-98% Sulphuric Acid was acquired from Merck. 95% Calcium hydroxide was acquired from Sigma-Aldrich. Nylon membrane filters (0.2 μm pore size) were acquired from Whatman. Nylon membrane filters (0.2 μm pore size) were acquired from Whatman. The leaching experiments were performed in a 400 ml glass beaker provided with a magnetic stirrer and ultrapure water (Mili-Q) was used to reach the desired liquid to solid ratio. For the purification experiments a glass column with fritted glass at the bottom was used as the exchange column. 2 mm glass beads were acquired from VWR. The strong cation resin MTC1600H was provided by Purolite. The precipitation experiemnts were performed in a 400 ml glass beaker provided with a magnetic stirrer. For all experiemnts, continuous stirring was achieved using a hotplate (Heidolph Hei-Tec) and pH and temperature were measured using a VWR Phenomenal 1100 L pH meter.

2.2 Method

2.2.1 Digestion and leaching experiments

We performed microwave digestion with aqua regia and sent the liquid phase to ICP to know the composition of the solid residue. Leaching experiments were also performed, to push the P recovery following the protocol followed in the first report. We sent the liquid phase to ICP to know the concentration of ions. Refer to the previous report for details.

2.2.2 Dicalcium phosphate precipitation

The experiments were performed by adding calcium hydroxide (aqueous, 1M) to the leachate at room temperature, under stirring for 2 hours and measuring the pH of the solution in intervals of 1 to 5 minutes. Then the solids were separated from

the liquid phase using a nylon membrane filter (0.2 μm pore size) under vacuum and then dried overnight at 100°C.

2.2.3 Purification experiments

We performed six purification experiments using the leachate from the six leaching experiments performed.

The setup consisted of a glass column with fritted glasss at its lower part and glasss valves at its ends plus a vent. The total height of the column is 53 cm whereas the height from the top to the fritted glass is 34 cm. The internal diameter is 29 mm. First, we filled the column with 30 ml water and up to 2 cm above the fritted glass with glass beads of 2 mm of diameter. Then, we washed around 125 ml of resin twice with 200 ml of fresh ultra pure water before filling the column with the water/resin mixture. Finally, we added glasss beads (2 mm diameter) up to 2 cm on top of the resin. The liquid level on the column must always remain 2 to 3 cm above the bed to ensure that the column never dries up and we avoid bubles inside the bed. The inlet of the column was connected through plastic pipes to a 60 ml plastic syringe which acts as a manual pump to fill the column with our solution. Refer to figure A.1 for details of the setup.

Before pumping the leachate, we washed the bed with one liter of ultra pure water. Then, we pumped the leahate inside the column opening the lower valve to allow the solution to pass through the bed. We discarded the first 50 ml of product since they represent the water inside the bed before our leachate passes through. Then, we collected the purified leachate in a 250 ml bottle. To avoid losing part of our product, once the level of the leachate above the bed is around 2 cm, we pumped 150 ml of ultrapure water and collected the outlet of the column in the same bottle until the level is again 2 cm over the bed.

In order to clean the column for the next experiment, we pumped two liters of ultra pure water which is enough to increase the pH of the outlet until that of ultrapure water. Refer to figure A.2 for details of the change in pH.

For each experiment, we take 3 samples for ICP analysis. One from the 50 ml discarded at the begginning, one from the purified leachate bottle and one from the first liter of ultra pure water for cleaning.

3 Results and discussion

3.1 Preliminar precipitation experiments

Several preliminar precipitation experiments were performed using a solid residue mix from several hydrothermal treatments run in our salt separator prototype.

We wanted to see if we could produce calcium phosphates (without previous purification) by mimicking processes in which phosphates are precipitated from sewage sludge ashes leachate[19–21]. We expected to precipitate phosphorus in the form of dicalcium phosphate[19]. The conclusions we can draw from these preliminar experimens are the following.

- Dry precipitates were sent to XRD and no crystalline dicalcium phosphate was found. In fact, phosphorus was only found forming iron-phosphorus complexes in very low concentrations (XRD spectra in figures A.3 and A.4 in the appendix).
- Nonetheless, according to ICP, phosphorus is precipitating (refer to figure 3 for details). We just do not know in which form. Since XRD only shows crystalline phases, P could be in amorphous form.
- We hypothesize that the fact that our feed is not incinerated (but treated under supercritical conditions) might be influencing the precipitation products.
- We performed a leaching experiment (Exp 2) using ashes and then we precipitated phosphorus as previously. In this case we can see crystalline dicalcium phosphate through XRD (spectra in figure A.4 in the appendix). This could confirm the previous hypothesis.

3.2 Leaching experiments to push P recovery

As a feedstock we used the solid residue produced during the campaign run at the lab-scale prototype in June 2019. ICP analysis after aqua regia digestion revealed that the solid contains 6.2% wt. phosphorus which lies within the typical concentraiton of the element in the solid residues analysed before. However, we want to highlight that this solid contains much lower concentrations of heavy metals such as Cd, Pb, Ni or Cr compared to other solid residues. Refer to figure 4 for the complete composition.

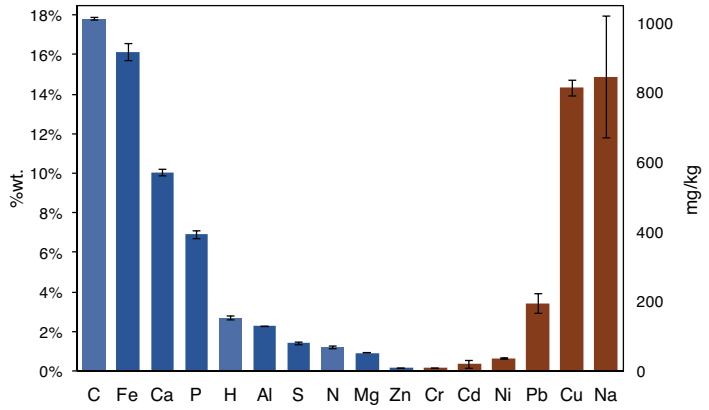


Figure 2. Composition (%wt in blue, mg/kg in orange) of the solid residue mix before leaching.

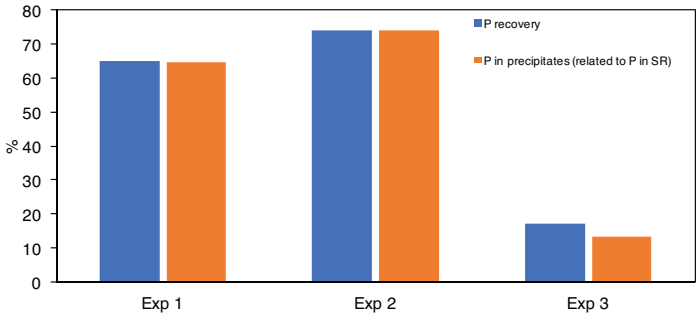


Figure 3. P recovery from the solid residue to the leachate and recovery of this P in the precipitates for the preliminar experiments. [Exp1] Feedstrock: solid residue. Leaching conditions: pH 1, 90 minutes, L/S 6, room temp. Precipitation conditions: 1.2% $Ca(OH)_2$, 120 minutes, room temp. [Exp 2] Feedstrock: sewage sludge ashes. Leaching conditions: pH 1, 90 minutes, L/S 6, room temp. Precipitation conditions: 2% $Ca(OH)_2$, 120 minutes, room temp. [Exp 3] Feedstrock: solid residue + $Ca(OH)_2$ (15% w/w). Leaching conditions: pH 4, 90 minutes, L/S 6, room temp. Precipitation conditions: 1.1% $Ca(OH)_2$, 120 minutes, room temp.

The conditions used will help choosing the apropriate liquid to solid ratio while not going too low on the pH scale to avoid excessive leaching of heavy metals (refer to table 1 for details). Experiments under columns A and B will be referred as 1.20.45.25 and 0,5.10.45.25 respectively, from now on.

	A	**B**
pH	1	0.5
Temp. (°C)	RT	RT
L:S	20	10
Time (min)	45	45

Table 1. Conditions for the leaching experiments to push P recovery. RT= room temperature, 25°C.

After leaching, the solids that remain in the filter are dried and sent to perform elemental analysis. In average, 87% and 97% of the carbon remains in the solid for the experiments at pH 1 and 0.5 respectively (figure 5). As the experiment at pH 0.5 is performed at half the liquid to solid ratio (10), we think that less carbon can solubilize in the liquid and hence, more carbon remains in the solid.

On the other hand, the liquid phase is analysed through ICP to evaluate the performance of the leaching experiments. For each of the two conditions mentioned (table 1), experiments were run in triplicates. In average, we were able to extract 87% and 84% wt. of the phosphorus in the solid residue for experiments 1.20.45.25 and 0,5.10.45.25 respectively (refer to table A.1 for results in mg/l). We can say that both conditions result in the same performance towards phosphorus recovery and improve by more than 20% the past results obtained for pH 1 and liquid to solid ratio of 10. Regarding the rest of the elements analysed, concentrations of Mg, Al, Fe, Ni, Cu, Zn, Cd and K are higher for lower pH while only Ca, Cr and Pb have slightly higher concentrations for a higher pH. This means that working at a higher pH will contaminate less our

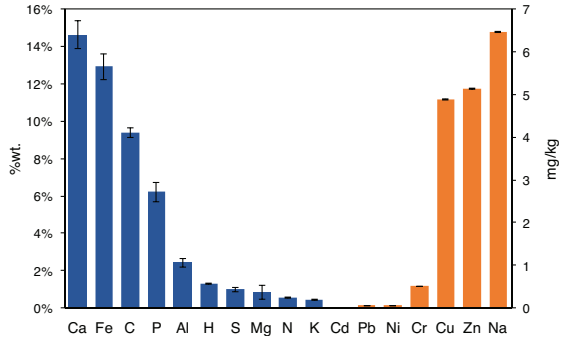


Figure 4. Composition (%wt in blue, mg/kg in orange) of the solid residue mix before leaching.

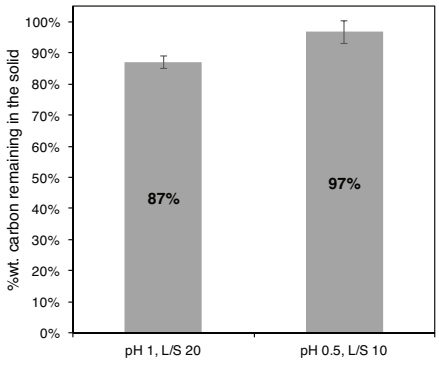


Figure 5. Percentage of the carbon in the solid residue that remains in the solids after leaching.

leachate. We should take special precautions when analysing the behavior of Cd, Pb, Ni and Cr since they have very low concentrations in the solid residue. This results in bigger inaccuracies and errors. Refer to figure 6 for all the recovery results.

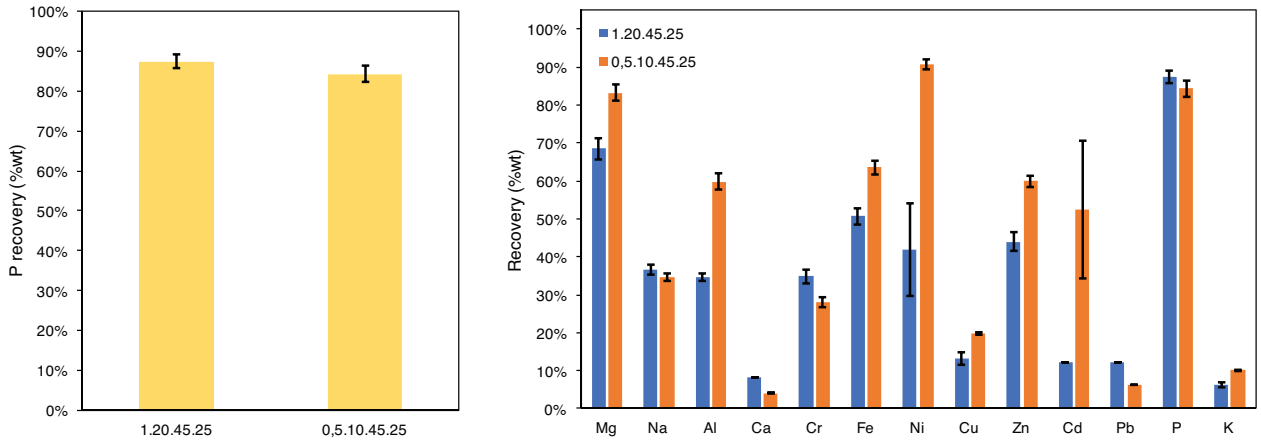


Figure 6. [Left] Percentage of P recovered in the leachate from the solid residue. [Right] Percentage recovered of all the elements analysed.

3.3 Purification of the leachate

One purification experiment was performed for each leachate produced. We took three samples for each one of them and analysed them through ICP. The three samples correspond to water exiting the column at the beginning of the experiments, purified leachate and water used to clean the column after the experiments.

For all six experiments performed, the discarded water at the beginning of them had negligible amounts of all the elements analysed. However, we found that, especially for Na and P, 14 to 20% of the amount present in the dirty leachate ended up in the cleaning water (refer to tables 2 and 3 for details). In view of these results, we will change the protocol of the purification experiments for the next trials. We should identify after how many ml of cleaning water, P stops coming out of the column and recover these ml as part of the purified leachate.

A part from this fact, we were able to recover, in the purified stream, 91% and 87% of the P that was present in the dirty leachate for conditions 1.20.45.25 and 0,5.10.45.25 respectively. Starting from the P in the solid residue, the overal recovery rate is 80% wt and 73% wt for conditions 1.20.45.25 and 0,5.10.45.25 respectively.

For the rest of the elements, for the 1.20.4.25 experiments, we could remove all the Mg, Al, Cu, Zn, Cd and Pb and almost all the Ca, Fe and K. In the case of the 0,5.10.45.25 experiments, the resin worked quite well for the first experiment, although giving worse results than for the more diluted conditions. However, for the second and third experiments, the

resins were unable to retain any cations, which means that the column was saturated and needed regeneration. Figure 7 show the results for each element and each of the triplicates for both leaching conditions. Refer to table A.2 for results in mg/l.

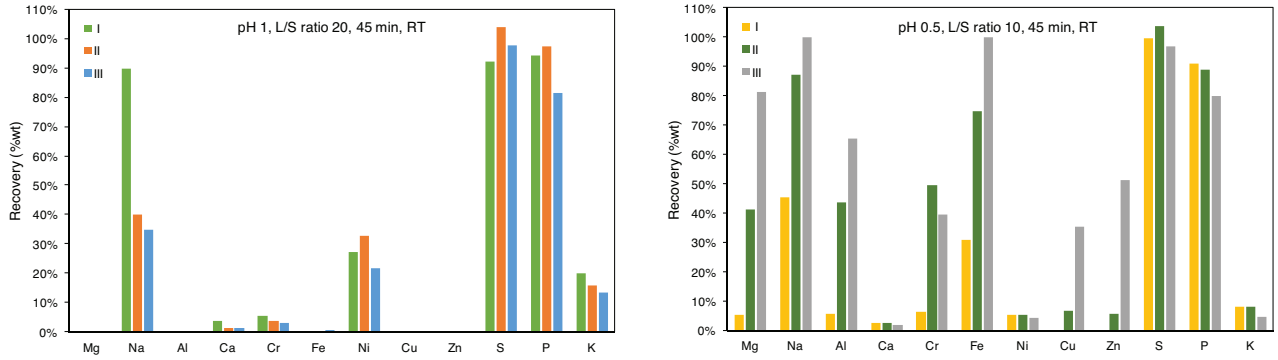


Figure 7. Percentage of each element that remains in the purified leachate (+ cleaning water) with respect to the mg of each element present in the dirty leachate.

	pH 1, L/S ratio 20, 45 min, RT											
	Mg	**Na**	**Al**	**Ca**	**Cr**	**Fe**	**Ni**	**Cu**	**Zn**	**S**	**P**	**K**
%wt. in the purified leachate	0.00%	40.24%	0.01%	1.51%	1.92%	0.16%	12.10%	0.00%	0.00%	93.94%	69.39%	7.55%
%wt. in the discarded water	0.00%	0.20%	0.00%	0.00%	0.04%	0.00%	0.30%	0.00%	0.00%	0.00%	0.03%	0.17%
%wt. in the cleaning water	0.00%	14.38%	0.01%	0.54%	2.12%	0.20%	14.85%	0.00%	0.00%	4.01%	21.58%	8.55%
%wt. total remaining from dirty leachate	0.00%	54.83%	0.01%	2.06%	4.09%	0.37%	27.25%	0.00%	0.00%	97.95%	91.00%	16.27%
% wt. total recovered from solid residue	0.00%	20.09%	0.00%	0.17%	1.42%	0.19%	11.17%	0.00%	0.00%	-	79.48%	1.03%

Table 2. For conditions 1.20.45.25, percentage of the elements present in the purified leachate, discarded water and cleaning water taking as a reference the mg of each element present in the dirty leachate. Recovery of S from the solid residue is not shown as sulphuric acid is added during leaching in much bigger quantities than the original present in the solid residue. RT= room temperature.

	pH 0.5, L/S ratio 10, 45 min, RT											
	Mg	**Na**	**Al**	**Ca**	**Cr**	**Fe**	**Ni**	**Cu**	**Zn**	**S**	**P**	**K**
%wt. in the purified leachate	42.19%	62.92%	38.01%	1.35%	29.62%	66.91%	1.92%	14.05%	18.96%	92.79%	68.73%	2.30%
%wt. in the discarded water	0.00%	0.15%	0.00%	0.00%	0.04%	0.00%	0.05%	0.00%	0.00%	0.02%	0.06%	0.07%
%wt. in the cleaning water	0.39%	22.88%	0.26%	0.96%	2.08%	1.54%	2.91%	0.00%	0.00%	7.15%	17.82%	4.55%
%wt. total remaining from dirty leachate	42.58%	85.96%	38.27%	2.31%	31.73%	68.45%	4.87%	14.05%	18.96%	99.96%	86.61%	6.93%
% wt. total recovered from solid residue	34.99%	29.82%	22.77%	0.10%	12.31%	43.21%	8.38%	2.72%	11.06%	-	73.11%	0.70%

Table 3. For conditions 0,5.10.45.25, percentage of the elements present in the purified leachate, discarded water and cleaning water taking as a reference the mg of each element present in the dirty leachate. Recovery of S from the solid residue is not shown as sulphuric acid is added during leaching in much bigger quantities than the original present in the solid residue. RT= room temperature.

4 Conclusions

We were able to push the recovery up to 87% by using a liquid to solid ratio of 20 at pH 1 and up to 84% by using a liquid to solid ratio of 10 at pH 0.5. The question of which condition is the optimal remains open as it depends on the costs associated to the evaporation of water and the amount of sulphuric acid used at large scale. Besides, it depends also on the final product targeted. If we target concentrated phosphoric acid, the evaporation cost could make the diluted conditions impractical. However, if precipitation of a solid product is targeted, we avoid the evaporation costs and add the costs related to the separation of the solid and liquid phases.

Regarding purification, the resins have proven to work as expected for the experiments with a liquid to solid ratio of 20. Most of the cations were trapped in the column and up to 91% of the phosphorus remained in the purified leachate. Most of the sulphates remained as well since they are anions. They will need to be removed through precipitation or membranes. For experiments with a liquid to solid ratio of 10, the column gradually stopped retaining cations probably because it got saturated and needed regeneration. The main disadvantage of ion exchange resins as a purification method, at lab scale and in batch mode of operation, is that as the column is always full of water and after the experiment we have to use a fair amount of water to clean the column, the concentration of phosphorus in the purified leachate sample will be very diluted

(less than 0.5% wt) requiring a lot of energy to evaporate water up to the point of having 60 to 80% phosphoric acid.

For the next steps we will perform precipitation experiments with the purified leachate in order to see if the problems encountered with precipitation out of the dirty leachate are solved after purification or if the problem lies within the nature of the solid residue.

References

1. White, S. & Cordell, D. Peak phosphorus: the sequel to peak oil. *Phosphorus Futur.* (2009).
2. Mohr, S. & Evans, G. New projection of peak phosphorus. *Philica* (2013).
3. Food and Agriculture Organization of the United Nations. World fertilizer trends and outlook to 2020 (2017).
4. Desmidt, E. *et al.* Global phosphorus scarcity and full-scale p-recovery techniques: A review. *Critical Rev. Environ. Sci. Technol.* **45**, 336–384, DOI: 10.1080/10643389.2013.866531 (2015).
5. Chen, M. & Graedel, T. E. A half-century of global phosphorus flows, stocks, production, consumption, recycling, and environmental impacts. *Glob. Environ. Chang.* **36**, 139–152, DOI: 10.1016/j.gloenvcha.2015.12.005 (2016).
6. van Dijk, K. C., Lesschen, J. P. & Oenema, O. Phosphorus flows and balances of the european union member states. *Sci. The Total. Environ.* **542**, 1078–1093, DOI: 10.1016/j.scitotenv.2015.08.048 (2016).
7. Lwin, C. M., Murakami, M. & Hashimoto, S. The implications of allocation scenarios for global phosphorus flow from agriculture and wastewater. *Resour. Conserv. Recycl.* **122**, 94–105, DOI: 10.1016/j.resconrec.2017.01.017 (2017).
8. Golroudbary, S. R., El Wali, M. & Kraslawski, A. Environmental sustainability of phosphorus recycling from wastewater, manure and solid wastes. *Sci. The Total. Environ.* **672**, 515–524, DOI: 10.1016/j.scitotenv.2019.03.439 (2019).
9. Donatello, S., Tong, D. & Cheeseman, C. Production of technical grade phosphoric acid from incinerator sewage sludge ash (issa). *Waste Manag.* **30**, 1634–1642, DOI: 10.1016/j.wasman.2010.04.009 (2010).
10. Dorozhkin, S. V. Calcium orthophosphates. occurrence, properties, biomineralization, pathological calcification and biomimetic applications, DOI: 10.4161/biom.18790 (2011).
11. Oliveira, C., Ferreira, A. & Rocha, F. Dicalcium phosphate dihydrate precipitation: Characterization and crystal growth. *Chem. Eng. Res. Des.* **85**, 1655–1661, DOI: https://doi.org/10.1016/S0263-8762(07)73209-4 (2007).
12. Ferreira, A., Oliveira, C. & Rocha, F. The different phases in the precipitation of dicalcium phosphate dihydrate. *J. Cryst. Growth* **252 (4)**, 599–611, DOI: https://doi.org/10.1016/S0022-0248(03)00899-6 (2002).
13. Mekmene, O. *et al.* Effects of pH and Ca/P molar ratio on the quantity and crystalline structure of calcium phosphates obtained from aqueous solutions. *Dairy Sci. Technol.* **89**, 301–316, DOI: 10.1051/dst/2009019 (2009).
14. Koga, D. Struvite recovery from digested sewage sludge. *Phosphorus Recover. Recycl.* 255–264, DOI: https://doi.org/10.1007/978-981-10-8031-9_17 (2019).
15. Pastor, L., Mangin, D., Ferrer, J. & Seco, A. Struvite formation from the supernatants of an anaerobic digestion pilot plant. *Bioresour. Technol.* **101**, 118–125, DOI: https://doi.org/10.1007/978-981-10-8031-9_17 (2010).
16. Uysal, A., Yilmazel, Y. & Demirer, G. The determination of fertilizer quality of the formed struvite from effluent of a sewage sludge anaerobic digester. *J. Hazard. Mater.* **181**, 248–254, DOI: 10.1016/j.jhazmat.2010.05.004 (2010).
17. Acelas, N. Y., Flórez, E. & López, D. Phosphorus recovery through struvite precipitation from wastewater: effect of the competitive ions. *Desalination Water Treat.* **54**, 2468–2479, DOI: 10.1080/19443994.2014.902337 (2015).
18. Kataki, S., West, H., Clarke, M. & Baruah, D. C. Phosphorus recovery as struvite: Recent concerns for use of seed, alternative Mg source, nitrogen conservation and fertilizer potential. *Resour. Conserv. Recycl.* **107**, 142–156, DOI: 10.1016/j.resconrec.2015.12.009 (2016).
19. Franz, M. Phosphate fertilizer from sewage sludge ash (SSA). *Waste Manag.* **28**, 1809–1818, DOI: 10.1016/j.wasman.2007.08.011 (2008).
20. Ash2phos – EasyMining. http://easymining.se/ash2phos/. Accessed on 2019-06-25.
21. Nättorp, A. & Stemann, J. Phosphorus recovery in Europe. *Results from Eur. P-REX project* .

A Appendix

A.1 Purification experiments

- Internal diameter: 2.9 cm
- Height of the resin: 14 cm
- Bed volume: 92.5 cm3



Figure A.1. Lab setup for the purification experiments.

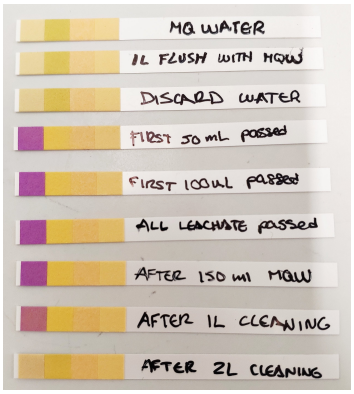


Figure A.2. Change in pH throughout purification of the leachate and cleaning of the column with ultra pure water.

A.2 ICP results

		Mg	Na	Al	Ca	Cr	Fe	Ni	Cu	Zn	Cd	Pb	S	P	K
1.20.45.25	LI	298.725	19.548	443.307	609.755	1.493	3289.062	0.291	4.986	17.849	0.010	0.070	4238.939	2847.564	15.845
	LII	294.576	18.762	432.357	614.632	1.375	3254.461	0.161	4.916	17.782	0.010	0.070	4247.056	2740.591	13.508
	LIII	317.823	20.034	418.489	604.751	1.522	3523.857	0.220	6.050	19.560	0.010	0.070	4727.913	2781.861	14.423
0,5.10.45.25	**LI**	725.128	34.493	1440.415	594.019	2.304	8329.555	0.948	15.579	49.408	0.100	0.070	13510.016	5223.990	45.544
	LII	729.192	36.560	1497.039	602.106	2.394	8310.117	0.953	15.554	49.460	0.100	0.070	12703.486	5351.273	46.796
	LIII	693.672	35.540	1393.349	598.930	2.173	7890.033	0.925	15.000	47.096	0.050	0.070	12108.644	5081.936	44.017
1.20.45.25	AVERAGE	303.708	19.448	431.384	609.713	1.463	3355.793	0.224	5.318	18.397	0.010	0.070	4404.636	2790.005	14.592
0,5.10.45.25	AVERAGE	715.997	35.531	1443.601	598.352	2.290	8176.568	0.942	15.378	48.655	0.083	0.070	12774.048	5219.066	45.452
1.20.45.25	STDEV	12.399	0.642	12.437	4.940	0.078	146.572	0.065	0.635	1.008	0.000	0.000	279.996	53.949	1.178
0,5.10.45.25	STDEV	19.441	1.034	51.918	4.075	0.111	248.337	0.015	0.327	1.350	0.029	0.000	703.346	134.736	1.392
1.20.45.25	Error	0.041	0.033	0.029	0.008	0.053	0.044	0.291	0.120	0.055	0.001	0.001	0.064	0.019	0.081
0,5.10.45.25	Error	0.027	0.029	0.036	0.007	0.048	0.030	0.015	0.021	0.028	0.348	0.002	0.055	0.026	0.031

Table A.1. ICP results (mg/l) for the leaching experiments performed.

			Mg	Na	Al	Ca	Cr	Fe	Ni	Cu	Zn	Cd	Pb	S	P	K
1.20.45.25	**Purified leachate**	LI	0.000	9.010	0.030	11.159	0.030	2.504	0.030	0.000	0.000	0.030	0.209	2264.850	1319.551	1.196
		LII	0.000	2.475	0.010	2.648	0.010	2.163	0.010	0.000	0.000	0.010	0.071	2305.676	1083.847	0.405
		LIII	0.000	2.450	0.010	2.640	0.010	5.019	0.010	0.000	0.000	0.010	0.070	2597.232	960.953	0.401
		Average	0.000	4.645	0.017	5.482	0.017	3.229	0.017	0.000	0.000	0.017	0.117	2389.253	1121.450	0.667
		STDEV	0.000	3.780	0.011	4.916	0.011	1.560	0.011	0.000	0.000	0.011	0.080	181.269	182.233	0.458
		Error	0.000	0.814	0.686	0.897	0.686	0.483	0.686	0.000	0.000	0.686	0.686	0.076	0.162	0.686
	Discarded water	LI	0.000	0.142	0.002	0.104	0.002	0.024	0.002	0.000	0.000	0.002	0.014	0.016	0.068	0.080
		LII	0.000	0.106	0.002	0.064	0.002	0.038	0.002	0.000	0.000	0.002	0.014	0.193	1.729	0.080
		LIII	0.000	0.136	0.002	0.054	0.002	0.100	0.002	0.000	0.000	0.002	0.014	0.016	6.084	0.080
		Average	0.000	0.128	0.002	0.074	0.002	0.054	0.002	0.000	0.000	0.002	0.014	0.075	2.627	0.080
		STDEV	0.000	0.019	0.000	0.027	0.000	0.041	0.000	0.000	0.000	0.000	0.000	0.102	3.107	0.000
		Error	0.000	0.151	0.000	0.358	0.000	0.749	0.000	0.000	0.000	0.000	0.000	1.361	1.183	0.000
	Cleaning water	LI	0.000	0.475	0.005	0.563	0.005	0.877	0.005	0.000	0.000	0.005	0.035	35.411	88.653	0.199
		LII	0.000	0.422	0.005	0.520	0.005	0.535	0.005	0.000	0.000	0.008	0.035	16.556	96.818	0.199
		LIII	0.000	0.455	0.005	0.515	0.005	1.949	0.005	0.000	0.000	0.005	0.052	34.996	104.389	0.199
		Average	0.000	0.451	0.005	0.533	0.005	1.120	0.005	0.000	0.000	0.006	0.041	28.988	96.620	0.199
		STDEV	0.000	0.027	0.000	0.026	0.000	0.738	0.000	0.000	0.000	0.001	0.010	10.768	7.870	0.000
		Error	0.000	0.059	0.001	0.050	0.001	0.659	0.001	0.000	0.000	0.250	0.249	0.371	0.081	0.001
0,5.10.45.25	**Purified leachate**	LI	15.832	3.293	33.468	2.983	0.030	1002.354	0.010	0.000	0.000	0.010	0.070	4918.770	1344.110	0.400
		LII	112.579	7.072	243.183	3.155	0.418	2248.228	0.010	0.393	1.031	0.010	0.070	4495.117	1350.884	0.398
		LIII	217.813	15.864	355.406	3.323	0.651	3068.081	0.020	2.082	9.480	0.010	0.070	4509.098	1513.480	0.430
		Average	115.408	8.743	210.686	3.153	0.366	2106.221	0.013	0.825	3.504	0.010	0.070	4640.995	1402.824	0.410
		STDEV	101.020	6.450	163.411	0.170	0.314	1040.159	0.006	1.106	5.202	0.000	0.000	240.662	95.890	0.018
		Error	0.875	0.738	0.776	0.054	0.856	0.494	0.435	1.341	1.485	0.003	0.003	0.052	0.068	0.044
	Discarded water	LI	0.000	0.134	0.002	0.054	0.002	0.110	0.002	0.000	0.000	0.002	0.014	14.210	9.535	0.080
		LII	0.000	0.123	0.002	0.050	0.002	0.119	0.002	0.000	0.000	0.002	0.014	0.016	6.331	0.080
		LIII	0.000	0.000	0.000	0.000	0.000	0.000	0.000	0.000	0.000	0.000	0.000	0.000	0.000	0.000
		Average	0.000	0.086	0.001	0.035	0.001	0.076	0.001	0.000	0.000	0.001	0.009	4.742	5.289	0.054
		STDEV	0.000	0.074	0.001	0.030	0.001	0.066	0.001	0.000	0.000	0.001	0.008	8.199	4.852	0.046
		Error	0.000	0.869	0.866	0.868	0.866	0.868	0.866	0.000	0.000	0.866	0.866	1.729	0.917	0.866
	Cleaning water	LI	0.000	0.556	0.005	0.581	0.005	7.898	0.005	0.000	0.000	0.005	0.035	104.379	108.253	0.199
		LII	0.000	0.970	0.450	0.576	0.005	15.595	0.005	0.000	0.000	0.005	0.035	88.176	86.703	0.200
		LIII	0.642	1.806	2.217	0.773	0.010	28.916	0.010	0.000	0.000	0.010	0.070	93.581	86.247	0.401
		Average	0.214	1.111	0.891	0.643	0.007	17.470	0.007	0.000	0.000	0.007	0.047	95.379	93.734	0.267
		STDEV	0.371	0.637	1.170	0.112	0.003	10.634	0.003	0.000	0.000	0.003	0.020	8.250	12.576	0.117
		Error	1.732	0.573	1.314	0.174	0.437	0.609	0.437	0.000	0.000	0.437	0.437	0.086	0.134	0.437

Table A.2. ICP results (mg/l) for the purification experiments performed.

A.3 XRD spectrum

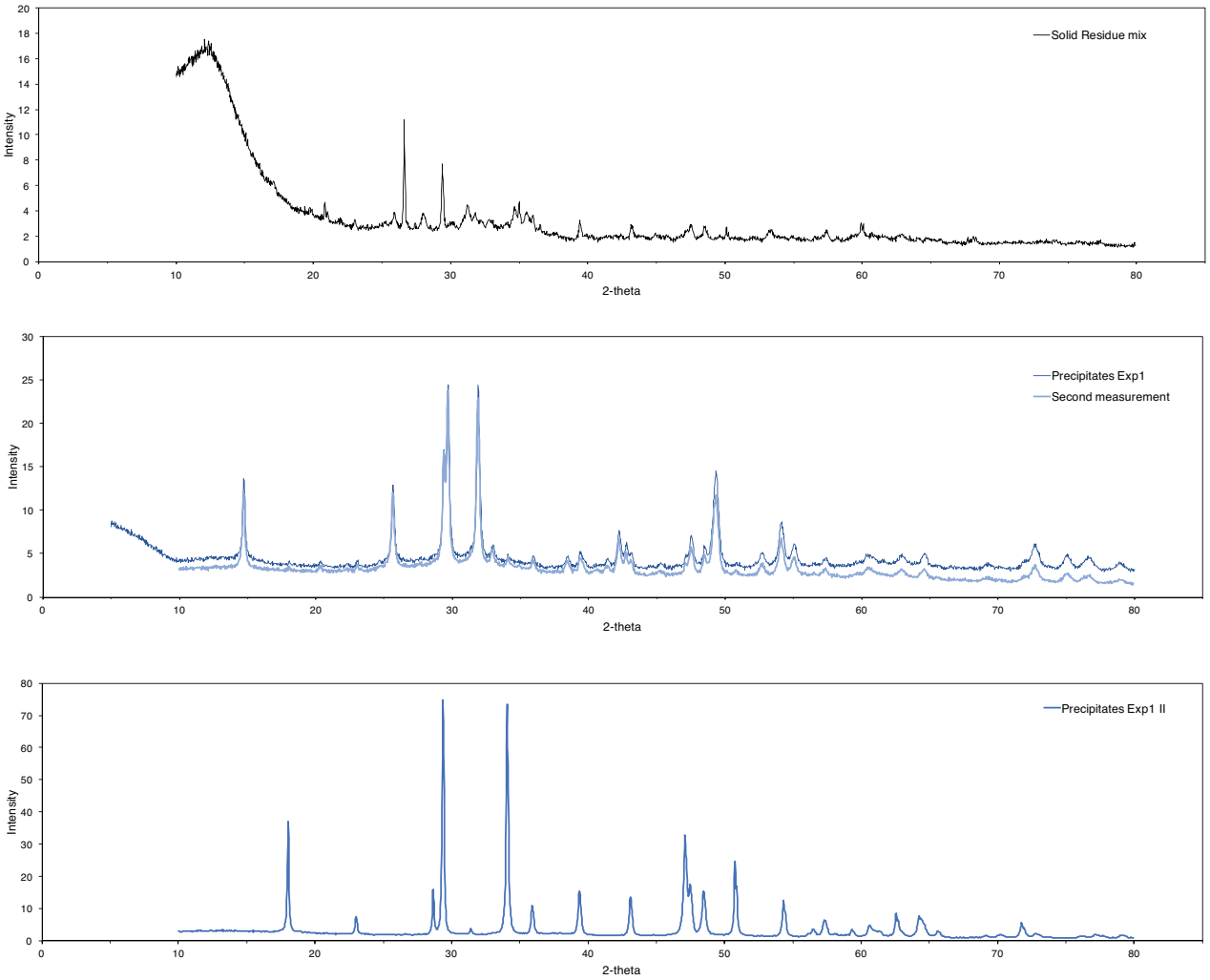


Figure A.3. XRD spectra from top to bottom: solid residue, precipitates Exp1 and precipitates Exp1 II.

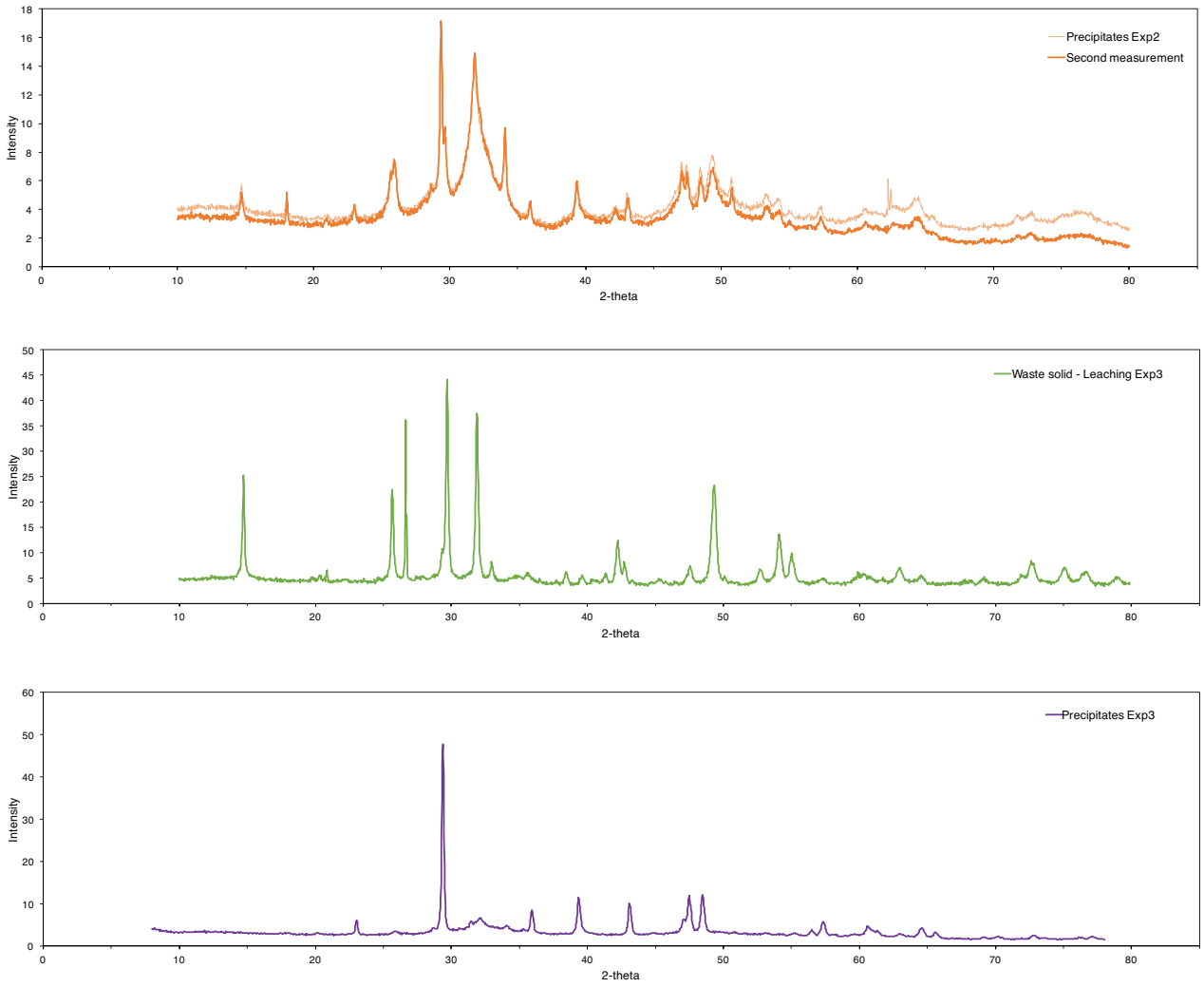


Figure A.4. XRD spectra from top to bottom: precipitates Exp2, waste solid after leaching Exp3, precipitates Exp3.

Phosphorus recovery from hydrothermally treated sewage sludge: Valorisation and regulation

August 2020

ABSTRACT

During this part of the phosphorus recovery project, we have focused on finding new options for the valorisation of phosphorus and testing the products to check their compliance with the national regulation for recycled mineral fertilizers (MinRec).

Leaching experiments were performed at pH 1 (sulfuric acid), liquid to solid ratio of 20 and a residence time of 45 min. The carbon content of the hydrothermally treated sewage sludge used was low (6%wt.). In average, 83%wt. of the phosphorus was recovered in the liquid phase. Following, the liquid phase (leachate) containing phosphorus and impurities, was purified using ion exchange resins (Purolite MTC1600H). It was shown that more than 99 %wt. of the cations present in the samples can be removed thanks to the ion exchange resins. After this purification step, about 86%wt. of the phosphorus still remained in the purified leachate. The next step concerns the precipitation experiments to produce either calcium phosphates or struvite by using the purified leachate. All the solid samples were analysed using XRD. High purity crystalline struvite was found in all cases confirming that a solid P-based fertilizer can be produced from hydrothermally treated sewage sludge. In the case of calcium phosphates, no crystalline forms were found.

Solid residue samples, extracted during hydrothermal gasification experiments, as well as purified leachate samples, were tested to find the concentration of organic and inorganic pollutants which require an upper limit according to the MinRec regulation. Concerning organic pollutants, we have performed analysis to determine the concentration of PCBs and PAHs. According to the results, for solid and liquid samples, the concentrations of PCBs and PAHs comply with MinRec requirements. Regarding inorganic pollutants, the concentrations of cadmium, arsenic, mercury, nickel, zinc, chrome, lead and copper are above the MinRec requirements for the solid sample but below for the purified leachate samples. Therefore, we can confirm that the precipitates (P-based fertilizer) from this liquid phase will comply as well with the regulation.

List of Figures

1 Summary of the process. . . . 3
2 Composition (%wt in blue, mg/kg in orange) of the deposits before leaching. . . . 6
3 Average %wt. leached to the liquid phase from the solid before purification. . . . 7
4 Average %wt. leached to the liquid phase from the solid before and after purification for both replicates. . . . 8
5 XRD patterns for calcium phosphate precipitates from hydrothermally treated sewage sludge. . . . 9
6 XRD patterns for struvite precipitates from hydrothermally treated sewage sludge. . . . 10
7 Chromatogram (intensity vs time in minutes) of the extracted organics from samples of solid residue. . . . 13
8 Structural formula of the main molecules found in the solid residues through solid-liquid extraction and GC-MS. 14
9 Composition (%wt in blue and gray, mg/kg in orange) of the calcined solid residue (ashes) before leaching. . 14
10 Average %wt. leached to the liquid phase from the ashes before purification. . . . 15
11 Average %wt. leached to the liquid phase from the solid before and after purification for both replicates. . . . 15
12 XRD patterns for calcium phosphate precipitates from hydrothermally treated sewage sludge ash. . . . 16
13 XRD patterns for struvite precipitates from hydrothermally treated sewage sludge ash. . . . 17

List of Tables

1 MinRec limits for inorganic pollutants in waste-derived fertilizers. All values in mg/kg of phosphorus. . . . 4
2 MinRec limits for organic pollutants in waste-derived fertilizers. . . . 4
3 Limit values for pollutants in solid wastes of type D and E, according to OLED[1]. . . . 5
4 Elemental composition of the hydrothermally treated sewage sludge used as feedstock (deposit). . . . 6
5 Leaching results. . . . 7
6 Concentration of carbon in all phases from leaching to precipitation. . . . 10
7 Concentration of PBCs in a sample of solid residue from hydrothermally treated sewage sludge (digested). . . 12
8 Concentration of PAHs in a sample of solid residue from hydrothermally treated sewage sludge (digested). . . 12
9 Concentration of inorganic pollutants in a solid residue sample and a purified leachate sample that must comply with MinRec. . . . 12

10 Organic molecules found through solid-liquid extraction and GC-MS. . . . 13
11 Leaching results. Numbers represent the %wt. of each element that is leached to the liquid phase from the calcined solid residue (ashes). . . . 14

Contents

1 Introduction **3**
1.1 Aim . . . 3
1.2 Framework . . . 3
1.3 Scope . . . 3
2 Experimental protocol **4**
2.1 Materials . . . 4
2.2 Method . . . 5
Digestion and leaching experiments • Purification experiments • Dicalcium phosphate precipitation • Struvite precipitation • Solid residue calcination
3 Results and discussion **6**
3.1 Leaching . . . 6
3.2 Purification of the leachate . . . 6
4 Valorisation of phosphorus **8**
4.1 Calcium phosphates . . . 8
4.2 Struvite . . . 9
5 Regulation regarding pollutants in the final product **11**
5.1 OLED . . . 11
5.2 MinRec . . . 11
Organic pollutants • Inorganic pollutants
5.3 GC-MS study of other organics . . . 13
6 Valorisation of P using calcined solid residue (ashes) **14**
6.1 Leaching . . . 14
6.2 Purification . . . 14
6.3 Valorisation . . . 15
CaP • Struvite
7 Conclusions and future works **16**
References **18**

1 Introduction

1.1 Aim

The goal is to show that a solid, P-based fertilizer can be produced from hydrothermally treated sewage sludge (SS) and that it complies with regulations.

1.2 Framework

Around 9 millions of tons of SS are produced every year in Europe as a side product of the treatment of wastewater, one of the major volumes of waste directly linked to the existence of humans. The current sludge disposal routes (landfilling, biosolids production, and incineration) cause severe environmental impacts (e.g. soil contamination, toxic gas emissions) and do not valorise its energetic and mineral content such as performing phosphorus (P) recovery. Treatech has developed a cost-efficient and eco-friendly technology for transforming waste streams (among which SS) into clean water, renewable gas and fertilizers precursors using the unique properties of supercritical water (refer to figure 1).

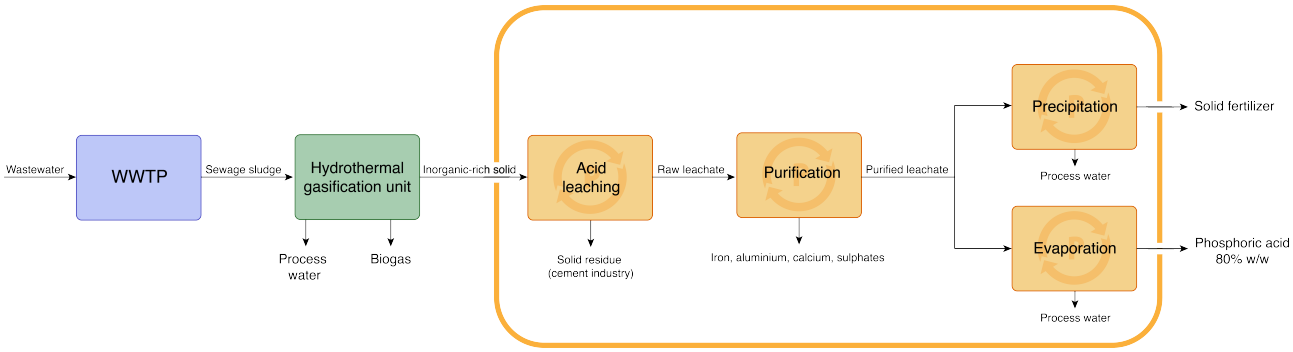


Figure 1. Summary of the process.

Phosphorus is a key component in crop growth and animal and human food manufacturing. Nowadays it is almost exclusively obtained in the form of phosphoric acid through mining of phosphate rock. The concern of depleting the current sources of this element has raised exponentially since its production from fossil resources is expected to peak between 2035 and 2075[2,3].

Switzerland is the first country in the world to establish a strict regulation regarding P-recovery from wastewater (OLED), which will enter into force in 2026[1,4]. According to this regulation, phosphorus must be recovered from sewage sludge. Since nowadays incineration is the only disposal route allowed in the country, P-recovery technologies are oriented towards the extraction of the element from sewage sludge ashes. After recovery, the residual solids must as well comply with the requirements of the OLED. Besides, concerning the extracted phosphorus, the Swiss government has carried out a study regarding the quality of the recycled phosphorus products to establish limits in the concentration of several pollutants (MinRec)[5].

Moreover, the government released a document where the cantons and the economic organizations concerned can find information to frame themselves in the context of phosphorus recovery. This document explains both the legal requirements and the state of the art. In addition, it provides instruments for calculating indicators and limit values.[6]

1.3 Scope

Valorization of phosphorus. We considered two possibilities for the valorization of phosphorus after leaching and purification: precipitation as calcium phosphates and precipitation as Struvite (magnesium-ammonium-phosphate).

The easiest phosphate to precipitate is dicalcium phosphate dyhydrate (DCPD). Corresponding to the formula $CaHPO_4 \cdot 2H_2O$, it can be produced from phosphoric acid by precipitation with $Ca(OH)_2$ in aqueous media at room temperature (5 steps reaction). Then, the anhydrous form (DCP) can be produced the same way as DCPD but at around 100 °C. Tricalcium phosphate (TCP, $Ca_3(PO_4)_2$) can also be precipitated from phosphoric acid and calcium hydroxide at high temperature in aqueous phase or low temperature in organic solvents.[7–10]

Struvite, or Magnesium Amounium Phosphate (MAP, $MgNH_4PO_4.6H_2O$), is a crystalline solid with low solubility in water or alkaline solutions. As its name indicates, it consists of magnesium, amonium and phosphate in a 1:1:1 molar ratio and it is normally hydrated by six water molecules. Struvite can be used as a low nutrient release fertilizer since it is a direct source of phosphorus (13%), nitrogen (6%) and magnesium (10%). Many wastewater plants precipitate Struvite to prevent scaling of the equipment due to a natural precipitation of the substance along the subsequent steps of the waste water treatment[11]. To ensure an efficient precipitation of phosphprus in the form of MAP, pH should between 8 and 10 for municipal waste[12–16]. Besides, although precipitation starts when the ratio between the three ions is 1:1:1, the process is favoured when the NH_4:PO_4 and Mg:PO_4 molar ratio is increased[12,14,17,18]. Finally, the presence of calcium in the mixture, as it is our case, can decrease the availability of phosphorus for the precipitation of struvite since dicalcium phosphate is formed. This can be easily avoided by removing calcium ions in the purification step.

MinRec regulation. As stated before, the Swiss government has carried out a study regarding the quality of the recycled phosphorus products to establish limits in the concentration of several pollutants (MinRec)[5]. MinRec sets limits for the concentration of inorganic and organic pollutants in recycled fertilizers based on the ALARA principle (as low as reasonably achievable). Table 1 and table 2 gather the values as well as the approach used to determine the minimum requirement (in the case of inorganic pollutants).

We need to analyze our precipitates (P-based fertilizer) to ensure the concentration of the pollutants indicated in tables 1 and 2 are below the limits set by MinRec.

Pollutant	Approach for the minimum requirement	Minimum requirement	Technically attainable value	Limit value MinRec
Cadmium	Balance	39	21	25
Arsenic	Balance	140	121	100
Mercury	Balance	12	8.7	2
Nickel	Balance	890	313	500
Zinc	Balance	14001	8879	10000
Chrome	Accumulation	1821	922	1000
Lead	Accumulation	2842	416	500
Copper	Accumulation	4931	2939	3000

Table 1. MinRec limits for inorganic pollutants in waste-derived fertilizers. All values in mg/kg of phosphorus.[5]

Pollutant	Limit value	Unit
PAH	25	g/t P
PCB	0.5	g/t P
PCDD + PCDF	120	ng I-TEQ/kg P

Table 2. MinRec limits for organic pollutants in waste-derived fertilizers.[5]

OLED regulation. We do not only need to ensure that our final product complies with MinRec but also all residues generated during P-recovery need to comply with regulation and be disposed adequately. Specifically, after acid leaching, P is extracted to the liquid phase and the solid remaining is filtered out and needs to be disposed as a waste.

In Switzerland all solid waste must be classified to ensure its adequate disposal. OLED[1] establishes 5 types of solid wastes (A to E) depending on its origin and composition. Our solid could be classified as type E or D. Table 3 gathers the concentration of pollutants allowed in solid wastes to be classified as types E or D.

We need to analyze the solids remaining after phosphorus extraction to ensure the concentration of the pollutants indicated in table 3 comply with the limits set by OLED for residue types D or E.

2 Experimental protocol

2.1 Materials

95-98% Sulphuric Acid was acquired from Merck. 95% Calcium hydroxide was acquired from Sigma-Aldrich. Magnesium chloride hexahydrate 99% was acquired from Sigma-Aldrich. Ammonium chloride 99% was acquired from Sigma-Aldrich. Sodium hydroxide 95% was acquired by Sigma-Aldrich. Hexane anhydrous, 95% and Toluene anhydrous, 99.8% were acquired from Sigma-Aldrich. Nylon membrane filters (0.2 μm pore size) were acquired from Whatman. The leaching experiments were performed in a 200 ml glass beaker provided with a magnetic stirrer and ultrapure water (Mili-Q) was

Table 3. Limit values for pollutants in solid wastes of type D and E, according to OLED[1].

Substance	Limit value in mg/kg of dry matter	
	Type D residues	Type E residues
Sb	50	50
As	50	50
Pb	2000	2000
Cd	10	10
Cr total	1000	1000
Cr (VI)	0.5	0.5
Cu	5000	5000
Ni	1000	1000
Hg	5	5
Zn	5000	5000
Volatile chlorinated hydrocarbons *	1	5
Polychloric biphenyls (PCB) **	1	10
Aliphatic hydrocarbons C5-C10 ***	10	100
Aliphatic hydrocarbons C10-C40	500	5000
Monocyclic aromatic hydrocarbons BTEX ****	10	100
Benzene	1	1
Polycyclic aromatic hydrocarbons (HAP) *****	25	250
Benzo[a]pyrene	3	10
Total organic carbon (TOC)	20000	50000

* ∑7 volatile chlorinated hydrocarbons: dichloromethane, trichloromethane, tetrachloromethane, cis-1,2-dichlorethylene, 1,1,1-trichlorethane, trichlorethylene (Tri), perchlorethylene (Per)

** ∑6 substances x 4,3 (UICPA n°): 28, 52, 101, 138, 153, 180

*** ∑HC C5-C10: surface of the FID chromatogramme between n-pentane and n-decane, multiplied by the response factor of n-hexane, minus ∑BTEX

**** ∑6 BTEX: benzene, toluene, ethylbencene, o-xylene, m-xylene, p-xylene

***** ∑16 HAP according to EPA: Naphtalene, Acenaphthylene, Acenaphtene, Fluorene, Phenanthrene, Anthracene, Fluoranthene, Pyrene, Benzo(a)anthracene, Chrysene, Benzo(b)fluoranthene, Benzo(k)fluoranthene, Benzo(a)pyrene, Indeno(1,2,3-c,d)pyrene, Dibenzo(a,h)anthracene, Benzo(g,h,i)perylene

used to reach the desired liquid to solid ratio. For the purification experiments a glass column with fritted glass at the bottom was used as the exchange column. 2 mm glass beads were acquired from VWR. The strong cation resin MTC1600H was provided by Purolite. The precipitation experiemnts were performed in a 200 ml glass beaker provided with a magnetic stirrer. For all experiemnts, continuous stirring was achieved using a hotplate (Heidolph Hei-Tec) and pH was measured using a VWR Phenomenal 1100 L pH meter.

2.2 Method

2.2.1 Digestion and leaching experiments

A laboratory at PSI performed microwave digestion with aqua regia and sent the liquid phase to ICP to know the composition of the solid residue. Leaching experiments were performed following the protocol used in the previous reports. We sent the liquid phase to ICP to know the concentration of ions. Refer to previous reports for details.

2.2.2 Purification experiments

Purification experiments were performed using the same setup and following the same protocol shown in the previous report. Please refer to this document for details.

2.2.3 Dicalcium phosphate precipitation

The experiments were performed by slowly adding a specific amount of calcium hydroxide to the purified leachate at room temperature, under stirring for 2 hours and measuring the pH of the solution in intervals of 1 to 5 minutes. Then the solids were separated from the liquid phase using a nylon membrane filter (0.2 μm pore size) under vacuum and then dried overnight at 50°C.

2.2.4 Struvite precipitation

The experiments were performed following the protocol shown by[14]. The purified leachate is kept under stirring at room temperature throughout the experience (2 hours). The NH_4:PO_4 and Mg:PO_4 molar ratios used are 1.1 and 2.6 respectively.

First of all, magnesium chloride hexahydrate is added to reach the Mg:P desired ratio. Following, the pH is raised to 9 using NaOH 5M. Finally, ammonium chloride is added to reach the N:P desired ratio and the mixture is left under stirring for the remaining time up to 2 hours.

2.2.5 Solid residue calcination

Around 20 grams of solid residue were placed in a crucible and calcined in a furnace according to the following program. Room temperature to 900°C at 2°C per minute ramp, then two hours at 900 °C and cool down to room temperature.

3 Results and discussion

3.1 Leaching

Following the usual procedure, we performed leaching experiments using hydrothermally treated sewage sludge that was extracted from the mineral separator unit after a 9 hours campaign (deposit). The elemental composition of the solids (table 4) shows a low carbon content (∼6% wt.) which will help us to understand the role of carbon in the valorisation of the residue since the experiments run in the past were done using a residue with a carbon content between 10 and 20% wt. Until now, we were not able to precipitate phosphorus in crystalline form using these high carbon content solid residues. We hypothesize that carbon, specifically organic carbon, can influence the precipitation process avoiding the formation of crystalline calcium phosphate probably by trapping phosphorus and precipitating as a carbon-phosphorus complex.

Figure 2 shows the composition of the hydrothermally treated sewage sludge used as feedstock for the leaching experiments. Phosphorus is the fourth most abundant element representing 8.8% wt. of the solids.

Table 4. Elemental composition of the hydrothermally treated sewage sludge used as feedstock (deposit). Values as %wt of dry matter.

Ash	C	N	H	S	O[a]
89 ± 0.4	5.7 ± 0.1	0.29 ± 0.01	0.98 ± 0.01	0.66 ± 0.01	3.37

[a] The percentage of oxygen has been calculated as O=100-Ash-C-N-H-S.

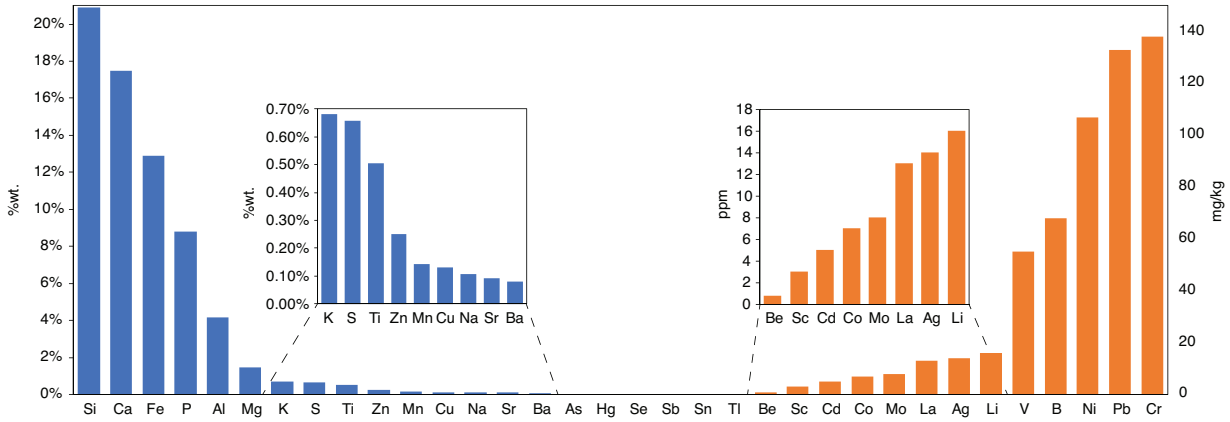


Figure 2. Composition (%wt in blue, mg/kg in orange) of the deposits before leaching.

Leaching experiments were done in triplicate in order to prove the repeatability of the method. Table 5 gathers the results for each of the replicates and figure 3 shows the average %wt. of each measured element that was leached from the solids to the liquid phase. Regarding phosphorus, 78%wt. of the element was recovered in the liquid phase for experiments in average. The rest of the elements were more prone to remain in the solid phase, with iron being the most leached one (44%wt.).

3.2 Purification of the leachate

One purification experiment was performed for each leachate produced. We took three samples for each one of them and analysed them through ICP. The three samples correspond to water exiting the column at the beginning of the experiments, purified leachate and water used to clean the column after the experiments.

Table 5. Leaching results. Numbers represent the %wt. of each element that is leached to the liquid phase from the solid residue (deposit).

	Al	Ca	Cd	Cr	Cu	Fe	Mg	Ni	P	Pb	Zn	As
I	37.13	6.46	<LOQ	18.29	18.93	48.16	42.64	31.93	**85.42**	<LOQ	27.17	<LOQ
II	35.38	7.10	<LOQ	26.29	18.03	45.46	42.17	47.95	**79.17**	<LOQ	24.91	<LOQ
III	30.87	7.02	<LOQ	21.07	17.24	39.75	38.55	36.68	**69.45**	<LOQ	23.44	<LOQ

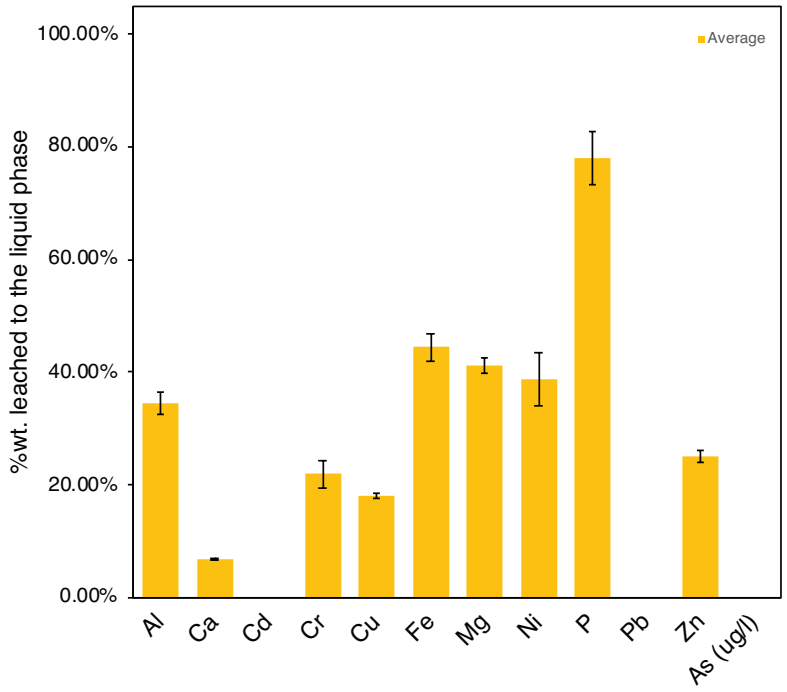


Figure 3. Average %wt. leached to the liquid phase from the solid before purification.

We were able to recover, in the purified stream, an average of 80%wt. of the phosphorus that was present in the dirty leachate. Starting from the phosphorus in the solid residue, the overall recovery rate is 72%wt. For all experiments, the discarded water at the beginning of them had negligible amounts of all the elements analysed. On the other hand, the analysis of the cleaning water revealed that between 2% and 7.4%wt. of the phosphorus in the dirty leachate ends up in this phase.

For the rest of the elements, in all cases, between 99% and 99.99%wt. of the amount present in the dirty leachate was removed by the column. Therefore, the purified leachates are composed almost exclusively by water, phosphates and sulphates (from sulfuric acid). Refer to figure 4 for details.

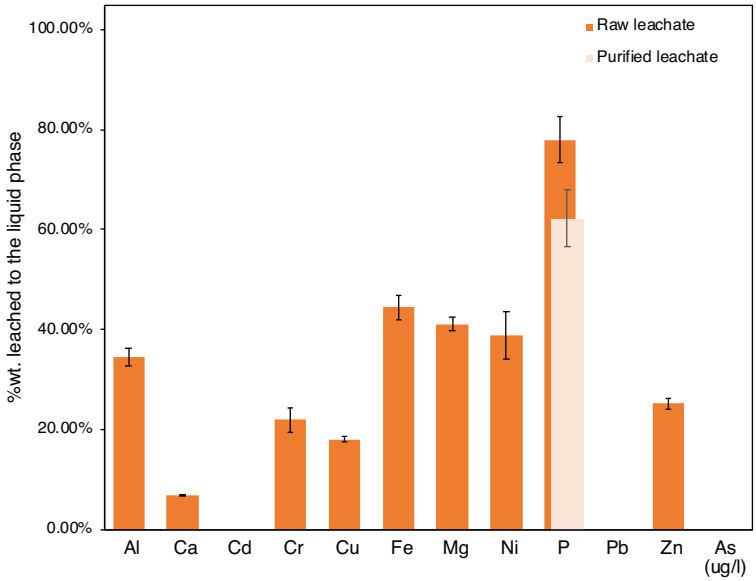


Figure 4. Average %wt. leached to the liquid phase from the solid before and after purification for both replicates.

4 Valorisation of phosphorus

We considered two possibilities for the valorization of phosphorus after leaching and purification: precipitation as calcium phosphates and precipitation as Struvite (magnesium-ammonium-phosphate).

4.1 Calcium phosphates

Following the protocol shown in section 2.2.3, we precipitated phosphorus with calcium hydroxide using the purified leachates from experiments I and II (section 3.2). The solid precipitates were analysed through XRD to identify the crystalline phases formed. Figure 5 shows the results. Reference patterns of the substances that could be expected are shown as well. These substances are:

- Bassanite: calcium sulphate demihydrate $CaSO_4 \cdot 1/2H_2O$. Precipitates easily in the presence of sulphates (from sulfuric acid leaching) and calcium (added as calcium hydroxide for precipitation).
- Gypsum: calcium sulphate dihydrate $CaSO_4 \cdot 2H_2O$. More hydrated version of the previous one. It also precipitates easily in the presence of sulphates (from sulfuric acid leaching) and calcium (added as calcium hydroxide for precipitation).
- Monetite: dicalcium phosphate $Ca(HPO_4)$. Desired product.
- Brushite: dicalcium phosphate dihydrate $Ca(HPO_4) \cdot 2H_2O$. Desired product as well.

No crystalline calcium phosphate was found in either of the samples. The sample from experiment I (LI-CaP) is mainly composed of a mixture of bassanite and gypsum. There is also some unreacted calcium hydroxide as a minor phase. The quality of the pattern is not very clear, probably due to defects on the surface of the solids. The sample from experiment II (LII-CaP) is nearly phase-pure gypsum. The difference between both samples may be due to different drying protocols for sample I and II. Sample I was dried overnight at 80°C and sample II was dried overnight at 50°C.

In addition, CHN analysis of the solids and TC/TOC of the liquid phases were performed to study the distribution of carbon during precipitation. Table 6 summarizes the concentration of carbon in all phases from leaching to precipitation. According to the data for experiment I, after leaching, 9% of the carbon is transferred to the leachate, then about 1% is trapped in the ion exchange column and finally all carbon remaining in the clean leachate precipitates during the precipitation experiment. This means that if we start with 100 grams of solid residue, 5.7 grams of it will be carbon and 0.46 grams of this carbon will end up in the precipitates. Looking at data from experiment II, after leaching, 9.8% of the carbon is transferred to the leachate, then about 5.4% is trapped in the ion exchange column and finally all carbon remaining in the clean leachate precipitates during the precipitation experiment. This means that if we start with 100 grams of solid residue, 5.7 grams of it will be carbon and 0.25 grams of this carbon will end up in the precipitates.

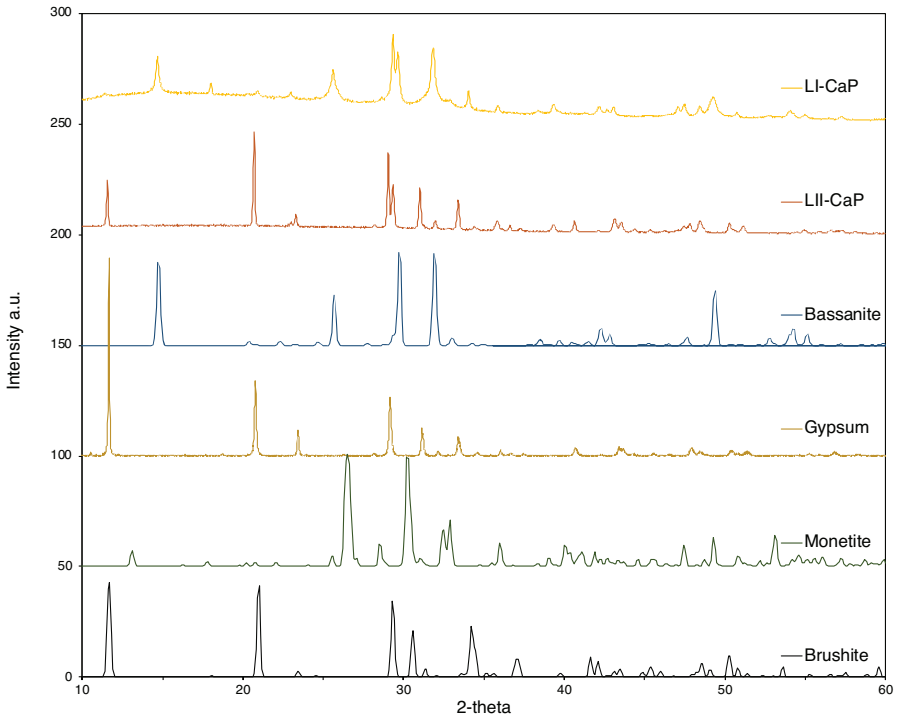


Figure 5. XRD patterns for calcium phosphate precipitates from hydrothermally treated sewage sludge (LI-CaP and LII-CaP) and reference substances patterns[19].

4.2 Struvite

Following the protocol shown in section 2.2.4, we precipitated phosphorus as magnesium ammonium phosphate (Struvite) using the purified leachates from experiments I and II (section 3.2). In addition, we prepared a model leachate using ultra-pure water and reagent phosphoric acid and then used this liquid phase to precipitate Struvite following the same protocol as for leachates I and II.

The precipitates were analysed through XRD to identify the crystalline phases formed. Figure 6 shows the results and the reference pattern. Samples for both experiments, as well as for the model leachate are composed by nearly pure Struvite. Therefore, opposite to what happened with calcium phosphates, we were able to precipitate phosphorus as crystalline Struvite.

Regarding carbon balance, table 6 summarizes the concentration of carbon in all phases from leaching to precipitation. Up to precipitation, the results are the same as for the previous section 4.1. After precipitation of Struvite, all carbon remaining in the clean leachate precipitates during the precipitation experiment. The concentration of carbon in the Struivite precipitates is lower than in the CaP precipitates (e.g. 1.65% vs 4.13% for experiment I) because the total mass in the case of Struvite is bigger. The reason for this is that Struvite molecules are heavier than gypsum or bassanite which are the main molecules found in the CaP precipitates.

Concerning the influence of carbon concentration, previous Struvite precipitation experiments using solid residues

with higher carbon content (10-20%wt.) were unsuccessful which confirms that carbon does have a role in precipitation since we were able to precipitate Struvite using a residue with 6%wt. C. However we still could not precipitate crystalline calcium phosphates. We need to further study if this difference lies in the different nature of the reagents used for both precipitations and its interaction with the organic molecules in the purified leachate.

Furthermore, we will need to know if, for the Struvite case, the sulphates precipitate (although we can't see any crystalline form of them through XRD) or if they remain in the liquid phase.

Table 6. Concentration of carbon in deposits before leaching, dirty and clean leachate, precipitates and liquid phase after precipitation. [a] TOC>TC due to high concentration of inorganic carbon[20]. [b] %wt. of carbon from the mass of carbon in the feedstock (solid residue).

	Experiment I		Experiment II	
	TC	TOC	TC	TOC
%wt. C in solid residue	5.70%		5.70%	
C in dirty leachate (mg/l)	227.8	207.7	285.9	237
C in purified leachate (mg/l)	129.3	118.4	80.6	108.3
C[a] in liquid after CaP precipitation (mg/l)	41.44	51.38	n.a.	n.a.
C in liquid after Struvite precipitation (mg/l)	78.69	109.8	n.a.	121.7
%wt. C in CaP precipitates	4.13%		3.45%	
%wt. C in Struvite precipitates	1.65%		1.26%	
%C[b] transferred to dirty leachate	8.93%		9.78%	
%C[b] remaining in clean leachate	8.13%		4.4%	
%C[b] precipitates in CaP solids	8.13%		n.a.	
%C[b] precipitates in Struvite solids	8.13%		4.4%	

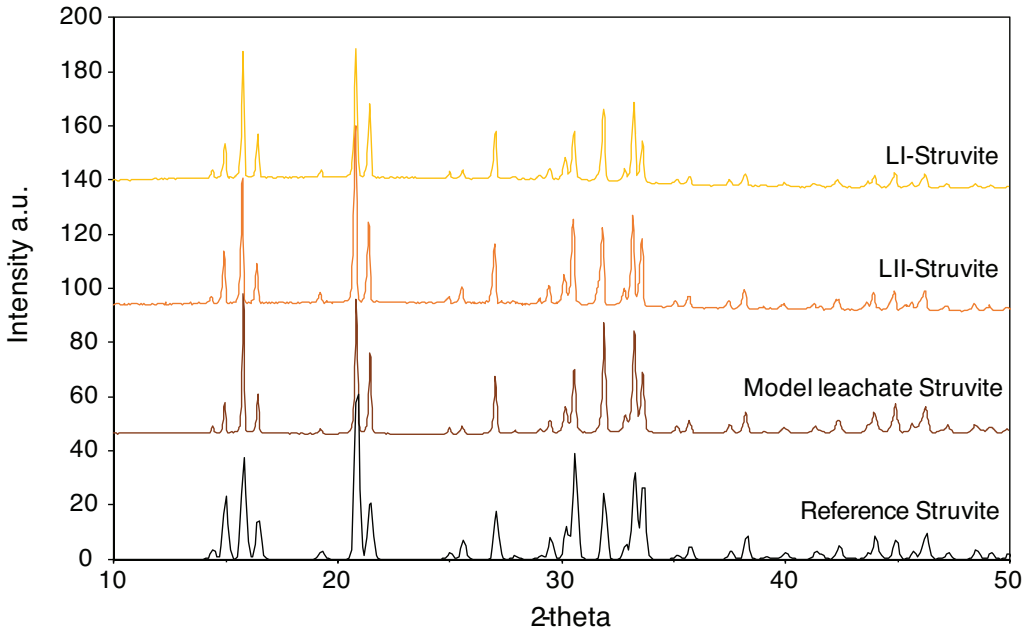


Figure 6. XRD patterns for struvite precipitates from hydrothermally treated sewage sludge (LI-CaP and LII-CaP), for struvite precipitates from a model leachate and XRD reference substance pattern[19].

5 Regulation regarding pollutants in the final product

5.1 OLED

During the P-recovery process, only one solid waste stream is produced. After acid leaching, phosphorus is extracted to the liquid phase and the solid remaining is filtered out and needs to be disposed as a waste.

In Switzerland all solid waste must be classified to ensure its adequate disposal according to OLED[1]. This regulation establishes 5 types of solid wastes (A to E) depending on its origin and composition. Our solid could be classified as type E or D. Table 3 gathers the concentration of pollutants allowed in solid wastes to be classified as types E or D.

From all the set of pollutants, our bottle neck is the organic carbon concentration which depends highly on the conditions of the hydrothermal gasification process. After leaching, around 90%wt. of the carbon in the solid residue will remain in the solids filtered out so it is important that the solid residues extracted during hydrothermal gasification have the lowest %wt. of carbon possible. The solids used for P-recovery experiments for this report, have a concentration of carbon of around 57000 ppm , which after leaching remains more or less the same (∼53600 ppm) since other elements are being removed from the solids (calcium, phosphorus, iron, etc.). This concentration is slightly above the limit concentration for type E residues (50000 ppm) but other experiments have confirmed that we can go as low as 34000 ppm.

5.2 MinRec

As stated before, in Switzerland, the composition of recycled phosphorus products must comply with the MinRec regulation[5]. MinRec sets limits for the concentration of inorganic and organic pollutants in recycled fertilizers based on the ALARA principle (as low as reasonably achievable). Table 1 and table 2 gather the values as well as the approach used to determine the minimum requirement (in the case of inorganic pollutants).

Even though this requirement must be fulfilled by the final recycled product, we analyzed a solid residue before leaching and its corresponding liquid phase after leaching and purification. This way, we could find out if those phases already complied with regulations and it also allowed us to have information about the quality of the solids and its corresponding purified leachate that we will later use to precipitate our P-based fertilizer. The solid residue used was extracted during hydrothermal gasification and contained around 30%wt. of carbon. The leachate used was obtained using the mentioned solid residue as a feedstock and performing acid leaching at standard conditions (pH 1, S/L=20, 45 min) and purification with ion exchange resins (Purolite MTC1600H).

5.2.1 Organic pollutants

MinRec regulates the concentration of three groups of organic pollutants: polychlorinated biphenyls (PCBs), polycyclic aromatic hydrocarbons (PAHs) and polychlorinated dibenzo-p-dioxins and dibenzofurans (PCDD/F) (table 2). We were able to get results for the concentration of PCBs and PAHs. Nonetheless, the unit in charge of the analysis did not have resources to analyse PCDD/F.

Tables 7 and 8 show the concentration of PCBs and PAHs respectively in the solid residue sample. The total concentration of PCBs (0.07 g per ton of P) found represents only the 14% of the limit set by MinRec (0.5 g per ton of P). On the other hand, PAHs in the sample (5.8 g per ton of P) account for 23% of the limit established by MinRec (25 g per ton of P). Therefore, our solid residue comply with the regulation. Regarding the results for the purified leachate, all concentrations measured for PCBs and PAHs, were under the limit of detection (LOD). Therefore, we can predict that the precipitates (P-based fertilizer) from this purified leachate will comply as well with the regulation for PCBs and PAHs. We still need to analyse the samples to find out if the concentration of PCDD/F is also below the MinRec limit (120 ng I-TEQ/kg P).

5.2.2 Inorganic pollutants

MinRec regulates the concentration of the following elements: cadmium, arsenic, mercury, nickel, zinc, chrome, lead and copper (table 1). Table 9 shows the concentration of these elements in the solid residue and in the purified leachate obtained after acid leaching of that solid (same samples as in section 5.2.1). For the solid residue, concentrations for all elements except cadmium and lead, are above the limits. Therefore, this solid residue could not be used as a solid fertilizer as it is. Nonetheless, the concentration of all elements in the purified leachate are below the limits. Hence, precipitates obtained from this liquid phase will comply with MinRec and could be used as a recycled P-based fertilizer provided they comply with the organic pollutants' regulation as well.

Table 7. Concentration of PBCs in a sample of solid residue from hydrothermally treated sewage sludge (digested).

PCBs	LOD	Concentration in sample	Concentration by P content
	ng/g	ng/g	g/t of P
CB 28	0.05	0.55	0.009
CB 52	0.05	0.55	0.009
CB 101	0.05	0.91	0.015
CB 138	0.05	0.89	0.014
CB 153	0.05	1.07	0.017
CB 180	0.05	0.39	0.006
∑ PCBs		4.34	**0.070**
MinRec limit			0.5

Table 8. Concentration of PAHs in a sample of solid residue from hydrothermally treated sewage sludge (digested).

PAHs	LOD	Concentration in sample	Concentration by P content
	ng/g	ng/g	g/t of P
Naphthalene	10.0	15.7	0.252
Acenaphthylene	1.0	2.0	0.031
Acenaphthene	2.1	2.9	0.046
Fluorene	0.7	5.3	0.085
Phenanthrene	2.1	44.3	0.712
Anthracene	0.8	7.6	0.123
Fluoranthene	1.3	56.8	0.912
Pyrene	1.1	36.6	0.588
Benzo (a) anthracene	0.3	20.6	0.331
Chrysene	0.4	43.0	0.692
Benzo (b) fluoranthene	2.5	41.2	0.662
Benzo (k) fluoranthene	0.7	16.5	0.266
Benzo (a) pyrene	0.8	23.6	0.380
Indeno (1,2,3-cd) pyrene	2.0	4.4	0.071
Dibenzo (a,h) anthracene	0.2	8.3	0.134
Benzo (g,h,i) perylene	1.3	29.4	0.472
∑ PAHs		358.1	**5.758**
MinRec limit			25

Table 9. Concentration of inorganic pollutants in a solid residue sample and a purified leachate sample that must comply with MinRec.

	Limit value MinRec (mg/kg P)	Solid Residue %wt.	Solid Residue mg/kg P	Purified leachate mg/l	Purified leachate mg/kg P
Cadmium	25	<LOD	<LOD	<LOD	<LOD
Arsenic	100	0.0007	208	<LOD	<LOD
Mercury	2	0.0002	62	<LOD	<LOD
Nickel	500	0.0042	1310	0.017	15
Zinc	10000	0.0813	25347	<LOD	<LOD
Chrome	1000	0.0048	1487	0.017	15
Lead	500	<LOD	<LOD	0.117	104
Copper	3000	0.0489	15252	<LOD	<LOD
P		3.21		1121	

LOD for solid samples (ppm): Cd 1.015, As 12.6, Hg 4.325, Ni 1.59, Zn 2.185, Cr 0.068, Pb 8.8, Cu 1.6.
LOD for liquid samples is 0.5 mg/l for all elements except As which has a LOD of 0.5 μg/l.

5.3 GC-MS study of other organics

As shown in section 5.2, the concentration of PCBs and PAHs in the purified leachate are below the limits of detection. Nonetheless, we observe that the total organic carbon (TOC) in the purified leachate is normally between 80 and 150 mg/l depending on the feedstock used. Therefore, even though we have discarded that these organic molecules correspond to PCBs and PAHs, we still need to identify them.

We performed preliminary liquid-liquid extractions using an organic solvents (hexane) as the liquid phase and the purified leachate that has been used for the analysis of the previous sections (5.1,5.2) as the second liquid phase. After extraction, the organic liquid phase was analysed through GC-MS. Results were not conclusive and the GC-MS spectra were practically flat. Only ethyl acetate (reliability of 90.5%) was found. We need to turn to other, more precise methods, such as LC-ICP-QQQ to identify them.

Moreover, we performed some solid-liquid extractions using organic solvents (hexane and toluene) as the liquid phase and the solid residues that have been used for the analysis of the previous sections (5.1,5.2) as the solid phase. The spectra obtained through GC-MS for all the extractions (two with hexane for repeatability and one with toluene to compare) are very similar to each other (figure 7). Table 10 gathers the main molecules found (structural formulas in figure 8).

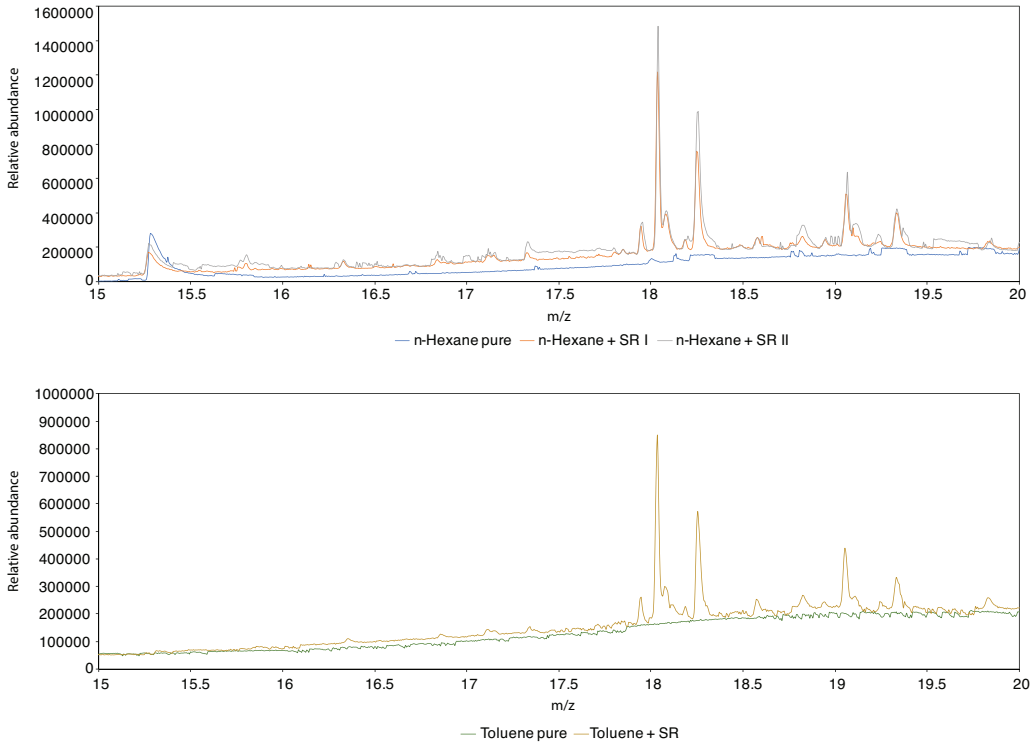


Figure 7. Chromatogram (intensity vs time in minutes) of the extracted organics from samples of solid residue.

Table 10. Organic molecules found through solid-liquid extraction and GC-MS.

Organic solvent	Main molecules found	Reliability
n-Hexane	Stigmastane	90%
	Coprostane	76%
	Bisphenol	51%
	Cholestane	45%
Toluene	Stigmastane	84%
	Coprostane	75%
	Cholestane	47%

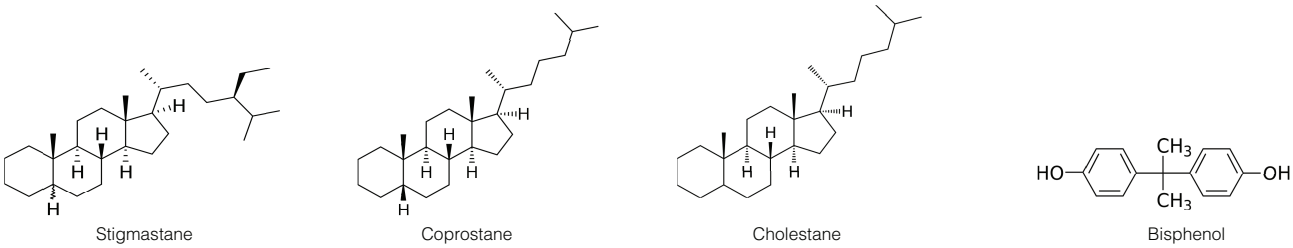


Figure 8. Structural formula of the main molecules found in the solid residues through solid-liquid extraction and GC-MS.

6 Valorisation of P using calcined solid residue (ashes)

We calcined solid residue from the same hydrothermal gasification experiment from which we obtained the deposits used in the experiments of this report (figure 2). The main difference in composition between the deposits and the solid residue ashes is the %wt. of carbon (figure 9). The ashes contain 1.35%wt. of carbon (vs 5.7%wt. in the deposits) which can be mostly attributed to carbonates which only decompose at temperatures above 900°C[21,22].

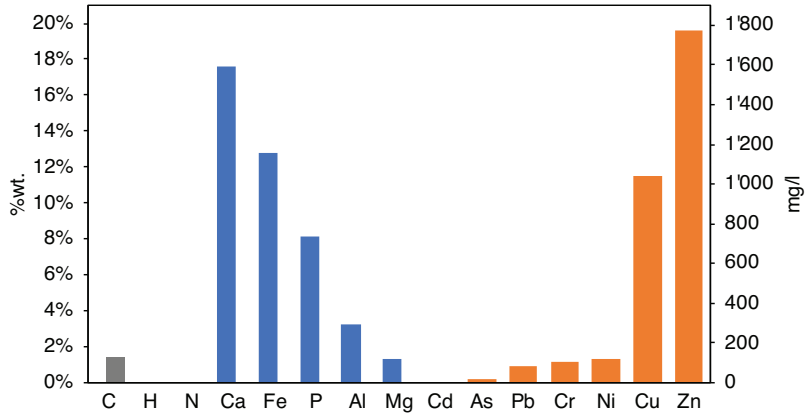


Figure 9. Composition (%wt in blue and gray, mg/kg in orange) of the calcined solid residue (ashes) before leaching.

6.1 Leaching

The ashes were leached in duplicates with sulphuric acid following the same protocol as for the deposits (refer to section 2.2.1 for details). Results (figure 10 and table 11) show that the percentage of P recovered is very similar (around 80%wt. for the deposits vs 83% for the ashes). However, we found remarkable differences for other elements such as Al, Cr, Ni and Zn for which the percentage leached to the liquid phase is smaller when ashes are used as a feedstock. Future works should include studying the influence of carbon concentration on the ability of the elements to transfer to the liquid phase during leaching.

Table 11. Leaching results. Numbers represent the %wt. of each element that is leached to the liquid phase from the calcined solid residue (ashes).

	Al	Ca	Cd	Cr	Cu	Fe	Mg	Ni	P	Pb	Zn	As
I	12.94%	5.69%	0.00%	0.00%	40.01%	1.58%	59.07%	0.00%	84.09%	0.00%	0.00%	64.87%
II	12.42%	5.59%	0.00%	0.00%	41.10%	1.55%	58.31%	0.00%	81.75%	0.00%	0.00%	64.39%
Average	12.68%	5.64%	0.00%	0.00%	40.55%	1.57%	58.69%	0.00%	**82.92%**	0.00%	0.00%	64.63%
Error	0.26%	0.05%	0.00%	0.00%	0.54%	0.02%	0.38%	0.00%	1.17%	0.00%	0.00%	0.24%

6.2 Purification

One purification experiment was performed for each leachate produced using ion exchange resins (refer to section 2.2.2 for details). We took three samples for each one of them and analysed them through ICP. The three samples correspond to water exiting the column at the beginning of the experiments, purified leachate and water used to clean the column after the experiments. We were able to recover, in the purified stream, 85% and 65%wt. (75%wt. average) of the phosphorus that

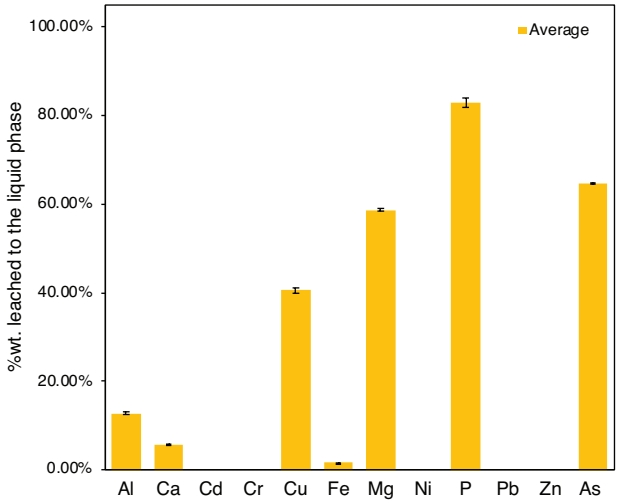


Figure 10. Average %wt. leached to the liquid phase from the ashes before purification.

was present in the dirty leachate for experiments I and II respectively. Starting from the phosphorus in the solid residue, the overall recovery rate is 71.5% wt and 53.1% wt for experiments I and II respectively. For both experiments, the discarded water at the beginning of them had negligible amounts of all the elements analysed. On the other hand, the analysis of the cleaning water revealed that between 19% and 27%wt. of the phosphorus in the dirty leachate ends up in this phase for experiments I and II respectively. Specially for experiment II, the losses in the cleaning water lower dramatically the P recovered in the purified stream. If we count the phosphorus in the cleaning water, the total P recovery from the phosphorus in the solid residue would be 88% and 75% for experiments I and II respectively. For the rest of the elements, in both cases, between 99% and 99.99%wt. of the amount present in the dirty leachate was removed by the column. Therefore, the purified leachates are composed almost exclusively by water, phosphates and sulphates (from sulfuric acid). Refer to figure 11 for details.

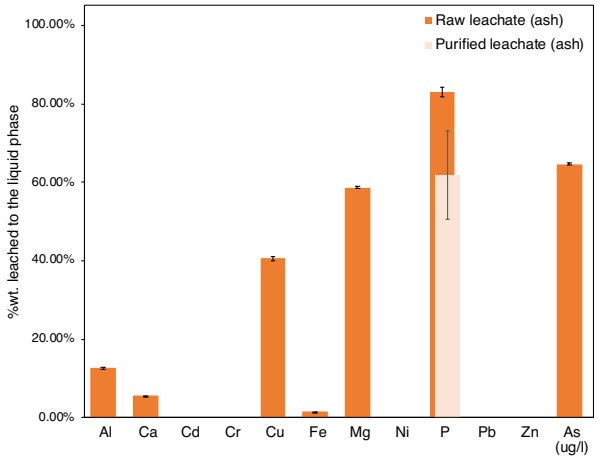


Figure 11. Average %wt. leached to the liquid phase from the solid before and after purification for both replicates.

6.3 Valorisation

6.3.1 CaP

Following the protocol shown in section 2.2.3, we precipitated phosphorus with calcium hydroxide using the purified leachates from experiments I and II (section 6.2). The solid precipitates were analysed through XRD to identify the crystalline phases formed. Figure 12 shows the results. Reference patterns of the substances that could be expected are shown as well. Both LI and LII crystalline phases are composed of 60% Brushite ($CaHPO_4) \cdot 2H_2O$) and 40% calcium carbonate ($CaCO_3$). Hence, we can confirm that, when using ashes as feedstock, phosphorus precipitates as

crystalline dicalcium phosphate dihydrate (brushite). Moreover, ICP analysis of the purified leachate and waste liquid after precipitation, confirmed that all the phosphorus in the purified leachate precipitates.
Elemental analysis revealed that the precipitates contained 4.7%wt. and 5.79%wt. C for samples I and II respectively. This carbon content corresponds to the $CaCO_3$ which comes from the inorganic carbon in the ashes.

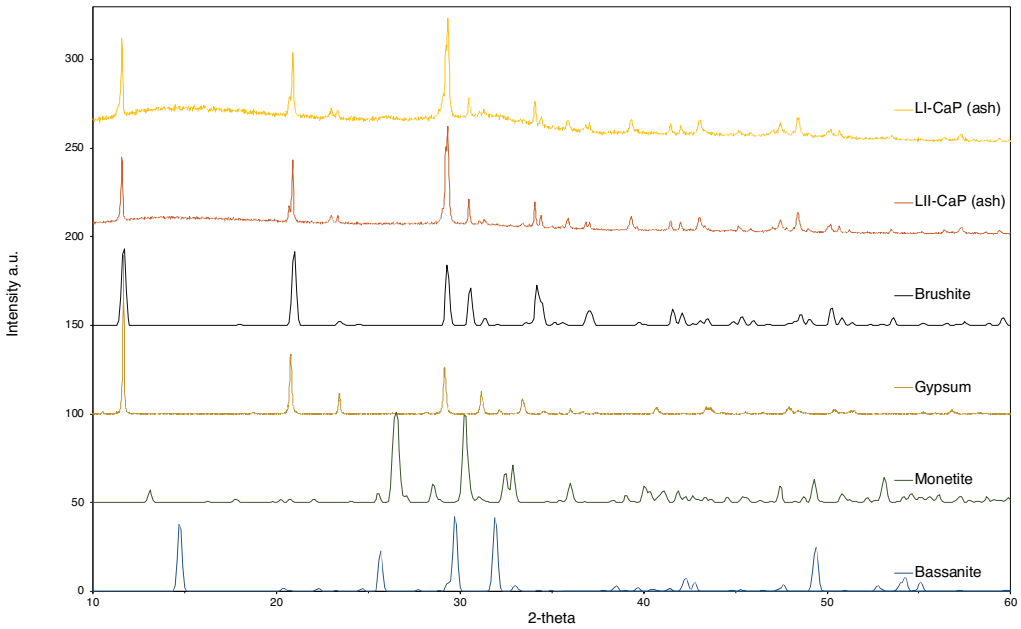


Figure 12. XRD patterns for calcium phosphate precipitates from hydrothermally treated sewage sludge ash (LI-CaP (ash) and LII-CaP (ash)) and reference substances patterns[19].

6.3.2 Struvite

Following the protocol shown in section 2.2.4, we precipitated phosphorus as magnesium ammonium phosphate (Struvite) using the purified leachates from experiments I and II (section 6.2). In addition, we prepared a model leachate using ultra-pure water and reagent phosphoric acid and then used this liquid phase to precipitate Struvite following the same protocol as for leachates I and II.

The precipitates were analysed through XRD to identify the crystalline phases formed. Figure 13 shows the results and the reference pattern. Samples for both experiments, as well as for the model leachate are composed by nearly pure Struvite. Therefore, as for experiments using the deposits (4.2), we were able to precipitate phosphorus as crystalline Struvite when using ashes. Moreover, as for CaP precipitation experiments, ICP analysis of the purified leachate and waste liquid after struvite precipitation, confirmed that all the phosphorus in the purified leachate precipitates.
Elemental analysis revealed that the precipitates contained 2.016%wt. and 1.74%wt. C for samples I and II respectively. This carbon content corresponds to the inorganic carbon in the ashes.

7 Conclusions and future works

We could precipitate high purity crystalline Struvite from phosphorus extracted from hydrothermally treated sewage sludge confirming that a solid P-based fertilizer can be produced from hydrothermally treated sewage sludge. In the case of calcium phosphates, no crystalline forms were found. Nonetheless, when the feedstock is calcined residue (ashes) with no organic carbon, both crystalline struvite and dicalcium phosphate can be identified. We hypothesize that, in the case of hydrothermally treated sewage sludge (not calcined), phosphorus in the liquid phase might be attached to organic functional groups and that, calcium cations (from calcium hydroxide) are unable to precipitate phosphorus and only precipitate sulphates in the form of bassanite and/or gypsum. We have two ideas to identify the form in which phosphorus is present in the purified leachate. On the one hand, we could do LC-ICP-QQQ-MS with the appropriate column to perform phosphorus speciation. First we would identify different peaks using liquid chromatography. Then we would isolate the compounds corresponding to the peaks through HPLC fractionation and finally, we would send each fraction to ICP-QQQ-MS. On the other hand, we could use NMR. Specifically, we could use deuterated sulfuric acid to extract phosphorus from solid residue

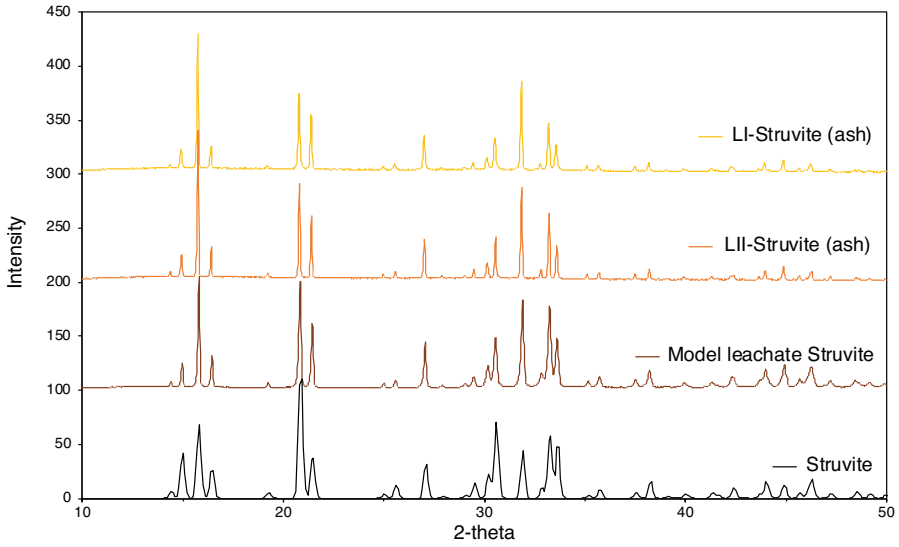


Figure 13. XRD patterns for struvite precipitates from hydrothermally treated sewage sludge ash (LI-Struvite (ash) and LII-Struvite (ash)), for struvite precipitates from a model leachate and XRD reference substance pattern[19].

and identify the functional groups to which phosphorus is attached through NMR. Identifying the organic molecules in the purified leachate, and how are they related to phosphorus, is the key to understand how phosphorus behaves when we valorize it through precipitation.

Regarding regulation, the analysis performed until know are very positive since our purified leachate complies with MinRec for organic and inorganic pollutants. Nonetheless, we still need to find resources or an external company to find the concentration of polychlorinated dibenzo-p-dioxins and dibenzofurans (PCDD/F) since we could not do it within this project.

References

1. Office fédéral de l'agriculture (OFAG). Ordonnance sur la limitation et l'élimination des déchets (ordonnance sur les déchets, oled) (2015).
2. White, S. & Cordell, D. Peak phosphorus: the sequel to peak oil. *Phosphorus Futur.* (2009).
3. Mohr, S. & Evans, G. New projection of peak phosphorus. *Philica* (2013).
4. Office fédéral de l'environnement (OFEV). Récupération du phosphore contenu dans les eaux usées (2009).
5. Office fédéral de l'agriculture (OFAG). Détermination des valeurs limites pour la nouvelle catégorie d'engrais «engrais minéraux de recyclage» (2018).
6. Office fédéral de l'environnement (OFEV). Déchets riches en phosphore. module de l'aide à l'exécution relative à l'ordonnance sur la limitation et l'élimination des déchets (ordonnance sur les déchets, oled) (2019).
7. Dorozhkin, S. V. Calcium orthophosphates. occurrence, properties, biomineralization, pathological calcification and biomimetic applications, DOI: 10.4161/biom.18790 (2011).
8. Oliveira, C., Ferreira, A. & Rocha, F. Dicalcium phosphate dihydrate precipitation: Characterization and crystal growth. *Chem. Eng. Res. Des.* **85**, 1655–1661, DOI: https://doi.org/10.1016/S0263-8762(07)73209-4 (2007).
9. Ferreira, A., Oliveira, C. & Rocha, F. The different phases in the precipitation of dicalcium phosphate dihydrate. *J. Cryst. Growth* **252 (4)**, 599–611, DOI: https://doi.org/10.1016/S0022-0248(03)00899-6 (2002).
10. Mekmene, O. *et al.* Effects of pH and Ca/P molar ratio on the quantity and crystalline structure of calcium phosphates obtained from aqueous solutions. *Dairy Sci. Technol.* **89**, 301–316, DOI: 10.1051/dst/2009019 (2009).
11. Koga, D. Struvite recovery from digested sewage sludge. *Phosphorus Recover. Recycl.* 255–264, DOI: https://doi.org/10.1007/978-981-10-8031-9_17 (2019).
12. Pastor, L., Mangin, D., Ferrer, J. & Seco, A. Struvite formation from the supernatants of an anaerobic digestion pilot plant. *Bioresour. Technol.* **101**, 118–125, DOI: https://doi.org/10.1007/978-981-10-8031-9_17 (2010).
13. Uysal, A., Yilmazel, Y. & Demirer, G. The determination of fertilizer quality of the formed struvite from effluent of a sewage sludge anaerobic digester. *J. Hazard. Mater.* **181**, 248–254, DOI: 10.1016/j.jhazmat.2010.05.004 (2010).
14. Ovsyannikova, E., Kruse, A. & Becker, G. Feedstock-dependent phosphate recovery in a pilot-scale hydrothermal liquefaction bio-crude production. *Energies* **13 (2)**, 379–400, DOI: https://doi.org/10.3390/en13020379 (2020).
15. Shi, Y., Luo, G., Rao, Y., Chen, H. & Zhang, S. Hydrothermal conversion of dewatered sewage sludge: Focusing on the transformation mechanism and recovery of phosphorus. *Chemosphere* **228**, 619–628, DOI: 10.1016/j.chemosphere.2019.04.109 (2019).
16. Xu, H., He, W., P. Gu, Wang, G. & Shao, L. Recovery of phosphorus as struvite from sewage sludge ash. *J. environmental sciences* **24(8)**, 1533–1538, DOI: https://doi.org/10.1016/S1001-0742(11)60969-8 (2012).
17. Acelas, N. Y., Flórez, E. & López, D. Phosphorus recovery through struvite precipitation from wastewater: effect of the competitive ions. *Desalination Water Treat.* **54**, 2468–2479, DOI: 10.1080/19443994.2014.902337 (2015).
18. Kataki, S., West, H., Clarke, M. & Baruah, D. C. Phosphorus recovery as struvite: Recent concerns for use of seed, alternative Mg source, nitrogen conservation and fertilizer potential. *Resour. Conserv. Recycl.* **107**, 142–156, DOI: 10.1016/j.resconrec.2015.12.009 (2016).
19. FIZ Karlsruhe - Leibniz Institute for Information Infrastructure. Icsd - the world's largest database for completely identified inorganic crystal structures. https://icsd.fiz-karlsruhe.de/search/basic.xhtml. Accessed: 2020.03.
20. Findlay, S. *et al.* Total carbon analysis may overestimate organic carbon content of fresh waters in the presence of high dissolved inorganic carbon. *LIMNOLOGY OCEANOGRAPHY: METHODS* **8**, 196–201 (2010).
21. Kim, J.-W. & Lee, H.-G. Thermal and carbothermic decomposition of na2co3 and li2co3. *Metall. Mater. Transactions B* **32**, DOI: 10.1007/s11663-001-0003-0 (2001).
22. L'vov, B. Mechanism and kinetics of thermal decomposition of carbonates. *Thermochimica Acta* **386**, 1–16, DOI: 10.1016/S0040-6031(01)00757-2 (2002).

Methodology for the estimation of the capital expenditure (CAPEX) and the operating expenditure (OPEX) of TreaTech's P- recovery process

Methodology for the estimation of the capital expenditure (CAPEX):

For scenario A, the estimation of equipment cost includes the purchase of the following equipment: solid/acid/water/buffer tanks, a solid screw, a water demineralization unit, a leaching jacketed reactor with a stirrer, pH controller and an acid dosing unit, acid/water/liquid-solid pumps, press filters, an ion exchange resin and a column, a precipitation reactor with a stirrer and a pH controller, solid/liquid-solid pumps, solid tanks, press filter and a low temperature dryer.

For the scenario B, the estimation of equipment cost includes the purchase of the following equipment: solid/acid/water/buffer tanks, a solid screw, a water demineralization unit, a leaching jacketed reactor with a stirrer, pH controller and an acid dosing unit, acid/water/liquid-solid pumps, press filters, an ion exchange resin and a column and a vacuum evaporator with double effect thermal power supply.

The cost estimate was based on three methodologies: the providers' quotes, the « Six-Tenths Factor » rule and the « percentage of equipment purchase costs ». The results obtained were verified with the « Lang Factor ». Although the Lang factor is relatively obsolete, it remains useful to estimate the fixed costs for building a plant. The « Six-Tenths Factor » rule is used when the evaluator is faced with the problem of costing equipment at a processing capacity for which no cost data are immediately available, which is the case for the P-recovery technology. According to this rule, the approximate cost of the equipment can be determined if the cost of a similar facility but with a different scale is known. It is calculated as follows: $C_B = C_A \left(\frac{TB}{TA}\right)^{0.6}$ where C_B is the approximate cost of the equipment with a T_B size and C_A is the known cost of the equipment with a size T_A. As there is not yet any available P-recovery plant at industrial scale, the approximate cost of the equipment is based on providers' quotes and economic analysis of similar installations. It allows a relatively precise cost estimation (± 30%).

Once the approximate costs related to the purchase of equipment have been determined, the method based on "percentages of equipment purchase costs", allows direct and indirect costs (e.g. installation costs, instrumentation and control, piping, etc.) to be estimated on the basis of individual percentages of the main equipment purchase cost. The percentages used for estimating direct and indirect costs are based on the study of Gasafi et al.[1]
A detailed description of the direct and indirect cost was described by Sari et al.[2] The following percentages of direct and indirect costs were taken into account:
Direct costs:

- Major purchased equipment (**100%**)
- Installation cost (**39%**)
- Instrumentation and control (**26%**)
- Piping (**31%**)
- Electrical (**10%**)
- Building (**18%**)
- Service facilities (**25%**)

Indirect costs:

- Engineering and Supervision (**35%**)
- Construction expenses (**40%**)
- Contractor's fee (**5%**)
- Contingency (**10%**)

Contractor's fees and contingencies were calculated as a fraction of total direct costs, taking into account engineering and supervision costs as well as construction costs.

Finally, "Working Capital Investment" is the capital needed to start up the plant and operate it before revenues are generated. This corresponds to 5% of the direct and indirect costs.

Methodology for the estimation of the operating expenditure (OPEX):

On the basis of the CAPEX, the OPEX can be estimated. The operating expenditure includes the chemicals costs, power consumption costs, waste disposal, maintenance, labor costs, insurance, amortization and product revenues for the two scenarios according to the two possible output products (PA and struvite).

Chemicals costs comprise the costs of all the chemicals needed for each of the scenarios including water (process water deionized with the deionization unit). The bulk price of the chemicals was taken from Chembid.

Concerning power consumption costs, the sale price for electricity is based on the sale price in Switzerland (0.15 CHF/kWh). The cost of the thermal energy needed for the concentration of phosphoric acid (PA, scenario B) was calculated based on the price of the natural gas that would need to be burned (provided by the cement producer, 7.10 CHF/GJ). This cost translates to 0.026 CHF/kWh.

The unit with the most significant power consumption for P-recovery was the evaporator (PA, scenario B). Its power consumption was calculated based on a double effect vacuum evaporator (IWE, HWS 6000 DE). For this evaporator, the electrical consumption and thermal energy consumption are 13 kWh and 350 kWh per m^3 evaporated respectively.

The disposal costs of the various residues from the process are based on costs in Europe[1]. Waste disposal includes disposal of the solids after leaching (if not reused in the cement plant), the ion exchange resins (lifetime of 10 years), the HCl regeneration and the treatment of the cleaning water from the purification process.

Maintenance costs are calculated on the basis of a fixed percentage of the CAPEX (2%[3]) of each of the scenarios. Similarly, insurance costs are calculated on the basis of a fixed percentage of the CAPEX (0.5%[3]).

Labor requires three full shifts spread over a 24-hour period for remote supervision, operation and maintenance work[3].The annual operating time corresponds to 8'000 h/a.

Finally, amortization costs were calculated according to literature[3] for similar processes. It is based on an interest rate of 3%, amortization periods of 10 and 30 years for the equipment and the building respectively, an annuity of 12% and 5% for the equipment and the building respectively and building costs (excluding land) of 270 CHF/m^3. Land was not included as it is assumed to be available on site.

Revenues were also estimated using market prices for phosphoric acid 54% (Chembid) and struvite (Chembid).

References

1. E. Gasafi, M. Y. Reinecke, A. Kruse and L. Schebek, *Biomass and Bioenergy*, 2008.
2. R. M. Sari and K. Kolmetz, *KLM Technol. Gr.*, 2014.
3. A. Nättorp and K. Remmen. P-Rex report. Sustainable sewage sludge management fostering phosphorus recovery and energy efficiency. Seventh Frame-work Programme Grant agreement No. 308645